

University of Nottingham
UK | CHINA | MALAYSIA

Alternative splicing and the inhibition of splicing kinases in Alzheimer's Disease

Roaa Alalwany

A thesis submitted to the University of Nottingham for the degree of Doctor of Philosophy (PhD)

Under supervision of Professors David Bates, Lucy Donaldson and Kevin Morgan

March 2021

Abstract

Alzheimer's disease (AD) is the most common cause of dementia, the chronic and progressive deterioration of memory and cognitive abilities. AD can be pathologically characterised by neuritic plaques and neurofibrillary tangles, formed by the aberrant aggregation of β-amyloid and tau proteins, respectively. As the global population living with dementia is projected to reach 132 million by the year 2050, treatment of AD has become a top public health priority. Unfortunately, there are currently no disease-modifying drugs available for AD patients, so it is critical to develop novel therapeutic strategies for better disease management.

Alternative splicing (AS) was first implicated in AD through key genes *APP* and *MAPT* which have splicing isoforms that differentially affect susceptibility for disease. More recently, transcriptome analyses of the ROSMAP dataset revealed an altered splicing profile in association with AD. Indeed, my analysis of this dataset found that individuals with mild cognitive impairment (MCI) and AD expressed a greater number of known splicing transcripts per gene, indicating more AS than individuals with no cognitive impairment. Additionally, multivariate analysis of transcript splicing of the BDR dataset discovered that the frontal cortex, a brain region with high susceptibility for AD pathology, exhibited differential splicing events compared to the cerebellum, a protected region of the brain. Differential splicing most notably occurred in genes related to synaptic function and calcium signalling. Therefore, I hypothesised that the expression of splicing kinases, known regulators of AS, can be associated with AD. Accounting for sex and age, individuals with low splicing kinase expression were identified to have a higher proportion of clinical AD and AD-related pathologies compared to high expression groups.

Next, I hypothesised that regulation of splicing kinase activity could have protective effects on AD-related neurotoxicity *in vitro*. Using oxidative stress, β-amyloid, and tau hyperphosphorylation models, I investigated the effect of VEGF-A splicing isoforms, previously established to be neurotrophic agents, as well as novel small molecule kinase inhibitors, which selectively inhibit SRPK1 and CLK. Both VEGF-A_{165}a and VEGF-A_{165}b isoforms, produced by differential splice site selection in exon 8, were protective against AD-related neurotoxicity, measured by increased metabolic activity and neurite outgrowth. However, VEGF-A_{165}b was more protective against decreased neurite outgrowth. SRPK1 inhibition was found to significantly protect neurite outgrowth through shifting AS of *VEGFA* towards the VEGF-A_{165}b isoform. The use of CLK inhibitors also exerted neuroprotective effects *in vitro*, but this was not VEGF-A isoform dependent. Since CLK inhibition modulated AS of *MAPT* through increased exon 10 inclusion, I postulated that CLK inhibitors may be neuroprotective through tau-mediated mechanisms.

Overall, these findings demonstrate that splicing kinase inhibitors can be used to modulate AS and could potentially have beneficial effects in AD-related pathologies Global changes in AS are implicated in AD and these are likely to occur upstream of pathogenic pathways, including the toxic accumulation of β-amyloid and tau proteins. As a result, I propose further investigation of splicing kinase inhibitors as a novel therapeutic strategy for treatment of AD and other tauopathies that similarly cause neurodegeneration.

Acknowledgments

Firstly, I would like to thank my primary supervisor, David Bates, for his wisdom and guidance over the last four years. From the very first day to the last, your passion for science has been inspirational and kept me motivated through the difficulties we faced along the way. I would also like to thank my co-supervisors, Lucy Donaldson and Kevin Morgan, for their incredible support and valuable input to various aspects of my work. I must likewise acknowledge our collaborator Nigel Mongan, for his mentorship and his many contributions to this project. I am very grateful to have had the opportunity to work with you all and I learnt a lot from the experience.

They say the only constant in this world is change, and indeed there were many during the progression of this project. Through all the preliminary plans, revised plans, amended plans and doomed-to-fail plans, I can only be grateful to the friendship and support of the wonderful people in TVBL/Exonate who helped me along the way. There are too many of you to name individually, but I hope you know that your kindness (and precious tea-breaks) got me through this process only slightly less sane than I was at the start.

I must mention my comrade Nas, who has been the absolute best PhD pal a girl could ask for. I have so much respect for you, both as a scientist and a friend, and I am grateful we got to do this together. I would also like to thank Zoe and Kiren for taking me in as a rotation student and teaching me how to “do science”. Thanks to the rest of Team Neuro, especially Matt and Nick, who were always generous with their time and advice. Jason, thanks for being my ELISA buddy and taking shifts on the world’s longest protocol. Mussarat and Nahlah, for all our bench-side conversations; Amany, for all the encouragement; Vicky, for all the laughs. Collectively, you guys made the lab a truly fantastic place to work.

Finally, I would be greatly amiss if I did not thank my family, and my friends who have become family. To my brother and sister-in-law: thanks for listening to me ramble on about my thesis and patiently suffering alongside me. To my girls made in Southall: thanks for the travel, the laughs, the late-night Skype calls, and the love. I cannot even attempt to tell you how much you mean to me. The biggest honour, however, must go to my parents. I simply would not be here without your loving care and unwavering support. You had to endure four years’ worth of doubts and woes, and not once did you stop believing in me. For that, and for so much more, thank you. I feel incredibly blessed to call you mum and dad.

Author's declaration

I, Roaa Alalwany, confirm that the work presented in this thesis was carried out in accordance with the requirements of the University's Regulations and Code of Practice for Research Degree Programs and that it has not been submitted for any other academic award. I confirm that the work and views demonstrated in this thesis are my own. Where information has been derived from other sources, I confirm this has been indicated in the thesis.

SIGNED ……..... DATE……

Conferences

Alalwany R.H., Bates D.O., Morgan K., Donaldson L.F. Alzheimer's Association International Conference; Chicago, Illinois, USA 2018 – Poster presentation (absent). Neuroprotective effects of VEGF-A in model of β-amyloid induced neurotoxicity.

Alalwany R.H., Donaldson L.F., Morgan K., Morris J.C., Hawtrey T., Mongan N.P., Bates D.O. 6th UK RNA Splicing Workshop; Cumbria, UK 2019 – Poster presentation (present). Use of dual-specificity kinase inhibitors to alter tau splicing.

Alalwany R.H., Donaldson L.F., Morgan K., Morris J.C., Hawtrey T., Bates D.O. Alzheimer's Association International Conference; Amsterdam, Netherlands 2020 – Poster presentation (online). CLK inhibition alters tau splicing and has a protective effect in neuronal cells *in vitro*.

Alalwany R.H., Donaldson L.F., Morgan K., Morris J.C., Hawtrey T., Bates D.O. 7th UK RNA Splicing Workshop – Oral presentation (online). Novel small molecule splicing kinase inhibitors have neuroprotective effects *in vitro*.

List of abbreviations

Aβ	β-Amyloid protein
ACh	Acetylcholine
AChE	Acetylcholinesterase
AD	Alzheimer's Disease
ANOVA	Analysis of Variance
ANCOVA	Analysis of Co-variance
APP	Amyloid Precursor Protein
AS	Alternative Splicing
ATP	Adenosine Triphosphate
BBB	Blood Brain Barrier
BDNF	Brain-derived neurotrophic factor
BDR	Brains for Dementia Research
BIN1	Bridging Integrator 1
bp	Base pairs
BSA	Bovine Serum Albumin
cDNA	complementary DNA
CI	Cognitive Impairment
CLK	CDC2 Like Kinase
CNS	Central Nervous System
Df	Degrees of freedom
dH_2O	distilled water
DMEM	Dulbecco's Modified Eagle Medium
DMSO	Di-methyl Sulfoxide
DNA	Deoxyribonucleic acid
DRG	Dorsal Root Ganglia
Dyrk1A	Dual specificity tyrosine phosphorylation regulated kinase 1A
EC50	Concentration required for 50% Efficacy
ELISA	Enzyme-linked immunosorbent assay
ESE	Exonic Splicing Enhancer

ESS	Exonic Splicing Silencer
FBS	Foetal Bovine Serum
FTD	Frontotemporal Dementia
GO	Gene Ontology
GSEA	Gene Set Enrichment Analysis
HIF-1	Hypoxia Inducible Factor 1
hnRNP	heterologous nuclear Ribonucleoprotein
IC50	Concentration required for 50% Inhibition
IgG	Immunoglobulin G
kb	kilobase
MAPK	Mitogen Activated Protein Kinase
MAPT	Microtubule-Associated Protein Tau
MCI	Mild Cognitive Impairment
MNK	MAP-Kinase Interacting Kinase
MKNK2	MAPK Interacting Serine/Threonine Kinase
MYC	Myelocytomatosis
mRNA	messenger RNA
mTOR	Mammalian Target of Rapamycin
NCI	No Cognitive Impairment
NFT	Neurofibrillary Tangle
NGF	Nerve Growth Factor
NMD	Nonsense Mediated Decay
NP1	Neuropilin 1
ORA	Over representation analysis
PBS	Phosphate Buffered Saline
PCR	Polymerase Chain Reaction
PFA	Paraformaldehyde
PI3K	Phosphoinositide 3-Kinase
PKC	Protein Kinase C
PNS	Peripheral Nervous System
pSR	phosphorylated SR protein

RAGE	Receptor for Advanced Glycation End Products
RNA	Ribonucleic acid
RNA-seq	RNA sequencing
ROSMAP	Religious Orders Study and the Memory and Ageing Project
RPE	Retinal Pigmented Epithelium
RPMI	Roswell Park Memorial Institute
RT-PCR	Reverse Transcription Polymerase Chain Reaction
SD	Standard Deviation
SEM	Standard Error of the Mean
snRNP	small nuclear Ribonucleoprotein
SRE	Splicing Regulatory Elements
SRPK	Serine/Threonine Protein Kinase
SRSF	Serine/Arginine Rich Splicing Factor 1
SS	Sum of Squares
TNF-α	Tumour Necrosis Factor Alpha
TGF-β	Transforming Growth Factor Beta
TRPV1	Transient Receptor Potential Vanilloid 1
VEGF	Vascular Endothelial Growth Factor
VEGFR	Vascular Endothelial Growth Factor Receptor
VD	Vascular Dementia

List of Tables

Table 1.1 Summary of core clinical features observed in different dementia types 2
Table 1.5 Braak stages as a characterisation of neurofibrillary changes seen in the AD brain 13
Table 2.1 Media composition for cell culture of SHSY5Y and Neuro2a cells 30
Table 2.5.1 List of components for cell lysis buffer 35
Table 2.5.2 List of buffers for Western blot 36
Table 2.5.3 Antibodies used for Western blot 36
Table 2.5.4 List of buffers for ELISA 37
Table 2.5.5 Antibodies used for VEGF-A ELISA 37
Table 3.3.1 Top 10 up- and down-regulated GO pathways identified from genes differentially expressed in cerebellum compared to the frontal cortex in normal brain 52
Table 3.3.2.1 Top 10 GO pathways identified from genes that have significantly more or less skipped exons in cerebellum compared to the frontal cortex of normal brain 55
Table 3.3.2.2 Top 10 biological processes identified by ORA of genes that show significantly differential exon skipping between the cerebellum and frontal cortex 56
Table 3.3.2.3 Top 10 GO pathways identified from genes that have significantly more or less retained introns in cerebellum compared to the frontal cortex of normal brain..... 58
Table 3.3.2.4 Top 10 biological processes identified by ORA of genes that show significantly differential intron retention between the cerebellum and frontal cortex 59
Table 3.3.2.5 Top 10 biological processes identified by ORA of genes that show significantly differential splicing of mutually exclusive exons in the cerebellum and frontal cortex..... 60
Table 3.3.2.6 Top 10 biological processes identified by ORA of genes that show significantly differential 5’ splice site selection between the cerebellum and frontal cortex 61
Table 3.3.2.7 Top 10 biological processes identified by ORA of genes that show significantly differential 3’ splice site selection between the cerebellum and frontal cortex 62
Table 3.3.3.1 Top 10 upregulated and 5 downregulated GO pathways identified from genes differentially expressed between NCI and AD groups 67
Table 3.3.3.2 Top 10 upregulated and 5 downregulated GO pathways identified from genes differentially expressed between control and AD groups..... 71
Table 3.3.3.3 Top 10 upregulated and 5 downregulated GO pathways identified from genes differentially expressed between individuals with NCI and SCI 74
Table 3.3.5.1 The relative expression of full-length transcript for splicing kinases in subgroup of females and males 79
Table 4.3.3: Summary of the effect size and IC50 of VEGF-A isoforms on OA-induced neurite “dieback” in SHSY5Y cells 128
Table 5.3.3.1 The percent remaining activity of splicing kinases with 1μM GRIFFIN treatment in a cell-free in vitro assay..... 157

Table 5.3.3.2 The half maximal inhibitory concentration (IC50) for GRIFFINs for splicing kinases based on a cell-free in vitro assay 158
Table 5.3.3.3 The percent remaining activity of splicing kinases with 1μM GRIFFIN42 and 53 treatment in a cell-free in vitro assay 163
Table 5.3.3.4 The half maximal inhibitory concentration (IC50) for GRIFFINs for splicing kinases based on a cell-free in vitro assay 164
Table 7.3.1 List of PCR primer sequences 197
Table 7.3.2 List of genes from GSEA analysis that show significant differential expression in cerebellum compared to the frontal cortex..... 198
Table 7.3.3 List of genes from GSEA analysis that show significant increased or decreased exon skipping in cerebellum compared to the frontal cortex..... 200
Table 7.3.4 List of genes from ORA analysis that show significant differential exon skipping between cerebellum and frontal cortex 201
Table 7.3.5 List of genes from GSEA analysis that show significant increased or decreased intron retention in cerebellum compared to the frontal cortex..... 202
Table 7.3.6 List of genes from ORA analysis that show significant differential intron retention between cerebellum and the frontal cortex 202
Table 7.3.7 List of genes from ORA analysis that show significantly differential splicing of mutually exclusive exons in the cerebellum and frontal cortex..... 203
Table 7.3.8 List of genes from ORA analysis that show significant differential 5’ splice site selection between cerebellum and the frontal cortex..... 203
Table 7.3.9: List of genes from ORA analysis that show significant differential 3’ splice site selection between cerebellum and the frontal cortex..... 204
Table 7.3.10 List of genes from GSEA analysis that have significantly different transcriptional expression in control and clinical AD 205
Table 7.3.11 List of genes from GSEA analysis that have significantly different transcriptional expression in control and pathological AD..... 208
Table 7.3.12 List of genes from GSEA analysis that have significantly different transcriptional expression in control and SCI groups 211

List of Figures

Figure 1.1 Biomarkers for AD with progression of clinical stage 3
Figure 1.3.1 Schematic diagram for the production of Aβ through post-translational processing of APP 6
Figure 1.3.2 Proposed secretase cleavage sites on APP amino acid sequence 7
Figure 1.5 Tau protein variants produced from alternative splicing of MAPT gene at exons 2/3 and exon 10 15
Figure 1.7 The structure of human *VEGFA* gene and its alternative splicing isoforms 18
Figure 1.8 Downstream signalling pathways of VEGF-A_{165} and VEGF-A_{165}b in endothelial cells 20
Figure 1.9: Schematic for the types of RNA splicing events 22
Figure 1.10 Schematic diagram for proposed phosphorylation of SRSF1 by splicing kinases SRPK1 and CLK1 24
Figure 1.12 The chemical structure of SPHINX31 26
Figure 2.3 Neurite outgrowth assay analysis 33
Figure 2.5.4 VEGF-A_{165}a ELISA optimisation of antibody concentration and blocking reagent 38
Figure 2.6 Structure of Tau minigene 39
Figure 3.3.1.1 Volcano plot reveal genes that are differentially expressed between cerebellum and frontal cortex in normal brain 52
Figure 3.3.1.2 Clustered heat map illustrating the differential expression of splicing factors in frontal cortex and cerebellum of control brain 53
Figure 3.3.2.1 The differential splicing of genes in cerebellum and frontal cortex 54
Figure 3.3.2.2 Synaptic gene *NRXN2* exon 20 is alternatively spliced in cerebellum and frontal cortex of normal brain 57
Figure 3.3.2.3 Summary of GO pathways for synaptic function enriched by ORA of alternatively spliced genes 62
Figure 3.3.2.4 Vesicle trafficking gene *EXOC1* is alternatively spliced in cerebellum and frontal cortex of normal brain 63
Figure 3.3.2.5 IP3 receptor gene *ITPR1* is alternatively spliced in cerebellum and frontal cortex of normal brain 64
Figure 3.3.3.1 Differential expression of genes in control, MCI, and AD groups according to clinical diagnosis 66
Figure 3.3.3.2 Protein interactions produced from genes which are differentially expressed in AD compared to both control and MCI groups 68
Figure 3.3.3.3 Differential expression of genes in control (no AD), predicted AD, and definite AD groups according to CERAD score 70
Figure 3.3.3.4 Differential expression of genes in control (no CI), MCI, and severe CI groups according to MMSE score 73

Figure 3.3.4.1 Percent of genes expressed in control, MCI, and AD groups with a single transcript or multiple known transcripts produced through alternative splicing 75
Figure 3.3.4.2 Increased alternative splicing in MCI and AD 76
Figure 3.3.4.3 Expression of splicing kinases (sum of all transcripts) in control, MCI and AD groups 77
Figure 3.3.4.4 Expression of splicing kinases is related to 4R:3R tau ratio 78
Figure 3.3.5.1 Normal distribution of age and sex in ROSMAP cohort 79
Figure 3.3.5.2 Low SRPK1 expression in females is related to AD phenotype in ROSMAP dataset 81
Figure 3.3.5.3 SRPK1 expression in males is not significantly related to AD phenotype in ROSMAP dataset 82
Figure 3.3.5.4 Low SRPK2 expression in females is related to AD phenotype in ROSMAP dataset 84
Figure 3.3.5.5 SRPK2 expression in males is not significantly related to AD phenotype in ROSMAP dataset 85
Figure 3.3.5.6 Low Dyrk1A expression in females is related to clinical diagnosis of AD 87
Figure 3.3.5.7 Dyrk1A expression in males is not significantly related to AD phenotype in ROSMAP dataset 88
Figure 3.3.5.8 CLK1 expression in females is not significantly related to AD phenotype in ROSMAP dataset 90
Figure 3.3.5.9 Low CLK1 expression in males is related to clinical diagnosis of AD 91
Figure 3.3.5.10 Low CLK2 is related to AD pathology in females but not significantly implicated in clinical outcome 93
Figure 3.3.5.11 CLK2 expression in males is not significantly related to AD phenotype in ROSMAP dataset 94
Figure 3.4.5.1 Schematic diagram of potential SRPK mediated regulatory mechanisms in neurodegeneration 105
Figure 3.4.5.2 Amino-acid sequence for N-terminus of SRPK2 106
Figure 3.4.7 Alternatively spliced isoforms of CLK1 protein 110
Figure 4.3.1.1 NGF increases metabolic activity of SHSY5Y cells and N2a cells co-treated with hydrogen peroxide 118
Figure 4.3.1.2 VEGF-A_{165}a increases metabolic activity of SHSY5Y cells and N2a cells co-treated with hydrogen peroxide 119
Figure 4.3.1.3 VEGF-A_{165}b increases metabolic activity of SHSY5Y cells and N2a cells co-treated with hydrogen peroxide 120
Figure 4.3.2.1 β-amyloid (Aβ) caused modest decrease in metabolic activity of SHSY5Y cells and N2a cells 122
Figure 4.3.2.2 VEGF-A_{165}a or VEGF-A_{165}b treatment recovers Aβ-induced decrease in metabolic activity in SHSY5Y cells 122
Figure 4.3.2.3 Aβ treatment did not replicate decreased in metabolic activity in N2a cells 123

Figure 4.3.3.1 Reduced neurite outgrowth with increased concentration of OA 124
Figure 4.3.3.2 VEGF-A_{165}a increased neurite outgrowth in SHSY5Y cells co-treated with OA 126
Figure 4.3.3.3 VEGF-A_{165}b recovered OA-induced decrease in neurite outgrowth 127
Figure 4.3.4.1 VEGF-A_{165}b bands are not detectable by conventional RT-PCR in SPHINX31 treated SHSY5Y samples 128
Figure 4.3.4.2 Standard curves for VEGF-A_{165}a and VEGF-A_{165}b ELISA show detection window for protein expression 129
Figure 4.3.4.3 SPHINX31 treatment significantly reduces VEGF-A_{165}a:VEGF-A_{165}b ratio expression in SHSY5Y cells 131
Figure 4.3.5.1 SPHINX31 significantly ameliorates OA-induced decline in neurite outgrowth from SHSY5Y cells 132
Figure 4.3.5.2 OA and SPHINX31 treatments do not significantly alter the 4R:3R tau ratio in SHSY5Y cells 133
Figure 4.3.5.3 VEGF-A_{165}b neutralisation with 56/1 antibody significantly reduces the neuroprotective effect of SPHINX31 treatment 135
Figure 4.4.4 Schematic summarising proposed action of VEGF-A_{165}a and VEGF-A_{165}b 139
Figure 5.1 The sequence of the stem-loop located immediately after exon 10 of MAPT gene 143
Figure 5.2.1: Chemical structures for GRIFFIN compounds 147
Figure 5.3.1 Expression of 4R and 3R tau isoforms in SHSY5Y and Neuro2a cells 149
Figure 5.3.1.1 Transient knockdown of SRSF1 and SRSF2 in Neuro2a cells 150
Figure 5.3.1.2 SRSF2 knockdown with targeted siRNA treatment of Neuro2a cells increases MAPT exon 10 skipping and decreases 4R:3R tau ratio 151
Figure 5.3.1.3 SRSF1 knockdown with targeted siRNA treatment of Neuro2a cells increases MAPT exon 10 skipping and decreases 4R:3R tau ratio 153
Figure 5.3.2.1 SPHINX31 treatment of SHSY5Y cells for 24h does not significantly alter 4R:3R tau ratio in concentration range 10-3000nM 154
Figure 5.3.2.2 SRPN56 treatment significantly increases 4R:3R tau ratio in SHSY5Y cells156
Figure 5.3.2.3 SPHINX31 and SRPN56 treatment of Neuro2a cells does not significantly increase 4R:3R tau ratio 157
Figure 5.3.3.1 GRIFFIN6 treatment significantly increases 4R:3R tau ratio in SHSY5Y cells 159
Figure 5.3.3.2 GRIFFIN8 treatment significantly increases 4R:3R tau ratio in SHSY5Y cells 161
Figure 5.3.3.3 GRIFFIN33 treatment significantly increases 4R:3R tau ratio in SHSY5Y cells 162
Figure 5.3.3.4 Summary of the effect size and EC50 of GRIFFINs 6, 8 and 33 increasing 4R:3R tau ratio in SHSY5Y cells 163

Figure 5.3.3.5 GRIFFIN42 treatment does not significantly change 4R:3R tau ratio in SHSY5Y cells 165
Figure 5.3.3.6 CLK1 knockdown (65%) is insufficient to change MAPT exon 10 splicing in SHSY5Y cells 166
Figure 5.3.3.7 1μM GRIFFIN53 treatment significantly increases 4R:3R tau ratio in SHSY5Y cells 167
Figure 5.3.4.1 GRIFFIN6 and SPHINX31 treatment of SHSY5Y cells induces a significant decrease in SRSF1 phosphorylation 168
Figure 5.3.4.2 GRIFFIN6 treatment of SHSY5Y cells induces a significant decrease in pSR at 55kDa 169
Figure 5.3.5.1 Griffin6 treatment protects against OA-induced decline in neurite outgrowth 171
Figure 5.3.5.2 Griffin6 treatment of SHSY5Y cells increases 4R:3R tau ratio in both absence and presence of OA 172
Figure 5.3.5.3 VEGF-A_{165}b bands are not detectable by conventional RT-PCR in GRIFFIN6 treated SHSY5Y samples 173
Figure 5.3.5.4 Griffin6 treatment does not significantly change VEGF-A_{165}a:VEGF-A_{165}b ratio in SHSY5Y cells 175
Figure 5.3.5.5 Griffin6 amelioration of OA-induced decline in neurite outgrowth is not dependent on VEGF-A_{165}b expression 176
Figure 5.4.7 Summary schematic for the role of regulatory splicing kinases in the inclusion of *MAPT* exon 10 185
Figure 7.3.1 Enrichment plots for biological processes that are significantly enriched in gene list of differential expression between the cerebellum and frontal cortex 199
Figure 7.3.2 Enrichment plots for biological processes that are significantly enriched in gene list of differential expression between the control and clinical AD 207
Figure 7.3.3 Enrichment plots for biological processes that are significantly enriched in gene list of differential expression between control and pathological AD 210
Figure 7.3.4 Enrichment plots for biological processes that are significantly enriched in gene list of differential expression between the NCI and SCI 213

Table of Contents

Abstract ... **2**
Acknowledgments ... **3**
Author's declaration ... **4**
Conferences ... **5**
List of abbreviations ... **6**
List of Tables ... **9**
List of Figures ... **11**
Table of Contents ... **15**
Chapter 1. Introduction ... **1**
1.1 Alzheimer's Disease (AD) ... 1
1.2 The management and treatment of AD ... 4
1.3 Amyloid in AD ... 5
1.4 Apolipoprotein E (ApoE) and genetic risk for AD ... 10
1.5 Neurofibrillary tangles (NFTs) ... 12
1.6 Vascular dysfunction ... 16
1.7 Vascular Endothelial Growth Factor A (VEGF-A) ... 17
1.8 VEGFR2 activation ... 19
1.9 Alternative splicing (AS) ... 21
1.10 Regulation of SR Splicing Factor 1 (SRSF1) function ... 23
1.11 AS of VEGF-A ... 25
1.12 Use of kinase inhibitors ... 25
1.13 Use of *in vitro* models for AD ... 27
1.14 Hypotheses and Aims ... 28
Chapter 2. Methods ... **30**
2.1 Cell culture ... 30
2.1.1 Cell splitting ... 30
2.1.2 Cell counting ... 30
2.1.3 Cell plating ... 31
2.1.4 Cell differentiation ... 31
2.1.5 Cell transfection with siRNA ... 31
2.2 Cell viability assay ... 32
2.3 Immunofluorescence ... 32
2.4 Reverse transcription PCR (RT-PCR) ... 33
2.4.1 RNA extraction ... 33
2.4.2 cDNA generation ... 34
2.4.3 Polymerase Chain Reaction (PCR) ... 34
2.5 Protein-based assays ... 34
2.5.1 Cell lysis ... 34
2.5.2 Protein quantification ... 35
2.5.3 Western blot ... 35
2.5.4 ELISA ... 36

2.6 Tau minigene 38
2.6.1 DNA extraction 39
2.6.2 Bacterial transformation 39
2.6.3 Plasmid preparation 39
2.6.3 Plasmid transfection 40
2.7 Brains for Dementia Research (BDR) 40
2.7.1 RNA extraction 40
2.7.2 Library preparation 41
2.7.3 RNA-seq analysis 41
2.7.4 Splicing analysis 41
2.8 Religious Orders Study and Memory and Aging Project (ROSMAP) 41
2.8.1 Data acquisition 42
2.8.2 Library preparation 42
2.8.3 RNA-seq analysis 42
2.8.4 Relation of transcript abundance to clinical and pathological outcomes 43
2.9 Statistical analyses 43
2.9.1 Differential gene expression 43
2.9.2 Covariance 43
2.9.3 Variance 44
Chapter 3. Bioinformatic analyses of alternative splicing in Alzheimer's disease 45
3.1 Introduction 45
3.1.1 The role of different brain regions in AD 45
3.1.2 Alternative splicing in AD 46
3.1.3 The regulatory role of splicing kinases 47
3.1.4 Hypotheses 48
3.2 Methods 49
3.2.1 BDR dataset 49
3.2.2 ROSMAP dataset 49
3.2.3 Clinical and pathological outcomes 49
3.2.4 Statistical Analysis 50
3.3 Results 51
3.3.1 Differential gene expression in brain regions 51
3.3.2 Differential AS events in brain regions 53
3.3.3 Differential gene expression in AD brain 65
3.3.4 Characterisation of splicing transcripts and splicing kinases in AD brain 75
3.3.5 The relationship between splicing kinase expression and the occurrence of AD 79
3.4 Discussion 95
3.4.1 Differential expression in the frontal cortex and cerebellum 95
3.4.2 Differential splicing of AD-related genes in frontal cortex and cerebellum 96
3.4.3 Differential expression in AD 98
3.4.4 Differential splicing transcripts in AD brain and splicing kinase expression in relation to 4R:3R tau ratio 101
3.4.5 Relation between low SRPK expression and AD pathology 103
3.4.6 Relation between Dryk1A expression and AD 107
3.4.7 Relation between low CLK expression and AD pathology 109

3.4.8 Targeting splicing kinases as a therapeutic strategy for AD ... 111
3.4.9 Concluding remarks ... 111
Chapter 4: The effect of VEGF-A on AD-related neurotoxicity ... 113
4.1 Introduction ... 113
4.1.1 Amyloid and VEGF-A ... 113
4.1.2 Neurofibrillary tangles and VEGF-A ... 114
4.1.3 AD-related neurotoxicity *in vitro* ... 114
4.1.4 Hypotheses ... 115
4.2 Methods ... 117
4.3 Results ... 118
4.3.1 VEGF-A isoforms are neuroprotective against oxidative stress ... 118
4.3.2 VEGF-A isoforms are neuroprotective against Aβ-induced neurotoxicity ... 121
4.3.3 VEGF-A isoforms are protective in neuronal outgrowth assay ... 123
4.3.4 SRPK1 inhibition can shift splicing of VEGF-A in SHSY5Y cells ... 128
4.3.5 SRPK1 inhibition is protective of neuronal outgrowth through a VEGF-A_{165}b mediated mechanism ... 131
4.4 Discussion ... 136
4.4.1 VEGF-A_{165} isoforms increase viability of SHSY5Y cells in oxidative stress *in vitro* model 136
4.4.2 VEGF-A_{165} isoforms increase viability of SHSY5Y cells in amyloid *in vitro* model ... 137
4.4.3 VEGF-A_{165}a increases neurite outgrowth of SHSY5Y cells ... 138
4.4.4 VEGF-A_{165}b recovers the decrease in neurite outgrowth of SHSY5Y cells ... 139
4.4.5 SRPK1 inhibitor SPHINX31 significantly decreases VEGF-A_{165}a:VEGF-A_{165}b ratio in SHSY5Y cells ... 140
4.4.6 SRPK1 inhibition recovers OA-induced decrease in neurite outgrowth and recovery is dependent on endogenous VEGF-A_{165}b ... 140
4.4.7 Concluding remarks ... 142
Chapter 5: The regulation of *MAPT* splicing ... 143
5.1 Introduction ... 143
5.1.1 Role of regulatory splicing kinases ... 144
5.1.2 Splicing models ... 145
5.1.3 Hypotheses ... 146
5.2 Methods ... 147
5.2.1 GRIFFIN compounds ... 147
5.2.2 The *MAPT* RT-PCR ... 148
5.3 Results ... 149
5.3.1 Knockdown of SRSF1 and SRSF2 promotes *MAPT* exon 10 skipping ... 149
5.3.2 Selective inhibition of SRPK1 does not conclusively increase *MAPT* exon 10 inclusion ... 153
5.3.3 GRIFFIN treatment of SHSY5Y cells increases *MAPT* exon 10 inclusion ... 157
5.3.4 Griffin6 treatment of SHSY5Y cells reduces SR protein phosphorylation ... 168
5.3.5 Griffin6 treatment of SHSY5Y cells ameliorates OA-induced decrease in neurite outgrowth ... 170
5.4 Discussion ... 177
5.4.1 Knockdown of SRSF1 and SRSF2 in Neuro2a cells confirmed to increase *MAPT* exon 10 skipping ... 177
5.4.2 Selective SRPK1 inhibition does not conclusively promote *MAPT* exon 10 inclusion ... 177
5.4.3 Selective CLK inhibitor promotes *MAPT* exon 10 inclusion and reduces SRSF1/6 phosphorylation ... 179

5.4.4 CLK2 is more important in *MAPT* exon 10 splicing than CLK1 181
5.4.5 SRPK2 inhibition may partially block increased *MAPT* exon 10 inclusion mediated by other kinases 182
5.4.6 Combined CLK and Dyrk1A inhibition has a synergistic effect on *MAPT* exon 10 inclusion 183
5.4.7 Other kinases also play a role in regulation of MAPT exon 10 inclusion 183
5.4.8 Griffin6 is neuroprotective against OA-induced neurotoxicity 185
5.4.9 The neuroprotective effect of Griffin6 is not dependent on VEGF-A_{165}b isoform expression 187
5.4.10 Concluding remarks 188
Chapter 6. Summary and future directions 189
6.1 Alternative splicing in AD 189
6.2 Targeting splicing kinases to modulate alternative splicing 190
6.3 Models to investigate AD pathology 192
6.4 Summary 193
Chapter 7. Appendix 194
7.1 PIPS Review 194
7.2 COVID Statement 196
7.3 Supplementary Tables and Figures 197
References 214

Chapter 1. Introduction

1.1 Alzheimer's Disease (AD)

Dementia is the chronic and progressive deterioration of memory and cognitive abilities, which may be accompanied by other behavioural symptoms, and impedes a person's ability to carry out daily activities (Pink *et al.*, 2018). There are 850,000 people estimated to be living with dementia in the UK today, and as our population ages its prevalence has been projected to increase to >2 million by the year 2050 (Prince *et al.*, 2014). Not only does dementia devastate lives, it has an enormous financial burden of £26 billion, amounting higher health and social care costs than cancer and chronic heart disease combined (Luengo-Fernandez *et al.*, 2015).

The clinical presentation of dementia usually entails three main components: (i) neuropsychological features, (ii) neuropsychiatric features, and (iii) deficits in activities of daily living (ADL) (Grand *et al.*, 2011). Neuropsychological features comprise the most recognisable element of dementia as they include memory impairments, aphasias (language difficulties), apraxias (inability to carry out coordinated movements), agnosias (inability to recognise elements of one's environment or self) and other difficulties with attention and executive function (Manning, 2004). The neuropsychiatric features, also referred to as Behavioural and Psychological Symptoms of Dementia (BPSD), are present in a substantial proportion of dementia patients and include anxiety, depression, paranoid ideation, delusions, and aggression (Mirakhur *et al.*, 2004). The third component, deficits in ADL, may first manifest as self-neglect of diet, personal hygiene, and household tasks, but can progress in the later stages of dementia to affect basic activities, e.g., problems with independently bathing and dressing oneself, at which point full-time care becomes necessary (Geldmacher, 2004; Grand *et al.*, 2011).

Alzheimer's disease (AD), the most common cause for dementia, is a neurodegenerative disease that is pathologically characterised and distinguished by amyloid plaques and neurofibrillary tangles (Gorelick *et al.*, 2016). In its typical form, AD first presents with an insidious decline of episodic memory (Lane *et al.*, 2018). As the disease progresses, memory problems are usually accompanied by confusion, aphasias, visuospatial problems, and emotional withdrawal (Geldmacher, 2004; Kester & Scheltens, 2009). AD was first described by Alois Alzheimer in 1905, based on his 51-year-old female patient who had been admitted with dementia; Alzheimer performed a histopathology study of her brain and linked her psychiatric

symptoms to her brain lesions (Alzheimer *et al.*, 1995). Diagnosis of AD, however, still depends on clinical assessment of cognitive impairment; this is usually done in accordance to national guidance which includes ruling out reversible causes (e.g., delirium, depression, sensory impairment) and specifies criteria related to AD, including (1) insidious onset, (2) progressive course of cognitive impairment, and (3) non-amnestic presentations typical to AD, e.g., language or executive dysfunction (McKhann *et al.*, 2011; National Institute for Health and Care, 2018). Both neuropsychological and cognitive examinations can help differentiate between AD and other causes of dementia, as summarised in Table 1.1 below.

	Alzheimer's disease	**Frontotemporal lobar degeneration**	**Vascular Dementia**	**Dementia with Lewy bodies**
Patient history	Short-term memory impairment, aphasia, apraxia, executive dysfunction	Compulsive and stereotyped behaviour, apathy, isolated language problems	Abrupt or fluctuant cognitive deterioration, vascular risk factors	Fluctuant cognitive disturbances, visual hallucinations, falls, sleep disorders
Cognitive neurological examination	Episodic memory impairment, executive dysfunction	Disinhibition, stereotypy, inertia, speech disorders	Apathy, slowness of thinking	Hallucinations and delusions

Table 1.1 Summary of core clinical features observed in different dementia types (Geldmacher, 2004)

The appearance of clinical symptoms often occurs much later (>10 years) than the development of AD pathology. This long pre-clinical phase of AD (during the pathophysiological process) is critical for therapeutic intervention. However, effective intervention requires accurate risk assessment for progression to Mild Cognitive Impairment (MCI) and further to AD dementia (Sperling *et al.*, 2011). Herein lies the difficulty, as individuals with AD pathology have increased risk for cognitive impairment, but some will never manifest clinical symptoms in their lifetime. To overcome this challenge, it is necessary to better characterise the pre-clinical phase of AD and identify biomarkers for the emergence of clinical symptoms.

The "continuum of AD" has been proposed to take individuals from completely asymptomatic to a clinical diagnosis of AD dementia. This model is based on the longitudinal study of AD patients, providing a timeline for neuropathology and cognitive decline relative to diagnosis and eventual death (Bennett *et al.*, 2012). Based on this model, individuals who exhibit AD pathology (positive for biomarkers in Figure 1.1) whilst having very subtle cognitive symptoms would be most likely

beneficiaries of early intervention. These individuals would not yet meet the requirements of MCI or AD and would be considered “asymptomatic but at risk for AD dementia” (Jack *et al.*, 2010; Sperling *et al.*, 2011). The continuum of AD has been reliably differentiated from normal ageing, wherein very little cognitive decline is evident in people who do not develop AD (Wilson *et al.*, 2011). On the other hand, AD diagnosis is preceded by five to six years of accelerated (15-fold) decline in cognitive abilities, with semantic memory and working memory showing the earliest decline. Visuospatial abilities similarly show a sharp decline about three years before clinical diagnosis (Johnson *et al.*, 2009), often preceding decline of other cognitive abilities. Johnson et al. commented that research into early detection of AD may not be sensitive to earliest manifestations of the condition if they exclusively test episodic memory and should include other aspects of cognition. In end-stage dementia, AD patients exhibit a “terminal decline”, which occurs in the last four years of life, and the rate of cognitive decline accelerates more than six-fold (Bennett *et al.*, 2012).

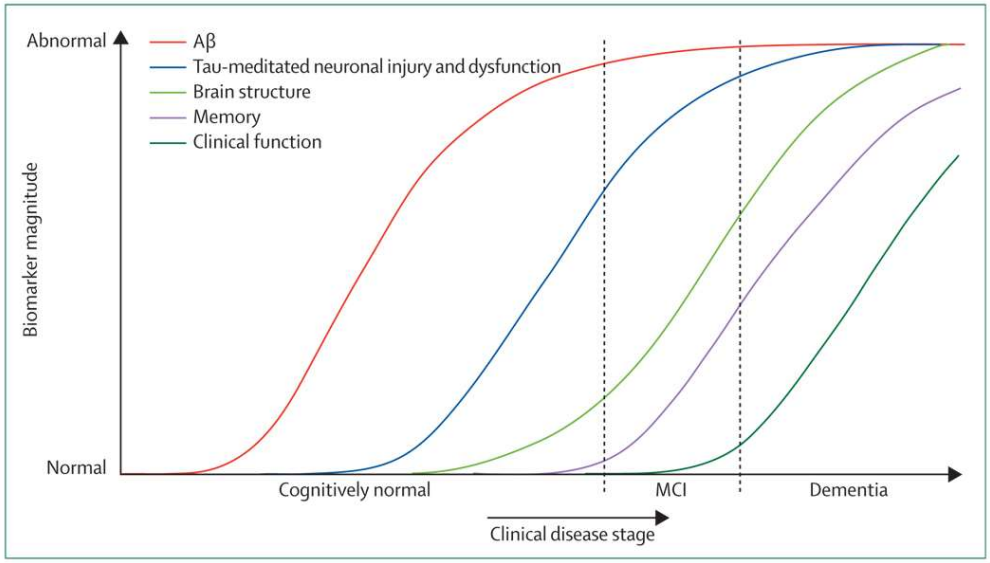


Figure 1.1 Biomarkers for AD with progression of clinical stage. Cognitively normal is equivalent to the pre-clinical stage, during which Aβ and tau pathologies have the largest impact. This model for pathological cascade was presented by (Jack *et al.*, 2010): The impact of Aβ and tau-mediated neuronal injury was quantified by CSF concentration or PET imaging. The impact of brain structure was measured by structural MRI.

1.2 The management and treatment of AD

There are currently no disease-modifying treatments available for AD. However, there are some symptomatic treatments options for disease management, which can be adapted to the individual patient and the course of progression. Acetyl-cholinesterase inhibitors (AChEIs, e.g., donepezil, galantamine and rivastigmine) are often used in cases of mild to moderate AD. Although they have shown consistent benefit to patients, their efficacy is considered modest at best (Di Santo *et al.*, 2013) and on average, AChEIs only arrest symptoms for less than six months (Ashford, 2015). The use of this therapeutic approach was developed in response to the "cholinergic hypothesis" of AD, which describes decreased AChE in AD patients, leading to neuronal loss and eventually the development of cognitive decline (Hampel *et al.*, 2018). Treatment with AChEIs has been shown to protect against atrophy, particularly in the hippocampus (Dubois *et al.*, 2015), and most crucially for the patient, improve both cognitive and behavioural outcomes (Tan *et al.*, 2014). By blocking the breakdown of neurotransmitter acetylcholine, these drugs increase its availability in the synapse of surviving cholinergic neurones, which are particularly vulnerable to AD pathology. However, AD progression is indiscriminate and damages a much greater population of cell types, including noradrenergic, serotonergic and glutamatergic neurones, so it is perhaps unsurprising that many patients that do not respond well to AChEIs, particularly if they have more advanced dementia (Di Santo *et al.*, 2013).

The only other drug available for AD is Memantine, which is licensed for moderate to severe AD. Memantine is a low-affinity, uncompetitive NMDA receptor antagonist which aims to reduce the glutamate-induced neurotoxicity that occurs in the AD brain (Matsunaga *et al.*, 2018). The fact memantine has low affinity and rapid off-rate kinetics is key to its therapeutic action, as this preserves the physiological function of NMDAR channels and gives the drug a low adverse event profile (Rogawski & Wenk, 2003). It has been shown to have slight but appreciable benefit on cognition in cases of moderate-severe AD but there is no evidence for benefit in cases of mild cognitive impairment (McShane *et al.*, 2019). Interestingly, memantine is reported to reduce amyloid levels, which make up neuritic plaques, through regulation of the endocytosis pathway and intracellular trafficking of its precursor protein, APP (Ito *et al.*, 2017). Treatment with memantine may have additive effects in patients who already received stable does of AChEI donepezil (Tariot *et al.*, 2004); a combinatory treatment plan is usually well-tolerated and the two treatments can work synergistically to improve standard of care (Olivares *et al.*, 2012).

1.3 Amyloid in AD

Etiologically, there are two main forms of AD: sporadic and familial. Sporadic AD, also known as the late-onset form, involves complex interplay between multiple genetic and environmental factors. As of yet, the ε4 allele for transport protein apolipoprotein E (APOEε4) is best known genetic polymorphism associated with AD pathology and cognitive decline (Del Bo *et al.*, 2009; Rodrigue *et al.*, 2013). Apolipoprotein E is discussed further in section 1.3. Familial AD, also known as the early-onset form, is considerably less common and accounts for only 5% cases of AD (Mendez, 2019). Individuals with familial AD will experience clinical symptoms before the age of 65, caused by mutations of amyloid precursor protein (APP) and/or presenilins, which form crucial catalytic components of enzymes required to cleave APP into amyloid (Zhang *et al.*, 2011). Since neuritic plaques in AD are primarily made up of amyloid protein (Glenner & Wong, 1984), there have been many studies on amyloid as well as its precursor protein, most notably research carried out by Hardy and Higgins which first introduced the amyloid-cascade hypothesis (Hardy & Higgins, 1992). Although there have been numerous revisions to this theory over the last 30 years, it remains crucial to our understanding of AD pathology and is widely-accepted in the scientific community (Hardy, 2017).

The amyloid-cascade hypothesis is based upon malfunction of proteolytic processing of amyloid precursor protein (APP). The physiological function of APP is not well understood, but it is known to regulate metabolic activity, both in its full-length form and through its cleaved peptides (Guo *et al.*, 2021). Abnormal accumulation of APP in the mitochondrial compartment is thought to disrupt transport across the mitochondrial membrane and lead to metabolic dysfunction in the AD brain (Anandatheerthavarada *et al.*, 2003). In fact, decreased energy metabolism is one of the earliest detectable hallmarks of AD (Devi *et al.*, 2006). APP is normally cleaved by a series of proteases named α, β and γ secretases; since these are functionally mutated in familial AD, they have been linked to its pathophysiology through over-production and accumulation of β-amyloid (Aβ) (Rodrigue *et al.*, 2013). As shown in Figure 1.2.1, non-amyloidogenic processing of APP involves α-secretase cleavage within the Aβ domain, preventing the formation of Aβ peptides; instead, soluble APPα is produced and the remaining C-terminal fragment α is subsequently cleaved by γ secretases into peptide P3. The amyloidogenic pathway involves β secretase cleaving APP to produce soluble APPβ and C-terminal fragment β, which is further cleaved by γ secretases into Aβ, most commonly in its Aβ40 form (where 40 denotes number of amino acids) but

sometimes in its Aβ42 form or other longer peptides (Selkoe, 2001; Bernabeu-Zornoza & Zambrano, 2019). Crucially, longer Aβ peptides are more hydrophobic and highly self-aggregating, thus they are more likely to oligomerise and form amyloid fibrils, which in turn assemble into neuritic plaques (Selkoe & Hardy, 2016). In this way, Aβ40 can actually be considered anti-amyloidogenic as it inhibits Aβ42 deposition (Kim *et al.*, 2007b).

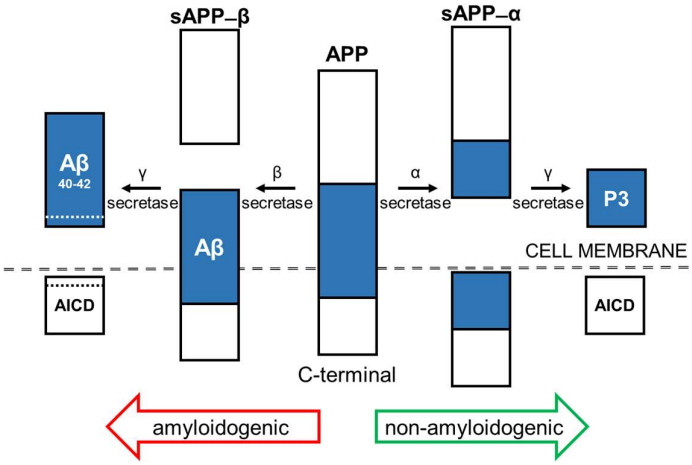


Figure 1.3.1 Schematic diagram for the production of Aβ through post-translational processing of APP, adapted from (Chen & Mobley, 2019). In the non-amyloidogenic pathway, the sequential cleavage of APP by α- and γ-secretases produces P3 and APP intracellular domain (AICD). In the amyloidogenic pathway, sequential cleavage by β- and γ-secretases produces Aβ (aa length 40-42) and AICD.

To understand why there is a proportional increase in Aβ42 peptides in AD, it is necessary to study the function of presenilins, as they comprise the active site of the intramembrane γ secretase enzyme and thus mediate APP proteolysis (De Strooper *et al.*, 1998). The enzyme complex acts as a carboxypeptidase to progressively cleave 3 or 4 C-terminal amino acids along two product lines, with Aβ40 being produced from Aβ49, and Aβ42 being produced from Aβ48 (see Figure 1.2.2), leaving behind APP intracellular domain with amino acid residues 50-99 and 49-99, respectively (Fernandez *et al.*, 2014). Presenilin mutation has been long established to cause AD (Scheuner *et al.*, 1996) and some literature goes insofar as to propose that the AD phenotype is fundamentally due to a loss of presenilin function, focusing on mutations that typically reduce Aβ40 and enhance Aβ42 production (Shen & Kelleher, 2007). However, strong counterarguments include that a) Aβ42 accumulation precedes AD symptoms by a long time, and b) >99% of AD patients express wildtype presenilin, which makes this theory much less convincing as the sole mechanism for AD pathogenesis.

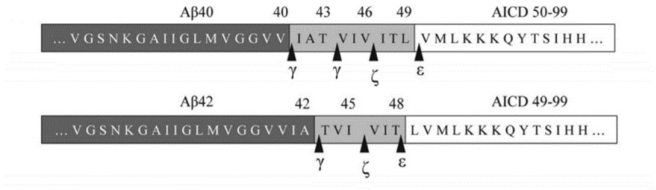


Figure 1.3.2 Proposed secretase cleavage sites on APP amino acid sequence to produce Aβ40 and longer peptide Aβ42 with corresponding AICDs (APP intracellular domains). Secretase subtype labelled on arrowhead, as presented by (Fernandez *et al.*, 2014).

Regardless of how they are produced, the oligomerisation of Aβ peptides are known to exert neurotoxic effects (through the amyloid cascade hypothesis), leading to neuronal loss (Sakono & Zako, 2010). This occurs either by direct injury to neurons, or by microglial (and astrocytic) activation which in turn alters ionic homeostasis. Ultimately, both can lead to altered kinase/phosphatase activities, aggregation of neurofibrillary tangles, microtubular dysfunction, and axonal loss. This develops into widespread neuronal dysfunction which underlies the clinical symptoms of AD (Selkoe & Hardy, 2016). Neuritic plaques in AD exist in a range of compositions, some being dense with fibrillar amyloid and others being loose, more diffuse amyloid deposits (Selkoe, 2004). The fibrillar form of Aβ is most infamous for accumulating into plaques, and fibrillar aggregates are known to be neurotoxic both *in vivo* and *in vitro*. At first glance, this makes them the most obvious cause for neurodegeneration (Hardy & Higgins, 1992). However, the number of neuritic plaques in the AD brain does not reliably correlate with the extent of neuronal loss, not is it an accurate indicator of cognitive impairment (Sakono & Zako, 2010). Indeed, there is evidence to suggest that fibrillar Aβ is less toxic than soluble Aβ oligomers (Stine *et al.*, 2011), and the latter have demonstrated closer relation with both the degree of neuronal loss and dementia (Caughey & Lansbury, 2003; Haass & Selkoe, 2007). Soluble Aβ oligomers have also been reported to inhibit long-term potentiation, a model for synaptic plasticity and memory consolidation (Walsh *et al.*, 2002), supporting the idea that soluble Aβ is the main driver for cognitive decline. Mechanistically, it has been suggested that Aβ oligomers are formed in the extracellular space and bind to a number of neuronal receptors, triggering toxicity pathways. For example, binding at NMDA receptors disrupts calcium homeostasis, leading to oxidative stress and eventually synaptic loss (Shankar *et al.*, 2007). Additionally, Aβ is known to cause a substantial loss of surface insulin receptors, interrupting receptor signalling and ultimately causing insulin resistance often associated with AD (Zhao *et al.*, 2008). In a murine model of AD, reduced insulin receptor levels have also been associated

with decreased LRP-1, a receptor protein related to lipid metabolism, suggesting that Aβ may accelerate their mutual degradation in endothelial cells and cause downstream cerebrovascular impairment (Gali *et al.*, 2019).

Despite amyloid being the key pathological marker of AD, there is contentious debate over its role as a driver of the disease. One reason is that many people have abundant Aβ deposits without dementia, but often these are more diffuse plaques. In fact, oligomer levels per plaque are much lower in AD brains, which suggests that plaques in non-demented people act to sequester Aβ oligomers (Esparza *et al.*, 2013). Another reason is that several phase three clinical trials of Aβ-targeting agents have not been successful in meeting clinical endpoints (Selkoe & Hardy, 2016). One such trial was for Semagacestat, a γ secretase inhibitor. However, this failure has been rationalised by a poor choice of dose that had not demonstrated any significant impact on levels of Aβ in the CSF during phase II trials (Doody *et al.*, 2013), limited by side-effects on Notch signalling (as a target for presenilins) (Henley *et al.*, 2014). The Semagacestat trial has also been criticised for selection of a drug that had poor brain penetration and selection of a treatment regimen that induced short peaks of γ secretase inhibition alternated with periods of normal activity (De Strooper, 2014). Based to these stipulations, it has been argued that the Semagacestat trial did not truly test the amyloid cascade hypothesis, since it did not reliably lower brain Aβ levels (Lanz *et al.*, 2006) nor the Aβ42:Aβ40 ratio (Doody *et al.*, 2013).

Another key strategy targeting Aβ is immunotherapy. There have been several attempts to adopt this method for treatment of AD, including clinical trials for the monoclonal antibody solanezumab, which was investigated by Eli Lilly as an anti-Aβ treatment in cases of mild dementia (Honig *et al.*, 2018). The use of anti-Aβ antibodies looked promising during the pre-clinical phase as it was found to prevent the formation of fibrillar Aβ aggregates and significantly reduce the deposition of Aβ plaques, as well as associated neuritic dystrophy and cognitive decline (Schenk *et al.*, 1999; Morgan *et al.*, 2000). This was hypothesised to occur by a number of mechanisms, including (1) plaque phagocytosis by microglia, (2) blocking oligomer formation and neutralisation of Aβ oligomers and attenuation of fibrilisation, as well as (3) efflux of Aβ monomers from the CNS (Mantile & Prisco, 2020). The latter was referred to as the peripheral sink hypothesis, and crucially provided the underlying rationale for development of solanezumab. Since the BBB severely restricts entry of antibodies into the brain, the CSF antibody concentration would be very low, in fact only 0.1-0.2% of blood plasma concentration (Poduslo *et al.*, 1994). Nonetheless, it

was proposed that Aβ levels in the brain and periphery were in equilibrium, so degrading Aβ in the blood would lead to an efflux from the brain, and therefore still reduce brain Aβ burden (DeMattos *et al.*, 2001). Unfortunately, this was proven not to be the case, as solanezumab failed to affect levels of Aβ in the brain (Honig *et al.*, 2018). Interestingly, immunised patients showed a measured increase in peripheral Aβ, but this was accounted for by the fact the Aβ-antibody complex has a longer half-life than free Aβ, rather than efflux from the CNS.

Vaccine AN179 was another anti- Aβ active immunisation attempt which successfully elicited an antibody response to Aβ42 (Bayer *et al.*, 2005). However, clinical trials for AN1792 had to be terminated when 6% of immunised patients (18/300) developed meningoencephalitis (Schenk, 2002). Long term follow-up of the participants revealed mixed results with regards to disease progression, but unlike solanezumab, Vaccine AN179 did demonstrate reliable reduction of Aβ burden in the brain (Mantile & Prisco, 2020). The phase I trial reported that the degree of plaque removal varied significantly with mean antibody response but was unable to present evidence for decelerated progression to severe dementia and/or greater patient survival (Holmes *et al.*, 2008). This was supported by the 15-year post-mortem study which determined that 88% of immunised patients had reduced Aβ plaques, among whom two patients had only very sparse or no detectable plaques at all, but most of these patients still progressed to severe dementia despite modification of AD pathology (Nicoll *et al.*, 2019). On the other hand, a larger study conducted on the phase IIa trial identified “antibody responders” who retained low but persistent antibody titres 4.6 years after immunisation; this subgroup did report better clinical outcomes than the placebo group, as they scored higher in memory tests and were significantly less dependent on care-givers (Bruno *et al.*, 2009). Based on these (albeit modest) successes, and despite cases of meningoencephalitis, the AN1792 clinical trials have encouraged further research into anti-Aβ immunotherapy and further anti-Aβ vaccines are currently undergoing phase II trials (Mantile & Prisco, 2020).

Although it is clear that progression of AD dementia is not necessarily prevented by clearance of Aβ plaques, it can be maintained that amyloid is still a major target for AD research. Perhaps the most reasonable argument is that amyloid cleavage and deposition is a consequence of another common factor or related to multiple factors equally critical for development of AD (Grammas, 2011) but will continue to play a key role in the characterisation of AD dementia.

1.4 Apolipoprotein E (ApoE) and genetic risk for AD

Closely tied to AD pathology is apoE, which can be found co-localised with amyloid in senile plaques in the AD brain (Namba *et al.*, 1991). The ε4 allele of apoE is the strongest genetic risk factor for AD (Corder *et al.*, 1993) and has been pathologically linked to high abundancy of senile plaques (Schmechel *et al.*, 1993). As such, *APOEε4* has been widely studied for its role in the brain and how that may be associated with AD pathology. It is one of three polymorphic alleles for the *APOE* gene; ε2, ε3 and ε4, which present in the Caucasian population at an average frequency of 8.4%, 77.9% and 13.7% respectively (and varies between ethnicities). However, the ε4 allele makes up a more significant proportion of Caucasian AD patients, shifting the ε2, ε3 and ε4 allele frequencies to 3.9%, 59.4% and 36.7% respectively (Farrer *et al.*, 1997). Physiologically, the apoE protein mediates lipid transport from one cell to another, hence it is integral for the regulation of lipid homeostasis. In the brain, apoE is mainly produced by astrocytes and lipidated through ATP-binding cassette transporter ABCA1, which acts in neurones and other cell types to transfer both phospholipids and cholesterol to apoE, and in this manner apoE regulates their distribution (Mahley & Rall, 2000; Hirsch-Reinshagen *et al.*, 2004). In AD, apoE binds amyloid and alters its propensity to form neuritic plaques. Both *in vitro* and *in vivo* studies have found that expression of apoE significantly reduces and delays plaque deposition in an isoform specific manner, ε2>ε3>ε4, even while amyloid expression itself remains unchanged in the brain (Reiman *et al.*, 2009). As a result, it has been suggested that apoE works independently of amyloid production, but rather facilitates its clearance, with the ε4 allele being least effective in this process.

Supporting the theory that *APOEε4* has reduced function, this allele has been associated with hyperlipidaemia and hypercholesterolemia, which can lead to atherosclerosis, coronary heart disease and stroke (Lahoz *et al.*, 2001), all of which in turn increase vascular risk for developing AD. Based on these comorbidities, it has been suggested that cholesterol, as a target for apoE, plays a key role in AD pathology. Investigating crosstalk between apoE, cholesterol and amyloid revealed that cholesterol efflux in microglia is sufficient to promote amyloid degradation whereas apoE binding to amyloid is not necessary for apoE-mediated amyloid degradation (Lee *et al.*, 2012). Together, these findings indicate that apoE acts through its ability to enhance cholesterol efflux rather than direct interaction with amyloid. Since measured expression of proteolytic enzymes remained unchanged, it has been proposed that trafficking of amyloid to lysosomes is a crucial step that is

being controlled through apoE and cholesterol. While increased cholesterol effectively paralyses endosomal transport (Chen *et al.*, 2008), apoE-mediated decrease in cholesterol promotes recycling of Rab7, a known regulator of endocytic trafficking, which therefore accelerates transport of Aβ-containing vesicles toward lysosomes for degradation (Lee *et al.*, 2012).

Since apoE4 lipoproteins bind to amyloid with lower affinity (LaDu *et al.*, 1994), this has been offered as an explanation for their impaired ability to mediate amyloid clearance. However, if amyloid binding is unnecessary for apoE-mediated amyloid degradation (as previously postulated), this is not a very convincing argument. Alternatively, apoE4 has been shown *in vitro* as deficient in promoting cholesterol efflux from neurones and astrocytes compared to apoE2 and apoE3 isoforms (Michikawa *et al.*, 2000; Rapp *et al.*, 2006). Furthermore, it has been demonstrated that apoE4 lipoproteins are less efficient at promoting enzyme-mediated proteolysis of amyloid (Jiang *et al.*, 2008). Together, this evidence supports clinical data that demonstrates association between the ε4 allele and higher AD prevalence at a lower age of clinical onset; 91% of ε4 homozygotes develop AD at a mean age of 68 years whereas only 20% of ε4 noncarriers develop AD at a mean age of 84 years (Rebeck *et al.*, 1993). In terms of sporadic AD, apoE4 thus presents as a crucial mechanism for failure of amyloid clearance and gradual rising of Aβ42 levels in the brain (Selkoe & Hardy, 2016). Accordingly, *APOE* genotype has been reported to account for up to 15-fold greater risk for AD (Farrer *et al.*, 1997).

Genome-wide associated studies (GWAS) have discovered many other genomic loci associated with AD; these loci comprise common risk variants, e.g., *CLU*, *PICALM*, and *CR1*, which increase susceptibility for late-onset AD, although individually they tend to have a very small effect (Harold *et al.*, 2009; Lambert *et al.*, 2009). This fits into the polygenic model for the complexity of late-onset AD, where there are thousands of risk alleles, each of which contribute a small (statistically significant) increase in relative risk, in contrast to the rare alleles which have a stronger individual effect, often causing early-onset AD (Manolio *et al.*, 2009; Seshadri *et al.*, 2010). Other common risk variants include *ABCA7*, the *MS4A* cluster, *EPHA1*, *CD33* and *CD2AP*, all of which were found to have genome-wide significance in meta-analyses of GWAS data (Hollingworth *et al.*, 2011). Functionally, these AD susceptibility loci affect pathology through various pathways, e.g., lysosomal trafficking gene *CD2AP* has been related to cell membrane APP, Aβ release, and greater plaque burden (Liao *et al.*, 2015). ATP-binding cassette *ABCA7* and myeloid-associated *CD33* have been proposed to affect AD risk though the

impairment of microglia mediated Aβ clearance, lipid metabolism, and phagocytosis (Jiang *et al.*, 2014; Zhao *et al.*, 2015). Some rare variants, such as AD-associated missense mutation of *TREM2*, have also provided valuable insight into AD pathogenesis (Jonsson *et al.*, 2013); the anti-inflammatory role of TREM2 in the brain has consolidated hypotheses for disrupted inflammatory processes causing vulnerability and predisposition to AD pathology. With continuation of GWAS on ever-growing sample sizes, the discovery of more AD susceptibility loci will begin to account for the high heritability of AD (Gatz *et al.*, 2006), which currently known genetic variation cannot explain (Ertekin-Taner, 2007). Overall, it is clear that AD is a heterogeneous condition, and it is not possible to understand its aetiology or pathology by only considering amyloid or any other single factor; in light of this, other components and related hypotheses for AD will be discussed in this thesis, including functional involvement of tau and the vascular system.

1.5 Neurofibrillary tangles (NFTs)

The intracellular accumulation of NFTs is a hallmark of AD pathology and many other neurodegenerative disorders, collectively referred to as tauopathies (Iqbal *et al.*, 2010). This is because NFTs are formed by misfolding and abnormal aggregation of tau protein into insoluble paired helical filaments (Gao *et al.*, 2018a). Under normal physiological conditions, tau plays an important role in stabilising the microtubule network and facilitating axonal transport and cellular trafficking. However, in pathological conditions tau undergoes conformational changes, usually due to hyper-phosphorylation, which leads to aforementioned protein dysfunction and detachment from microtubules (Weingarten *et al.*, 1975; Avila *et al.*, 2004). Once tau is polymerised into NFTs, it becomes inert and no longer binds to tubulin nor supports microtubule assembly. The density of NFTs in the brain has a direct physiological correlation with dementia (Wang *et al.*, 2013) and forms the basis of Braak staging for AD (Braak & Braak, 1991). This is because NFTs have been found to exhibit a certain pattern of distribution with progression of disease, spreading outward from layer II of the entorhinal cortex to the hippocampus (via the perforant pathway) and limbic regions of the brain. Braak staging is a standardised method of characterising these neurofibrillary changes in AD brain, as described in Table 1.5. Braak stages can be related with clinical outcomes; stages two and three tend to occur in pre-clinical AD and relate to aggregation of paired helical filaments and synaptic dysfunction, whilst stages four to six are proposed to occur in AD dementia and relate to NFT pathology (Mukaetova-Ladinska *et al.*, 2000). Consequently, the regulation of tau function has become a critical target for AD research.

Braak Stage	Affected region	Description
I-II	Transentorhinal	Mildly affected brains, NFTs confined to hippocampal region, these stages do not present with any cognitive impairment
III-IV	+ Limbic system	Severe changes are restricted to allocortical regions and adjoining areas, there is no macroscopically detectable atrophy, these stages present with cognitive impairment and subtle personality changes
V-VI	+ Isocortex	End stages of AD show many NFTs in most of the cerebral cortex and particularly severe destruction of neocortical areas, these stages present with AD dementia

Table 1.5 Braak stages as a characterisation of neurofibrillary changes seen in the AD brain. Descriptions for each stage adapted from (Braak & Braak, 1991).

In relation to formation of paired helical filaments, a number of kinases have been found to regulate the phosphorylation of tau, most notably GSK-3β (Song & Yang, 1995). Originally discovered for its role in glycogen metabolism, GSK-3β was coincidentally discovered as a "tau protein kinase" (Ishiguro *et al.*, 1993) that accumulates in AD brain and is responsible for the formation of paired helical filaments (Ishiguro *et al.*, 1992). Independent of its glycogen function, it is now known that GSK-3β phosphorylates tau at crucial sites related to AD pathology, and consequently can be found colocalised with tau during NFT formation (Lovestone *et al.*, 1994). GSK-3β inhibition has been shown to decrease the phosphorylation of tau as well as upregulate expression of neurogenesis markers GAP43, N-myc, and MAP2, which in turn promote neurite outgrowth (Shi *et al.*, 2020). This suggests that regulation of GSK-3β or downstream mediators could play a neuroprotective role in AD. Further tauopathy-related phosphorylation sites are targeted by other key kinases, including mitogen activated protein kinases and cell division cycle protein 2 (Drewes *et al.*, 1992; Ledesma *et al.*, 1992), as well as protein kinase C (Boyce & Shea, 1997).

The toxicity of tau, however, remains controversial as it is not definitively known at which stage tau pathology is most significant to AD. It has been argued that 1) soluble species of hyperphosphorylated tau are toxic when they abnormally accumulate in the cell and 2) aggregated fibrillar tau in NFTs is toxic and causative of cell death (Spires-Jones *et al.*, 2009). Since there is evidence for the toxicity for both forms of tau, it is most likely that both contribute to AD on different time scales (Kopeikina *et al.*, 2012). This is in opposition to the theory that formation of NFTs can be neutral or even protective by acting as a sink for toxic soluble tau species

(Spires-Jones *et al.*, 2011). In the face of overwhelming evidence for close correlation of NFTs with location and number of cell death (Gómez-Isla *et al.*, 1996) as well as severity of cognitive decline (Giannakopoulos *et al.*, 2003), there is a general consensus that NFTs are indeed harmful. It is also pertinent to note that axonal loss, caused by tau-driven microtubular dysfunction, precedes neuronal loss. Moreover, NFTs have been reliably linked with the amyloid cascade hypothesis, and Aβ immunotherapy treatment that alleviates cognitive dysfunction has been associated with reduction of both Aβ42 and phospho-tau, consolidating that they both play a role in AD-related neurodegeneration (Xiao *et al.*, 2020). Nonetheless, tau pathology in some instances has been linked to cognitive deficit whilst independent of NFT burden, e.g., Santacruz et al developed a transgenic mouse model which induces pathogenic tau mutation (linked to heredity tauopathy) and results in cognitive decline. They reported that suppression of mutated tau could ameliorate cognition despite NFTs persistently accumulating in the brain (Santacruz *et al.*, 2005). Interestingly, the opposite can also be true, as tau mutation in *Drosophila* was found to induce neurodegeneration without formation of NFTs (Wittmann *et al.*, 2001). These findings suggest that NFTs are not solely responsible for tau-related pathology nor are they always necessary for neuronal loss.

The Microtubule-Associated Protein Tau (*MAPT*) gene is alternatively spliced into numerous mRNA transcripts and translated to six known proteins (see Figure 1.4): cassette splicing of exons 2 and 3 produce tau isoforms with 0, 1 or 2 amino-acid terminal repeats and inclusion or skipping of exon 10 produces isoforms with four (4R) or three (3R) microtubule-binding repeats towards the carboxyl terminal (Goedert *et al.*, 1989; Trabzuni *et al.*, 2012). The human adult brain usually has an equimolar ratio of 4R/3R tau isoforms and dysregulation of exon 10 splicing has been implicated in tau pathology (Espindola *et al.*, 2018). About a third of *MAPT* mutations affect exon 10 splicing, the majority of which favour inclusion and lead to an increase in 4R tau (Spillantini & Goedert, 2013). Interestingly, *MAPT* mutations that favour 3R tau have also been linked with tau pathology (Stanford *et al.*, 2003), suggesting that isoform imbalance is detrimental in either direction and that maintenance of an equimolar ratio between 4R/3R tau isoforms is crucial to normal function (Espindola *et al.*, 2018). In AD, the ratio is most commonly shifted toward an excess of 4R tau (Kopeikina *et al.*, 2012).

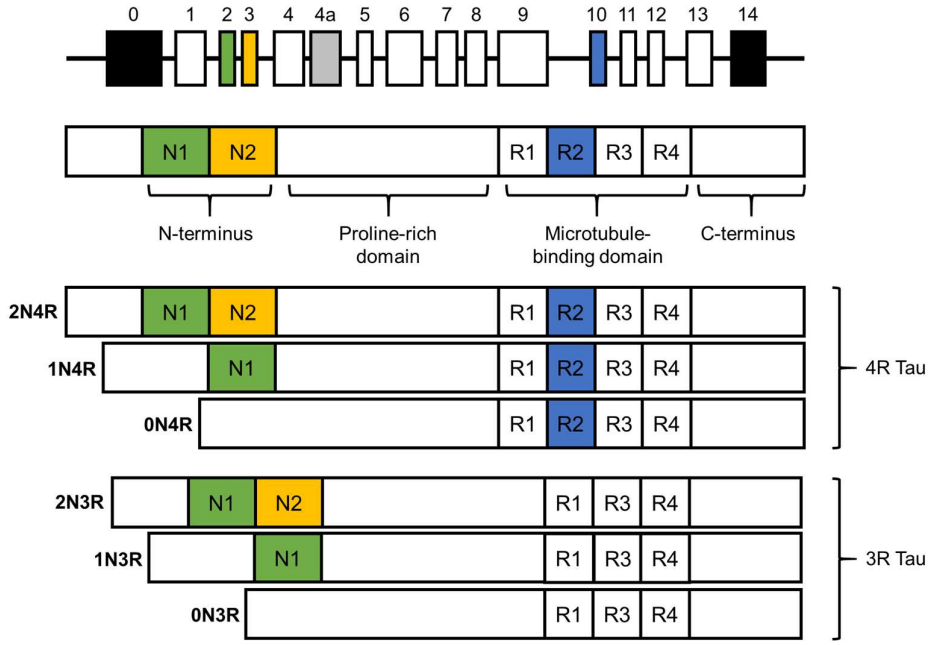


Figure 1.5 Tau protein variants produced from alternative splicing of MAPT gene at exons 2/3 and exon 10, adapted from (Gao *et al.*, 2018b). Exons 2 and 3 encode the N-terminal region of tau; inclusion of both produces 2N isoforms, skipping of exon 3 produces 1N isoforms, and skipping of both produces 0N isoforms. Exon 10 encodes the second of four microtubule-binding repeats and exon 10 skipping producing 3R tau isoforms.

Since 4R tau is able to bind microtubules with greater affinity due to its extra repeat, excess 4R tau is able to outcompete 3R tau and leave 3R tau unbound (Goedert & Jakes, 1990; Lu & Kosik, 2001). Compared to microtubule-bound tau, free tau is far more vulnerable to hyperphosphorylation (Sengupta *et al.*, 2006). It was therefore postulated that mutations shifting expression to 4R tau would lead to the aggregation of inclusion bodies from a pool of microtubule-dissociated 3R tau. However, in the case of FTDP-17-related mutations in the 5' splice site of exon 10 which promote exon 10 inclusion (Hutton *et al.*, 1998), it was found that inclusion bodies were in fact exclusively made of 4R tau (Clark *et al.*, 1998; Hong *et al.*, 1998). This was likely related to the high expression of 4R tau relative to the 3R isoform, but it also suggests that tau dissociation from microtubules is insufficient to cause inclusions. It has been proposed that tau mutations induce self-assembly and aggregation with involvement of other processes, including polyglutamylation (Lu & Kosik, 2001). Indeed, both 3R and 4R tau isoforms have been found to aggregate in NFTs in AD brain (Goedert *et al.*, 1992), providing further evidence that NFT pathology is not caused by simple dissociation of tau from microtubules. Further investigation is necessary to elucidate exactly how the 4R/3R ratio affects tau aggregation in AD and other tauopathies.

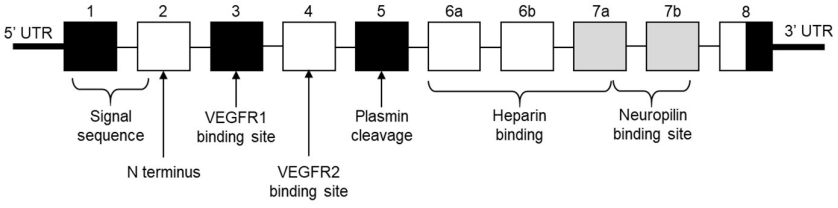
1.6 Vascular dysfunction

AD patients commonly have “mixed” or concomitant pathology, where further pathological changes from other neurodegenerative conditions are observed in addition to the defining lesions of AD: senile plaques and NFTs (Armstrong *et al.*, 2005). In persons with dementia, AD is most likely to coincide with infarcts in the brain, typically found in vascular dementia (Schneider *et al.*, 2007). In fact, pathological diagnosis of AD with cerebral infarction is associated with a higher probability of dementia than AD alone (Schneider *et al.*, 2004; James *et al.*, 2012). Considering such clinical manifestation, it is perhaps unsurprising that risk for AD and dementia is dramatically increased by cerebrovascular disease (Gorelick *et al.*, 2011) and significantly associated with incidence of atherosclerosis, diabetes, hypertension and obesity (Kovacic *et al.*, 2012). In fact, it was estimated that up to half of AD cases worldwide could be attributable to cardiovascular risk factors (Barnes & Yaffe, 2011) which strongly suggests that control of these risk factors could potentially prevent the development of AD, especially since receiving antihypertensive treatment has already been associated with a lower incidence of dementia (Forette *et al.*, 1998). On a physiological level, it has been long-established that cerebral blood flow, glucose metabolism and oxygen consumption are negatively correlated with severity of AD symptoms (Delatorre & Mussivand, 1993), supporting the theory that vascular dysfunction is implicated in AD pathogenesis. Various brain microvascular lesions can be seen in AD, including focal swelling, atrophy, and necrotic degeneration of capillary endothelial cells with loss of tight junctions; these lesions lead to chronic mismatch between blood flow and neural energy consumption, which may become self-perpetuating, progressive and destabilize neuronal transmission (Carmeliet & Storkebaum, 2002).

Vascular risk factors have also been related to other aspects of AD pathology; for example, being *APOEε4* positive and hypertensive can act synergistically on amyloid load. It was found that individuals who are both *APOEε4* positive and hypertensive have significantly higher Aβ deposition compared to individuals with neither or a single risk factor (Rodrigue *et al.*, 2013). In clinically normal individuals, vascular risk coupled with amyloid load have been associated with increased cortical tau burden (Rabin *et al.*, 2019) and shown to synergistically accelerate cognitive decline (Rabin *et al.*, 2018). Although it is unclear whether interplay between vascular risk and amyloid load is directly related to AD pathology, it is interesting to see amyloid more closely correlated with cognitive decline when alone it can be an unreliable indicator of dementia.

1.7 Vascular Endothelial Growth Factor A (VEGF-A)

VEGF-A is a hypoxia-induced factor that plays an integral role in the regulation of angiogenesis and vascular permeability (Melincovici *et al.*, 2018). It was the surgeon Judah Folkman who proposed there must be some stimulating factor that 'called forth blood vessels' in tumour microbiology and that tumour growth was dependent on this angiogenesis. Although Folkman's laboratory isolated a "tumour angiogenesis factor" and continued to work on its characterisation (Folkman *et al.*, 1971; Folkman, 1974) it was Harold Dvorak's laboratory that first identified the vascular permeability factor (Senger *et al.*, 1986; Senger *et al.*, 1990) after which Napoleone Ferrara and Dan Connolly's laboratories independently purified and cloned the factor for the first time (Keck *et al.*, 1989; Leung *et al.*, 1989). Originally termed vascular permeability factor, VEGF-A has become the fourth most-cited gene in the human genome. Numerous isoforms have been identified, including VEGF-A_{121}, VEGF-A_{145}, VEGF-A_{148}, VEGF-A_{165}, VEGF-A_{183}, VEGF-A_{189}, and VEGF-A_{206} (subscript indicating amino acid length), with VEGF-A_{165} being the most highly expressed (Hoeben *et al.*, 2004). As seen in the Figure 1.6 below, VEGF-A isoforms can be split into two major families: pro-angiogenic VEGF-A_{xxx}a and anti-angiogenic VEGF-A_{xxx}b. The two families differ by their last 6 amino acids, dependent on the selection of alternative splice sites in exon 8. Pro-angiogenic VEGF-A_{xxx}a isoforms are formed with the proximal splice site in exon 8a translating amino acid sequence CDKPRR and anti-angiogenic VEGF-A_{xxx}b are formed with the distal splice site in exon 8b translating amino acid sequence SLTRKD (Bates *et al.*, 2002). The control of angiogenesis is essential for accommodating physiological (and pathological) changes in tissue demand (Murakami & Simons, 2009). The ratio of pro- to anti-angiogenic isoforms VEGF-A_{xxx}a and VEGF-A_{xxx}b hence plays an important role in maintaining normal function in a tissue-specific manner (Qiu *et al.*, 2009). Subsequently, regulation of this ratio can have therapeutic potential in various angiogenesis-associated diseases, including cancers (Bates *et al.*, 2002), Denys Drash Syndrome (Schumacher *et al.*, 2007), diabetic retinopathy (Perrin *et al.*, 2005), age-related macular degeneration (Hua *et al.*, 2010) and glomerular diseases (Oltean *et al.*, 2012).



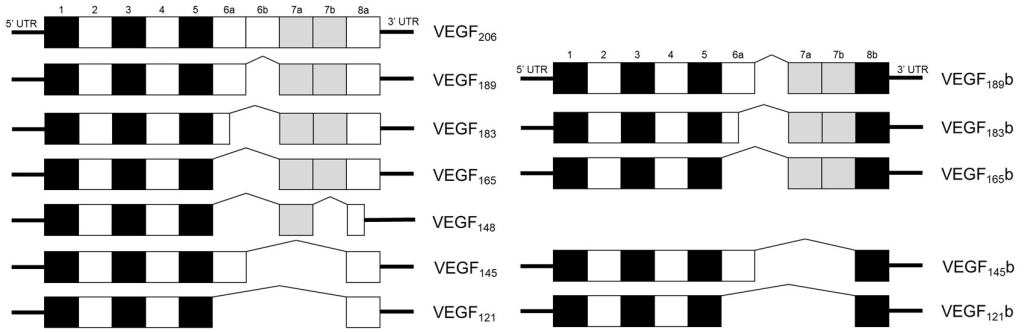


Figure 1.7 The structure of human *VEGFA* gene and its alternative splicing isoforms, adapted from (Nowak *et al.*, 2008). There are two families of VEGF-A isoforms: pro-angiogenic VEGF-A_{xxx} isoforms and anti-angiogenic VEGF-A_{xxx}b isoforms, which have alternate C-terminus produced from unique exon 8b sequence.

As a remarkably pleiotropic protein, VEGF-A has also been implicated in a number of neurological and neurodegenerative conditions (Carmeliet & Storkebaum, 2002): it not only acts on endothelial cells and regulate angiogenesis but also acts directly on nervous tissue, where it exerts neuroprotective effects (Greenberg & Jin, 2005). The majority of research on VEGF-A's neurotrophic role has been conducted in the peripheral nervous system, both *in vitro* and *in vivo*, whereby VEGF-A stimulates axonal growth and enhances cell survival, as well as promoting mitogenic activity in glial cells (Sondell *et al.*, 1999; Sondell *et al.*, 2000). In terms of pathology, VEGF-A has been notably related to amyotrophic lateral sclerosis; it was discovered that mutation of the VEGF-A promoter region causes late-onset degeneration of motor neurones resembling progression of the disease (Oosthuyse *et al.*, 2001) and that recombinant VEGF-A treatment is able to recover this degeneration (Lambrechts *et al.*, 2003). Additionally, VEGF-A has been shown to protect axotomized retinal ganglion cells from degeneration (Kilic *et al.*, 2006) and reduce infarct volume and neuronal damage after transient ischaemia in the brain (Hayashi *et al.*, 1998). Although regenerative effects of VEGF-A in the brain can be dependent on VEGF-A mediated angiogenesis enhancing neuronal perfusion (Hobson *et al.*, 2000), *in vitro* data clarifies the VEGF-A can directly increase survival of glutamate-treated hippocampal cells (Matsuzaki *et al.*, 2001) and increase neuronal outgrowth from midbrain tissue explants (Silverman *et al.*, 1999) independent of other factors. This puts forward VEGF-A as a potential tool to protect against other types of neurodegeneration.

Of particular relevance to AD, VEGF-A can be upregulated as a compensatory mechanism for reduced cerebral perfusion, most likely induced by hypoxia: It has been reported that AD patients have significantly higher VEGF-A expression in the

brain, specifically in glia and most commonly in perivascular cells (Kalaria *et al.*, 1998). This is further supported by elevated intrathecal levels of VEGF-A (Tarkowski *et al.*, 2002). Contradictory evidence associates low VEGF-A with NFTs and amyloid plaques in lesion-prone regions of AD brain (Provias & Jeynes, 2008) and suggests CSF VEGF-A remains unchanged in both AD and vascular dementia (Chakraborty *et al.*, 2018). Interestingly, serum levels of VEGF-A in AD are significantly lower than in mild cognitive impairment or control, and negatively correlated with severity of dementia (Huang *et al.*, 2013). Overall, this evidence implicates low VEGF-A (and VEGF-A mediated angiogenesis) in AD pathology and suggests measured upregulation of VEGF-A, particularly around micro-infarcts, is a consequence of AD rather than a driver of disease.

1.8 VEGFR2 activation

VEGF-A acts by activation of tyrosine-specific kinases and downstream intracellular signalling pathways. Named based on their catalytic activity, tyrosine-specific kinases (YKs) and serine/threonine-specific kinases (STKs) make up the largest superfamily of enzymes involved in cell signalling (Shen *et al.*, 2005). YKs, including both receptor-linked and cytoplasmic proteins, are known to regulate cell proliferation and differentiation, as well as other critical cellular processes such as metabolism, adhesion and motility (Schlessinger & Ullrich, 1992; Lemmon & Schlessinger, 2010). STKs include well-characterised proteins such as PKC and PKA which are activated by YKs, among other signal transduction systems, and mediate the end-effect on cell behaviour (Hardie, 1990). VEGF-A binds to the YKs VEGFR1 and VEGFR2 as well as members of the Neuropilin (NRP) family NRP1 and NRP2 (Simons *et al.*, 2016). Although VEGFR1 binds with the greatest affinity, it has only a tenth of the kinase activity of VEGFR2 (Shibuya, 2001). Alternative splicing of the *VEGFR1* gene can give rise to soluble isoforms (sVEGFR1) which do not have a kinase domain but are expressed at 10-fold molar excess over VEGF-A, effectively acting as a “decoy” receptor and negative regulator of VEGF-A function in endothelial cells (Kendall & Thomas, 1993; Shibuya, 2001).

The major positive signal from VEGF-A is transduced by VEGFR2. Binding of a VEGF-A_{xxx}a dimer at the extracellular domain promotes the activation of tyrosine kinase in the intracellular domain and consequent autophosphorylation of tyrosine residues (Claesson-Welsh & Welsh, 2013). Through a series of downstream events (illustrated in Figure 1.7 below), endothelial VEGFR2 activation ultimately leads to cell survival, proliferation, migration and increased vascular permeability (Harper &

Bates, 2008). VEGFR2 signal transduction from anti-angiogenic VEGF-A_{xxx}b dimer binding has not yet been fully characterised, but it has been reported as a partial agonist of VEGFR2, producing weaker phosphorylation of tyrosine residues which does not lead to PIP2 hydrolysis or PKC activation (Ballmer-Hofer *et al.*, 2011; Kisko *et al.*, 2011).

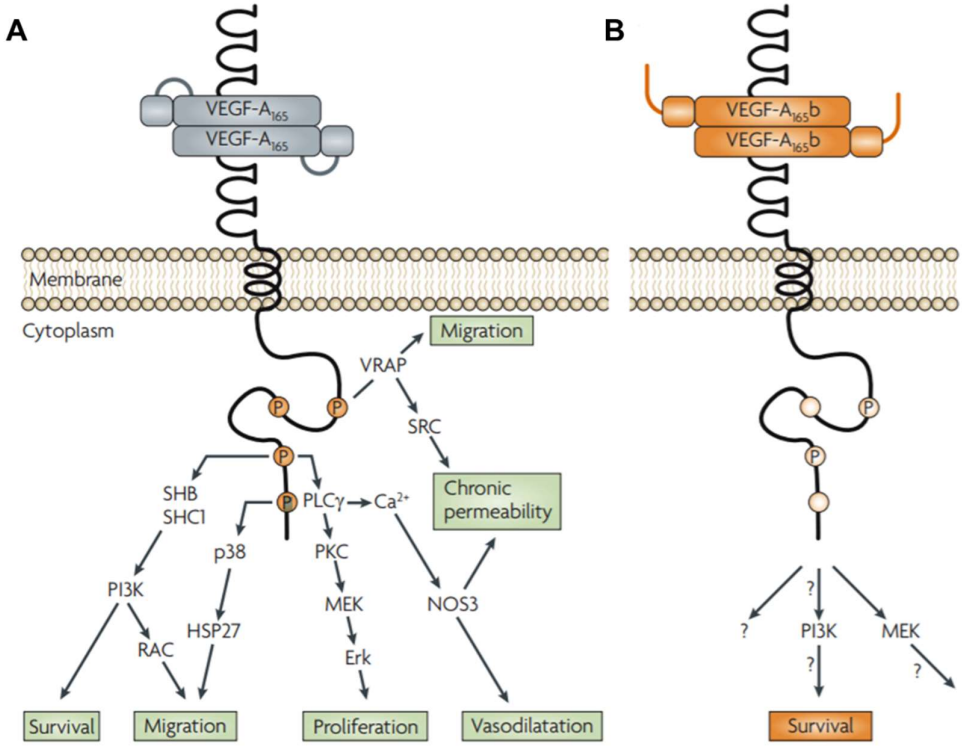


Figure 1.8 Downstream signalling pathways of VEGF-A_{165} and VEGF-A_{165}b in endothelial cells, presented in (Harper & Bates, 2008). **A** VEGF-A_{165} activation of VEGFR2 initiates downstream pathways which lead to increased cell survival, migration, proliferation and vascular permeability. **B** VEGF-A_{165}b binding to VEGFR2 results in weaker phosphorylation of downstream mediators and leads to increased cell survival. As denoted with "?" the signalling pathway for VEGF-A_{165}b remains largely uncharacterised. Erk, extracellular signal-regulated kinase; HSP27, heat shock protein 27; NOS3, endothelial nitric oxide synthase; PI3K, phosphoinositide 3-kinase; PKC, protein kinase C; RAC, Ras-related C3 botulinum toxin substrate; PLCγ, phospholipase Cγ; SHB, SH2 domain-containing adaptor protein B; SHC1, SH2 domain-containing transforming protein 1; VRAP, VEGF receptor-associated protein.

1.9 Alternative splicing (AS)

Splicing is a fundamental principle in RNA biology that can be categorised as either constitutive or alternative. Constitutive splicing is the process of intron removal and exon ligation in the order which they appear in a gene (Wang *et al.*, 2015b). However, a single gene can generate multiple mature mRNA products, and subsequently translate into multiple proteins, through differential selection of exonic and intronic sequences (Yap & Makeyev, 2016); this process is called alternative splicing (AS). The proportion of alternatively spliced genes in a species can be related to its complexity, with higher eukaryotes exhibiting the greatest degree of AS. Indeed, more than 95% of human genes are alternatively spliced, and the human genome is thus able to produce many more proteins than it has encoding genes (Pan *et al.*, 2008; Nilsen & Graveley, 2010). The process of AS mediates development of complex tissues with diverse cell types, particularly in the brain, and can play a role in the regulation of gene expression and most aspects of protein function, including ligand binding, membrane properties, intracellular localisation, and enzymatic function (Wang *et al.*, 2015b).

There several modes of AS modes, with exon skipping (or cassette exons) being the most common in vertebrates (Kim *et al.*, 2007a). Other modes include intron retention, which often leads to nonsense-mediated decay of mRNA, and alternative selection of 5' or 3 sites, which may lead to subtle changes in coding sequence (Wang *et al.*, 2015b) (see Figure 1.9 for schematic of splicing events). A splice site may not be selected when it has a weaker "signal"; in fact, AS can be distinguished from constitutive splicing by the strength of splice sites. In particular, a weaker splicing "signal" results from shorter exon length and/or higher sequence conservation surrounding orthologous alternative exons (Zheng *et al.*, 2005). However, there are other factors that play a crucial role in splice site selection, such as genomic position and association with exonic splicing enhancers (ESE) and/or exonic splicing silencers (ESS). These are cis-acting elements which promote and inhibit the assembly of the spliceosome at weaker splice sites, respectively (Wang & Burge, 2008).

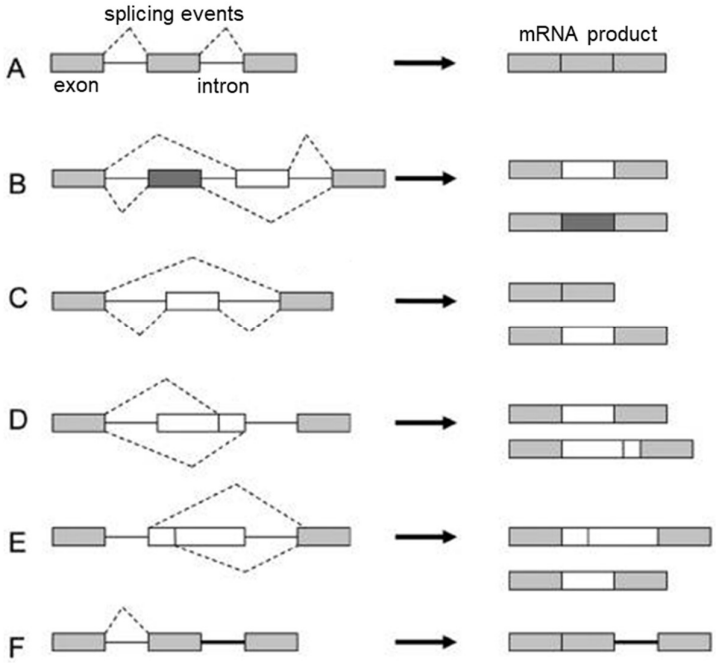


Figure 1.9: Schematic for the types of RNA splicing events. **A** Constitutive splicing removes introns and ligates exons in sequential order. Alternative splicing events include **B** mutually exclusive exons; **C** exon skipping; **D** alternative 3' splice site; **E** alternative 5' splice site; and **F** intron retention.

Regulation of AS occurs through the spliceosome, a macromolecular complex made up of five small ribonuclear-proteins (snRNPs): U1, U2, U4, U5 and U6, supported by more than 100 auxiliary proteins (Yang *et al.*, 2007). The complex recognises an intron via the its 5' splicing site and removes introns with two transesterification steps: first the 5' splice site cleavage and intron lariat formation, second the 3' splice site cleavage and covalent bonding of exons (Will & Lührmann, 2011). In order for the first step to occur, the U1 snRNP binds the 5' splice site and the U2 snRNP binds the branch point of the intronic sequence. Following this, the U5.U4/U6 tri-snRNP is recruited to the U1 snRNP and connects to the spliceosome. At this stage, the spliceosome undergoes conformational changes which activate its catalytic function, allowing the first transesterification reaction to occur. As a result, U1 and U4 snRNPs are released and intron lariat is formed at the 3' splice site. The second transesterification reaction excises the lariat containing U2, U5 and U5 snRNPs, leading to exon ligation and completion of the splicing process (Bowler & Oltean, 2019; Wilkinson *et al.*, 2020). Removed introns are decayed and the spliceosome deconstructs whereby its components are recycled for further use.

Recruitment of the spliceosome to maturing pre-mRNA and selection of a splice site is dependent on short cis-acting regulatory elements (SREs) in pre-mRNA sequence and trans-acting RNA binding proteins (RBPs) (Naro & Sette, 2013). RBPs recognise and interact with particular SREs, which leads to the selection of splice sites and determines the composition of the final mRNA transcript. As a result, the expression and relative activity of RBPs contributes toward regulation of AS (Bowler & Oltean, 2019). Among these RBPs are serine-rich (SR) proteins, a family of splicing factors that play a major role in the regulation of AS at multiple steps of the process. This includes establishment of 5' and 3' splice sites during spliceosome assembly and many post-splicing events such as mRNA export, translation regulation and genomic stability (Jurica & Moore, 2003). The function of SR proteins is highly dependent on their phosphorylation state, which controls their subcellular (and subnuclear) localisation and ability to promote spliceosome interaction with splicing enhancer sequences (Naro & Sette, 2013). Serine-Arginine protein kinases (SRPKs) and Cyclin-dependent Like Kinases (CLKs) are subfamilies of STKs that phosphorylate serine residues within Arginine-Serine (RS) dipeptide motifs (Giannakouros *et al.*, 2011), which make up the highly-conserved RS domain found in SR proteins. By extension, SRPKs and CLKs modulate the activity of SR proteins. SRPK-mediated phosphorylation of SR proteins enhances their interaction with nuclear transport factor transportin-SR2, promoting their nuclear localisation (Lai *et al.*, 2001). CLK-mediated phosphorylation of SR proteins leads to disassembly of speckles and their nuclear dispersion, facilitating interaction with target splice sites (Ghosh & Adams, 2011).

1.10 Regulation of SR Splicing Factor 1 (SRSF1) function

SRSF1 is an essential gene; it is constitutively expressed at the post-transcriptional level and tied to normal embryonic development (Gonçalves & Jordan, 2015). Among other SR proteins, SRSF1 is able to auto-regulate its expression through a negative feedback loop: it identifies highly conserved SREs in its own transcripts, leading to AS in the 3' untranslated region and causing the transcript to become a target for nonsense-mediated decay (Lareau *et al.*, 2007). Increased SRSF1 levels therefore promote an increase in their unproductive splice variants to regulate SRSF1 function.

SRPKs phosphorylate proteins containing RS domains (Bullock & Oltean, 2017). SRPK1 binds with high affinity to SRSF1 and phosphorylates about 10-12 serines in the RS domain in a directional (C-to-N terminal) manner. This is facilitated by a

docking groove in the large lobe of the kinase domain that feeds SRSF1 RS domain into the SRPK1 active site, an example of a “two-prong” recognition mechanism (Ma *et al.*, 2008). The SRPK1 active site is accessible to substrates without phosphorylation; this has been related to its relatively short activation loop which adopts a stable and open conformation (Ghosh & Adams, 2011). Phospho-SRSF1 is then imported into the nuclear speckles where it is co-localised with CLKs and further phosphorylated at remaining serine residues in the distal RS domain (Colwill *et al.*, 1996). This leads to nuclear dispersion of SRSF1 and facilitates association with RNA polymerase II and consequent regulation of splicing (Gonçalves & Jordan, 2015). Interestingly, CLKs do not possess a docking groove in the kinase domain yet are still able to phosphorylate up to 18 serines in SRSF1 RS domain. This impressive kinase activity has been attributed to CLKs disordered N-termini that bind tightly to RS domains (George *et al.*, 2019) as well as SRSF1 kinase domains, facilitating SRSF1 hyperphosphorylation and inducing RNA binding (Aubol *et al.*, 2014).

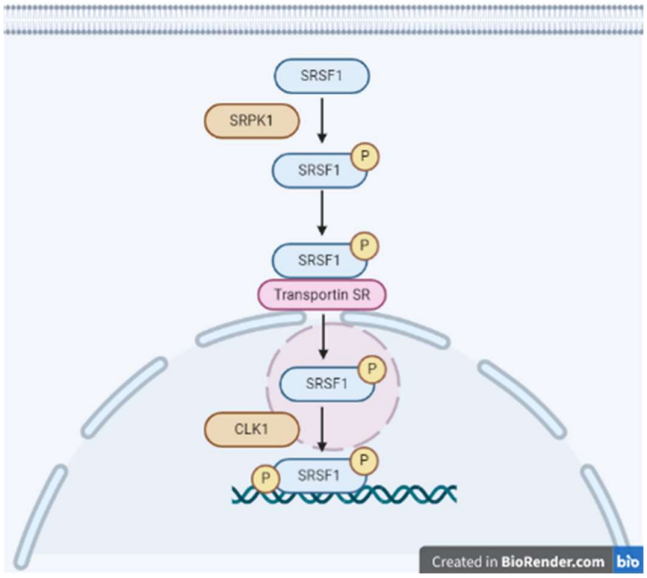


Figure 1.10 Schematic diagram for proposed phosphorylation of SRSF1 by splicing kinases SRPK1 and CLK1. SRPK1 phosphorylation enables translocation of SRSF1 from cytoplasm to cell nucleus through transportin SR but it is shuttled directly into nuclear speckles. SRSF1 is further phosphorylated by CLK1 to be released from nuclear speckles, enabling interaction with spliceosome and downstream splicing effects. Diagram created in BioRender, adapted from text (Aubol *et al.*, 2014).

1.11 AS of VEGF-A

VEGF-A splicing is regulated by SR proteins, particularly SRSF1, SRSF5 and SRSF6 (Biselli-Chicote *et al.*, 2017). As previously described, VEGF-A splicing at exon 8 produces two families of isoforms, VEGF-A_{xxx}a and VEGF-A_{xxx}b. Splicing factor SRSF1 has been found to promote selection of the proximal splice site in exon 8, leading to VEGF-A_{xxx}a, whereas SRSF6 promotes selection of the distal site, leading to VEGF-A_{xxx}b expression (Nowak *et al.*, 2008). Given its role in SRSF1 phosphorylation, SRPK1 is a key regulator of VEGF-A splicing; since SRSF1 supports the proximal site, inhibition of SRPK1, which subsequently prevents shuttling of SRSF1 to the nucleus, would favour selection of the distal site. As a result, SRPK1 inhibition can cause a shift toward VEGF-A_{xxx}b production, changing the physiological ratio of VEGF-A isoform expression (Nowak *et al.*, 2010). This has been shown in melanoma (Gammons *et al.*, 2014) as well as prostate and colon cancer cell lines (Amin *et al.*, 2011; Mavrou *et al.*, 2015), where SRPK1 knockdown increased VEGF-A_{xxx}b expression. The SRPK1-SRSF1 pathway has been further validated by assessing SRSF1 localisation with relation to VEGF-A isoform expression; cells that do not express VEGF-A_{165}b have high SRPK1 expression and SRSF1 is found strictly in the nucleus, whereas VEGF-A_{165}b-expressing cells have comparatively low SRPK1 and cytoplasmic SRSF1 in addition to nuclear SRSF1, evidence for reduced interaction with the spliceosome (Amin *et al.*, 2011).

1.12 Use of kinase inhibitors

The activity of SR proteins is dependent on phosphorylation of their RS domain, which is mainly controlled by three families of kinases: dual-specificity tyrosine-regulated kinases (DYRKs), CLKs and SRPKs. Pharmacological modulation of AS through activity of these kinases can affect cellular function and downstream physiology (Bates *et al.*, 2017). Hence, the development of small molecule inhibitors targeting splicing kinases has useful application as 1) investigative tools for understanding mechanisms that regulate AS and 2) potential therapeutic agents for diseases characterised by dysregulation of splicing. However, it can be difficult to directly link the biological effects of kinase inhibitors with cellular splicing; a link oftentimes confounded by interference from off-target effects associated with low-potency and/or less selective compounds (Effenberger *et al.*, 2017). SPHINX31 is a moderately potent and highly selective inhibitor of SRPK1. It is a 3-(trifluoromethyl)anilide scaffold developed by a screening campaign using differential scanning fluorimetry. The compound has an IC_{50} of 5.9nM and

approximately 50-fold affinity for SRPK1 over the closest related kinase SRPK2 (Batson *et al.*, 2017). It is challenging to produce selective type 1 kinase inhibitors (ATP competitive) because the kinase active site is very highly conserved and inhibitors conventionally target the ATP-binding site, located between two catalytic domain lobes (Müller *et al.*, 2015). However, in the case of SPHINX31, this challenge was overcome by targeting a hinge region unique to SRPK1. The trifluoromethyl group in SPHINX31 interacts with a glycine residue in the SRPK1 hinge region to flip the hinge outward and push the phosphorylation loop upward, blocking its kinetic activity (Batson *et al.*, 2017). In fact, by targeting this region, 1μM SPHINX31 is able to inhibit 96% SRPK1 activity *in vitro*.

Since its production, SPHINX31 has been used *in vitro* and *in vivo* to switch splicing of VEGF-A from pro-angiogenic VEGF-A_{xxx}a to anti-angiogenic VEGF-A_{xxx}b isoforms, with promising therapeutic applications in cancer, age-related macular degeneration, diabetic retinopathy and kidney diseases (Gammons *et al.*, 2013; Mavrou *et al.*, 2015; Ved *et al.*, 2017; Stevens & Oltean, 2018). Although VEGF-A has been related to AD pathology (see section 1.6), we do not have a clear understanding of the relationship between different VEGF-A splicing isoforms and neurodegeneration. However, a study of sera and CSF from AD patients found elevated levels of anti-SRPK1 antibodies, the function of which remains unclear (Daniilidou *et al.*, 2011). Other autoantibodies have been found in AD, most of which target neuronal proteins, but it is unknown if they have a pathogenic or protective role (Colasanti *et al.*, 2010). Either way, this study implicates SRPK1 function in AD, and presents rationale for further investigation.

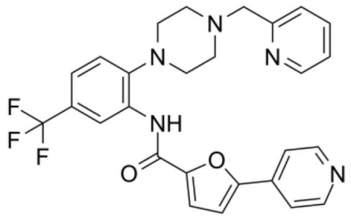


Figure 1.12 The chemical structure of SPHINX31, as published in Batson et al. 2007.

CLK inhibition has been proposed as a therapeutic strategy for autism spectra (Bidinosti *et al.*, 2016) and various cancers through regulation of abnormal splicing in tumour development and progression (Martín Moyano *et al.*, 2020). Small-molecule CLK inhibitors have been developed and tested for a number of conditions, particularly gliomas and renal tumours since they are associated with high CLK1 induction (Czubaty & Piekiełko-Witkowska, 2017). Indeed, high CLK1

tumour expression has been correlated with poor prognosis in renal cancer patients, indicating that CLK1 can play a critical role in cancer progression (Dominguez *et al.*, 2016). TG003 is an inhibitor of CLKs 1, 2 and 4, first developed in 2004 as a tool to investigate CLK-mediated regulation of SR proteins and splicing mechanisms (Muraki *et al.*, 2004). Since then, TG003 has been used in several studies on CLK function, including RNAseq analysis of TG003 treated cells. It was found that CLK1 inhibition significantly alters 892 AS events in 665 genes, and 156 of those genes have a role in cell cycle control, indicated by cell cycle periodic AS events. Since CLK1 expression itself is dependent on the cell cycle, increasing in late S-phase and G2 phase, it was suggested that CLK1 is required for normal cell cycle progression via regulation of periodic AS events, and dysregulation of these AS events may explain the association between CLK1 and cancer (Dominguez *et al.*, 2016).

Interestingly, CLKs have also been proposed as a target in AD (Jain *et al.*, 2014) since they are implicated in AS of *MAPT*. It has been reported that CLK2 increases exon 10 skipping and proportional increase in 3R tau expression, opposing upregulation of 4R tau seen in AD-affected brain regions (Glatz *et al.*, 2006). CLK1 has similarly been associated with increased exon skipping (Duncan *et al.*, 1997) but this has not been definitively related to AD through 3R:4R tau ratio. Nonetheless, the respective roles of SPRK1 and CLK in *VEGFA* and *MAPT* splicing makes them interesting targets in AD, and the use of splicing kinase inhibitors can therefore be proposed as a novel therapeutic approach for AD-related pathologies.

1.13 Use of *in vitro* models for AD

As with most complex diseases, it is very difficult to effectively model the pathology of AD *in vitro*. Several approaches have been adopted to facilitate research on particular aspects of disease progression, e.g., using CRISPR/Cas9 technology to knock-out of key genes *APP* and *PSEN1* that are mutated in familiar AD (Paquet *et al.*, 2016). This provides an alternative to transgenic mouse models and can reduce the number of animals used in AD research. Other methods depend on treatment of neurones with pathological agents that are known to induce excitotoxicity, e.g., exogenous Aβ (Tamagnini *et al.*, 2015), creating a simple model that maintains relevance to AD (Stine *et al.*, 2011). In order to be clinically relevant, it is crucial to model as aspect of pathogenesis that leads to cell death, i.e., a driver of disease, so that neuroprotective agents may have a good therapeutic window. Such assays include use of neurotoxins that lead to abnormal phosphorylation and aggregation of tau, since NFTs are closely related to cell death and the severity of cognitive decline

(Gómez-Isla *et al.*, 1996; Giannakopoulos *et al.*, 2003). For example, okadaic acid (OA) is a potent inhibitor of protein phosphatase 2A (PP2A) which regulates the phosphorylation state of tau; OA-mediated inhibition of PP2A has been established to induce tau hyperphosphorylation *in vitro* (Martin *et al.*, 2011). In this thesis, both Aβ and OA are used to model AD-related neurotoxicity and investigate the potential of VEGF-A_{165} isoforms and splicing kinase inhibitors as neuroprotective agents.

The appropriate selection of cell model is a crucial step for maintaining relevance to the AD brain. In recent years, the use of induced pluripotent stem cells has become a popular method for generating differentiated cortical neurones *in vitro* that represent the cell phenotype most affected by AD (Arber *et al.*, 2017). The method is made yet more attractive by the potential of patient-derived cells and development of personalised medicine (D'Souza *et al.*, 2021). However, stem cell culture requires a very long and particular protocol for neuronal differentiation, after which the "developmental age" of neurones remains relatively young. Considering that age poses the single most significant risk for AD, "ageing" neuronal cultures remains an obstacle for truly representative cell models. Direct use of patient-derived tissue circumvents need for cell models, but it is limited in experimental capacity due to inability to culture primary neurones, and it depends on rapid access to tissue that is limited, precious, and in high demand. Neuronal cell lines, including SHSY5Y cells described in Chapters 4 and 5 of this thesis, are a commonly used alternative method since they are widely available, relatively easy to culture and differentiate, and maintain key neuronal characteristics that represent brain tissue, albeit in a more limited way (de Medeiros *et al.*, 2019).

1.14 Hypotheses and Aims

There are two main hypotheses tested in this thesis:

- Brain regions susceptible to AD pathology and individuals with AD dementia will exhibit differential splicing patterns and differential expression of splicing kinases.
- The regulation of alternative splicing through inhibition of splicing kinases will ameliorate AD-related neurotoxicity *in vitro*.

The aims of this thesis are:

1. Use transcriptional analysis methods to elucidate differential expression and alternative splicing events between the cerebellum and the frontal cortex.
2. Determine the difference in alternatively spliced transcripts between individuals with no cognitive impairment, MCI, and AD.
3. Compare the proportion of individuals with AD diagnoses/pathology in groups of low and high splicing kinase expression.
4. Investigate the neuroprotective role of VEGF-A splicing isoforms in AD-related neurotoxicity *in vitro*.
5. Determine changes in *MAPT* exon 10 splicing with a panel of splicing kinase inhibitors.
6. Assess the effect of SRPK1 and CLK inhibitors on VEGF-A expression and neurite outgrowth.

Chapter 2. Methods

2.1 Cell culture

Unless otherwise stated, all cell culture reagents were purchased from Thermo Fisher Scientific. All cell culture was performed in cell culture hoods in class II facilities using aseptic technique and sterile culture medium. Cell culture flasks were kept in an incubator at 37°C in a humidified environment containing 5% CO_2.

2.1.1 Cell splitting

Cells were cultured for up to 4 days until they reached confluency of 80-90% in their flask (see Table 2.1 for media composition). To split cells, media was removed from cells with a sterile pipette and the flasks were washed with PBS (5mL for 25cm^2 flasks, 10mL for 75cm^2 flasks, 20mL for 175cm^2 flasks). Trypsin was then added (0.5mL for 25cm^2 flask, 1mL for 75cm^2 flask, 2mL for 175cm^2) and put in the incubator for 2-3 min. Flasks were removed from the incubator and briefly visualized on a light microscope (Leica DMIL) to ensure cells had detached from the bottom of the flask. After confirmation, growth media was added to the flask containing trypsin (5mL for 25cm^2 flask, 10mL for 75cm^2 or 175cm^2 flask) and the cell mixture was transferred to a 15mL Falcon tube. Tubes were then centrifuged at 1000 x g for 5 min to form a cell pellet and the supernatant was discarded. The cell pellet was thoroughly re-suspended in 2mL fresh growth media in the Falcon tube by gentle trituration. From this cell suspension, 400µL (for a 1 in 5 dilution) is added to a bigger volume of growth media and seeded into a new culture flask.

Cell line	Growth media composition
SHSY5Y	DMEM/F-12 GlutaMAX media + 10% Fetal Bovine Serum (FBS)
Neuro2a	RPMI media + 2mM L-glutamine + 10% FBS

Table 2.1 Media composition for cell culture of SHSY5Y and Neuro2a cells.

2.1.2 Cell counting

From this cell suspension, 10µL was placed underneath a sterilized 22 x 22mm glass coverslip (VWR International) into a haemocytometer chamber (Millscience Neubauer) and cells were counted in the four corner grids using a manual cell counter and a light microscope (Leica DMIL). The value from each grid was

averaged and multiplied by 10,000 to calculate cell number/mL. After cell counting, additional growth media was added to the cell suspension mixture and plated onto experimental plates.

2.1.3 Cell plating

For protein extraction, cells were plated at a density of 200,000 cells/well in 6-well plates or 800,000 cells per 10cm dish. For RNA extraction, cells were plated at a density of 100,000 cells/well in 12 well plates or 200,000 cells/well in 6-well plates. For imaging, cells were plated into black-sided flat clear bottom 96-well plates at a density of 10,000 cells/well.

2.1.4 Cell differentiation

After plating, cells were differentiated prior to treatment. SH-SY5Y cells were differentiated by reduction to 1% serum and treatment with 10μM all-trans retinoic acid for 7 days. Differentiation media was renewed at least every 3 days. Neuro2a cells were differentiated by serum starvation and treatment with 300μM dibutyryl cAMP for 48h.

2.1.5 Cell transfection with siRNA

Cells seeded in 6-well plates were transfected using Lipofectamine RNAiMAX reagent after their differentiation. All siRNA was made up at a stock concentration of 20μM in sterile water. For each treatment well, two separate Eppendorf tubes were prepared with 100μL Optimem; 10μL stock siRNA was added into one tube and 5μL Lipofectamine was added to the other. Solutions were gently mixed and incubated for 10 min at RT. Next, the Lipofectamine solution was transferred over to the siRNA solution and they were incubated together for 30 min at RT.

For Neuro2a cell transfection, differentiation media was removed, and cells were washed once with PBS. 800μL Optimem was added to each well, then total 200μL Lipofectamine-siRNA mix was added dropwise to the cells at a final concentration of 200nM siRNA (1:100 dilution from stock). The cells were incubated with Lipofectamine-siRNA mix for 6h at 37°C, then another 1mL Optimem was added to each well. Finally, the cells were incubated for 48h to achieve transient knockdown and RNA (or protein) was collected for downstream experiments. SHSY5Y cells were transfected with siRNA following an adapted protocol that involved a two-step knockdown. After 4 days of differentiation, SHSY5Y cells were treated with siRNA as previously described, and then re-treated for another 48h before tissue collection.

This method was optimised due to low transfection rate of differentiated SHSY5Y cells with the traditional protocol.

2.2 Cell viability assay

All cell viability assays were carried out on SHSY5Y cells and Neuro2a cells seeded in black-sided flat clear bottom 96-well plates. After differentiation and treatment, 10µL WST-1 reagent was added to 100µL media alone or cells with 100µL treatment media. After 1h, 2h and (only if necessary) 4h, plates were read at 450nm with a reference wavelength of 620nm. Incubations were performed under normal sterile cell culture conditions, at 37°C in a humidified environment containing 5% CO_2. Readings from treated cells were normalised against an assay control (media + WST-1 reagent) and the relevant experimental control (e.g., vehicle only). Data was analysed using GraphPad Prism software.

2.3 Immunofluorescence

SHSY5Y cells were fixed in black-sided flat clear bottom 96-well plates with 4% PFA for 10 min at RT (50µL per well). Fixed cells were washed once with 200µL PBS and then permeabilised with 100µL PBS 0.2% Triton X100 (PBSX) with 1% normal horse serum for 30 min. A mouse anti-human βIII tubulin antibody (R&D Systems) was used as a marker of neurite outgrowth. It was diluted 1:1000 in 1% normal horse serum PBS and 50µL was added to each well after cell permeabilisation, then incubated (in a humid box) overnight at 4ºC. The following day, wells were washed three times for 5 min each with 200µL PBS 0.5 mL/L Tween20. Donkey anti-mouse 488 secondary antibody and Hoechst were diluted 1:1000 in 1% BSA PBS and 50µL added to each well. Cells were incubated for 30 min in the dark at RT, and cells were washed again three times with 200µL PBS 0.5 mL/L Tween20. Cells were kept in 100µL PBS at 4ºC until imaged. Fluorescence was captured using a Leica SPE confocal microscope: three 20x images were taken per well with smart gain of 700 or 800 (always kept consistent across experimental groups). There were 4-6 wells per condition in each experiment, making a total of 12-18 images per condition. Images were analysed on Image J using simple neurite tracer, as demonstrated in Figure 2.3. The sum length of neurites per image was normalised to the number of cells, automatically calculated with a mask of Hoechst-stained nuclei. Average neurite length was then compared between treatment groups using GraphPad Prism software.

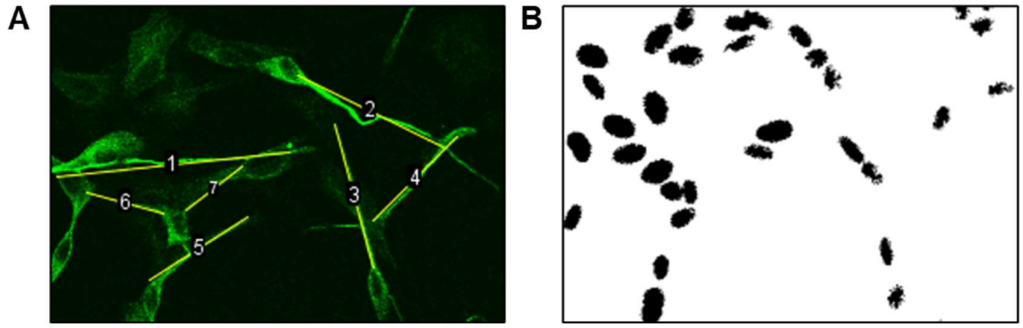


Figure 2.3 Neurite outgrowth assay analysis. **A** Images of βIII-tubulin in SHSY5Y cells imaged on the confocal microscope. Example traces are manually drawn over outgrowth which were then quantified using region of interest manager on Image J. **B** Mask over nuclei from same region stained with Hoechst according to set threshold. Number of cells were automatically counted using "Analyse particles" feature on Image J. The sum length of neurites per image was then normalised to the total number of cells.

2.4 Reverse transcription PCR (RT-PCR)

Unless otherwise stated, all RNA work was carried out at 4ºC (or on ice) to prevent sample degradation.

2.4.1 RNA extraction

RNA was extracted from cells after differentiation and treatment using a TRI-reagent protocol. Firstly, media was removed from cells and 500µL TRI-reagent was added directly to culture dish. The cell lysate was homogenised with a pipette before transfer to an Eppendorf tube. After 5 min incubation at RT, 250µL chloroform was added and samples were shaken vigorously by hand for 1 min, then left to incubate for 10 min at RT. Samples were centrifuged at 12,000 x g for 15 min at 4ºC for phase separation: a red organic phase (containing protein), an interphase (containing DNA) and a colourless aqueous phase (containing RNA). The top aqueous phase was transferred into an ice-chilled Eppendorf tube with equal-volume isopropanol. Samples were shaken for 15 sec and RNA was allowed to precipitate overnight at -20ºC. Next, samples were centrifuged at 12,000 x g for 15 min at 4ºC to pellet the RNA. The supernatant was discarded, and the RNA pellet was washed with 1mL 75% ethanol and re-pelleted by centrifugation at 7,500 x g for 15 min at 4ºC. The supernatant was discarded, and the RNA pellet was allowed to air-dry before being resuspended in 10-30µL sterile water. RNA was kept on ice for 30 min before being quantified using a spectrophotometer (Thermo-Scientific Nanodrop 2000) and stored at -80ºC.

2.4.2 cDNA generation

RNA was reverse transcribed to complementary DNA (cDNA) using the Takara PrimeScript™ RT Reagent Kit (RR037A). For each sample, 1µg RNA was combined with 25pM oligo dT, 200pM random hexamers and PrimeScript buffer, then made up to a reaction volume of 19µL with sterile water. The reaction mixtures were heated to 65ºC for 10 min for denaturation and then immediately placed on ice for the addition of 1µL PrimeScript RT enzyme. Following this, reaction mixtures were incubated at 25°C for 10 min and 37°C for 60 min for generation of 50ng cDNA. RT enzyme was inactivated by heating to 85°C for 1 min and cDNA samples were stored at -20ºC. For each experiment, a no-template control was run to check for contamination, including all components of the reaction mixture excluding the RNA sample.

2.4.3 Polymerase Chain Reaction (PCR)

All PCR reactions were performed on 50ng cDNA using GoTaq G2 Green Master Mix (Promega) at a total volume of either 15µL or 30µL. Primers were used at a final concentration of 0.4µM. DNA samples were denatured at 96°C for 5 min, followed by multiple cycles of denaturation at 96°C for 30 seconds, annealing at primer specific temperature (see Table 2.4) for 30 sec, and extension at 72°C for 1 min. PCR cycles were followed by a final extension step at 72°C for 10 min and samples were then held at 4°C until gel electrophoresis. PCR products were run in 2% agarose gels containing 50ng/ml ethidium bromide at 100V for approximately 1.5h. Gels were visualised using the BioRad Gel Doc™ EZ System. Full list of primer sequences can be found in Appendix Table 7.3.1.

2.5 Protein-based assays

Unless otherwise stated, all protein work was carried out at 4ºC (or on ice) to prevent sample degradation.

2.5.1 Cell lysis

Protein was extracted from cells after differentiation and treatment. Cells were washed with ice-cold PBS and kept on ice. Cell lysis buffer (see Table 2.5.1) was added to cells and left to incubate for 10 min. Cells adhered to the surface of culture plates were scraped and mechanically dissociated by trituration, then transferred to an ice-chilled Eppendorf. The cell suspension was vortexed for 15 sec three times over a 10 min incubation on ice. Samples were centrifuged at 12,000 x g for 10 min at 4ºC and the supernatant was collected in a fresh Eppendorf and stored at -80ºC.

Component	Concentration (Volume)
NP40	1X (1mL)
PMSF	1mM (10µL from 100mM stock)
Na_3VO_4	10mM (50µL of 200mM stock)
NaF	5-50mM (20µL from 0.5M stock)
Protease Inhibitor	1X Roche cOmplete cocktail (20µL)

Table 2.5.1 List of components for cell lysis buffer.

2.5.2 Protein quantification

A Bradford protein reagent assay (Bio-Rad) was used to quantify the protein concentration of samples against a 7-point standard curve of bovine serum albumin (BSA) in PBS (1000µg/mL serially diluted 1:1 to 15.625µg/mL). Samples were diluted 1:10 or 1:20 in PBS to bring them within range of the standard curve. 10µL of standards and samples were loaded in triplicate into a clear 96 well plate. Bradford reagent was diluted 1:5 in distilled water and 200µL was loaded to each well. Plates were agitated for 5 sec and then read immediately at 620nm using a Magellan microplate reader. A standard curve was plotted on Microsoft Excel using optical density readings from the BSA standards, and sample protein concentrations were calculated based on the equation of the curve.

2.5.3 Western blot

Cell lysates were diluted to contain a constant amount of total protein (per experiment, 25-100µg) in distilled water and 1X Laemmli sample buffer. Samples were heated to 95^{o}C for 5 min and immediately returned on ice until loaded in a 10% Mini-PROTEAN TGX Precast Protein gel alongside a molecular weight marker (PrecisionPlus dual colour standard, Bio-Rad). Gels were run in Tris buffer at 100V for approximately 90 min using the Mini-PROTEAN Tetra Cell 1-D vertical gel electrophoresis system (Bio-Rad). The separated proteins were transferred onto a nitrocellulose membrane using Transfer buffer in the Trans-Blot Turbo Transfer system (Bio-Rad). The membranes were subsequently incubated (on a roller) in blocking buffer for 90 min at RT. Primary antibody was diluted to the appropriate concentration (see Table 2.5.3) in blocking buffer. After block, membranes were incubated (on a roller) in primary antibody overnight at 4^{o}C. The composition of all buffers is described in Table 2.5.2.

Buffer	Components
Running (Tris) Buffer	25nM Tris, 192mM Glycine, 0.1% SDS, pH 8.3
Transfer Buffer	1X Transfer Buffer (Bio-Rad) with dH_2O and 10% ethanol
Wash Buffer	Tris-Buffered Saline (TBS) 1% Tween20 (TBS-T)
Blocking Buffer	5% Bovine Serum Albumin in TBS-T

Table 2.5.2 List of buffers for Western blot.

Next, membranes were washed three times for 5 min each at RT using wash buffer. Secondary antibodies were diluted to the appropriate concentration in blocking buffer, as detailed in Table 2.5.3 below. After washes, membranes were incubated (on a roller) in secondary antibody for 1h at RT. The membranes were washed again (as before) and imaged using the LI-COR Odyssey system. Results were analysed using LI-COR Image Studio software.

	Antibody	Dilution	Source
Primary	Goat anti-β actin	1:500	Abcam
	Rabbit anti-SRSF1	1:2000	Abcam
	Mouse anti-phospho SR	1:200	Merck millipore
Secondary	IRDye 800CW Donkey anti-Mouse IgG	1:5000	LiCor
	IRDye 680RD Donkey anti-Rabbit IgG	1:5000	LiCor

Table 2.5.3 Antibodies used for Western blot.

2.5.4 ELISA

High-binding 96-well clear microplates were coated with 100µL capture antibody (detailed in Table 2.5.5), sealed with parafilm and incubated (with agitation) overnight at RT. The following day, wells were washed three times with wash buffer. After each wash, plates were inverted and firmly tapped on tissue paper to completely empty wells and prevent carry-over of liquid or bubbles. 100µL blocking buffer was added to coated plates, sealed with parafilm, and incubated (with agitation) for 2h at RT. After block, wells were washed again (as before) and 100µL standards or samples were added in duplicate according to plate layout planned for the experiment. VEGF-A_{165}a and VEGF-A_{165}b recombinant proteins were used as standards, starting at 1000pg/mL and serially diluted 1:1 in diluent to a low concentration of 3.9pg/mL, making a 9-point standard curve. The opposite VEGF-A isoform was used at highest concentration as a negative control to ensure specificity

of the capture antibody. Samples were typically diluted 1 in 2, also using diluent. After addition of standards and samples, plate was resealed with parafilm and incubated (with agitation) for 2h at RT. The composition of all buffers used in this protocol are listed in Table 2.5.4.

Buffer	Components
Wash buffer	PBS + 0.05% Tween20
Blocking buffer	PBS + 1% BSA (sterile-filtered) or SuperBlock (ThermoFisher)
Diluent	PBS + 1% BSA (sterile-filtered)

Table 2.5.4 List of buffers for ELISA.

As detection antibody, 100µL biotinylated mouse monoclonal anti-human VEGF-A antibody was added to each well following another set of washes. Plates were resealed and incubated (with agitation) for another 2h at RT. Plates were washed (as before) and 100µL horseradish peroxidase conjugated streptavidin (made up in diluent) was then added to each well. Plates were sealed with foil to protect from light and incubated for 30 min at RT. Plates were washed a final time and 100µL tetramethylbenzidine (TMB) substrate was added to each well, then incubated in the dark for 1h (or until the colour change reached an appropriate intensity) at RT. The reaction was quenched with 50µL 1M HCL per well and shaking for 10 sec to ensure thorough mixing. Finally, plates were read at 450nm using a Magellan microplate reader. A standard curve was plotted on Microsoft Excel using optical density readings from the VEGF-A standards, and sample concentrations for VEGF-A isoforms were calculated based on the equation of the curve.

	Antibody	Concentration
Capture	HuCAL anti-human VEGF-A_{165}a	0.75µg/mL
	Mouse anti-human VEGF-A_{xxx}b 56/1	10µg/mL
Detection	Mouse monoclonal anti-human VEGF-A	100ng/mL
	Streptavidin-horseradish peroxidase	1:200 dilution

Table 2.5.5 Antibodies used for VEGF-A ELISA.

During the optimisation of the VEGF-A_{165}a ELISA, 0.25, 0.75 and 2.25µg/ml capture antibody were used to determine concentration-dependent effect on signal to noise ratio. 0.75µg/ml antibody was taken forward (Figure 2.5.4A) and the blocking step was selected for further optimisation. The use of SuperBlock (ThermoFisher) was compared to 2h incubation with PBS + 1% BSA. In accordance with manufacturer's instructions, SuperBlock was also used as a "wash" where 200µL was added to each well and shortly emptied in three consecutive steps. I found that SuperBlock provided a better signal to noise ratio, and 3x 1min steps were just as effective and 1-2h incubation, as presented in Figure 2.5.4B below. This optimised protocol was used to collect data for this thesis.

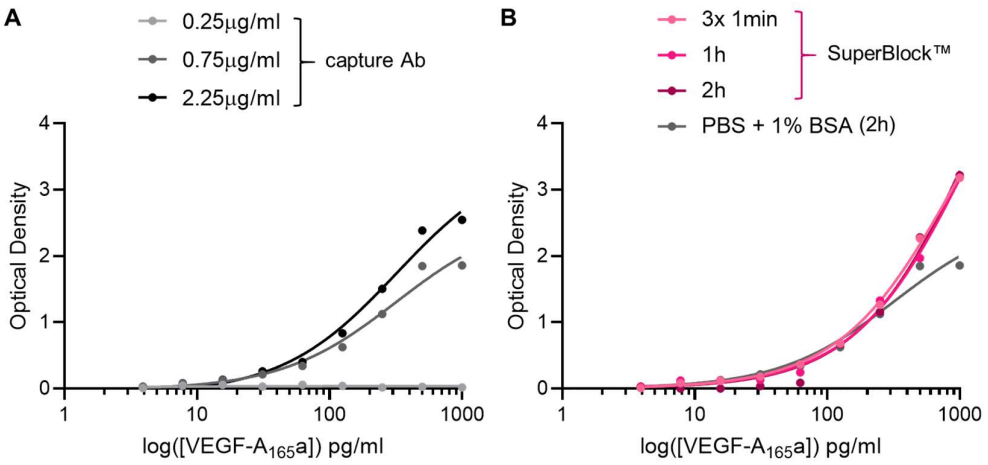


Figure 2.5.4 VEGF-A_{165}a ELISA optimisation of antibody concentration and blocking reagent. **A** Standard curves for VEGF-A_{165}a optical density reading using 0.25-2.25µg/ml capture antibody. **B** Standard curves for VEGF-A_{165}a optical density reading comparing the use of PBS + 1% BSA and SuperBlock as blocking buffers.

2.6 Tau minigene

Expression construct SV9/10L/11 is a minigene cloned into pSVIRB and sourced from Prof Stefan Stamm's lab group, originally published in Molecular and Cellular Neuroscience (Hartmann *et al.*, 2001). Tau exon 10 is flanked by proximal intronic regions (471 nucleotides downstream and 408 nucleotides upstream) as well as exons 9 and 11. Tau exon 9 (161 nucleotides) and 1.5kb of its downstream intron is fused to insulin exon 2 while tau exon 11 (68 nucleotides) and 324 nucleotides of its upstream intron is fused to insulin exon 3 (see Figure 2.6). The pSVIRB vector has ampicillin resistance for selection and a GFP tag for confirmation of transfection.

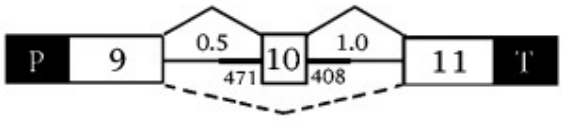


Figure 2.6 Structure of Tau minigene, sourced from Wang et al., P and T represent vector promoters and terminators. The numbers on each side of the exon 10 indicate kilobases of flanking introns. Solid and dashed lines represent splicing pathways of exon 10 inclusion and exclusion, respectively.

2.6.1 DNA extraction

The minigene was transported in a section of filter paper. Upon delivery, the paper containing DNA was cut and put in an Eppendorf, then 200µL distilled water was added to the tube. After 15 min incubation, the paper was broken down by trituration in a 200µL tip. DNA concentration was calculated using a spectrophotometer (Thermo-Scientific Nanodrop 2000) to be 180µg/mL and kept at 4°C or stored long term at -80°C.

2.6.2 Bacterial transformation

This protocol was carried out using commercially available TOP10 competent cells (Thermo Fisher) stored at -80°C. From stock, 2µL plasmid was added to 50µL competent cells and mixed very gently, then incubated on ice for 30 min. The mixture was then subjected to heat shock for 1 min at 42°C. Next, 450µL LB broth was added to the mixture and incubated in a shaker for 2.5h at 37°C. This was scaled up to 5mL by adding a further 4.5mL warm LB broth (with ampicillin) and incubated in a shaker overnight at 37°C. The lid of the Falcon tube was left slightly open to allow gas exchange. From this starter culture, 1mL was added to 49mL warm LB broth (with ampicillin) in four separate Falcon tubes and incubated in a shaker overnight at 37°C.

2.6.3 Plasmid preparation

Following transformation and scale-up, the plasmid was isolated using a Genopure Maxiprep Kit (Roche). Competent cells were centrifuged in 50mL batches at 5,000 x g for 10 min at 4°C. The supernatant was discarded, and cell pellets were carefully resuspended in 12mL suspension buffer + RNAse followed by addition of 12mL lysis buffer. Falcons were gently inverted six-eight times and incubated for 3 min at RT. Next, 12mL pre-chilled neutralisation buffer was added, and Falcons were gently inverted again until a homogenous suspension was formed. Falcons were then

incubated on ice for 5 min for the formation of a flocculent precipitate. Lysates were cleared through filtration with 6mL equilibration buffer and loaded onto an equilibrated column, allowing it to empty by gravity flow. The column was washed twice with 16mL wash buffer and finally the plasmid was eluted in 15mL elution buffer pre-warmed to 50°C. 11mL isopropanol was added to the elution and immediately centrifuged at 10,000 x g for 90 min at 4°C. The plasmid pellet was then washed with 4mL 70% (v/v) ethanol and centrifuged again for 30 min at 10,000 x g at 4°C to re-pellet the plasmid. The ethanol was carefully removed, and the DNA was allowed to air dry at RT before being resuspended in 100-200µL sterile water.

2.6.3 Plasmid transfection

Transfection mixture of 0.5µg plasmid and 1µL Lipofectamine 2000 was prepared in in 50µL Optimem per well in a 6-well plate. Neuro2a cells were added to each well at a density of 200,000 cells/well made up in 450µL Optimem. Cells were incubated overnight, and a further 500µL Optimem was added to each well. After a total of 48h, RNA was extracted as previously described in section 2.4.1.

2.7 Brains for Dementia Research (BDR)

BDR is an initiative jointly funded by Alzheimer's society and Alzheimer's Research UK where >3,300 participants have pledged to donate their brain post-mortem to advance dementia research. BDR operates through five brain banks across the UK and provides brain tissue to applicants for approved research projects. Dr Keeley Brookes (Human Genetics Group) obtained brain tissue from BDR to perform several experiments, including RNA-seq on different regions of three control (non-demented) brains.

2.7.1 RNA extraction

Brain tissue was stored at -80°C. Before use, a cryoPREP Automated Dry Pulverizer (Covaris) system was used to break down tissue into small pieces. Following this, between 80-250mg was weighed out into an Eppendorf and 1mL TRI-reagent was added onto the tissue. The mixture was briefly vortexed homogenise the tissue, then 500µL chloroform was added to each sample. The Eppendorf was shaken vigorously by hand for 1 min, then centrifuged at 12,000 x g for 15 min at 4°C for phase separation. After taking the aqueous phase, the RNeasy Mini Kit (Qiagen) was used according to manufacturer's instructions to elute RNA in 20-25µL elution

buffer. RNA was quantified by spectrophotometer (Thermo-Scientific Nanodrop 2000) and quality was evaluated by Agilent Bioanalyzer.

2.7.2 Library preparation

University of Nottingham Deep Seq facility performed RNA-seq library preparation. Samples were treated for ribosomal RNA depletion, leaving mRNA and other non-coding RNA. Deep Seq then generated a barcoded stranded library for each sample using an Illumina Preparation Kit, according to the manufacturer`s instructions.

2.7.3 RNA-seq analysis

Sequencing was performed on the Illumina NextSeq500 and generated 75bp paired end reads, achieving coverage of 60 million reads per sample. Deep Seq then carried out read quality control, trimming and alignment to rRNA and tRNA for filtering purposes. Next, RNA-seq reads were mapped against reference genome GRCh37 (hg19) using TopHat and then counted using HTSeq. Differential expression analysis was done across brain regions using DESeq2 on genes filtered FPKM>1. Significance was reported with false discovery rate (FDR) and Bonferroni correction.

2.7.4 Splicing analysis

RNA-seq reads were mapped against reference genome GRCh38.83 using STAR and counted using HTSeq. Multivariate Analysis of Transcript Splicing (MATS) was run on python to compare splicing between the frontal cortex and cerebellum. Input genes were filtered for FPKM>1 and differential splicing events were filtered for FDR <10%. The resultant gene list with significantly different splicing events was ranked by -log(adjusted P value) and then entered in Webgestalt (Vanderbilt University) and Gene Set Enrichment Analysis (GSEA) with selection of the biological processed (non-redundant) gene ontology functional database.

2.8 Religious Orders Study and Memory and Aging Project (ROSMAP)

The Religious Orders Study (ROS) is a longitudinal cohort study of ageing and Alzheimer's disease (AD) run from Rush University, Chicago, Illinois. Participants were enrolled from >40 groups of religious orders across the US for longitudinal clinical analysis and brain donation for pathological study. The Memory and Aging Project (MAP) is a second longitudinal cohort study of chronic conditions of ageing run from Rush University. This study was designed to complement ROS by enrolling

volunteers from a wider range of backgrounds and socioeconomic status. AD status was determined by algorithm based on cognitive test performance and a series of clinical judgements made by a neuropsychologist and a clinician. Persons were categorised in three groups: no cognitive impairment, mild cognitive impairment, or diagnosis with dementia and/or AD (by standard definitions).

2.8.1 Data acquisition

Access to ROSMAP dataset was obtained through permissions from Rush Alzheimer's Disease Center and Sage Bionetworks based on submission of an *Intended Data Use Statement* and in accordance with the terms of access detailed in *Data Use Certificate*. This agreement was authorised by the contracts team in University of Nottingham's Research and Innovation Department for signed users of the dataset, namely myself and my supervisors.

2.8.2 Library preparation

The Broad Institute Genomics Platform performed RNA-seq library preparation for Rush Alzheimer's Disease Center. RNA samples were extracted using Qiagen miRNeasy kit and the RNase free DNase Set, then quantified by spectrophotometer (Nanodrop). Following poly-A selection (for mRNA), the library was constructed using the strand specific dUTP method (Levin *et al.*, 2010), followed by fragmentation and Illumina adapter ligation.

2.8.3 RNA-seq analysis

RNA-seq was completed with 582 samples that met quality and quantity thresholds, specifically RIN score >5 (Agilent Bioanalyzer) and >5µg RNA. Sequencing was performed on the Illumina HiSeq and generated 101bp paired-end reads, achieving coverage of 50 million reads per sample. The first 12 samples sequenced (2 males and 2 females across non-impaired, mild cognitive impaired, and Alzheimer's disease groups) were employed as a deep coverage reference at 150 million reads. RNA-seq reads were trimmed and aligned to rRNA for filtering purposes. Originally, Bowtie was used to align reads to reference genome GRCh37 (hg19) and RSEM was applied to estimate expression levels for all transcripts. However, in re-processing of the data, Picard SamToFastq function was used to covert bam files back to fastq files, which were then re-aligned to GRCh38 reference genome using STAR. Gene counts were also calculated by STAR in quantMode and transcript abundance was estimated using Sailfish (De Jager *et al.*, 2018). In this thesis, re-processed data was used for analysis.

2.8.4 Relation of transcript abundance to clinical and pathological outcomes

Clinical and pathological data for each individual in the RNA-seq database was pulled by matching identification numbers. Individuals were ranked according to expression of target transcript, e.g. CLK1 or SRPK1, and then grouped according to clinical outcome, i.e. no cognitive impairment, mild cognitive impairment, or Alzheimer's disease. Analysis of covariance was conducted on R with the covariates age and sex. Individuals were then matched for sex and age range (85-88yrs and 88-93yrs for males and females respectively). Next, individuals in the top and bottom quintile for target transcript expression were selected and compared for clinical diagnosis, Mini-Mental State Exam score, CERAD score, and tau burden (quantified by histopathology).

2.9 Statistical analyses

2.9.1 Differential gene expression

DESeq2 is a programme which quantifies gene counts and then corrects for dispersion, producing a p-value for differential expression. DESeq2 was used to determine genes that were differentially expressed between brain regions in three non-cognitively impaired individuals from the BDR dataset. EdgeR is a similar method for determining differential gene expression that was used in the ROSMAP dataset to determine AD-associated changes. RobiNA is a graphical user interface that was used to run EdgeR on gene counts filtered for expression in all individuals. This method was selected for two main reasons: (1) EdgeR is more suitable for larger datasets such as ROSMAP and is faster to run, (2) DESeq2 is more stringent than EdgeR and can filter out significantly different genes based on low expression. All p-values were adjusted with False Discovery Rate (FDR) to produce q-values.

2.9.2 Covariance

Analysis of Co-variance (ANCOVA) was conducted on R statistical software. This analysis blends analysis of variance and linear regression. The ANCOVA evaluates whether population means on the dependent variable are the same across levels of the independent variable whilst controlling for the effects of other factors that are known to covary with the dependent variable i.e., covariates. The ANCOVA determines what proportion of the dependent variable can be explained by the covariates and how much it is affected by the independent (i.e., categorical) variable. Output tables summarised in each relevant results section reporting the following values: (1) df = degrees of freedom, equal to (n-1) where n is the number

of samples or observations, (2) SS = sum of squares, (3) *F* = *F* value, i.e., the ratio of explained to unexplained variance, and (4) Pr(>*F*) = the p value.

2.9.3 Variance

Analysis of Variance (ANOVA) was conducted on GraphPad Prism. This analysis determines whether two or more population means are equal, i.e., it is an expansion of the t-test beyond two means. Post hoc analyses, adjusting for multiple comparisons, can explain observed variation further by identifying which population means differ from one another. For specific experimental parameters, refer to relevant results chapter and accompanying figure legends. All statistical tests used a p-value <0.05 as a threshold for rejecting the null hypothesis. Tukey's multiple comparison test was conducted post hoc and all figures display mean ± standard error of the mean, unless otherwise stated.

Chapter 3. Bioinformatic analyses of alternative splicing in Alzheimer's disease

3.1 Introduction

RNA-seq is a powerful tool that uses next-generation sequencing technology to study the whole transcriptome. The quantification of relative transcript expression levels in groups or case control cohorts enables comprehensive characterisation of potential phenotype (Wang *et al.*, 2009), and gene ontology enrichment analyses provide valuable insight into biological processes that have differential expression profiles (Yon Rhee *et al.*, 2008). RNA-seq studies comparing AD and control have revealed a variety of results for genes that are differentially expressed in the brain; not only does this reflect the complexity of AD aetiology, it also suggests that genes will show differential expression in some brain regions but not others (Chappell *et al.*, 2018).

3.1.1 The role of different brain regions in AD

The progression of AD can be pathologically assessed by the distribution of amyloid plaques and NFTs as they often spread following a particular sequence. Different brain regions are hierarchically involved in amyloid deposition, with the first phase being limited to the neocortex, sequentially followed by allocortical regions, the striatum and basal forebrain, and finally the cerebellum (Thal *et al.*, 2002). Similarly, accumulation of NFTs can be used for staging AD pathology, as their distribution increases from the trans-entorhinal region to the whole entorhinal cortex and other parts of the limbic system, then further to the isocortex (Braak & Braak, 1991). The onset of AD neuropathology is proceeded by transcriptional changes in the brain, most notably associated with synaptic dysfunction (Bossers *et al.*, 2010). Proteomic analyses have revealed distinct expressional changes in different regions of the AD brain; proteins related to synaptic transmission and lipid transport, key pathogenic pathways, were significantly altered in limbic regions, the temporal cortex and sensorimotor areas (Schonberger *et al.*, 2001). Since brain regions have different susceptibility or vulnerability to AD, studies have sought to characterise their differences and reveal expression profiles that may be neuroprotective. As one of the last areas to be affected by AD, the cerebellum is known to have a distinct pattern of protein expression which allows it to maintain normal function (Xu *et al.*, 2019). Indeed, the cerebellum was recently found to have enhanced capability for Aβ clearance compared to the cerebral cortex, which protects the cerebellum

against Aβ deposition and neuritic plaques (Shahnur *et al.*, 2021). Based on this profile, comparison of gene expression in cerebellum and cortical areas of the brain can serve as a model of molecular changes associated with the pathology of AD. Neuroprotective shifts in gene or isoform expression between the frontal cortex and the cerebellum may reveal potential changes to convert gene expression of AD patients back to a 'normal' asymptomatic profile (Chappell *et al.*, 2018).

There has been some criticism for the neglect of cerebellum in AD research, reporting the cerebellum as more than an "innocent bystander" in AD pathogenesis since (a) it does exhibit amyloid pathology, albeit delayed, (b) structural neuroimaging studies have reported the same pattern of cerebellar atrophy, from vermis and posterior lobe to the anterior lobe, and finally, (c) functional neuroimaging has linked reduced cerebellar activation with disease progression as well as cognitive reserve (Jacobs *et al.*, 2018). Critically, this collection of evidence does not connote causation but rather characterises later stages of AD pathogenesis. In this chapter, the cerebellum of cognitively "normal" donors was selected as control tissue to compare with the frontal cortex, an area more commonly associated with AD, and as a learning paradigm for me to investigate changes in gene expression. Although it is agreed that the cerebellum should not be ignored in studies of AD, considering the cerebellum as a control was justified by evidence that this region is protected from pathology, at least in early pre-clinical stages of AD, and thus provides insight to pathways for disease prevention.

3.1.2 Alternative splicing in AD

AD can be characterised by the deposition of insoluble protein aggregates; study of the human brain-insoluble proteome in AD has revealed that U1-70K and other U1 snRNPs spliceosome components are among proteins that accumulate in disease (Bai *et al.*, 2013). U1 snRNPs have been found to colocalise with NFTs and aggregate in AD brain, but not in other neurodegenerative disorders (including Parkinson's disease and frontotemporal dementia), and positively correlate with both amyloid and tau burden (Bai *et al.*, 2013; Hales *et al.*, 2016). This suggests that RNA splicing is implicated in AD pathogenesis, but there have only been a limited number of AD studies that have investigated genome-wide changes in AS. Nonetheless, the available literature does link AS to AD through two main themes; (1) differential expression of trans-acting factors that are known to regulate pre-mRNA processing, such as RNA-binding proteins RBFOX1 (Alkallas *et al.*, 2017) or hnRNPA2/B1 (Berson *et al.*, 2012), and (2) differential splicing of AD-associated genes that are known to contribute amyloid or tau pathology (Johnson *et al.*, 2018;

Biamonti *et al.*, 2019). Pathway analysis of differential proteomic expression in AD has indicated that enriched modules comprising RNA binding proteins are mostly correlated with tau burden rather than amyloid pathology (Johnson *et al.*, 2018). Indeed, inducing overexpression of tau alone has been shown to replicate some of the splicing changes observed in AD; 11 out of 42 genes that are differentially spliced when tau is overexpressed overlap with differentially spliced genes that were associated with AD in the ROSMAP dataset (Raj *et al.*, 2018). Nonetheless, AS can still be implicated in amyloid (Aβ) pathology through altered presenilin activity; it was found that exclusion of exons four and five of *PSEN1* and *PSEN2* respectively causes altered processing of APP and consequently increases Aβ production and accumulation (Love *et al.*, 2015). Altogether, this highlights that AS could play an important role in the development of AD.

3.1.3 The regulatory role of splicing kinases

AS is regulated by splicing kinases, including SRPKs, CLKs and DYRKs, through phosphorylation of SR proteins. The SRPK family consists of three proteins, SRPK1-3, and while SRPK1 is ubiquitously expressed throughout the body, SRPK2 and SRPK3 have limited expression in the brain and muscle tissue respectively (Kuroyanagi *et al.*, 1998; Nakagawa *et al.*, 2005). Most research on SRPK1 is focused on alternative splicing in cancer (Mavrou *et al.*, 2015; Czubaty & Piekiełko-Witkowska, 2017), but as a brain-specific kinase, SRPK2 activity has been linked with cognitive decline in AD (Hong *et al.*, 2012). The cdc-like (CLK) family consists of four proteins, CLK1-4, with the ability to auto-phosphorylate at tyrosine residues as well as phosphorylate substrates at serine/threonine residues (Nayler *et al.*, 1997). CLKs play a unique role in regulation of SR protein conformation and activation since, in contrast to SRPKs, they do not exclusively phosphorylate serine dipeptides with arginine, but also serine dipeptides with proline (Keshwani *et al.*, 2015). In relation to AD, all four CLKs have been shown to affect tau splicing (Hartmann *et al.*, 2001), and CLK1 in particular has been proposed as a novel target for AD therapeutics (Jain *et al.*, 2014). Dyrk1A, another major splicing kinase, is a member of the DYRK family of proline-directed kinases, which plays an important role in neurodevelopment (Feki & Hibaoui, 2018). Dyrk1A is commonly associated with Down's Syndrome, but it has also been implicated in AD (Arbones *et al.*, 2019) as well as AD-type dementia in individuals with Down's Syndrome (Wisniewski *et al.*, 1985). In this chapter, expression of splicing kinases is related to the pathology and diagnosis of AD in order to characterise the regulation of AS in disease. This is

particularly interesting because splicing kinases could potentially be targeted by AD therapeutics to modulate kinase activity and provide neuroprotection.

3.1.4 Hypotheses

Using RNA-seq data from the BDR and ROSMAP cohort, I aimed to test the following hypotheses:

1. The cerebellum and frontal cortex have differential expression profiles that affect relative susceptibility to AD dementia.
2. The cerebellum and frontal cortex have differential splicing patterns that affect relative susceptibility to AD dementia.
3. In the ROSMAP cohort, individuals with clinical and pathological diagnosis of AD will have a differential expression profile to age-matched individuals with no cognitive impairment.
4. In the ROSMAP cohort, comparison of individuals with low and high expression of splicing kinases will reveal increased likelihood for AD pathology and cognitive decline.

3.2 Methods

The data analysed in this chapter were obtained from BDR and Rush University. Unless stated otherwise, analysis was performed on Excel or R and figures were produced using GraphPad Prism.

3.2.1 BDR dataset

I received data from an RNA-seq experiment conduced on tissue kindly donated to Brains for Dementia Research (BDR). This included different brain regions from three individuals who did not have cognitive impairment or AD, as described in section 2.7. Dr Keeley Brookes shared this data with me after publishing on differential expression between brain regions (Chappell *et al.*, 2018). In this chapter, I performed an independent investigation of expression and splicing events in the frontal cortex and cerebellum, with the help of Prof Nigel Mongan who performed rMATS analysis. A more detailed description of RNA-seq methods can be found in Chapter 2.

3.2.2 ROSMAP dataset

The Religious Orders Study (ROS) and the Memory and Ageing Project (MAP) were conducted by Rush University, Chicago, Illinois (Wilson *et al.*, 2012), as described in section 2.8. RNA-seq data, clinical data and pathological data was collected from the dorsolateral prefrontal cortex (DLPFC) of 636 donor and patient samples. I requested access to the ROSMAP dataset through the Rush Alzheimer's Disease Centre (RADC) and synapse portal. I used transcript counts as a measure of gene expression for all analyses presented in this chapter. Clinical and pathological data was matched to transcriptional analysis through conversion of project ID, which enabled sorting of data into control, MCI and AD groups. A more detailed description of bioinformatic methods can be found in Chapter 2.

3.2.3 Clinical and pathological outcomes

Diagnosis of Alzheimer's disease was considered to be the primary outcome in this study; this was determined by a three-stage process (1) computer scoring of 19 cognitive tests using a decision tree to mimic clinical judgement, (2) review of clinical impairment ratings and other information by a neuropsychologist to make clinical judgement regarding the presence of impairment or dementia, and (3) review of all data and examination of the participant by a clinician to render final diagnostic classification. For the purposes of my study, I excluded persons diagnosed with

another primary cause of dementia and no clinical evidence of Alzheimer's disease. Other persons were grouped in the following three categories:

- Control group: diagnosed as having no cognitive impairment.
- MCI: diagnosed with Mild Cognitive Impairment and possibly another contributing condition.
- AD: diagnosed with Alzheimer's disease and possibly another contributing condition.

Additionally, expression level of target genes was also related to outcomes from Mini-Mental State Exam (MMSE) score, Consortium to Establish a Registry for Alzheimer's Disease (CERAD) score, and tau burden. The MMSE is widely used standardised screening measure of dementia severity, scored out of 30 items. According to clinical evaluation, persons with scores <24 are considered to have no cognitive impairment, scores between 19-24 (inclusive) were considered to indicate mild cognitive impairment, and scores <19 indicated moderate to severe cognitive impairment. The CERAD score provides a neuropathologic diagnosis of AD based on density of neuritic plaques in one or more neocortical regions and is blinded to clinical data. The diagnosis was made in four categories: no AD, possible AD, probable AD, and definite AD (Mirra *et al.*, 1991). As an estimate of tau burden, neurofibrillary tangles were quantified by immunohistochemistry (AT8 antibody specific to abnormally phosphorylated tau) and average cortical density was determined by systemic sampling of eight different regions (Bennett *et al.*, 2018).

3.2.4 Statistical Analysis

For analysis of differential gene expression, FDR adjusted p-values were produced by DESeq2 or EdgeR. In the analysis of splicing events, FDR adjusted p-values were produced by rMATS analysis. Analysis of Covariance (ANCOVA) was performed on R. Power analyses were conducted using GPower 3.1. All other statistical tests, including Chi-Square test for occurrence of AD in different groups, were performed on GraphPad Prism.

3.3 Results

3.3.1 Differential gene expression in brain regions

In normal brain, brain regions have distinct gene expression profiles. To develop an understanding of the variation in expression and splicing between two regions, and to learn the bioinformatics pathway, I determined to assess differential expression between the cerebellum and frontal cortex. RNA-seq was performed on paired RNA samples extracted from normal human frontal cortex and cerebellum. Following the analysis pipeline described in Chapter 2, expression was quantified using the programme DESeq2, which quantifies gene counts and then corrects for dispersion, producing a p-value for differential expression. Values were adjusted with False Discovery Rate and $q<0.01$ was considered significant. Out of a total 21820 genes, 6945 were differentially expressed between the frontal cortex and cerebellum. This subset of differentially expressed genes was further filtered for logFC>2 and scored by "-log(q-value)*sign(logFC)". This ranked gene list was then used as an input for GSEA to quantify enrichment of biological processes between these two brain areas. Compared to the frontal cortex, the cerebellum showed significantly lower expression of genes related to cognition; this is unsurprising considering their respective functions. Additionally, GPCR and serotonin signalling pathways were significantly downregulated in the cerebellum. Although not to a significant degree, processes of DNA modification and repair were identified among genes that were upregulated in the cerebellum, annotated in Table 3.3.1 below. The differentially expressed genes within these GO pathways are listed in Appendix Table 7.3.2 and enrichment plots for GSEA analysis can be found in Appendix Figure 7.3.1.

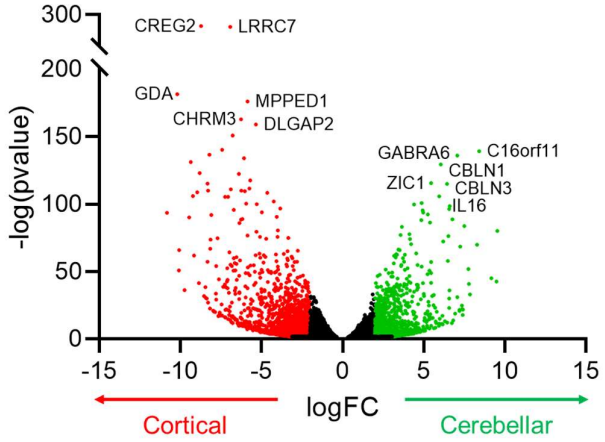


Figure 3.3.1.1 Volcano plot reveal genes that are differentially expressed between cerebellum and frontal cortex in normal brain (shown in red and green) by filtering for FDR adjusted p-value<0.01 and of $Log_2FC>2$. Genes that have smallest p-value are labelled on graph.

GO: gene set	GO: description	Enrichment Score (ES)	Normalised ES	P-value	FDR	Size	Edge Size
0055088	lipid homeostasis	0.570	1.757	<1.0E-6	0.652	37	10
0006289	nucleotide-excision repair	0.474	1.490	0.058	0.774	32	14
0006298	mismatch repair	0.720	1.603	0.056	0.793	7	5
0006304	DNA modification	0.561	1.548	0.044	0.812	20	12
0032200	telomere organization	0.380	1.260	0.160	0.807	44	13
0007187	**GPCR signalling pathway, coupled to cyclic nucleotide**	-0.694	-2.165	<1.0E-6	<1.0E-4 (*)	89	38
0050890	**cognition**	-0.661	-2.061	<1.0E-6	0.004 (*)	102	44
0007210	**serotonin receptor signalling pathway**	-0.852	-2.042	<1.0E-6	0.006 (*)	17	12
0007200	**PLC-activating GPCR signalling pathway**	-0.760	-1.997	<1.0E-6	0.013 (*)	31	15
0099072	regulation of postsynaptic membrane neurotransmitter receptor levels	-0.732	-1.891	0.003	0.058	28	11

Table 3.3.1 Top 10 up- and down-regulated GO pathways identified from genes differentially expressed in cerebellum compared to the frontal cortex in normal brain. Genes were filtered for FDR adjusted p<0.01 prior to GSEA using WebGestalt. Significantly enriched pathways in Biological processes database are shown with FDR (*) and in description in **bold** (normalised enrichment q<0.05). Up-regulated pathways shown in green, down-regulated pathways shown in orange.

To begin to explore splicing in these brain areas, I next quantified the expression of SR proteins known to regulate AS. Using hierarchical clustering on iDEP.91 (see Figure 3.3.1.2), it was found that some SR proteins, including SRSF1, 3, 5, 6, 10 and 11, show higher expression in the cerebellum compared to the frontal cortex. Other SR proteins, such as SRSF4 and 8, showed similar expression in both areas. This indicates differential control of splicing in the cerebellum.

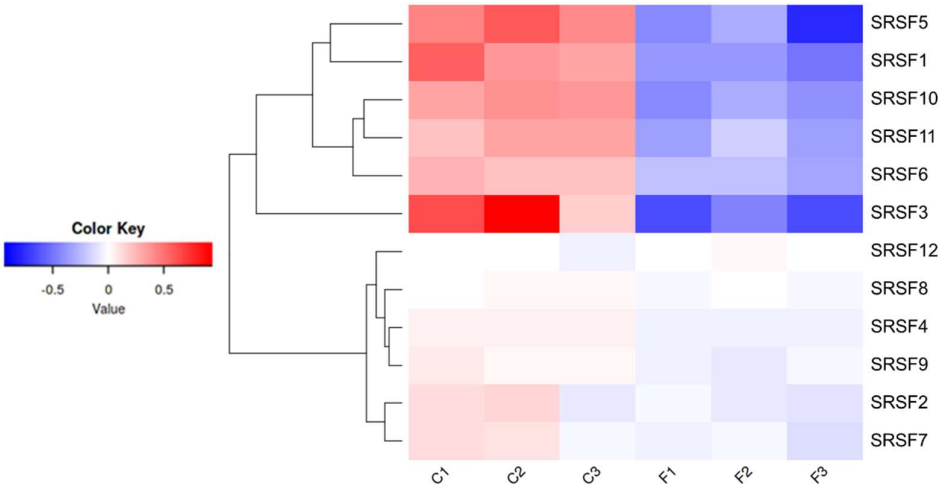


Figure 3.3.1.2 Clustered heat map illustrating the differential expression of splicing factors in frontal cortex and cerebellum of control brain. Colour key identifies relative change in transcript expression for each splicing factor. Produced on iDEP.91 using Transcripts Per Million (TPM). F1-3 are frontal cortex and C1-3 are matched cerebellum RNA samples from three BDR donors.

3.3.2 Differential AS events in brain regions

Multivariate Analysis of Transcript Splicing (rMATS) was used to assess alternative splicing events in the cerebellum and frontal cortex. The statistical model of MATS calculates FDR corrected p-values for the difference in the isoform ratio of a gene based on five different types of splicing events: skipped exons, retained introns, mutually exclusive introns, alternative 3' and 5' splice site selection. MATS identified a variety of genes that are differentially spliced in the two brain areas (FDR p-value<0.05). A subset of these genes that have above-threshold expression (FPKM>1) were used as input for enrichment and over-representation analyses to identify biological processes related to the altered splicing pattern of cerebellum and frontal cortex. This included 4999 skipped exons, 1570 retained introns, 1124 mutually exclusive exons, 830 alternative 5' splice sites and 1005 alternative 3' splice sites. GSEA, as previously described, produces up- or down-regulated biological processes based on a ranked gene list. Over representation analysis (ORA) is another method of enrichment analysis, but unlike GSEA, it does not utilise ranking of genes nor directional fold change. Instead, ORA simply determines the overlap between reference genes of interest (i.e., in gene ontology pathways) and the input gene list to calculate enrichment of biological processes and their statistical significance (Tokar *et al.*, 2020).

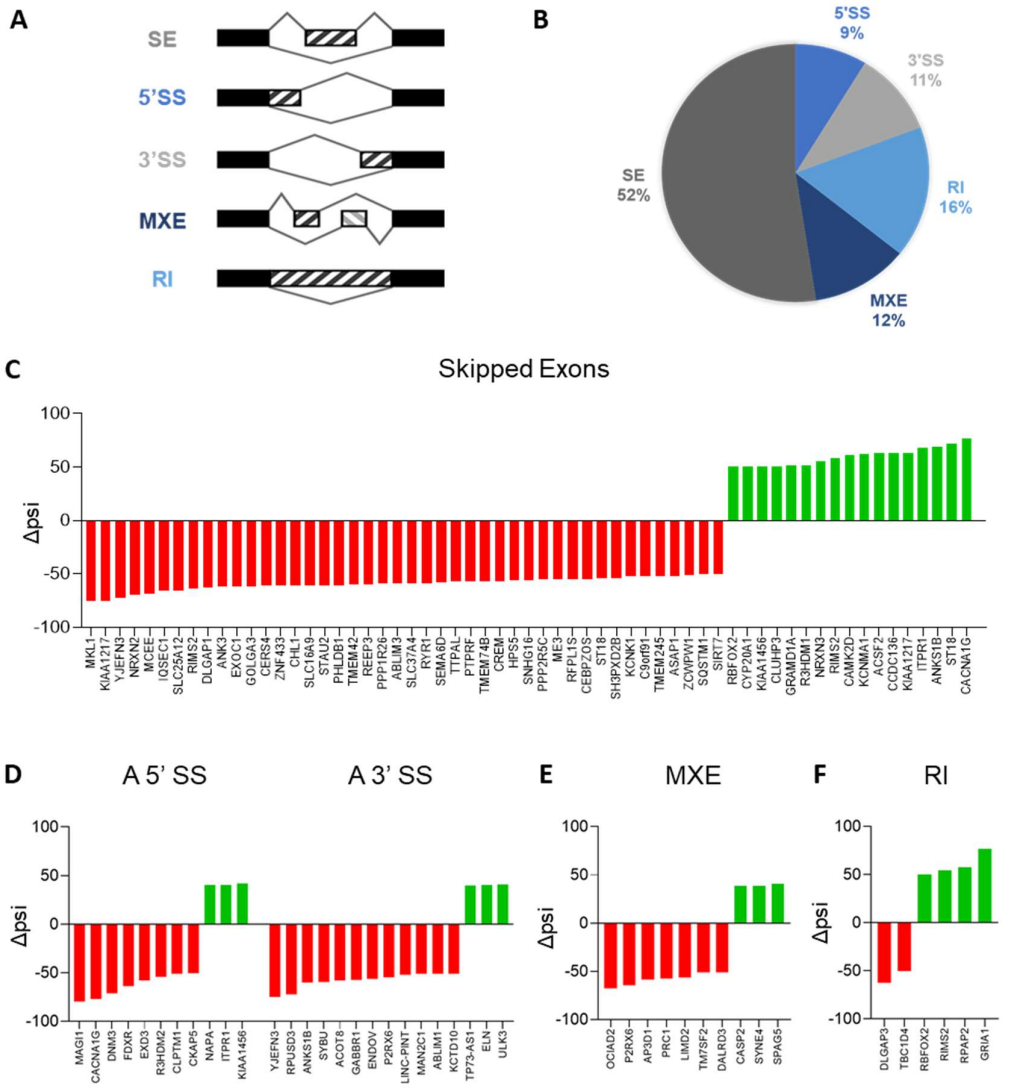


Figure 3.3.2.1 The differential splicing of genes in cerebellum and frontal cortex. **A** Schematic diagram for the splicing events detected and analysed by rMATS. **B** Pie chart representing the splicing events that significantly differ between brain regions. **C** Genes which show >50% difference in exon skipping between the frontal cortex and cerebellum: Genes which have increased skipped exons in frontral cortex are shown in red while genes with more skipped exons in the cerebellum are shown in green. **D** Selection of genes which show greatest difference in selection of 5' and 3' splice sites between frontal cortex and cerebellum. **E** Selection of genes which show greatest difference in mutually exclusive exons between frontal cortex and cerebellum. **F** Genes which show >50% difference in intron rentention between the frontal cortex and cerebellum. All genes filtered for FDR<0.05 and FPKM>1. SE= skipped exons, RI= retained introns, MXE= mutually exclusive exons, A 5'SS= alternative 5' splice site, A 3'SS= alternative 3' splice site. ΔPSI = change in difference spliced in.

Skipped exons were the most common differential splicing event that occurred between the cerebellum and frontal cortex. Differentially spliced genes were ranked for exon skipping by "-log(q-value)*sign(ΔPSI)" and then input for GSEA to quantify enrichment of biological processes. The GO pathway for "vesicle-mediated transport to plasma membrane" was significantly enriched with genes that showed significantly reduced exon skipping events in the cerebellum compared to the frontal cortex. Otherwise, processes related to exocytosis and signal release were also enriched, but not to a significant degree, as shown in Table 3.3.2.1 below. Enriched genes within each GO pathway can be found in Appendix Table 7.3.3.

GO: gene set	GO: description	Enrichment Score (ES)	Normalised ES	P-value	FDR	Size	Edge Size
0019932	second-messenger-mediated signaling	0.211	1.227	0.114	0.796	59	10
0010038	response to metal ion	0.209	1.211	0.205	0.800	59	15
0007059	chromosome segregation	0.207	1.172	0.216	0.814	53	12
0051604	protein maturation	0.212	1.135	0.283	0.815	40	8
0007187	GPCR signalling pathway, coupled to cyclic nucleotide	0.269	1.152	0.291	0.819	19	3
0098876	**vesicle-mediated transport to the plasma membrane**	-0.651	-2.131	<1.0E-5	0.008 (*)	22	12
0017156	calcium ion regulated exocytosis	-0.436	-1.709	0.004	0.323	52	22
0009896	positive regulation of catabolic process	-0.416	-1.710	<1.0E-5	0.349	78	42
0023061	signal release	-0.384	-1.655	0.003	0.371	100	38
0048013	ephrin receptor signalling pathway	-0.495	-1.688	0.009	0.372	26	10

Table 3.3.2.1 Top 10 GO pathways identified from genes that have significantly more or less skipped exons in cerebellum compared to the frontal cortex of normal brain. Genes were filtered for expression (FPKM>1) and FDR adjusted p<0.01 prior to GSEA using WebGestalt. Significantly enriched pathways in Biological processes database are shown with FDR (*) and in description in **bold** (normalised enrichment q<0.05).

Over-representation analysis (ORA) also identified GO pathways for vesicle-mediated transport and synaptic function to be enriched in genes with differential exon skipping between cerebellum and frontal cortex. Furthermore, neurone-specific axon and dendrite development genes were highlighted to have differential exon skipping in these brain areas. The top 10 significantly enriched processes are listed in Table 3.3.2.2 below and overlap genes from dataset can be found in Appendix Table 7.3.4.

GO: gene set	GO: description	Size	Overlap	Enrichment	P-value	FDR
0099003	vesicle-mediated transport in synapse	203	73	2.55 (*)	3.6E-15	3.0E-12
0099504	synaptic vesicle cycle	193	70	2.57 (*)	8.1E-15	3.4E-12
0010975	regulation of neuron projection development	475	128	1.91 (*)	6.1E-14	1.7E-11
0051648	vesicle localization	305	93	2.16 (*)	8.2E-14	1.7E-11
0051656	establishment of organelle localization	494	130	1.87 (*)	2.6E-13	4.4E-11
0016358	dendrite development	219	71	2.30 (*)	3.0E-12	3.7E-10
0099177	regulation of trans-synaptic signaling	417	112	1.91 (*)	3.0E-12	3.7E-10
0031346	positive regulation of cell projection organization	365	100	1.94 (*)	1.3E-11	1.4E-09
0050808	synapse organization	385	103	1.90 (*)	3.0E-11	2.8E-09
0061564	axon development	490	121	1.75 (*)	1.6E-10	1.4E-08

Table 3.3.2.2 Top 10 biological processes identified by ORA of genes that show significantly differential exon skipping between the cerebellum and frontal cortex. Significance shown by (*) next to enrichment score.

NRXN2 is among the genes which showed differential exon skipping between the frontal cortex and cerebellum, and it is a member of several GO pathways for synaptic function, including synapse organisation and neurotransmitter transport. This alternative splicing event was explored on Integrative Genomics Viewer (IGV), as seen in Figure 3.3.2.2. In all three individuals, there was significantly greater exon 20 junction coverage in the cerebellum compared to the frontal cortex. This suggests that *NRXN2* expression is differentially regulated in these brain areas, contributing to distinction of the cerebellar synaptic profile.

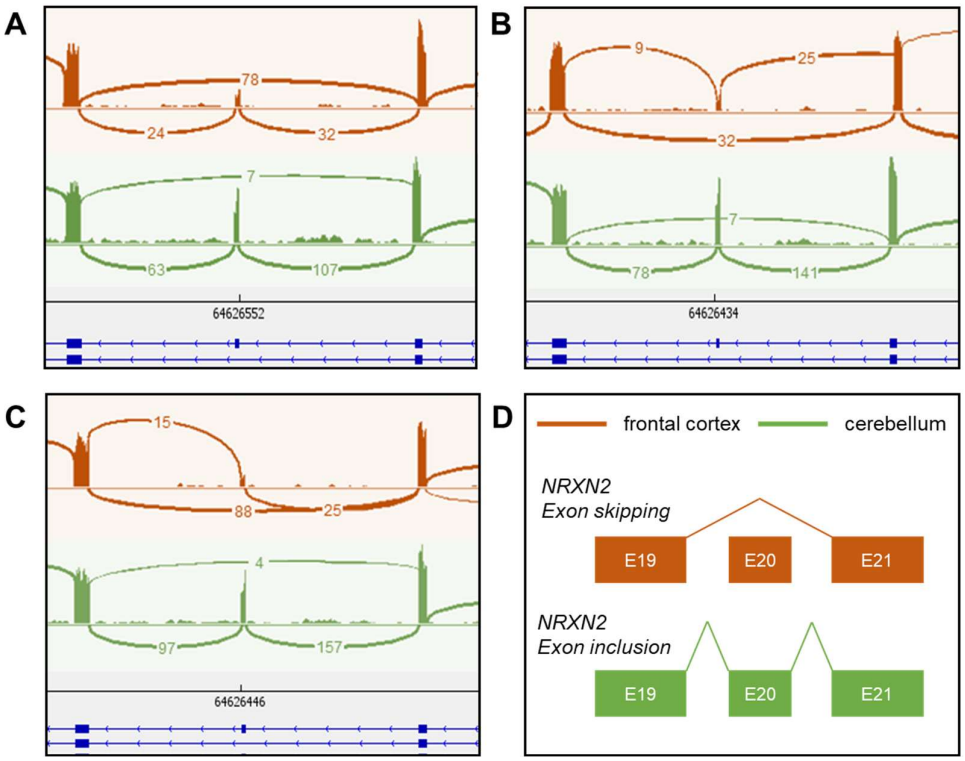


Figure 3.3.2.2 Synaptic gene *NRXN2* exon 20 is alternatively spliced in cerebellum and frontal cortex of normal brain. **A B C** Sashimi plots displaying relative inclusion of coding exon 20 in the cerebellum (red) and frontal cortex (black) in three individuals, respectively. Numbers on plot indicate exon coverage, as determined from sorted aligned bam files, visualised on IGV software. The exon is located in chromosome 11 between start position 64,626,463 and end position 64,626,552 on reference genome hg38. **D** Schematic for alternative splicing at *NRXN2* exon 20.

Intron retention was the next most frequent type of differential splicing event quantified between brain areas. As before, differentially spliced genes were ranked for intron retention by "-log(q-value)*sign(ΔPSI)" and then input for GSEA to quantify enrichment of biological processes. No GO pathways were significantly enriched for differential intron retention; nonetheless, the top 10 identified pathways are shown in Table 3.3.2.3 below. There is a trend of increased cerebellar intron retention in genes related to lipid metabolism and membrane fusion, while genes related to glutamate signalling and post-translation protein modification show reduced intron retention in the cerebellum. Differentially spliced genes within these GO pathways can be found in Appendix Table 7.3.5.

GO: gene set	GO: description	Enrichment Score (ES)	Normalised ES	P-value	FDR	Size	Edge Size
0032103	positive regulation of response to external stimulus	0.711	2.095	0.005	0.078	6	6
0048284	organelle fusion	0.318	0.992	0.422	0.893	7	7
0061025	membrane fusion	0.213	0.839	0.693	0.879	10	10
0006638	neutral lipid metabolic process	0.385	1.121	0.255	0.882	6	6
0032606	type I interferon production	0.422	1.082	0.342	0.884	5	5
0007215	glutamate receptor signalling pathway	-0.684	-1.513	0.029	0.594	5	3
0018209	peptidyl-serine modification	-0.445	-1.427	0.072	0.583	21	15
0006732	coenzyme metabolic process	-0.440	-1.508	0.033	0.579	29	14
0043687	post-translational protein modification	-0.418	-1.412	0.072	0.594	29	11
0006898	receptor-mediated endocytosis	-0.481	-1.434	0.063	0.598	15	7

Table 3.3.2.3 Top 10 GO pathways identified from genes that have significantly more or less retained introns in cerebellum compared to the frontal cortex of normal brain. Genes were filtered for expression (FPKM>1) and FDR adjusted p<0.01 prior to GSEA using WebGestalt. No pathways in Biological processes database were significantly enriched (normalised enrichment q>0.05).

Over-representation analysis revealed biological processes related to the genes which have a significantly different level of intron retention between the cerebellum and frontal cortex. The annotation of these processes, listed in Table 3.3.2.4, indicates an emphasis on protein production, translation and localisation, as well as protein catabolism. A list of overlap genes from dataset can be found in Appendix Table 7.3.6.

GO: gene set	GO: description	Size	Overlap	Enrichment	P-value	FDR
0006413	translational initiation	192	36	3.49 (*)	3.7E-11	3.2E-08
0070972	protein localization to endoplasmic reticulum	137	27	3.67 (*)	3.4E-09	1.4E-06
0010498	proteasomal protein catabolic process	449	55	2.28 (*)	8.0E-09	1.8E-06
0048193	Golgi vesicle transport	366	48	2.44 (*)	8.4E-09	1.8E-06
0006605	protein targeting	412	50	2.26 (*)	5.3E-08	9.0E-06
0042176	regulation of protein catabolic process	370	44	2.22 (*)	5.9E-07	8.4E-05
0022613	ribonucleoprotein complex biogenesis	440	49	2.07 (*)	9.7E-07	1.2E-04
0090150	protein localization to membrane	313	38	2.26 (*)	2.1E-06	2.2E-04
0006401	RNA catabolic process	341	40	2.19 (*)	2.7E-06	2.6E-04
0034976	response to endoplasmic reticulum stress	268	33	2.29 (*)	7.3E-06	5.3E-04

Table 3.3.2.4 Top 10 biological processes identified by ORA of genes that show significantly differential intron retention between the cerebellum and frontal cortex. Significance shown by (*) next to enrichment score.

Next, genes that showed a significant difference in splicing of mutually exclusive exons were input in ORA to reveal further biological processes affected by AS between the cerebellum and frontal cortex of normal brain. Similar to results from differential exon skipping, GO pathways for synapse organisation and activity, as well as calcium-regulated exocytosis and neurotransmitter transport, were significantly enriched in this gene list. The top 10 GO pathways are shown in Table 3.3.2.5, and the overlap genes from the dataset can be found in Appendix Table 7.3.7.

GO: gene set	GO: description	Size	Overlap	Enrichment	P-value	FDR
0050808	synapse organization	385	47	3.67 (*)	9.5E-15	8.1E-12
0099504	synaptic vesicle cycle	193	27	4.20 (*)	2.6E-10	7.5E-08
0050803	regulation of synapse structure or activity	221	29	3.94 (*)	2.7E-10	7.5E-08
0099177	regulation of trans-synaptic signalling	417	39	2.81 (*)	5.8E-09	1.2E-06
0051648	vesicle localization	305	32	3.15 (*)	9.3E-09	1.6E-06
0010975	regulation of neuron projection development	475	40	2.53 (*)	6.9E-08	8.9E-06
0099003	vesicle-mediated transport in synapse	203	24	3.55 (*)	7.3E-08	8.9E-06
0017156	calcium ion regulated exocytosis	152	20	3.95 (*)	1.6E-07	1.7E-05
0006836	neurotransmitter transport	268	27	3.03 (*)	3.1E-07	2.9E-05
0043087	regulation of GTPase activity	472	38	2.42 (*)	4.6E-07	3.9E-05

Table 3.3.2.5 Top 10 biological processes identified by ORA of genes that show significantly differential splicing of mutually exclusive exons in the cerebellum and frontal cortex. Significance shown by (*) next to enrichment score.

Finally, MATS analyses use of alternative 5' and 3' splice sites in RNA-seq data. As previously described, genes that showed significantly differential selection of 5' splice sites were input in ORA to identify GO pathways related to this AS event. Among the most enriched GO pathways were microtubule-dependent biological processes, including anchoring, transport, intracellular organisation, and neuronal projection. Otherwise, genes for membrane docking also showed differential 5' splice site selection in these two areas of normal brain. The top 10 significantly enriched processes are displayed in Table 3.3.2.6 and overlap genes from the dataset are listed in Appendix Table 7.3.8.

GO: gene set	GO: description	Size	Overlap	Enrichment	P-value	FDR
0034453	microtubule anchoring	26	7	7.24 (*)	3.4E-05	7.2E-03
0030705	cytoskeleton-dependent intracellular transport	170	20	3.16 (*)	5.3E-06	4.5E-03
0031023	microtubule organizing center organization	134	15	3.01 (*)	1.4E-04	1.7E-02
0022406	membrane docking	177	18	2.73 (*)	1.1E-04	1.5E-02
0031503	protein-containing complex localization	280	26	2.50 (*)	1.8E-05	7.2E-03
0006401	RNA catabolic process	341	29	2.29 (*)	3.1E-05	7.2E-03
0007018	microtubule-based movement	271	23	2.28 (*)	2.1E-04	1.8E-02
0051656	establishment of organelle localization	494	36	1.96 (*)	9.5E-05	1.5E-02
0006091	generation of precursor metabolites and energy	469	34	1.95 (*)	1.6E-04	1.7E-02
0010975	regulation of neuron projection development	475	34	1.92 (*)	2.1E-04	1.8E-02

Table 3.3.2.6 Top 10 biological processes identified by ORA of genes that show significantly differential 5' splice site selection between the cerebellum and frontal cortex. Significance shown by (*) next to enrichment score.

The ORA of genes with differential 3' splice selection revealed GO pathways for neurone-specific biological processes such as synaptic function. These included pathways seen in ORA of skipped or mutually exclusive exons, namely synaptic vesicle cycle, vesicle-mediated transport in the synapse, vesicle localisation, and regulation of trans-synaptic signalling. It also includes related GO pathways such as calcium-regulated exocytosis and the exocytosis process. Altogether, this identified AS of genes is important for differential synaptic function in the cerebellum and frontal cortex. The top 10 enriched biological processes from genes with differential 3' splice site selection are displayed in Table 3.3.2.7, and the overlap gene list from this dataset can be found in Appendix Table 7.3.9. The GO pathways enriched by multiple splicing events are summarised in Figure 3.3.2.3: some genes within these pathways showed significantly different exon skipping, mutually exclusive exons, and/or 3' splice site selection.

GO: gene set	GO: description	Size	Overlap	Enrichment	P-value	FDR
0051656	establishment of organelle localization	494	53	2.53 (*)	4.4E-10	3.7E-07
0051648	vesicle localization	305	37	2.86 (*)	8.2E-09	2.6E-06
0099003	vesicle-mediated transport in synapse	203	29	3.37 (*)	9.1E-09	2.6E-06
0099504	synaptic vesicle cycle	193	26	3.18 (*)	1.8E-07	3.2E-05
1990778	protein localization to cell periphery	301	34	2.66 (*)	1.9E-07	3.2E-05
0060627	regulation of vesicle-mediated transport	499	47	2.22 (*)	2.5E-07	3.5E-05
0017156	calcium ion regulated exocytosis	152	22	3.41 (*)	4.5E-07	5.4E-05
0099177	regulation of trans-synaptic signalling	417	39	2.21 (*)	3.1E-06	3.3E-04
0010975	regulation of neuron projection development	475	42	2.09 (*)	5.5E-06	5.2E-04
0140029	exocytic process	84	14	3.93 (*)	1.1E-05	9.1E-04

Table 3.3.2.7 Top 10 biological processes identified by ORA of genes that show significantly differential 3' splice site selection between the cerebellum and frontal cortex. Significance shown by (*) next to enrichment score.

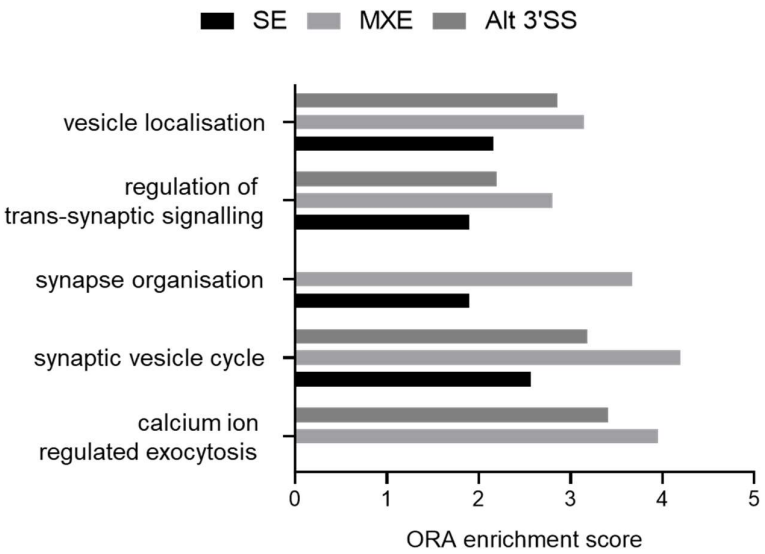


Figure 3.3.2.3 Summary of GO pathways for synaptic function enriched by ORA of alternatively spliced genes. The listed GO pathways were significantly differential skipped exons (SE), mutually exclusive exons (MXE) and alternative 3' splice site selection (Alt 3'SS).

The *EXOC1* gene, encoding a core component of the exocyst complex, showed differential splicing in between the frontal cortex and cerebellum. *EXOC1* is a member of the GO pathway for "vesicle-mediated transport to the plasma membrane" which was enriched by ORA of genes with differential exon skipping events. It is known to be involved in neurotransmitter relay as well as regulation of IP_3R activity and calcium signalling (Park *et al.*, 2015). Investigation of *EXOC1* exon coverage on IGV shows greater exon 10 inclusion in the cerebellum of three individuals. This indicates that regulation of *EXOC1* splicing is different in these brain regions, as presented below by the sashimi plots in Figure 3.3.2.4.

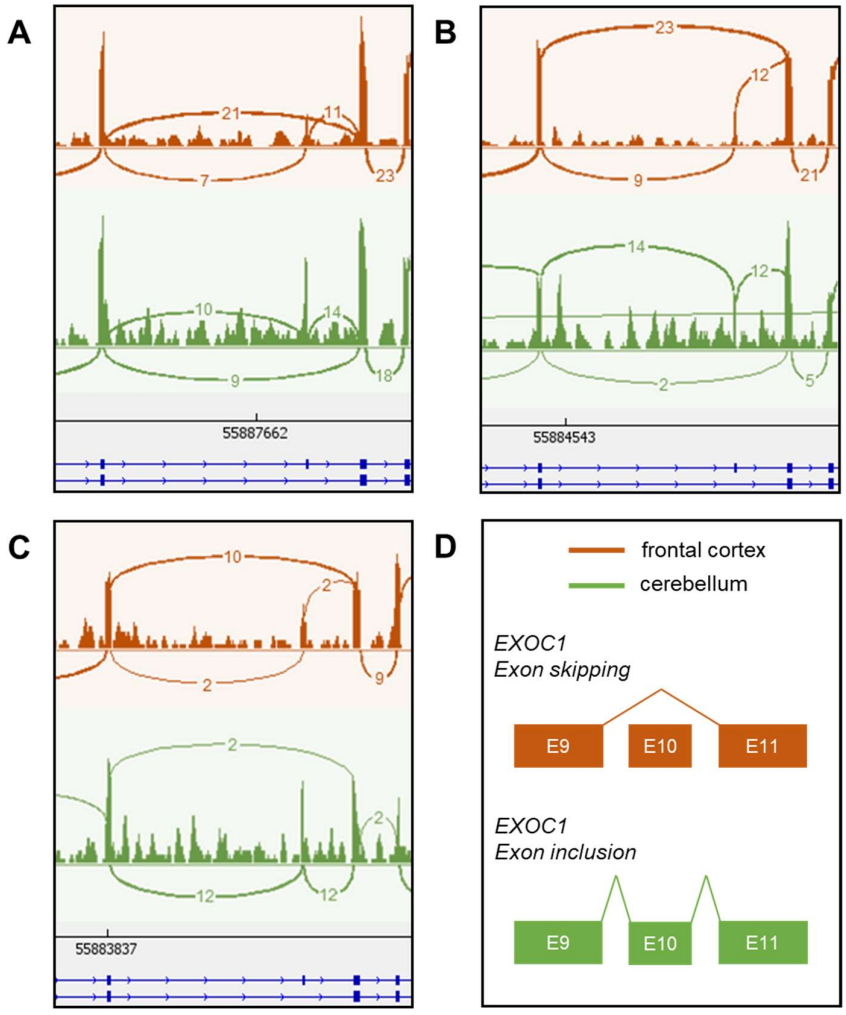


Figure 3.3.2.4 Vesicle trafficking gene *EXOC1* is alternatively spliced in cerebellum and frontal cortex of normal brain. Sashimi plots display relative inclusion of coding exon 11 in the cerebellum (red) and the frontal cortex (black) in three individuals without cognitive impairment. Numbers on plot indicate exon coverage, as determined from sorted aligned bam files, visualised on IGV software. The exon is located in chromosome 4 between start position 55,888,888 and end position 55,888,932 on reference genome hg38.

The *ITPR1* gene is a member of GO pathways for calcium signalling and calcium-regulated exocytosis, which were significantly enriched by ORA of differentially spliced genes. *ITPR1* encodes the intracellular receptor IP3R, which is a ligand-gated ion channel that mediates mobilisation of intracellular Ca^{2+} stores when activated by elevation of cytosolic IP_3 (Berridge, 2009). In addition to differential use of mutually exclusive exons and 3' splice sites, *ITPR1* also showed significantly differential exon 10 inclusion. As visualised by IGV in Figure 3.3.2.5 below, the cerebellum of all three individuals showed preferential exon 10 skipping whilst the frontal cortex showed greater exon 10 inclusion. AS of *ITRP1* in these brain regions supports the discovery of differential regulation of calcium signalling in these brain regions.

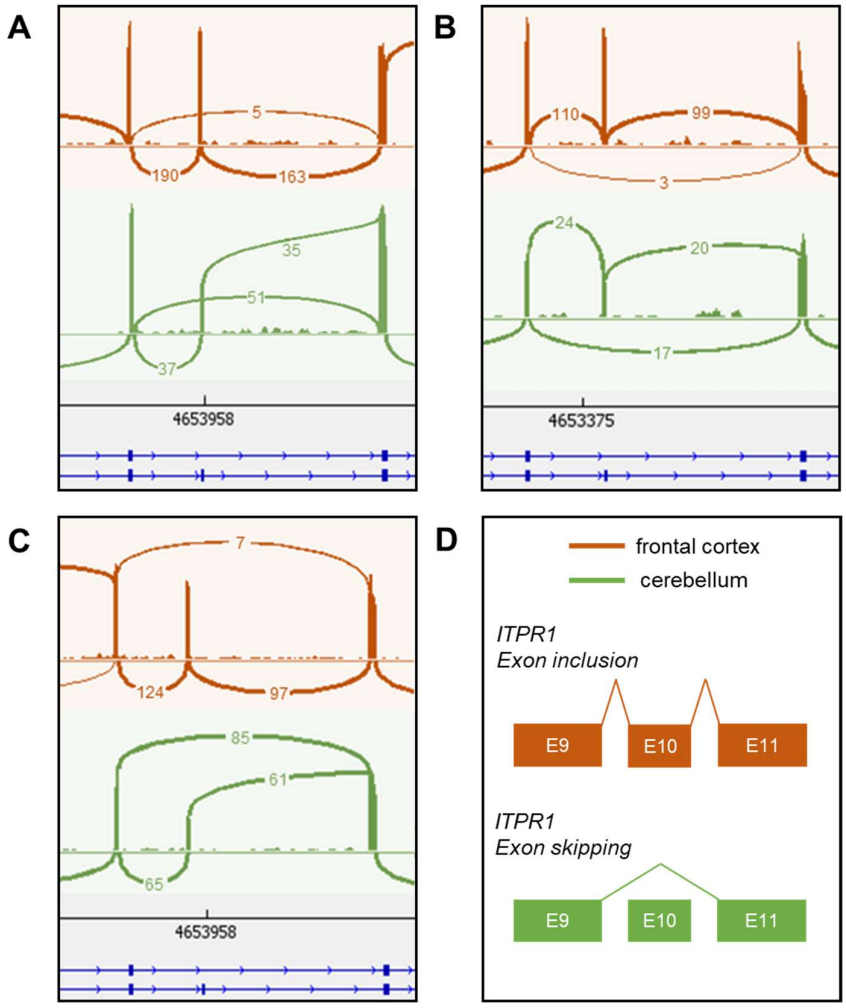
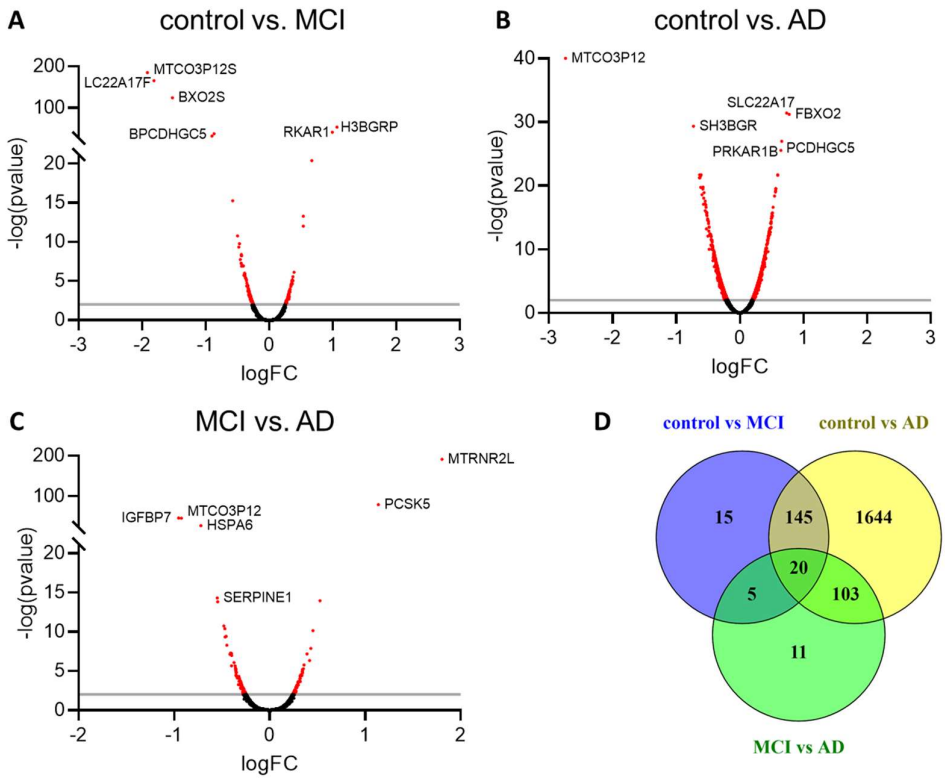


Figure 3.3.2.5 IP3 receptor gene *ITPR1* is alternatively spliced in cerebellum and frontal cortex of normal brain. Sashimi plots display relative inclusion of coding exon 10 in the cerebellum (red) and the frontal cortex (black) in three individuals without cognitive impairment. Numbers on plot indicate exon coverage, as determined from sorted aligned bam files, visualised on IGV software. The exon is located in chromosome 3 between start position 4,653,842 and end position 4,653,886 on reference genome hg38.

3.3.3 Differential gene expression in AD brain

To establish an understanding of transcriptome in AD brain, the ROSMAP dataset of 636 patient and donor samples was interrogated for differential transcript expression between no-cognitive impairment (NCI or control), mild-cognitive impairment (MCI) and AD groups. First, transcript counts were grouped according to clinical diagnosis and filtered for expression in all individuals (i.e. transcripts that were only detected in a subset of the population were excluded from the whole dataset). This produced a subset of expression data for total 27,268 transcripts (of 17,444 identified unique genes). Next, EdgeR was used to identify differentially expressed transcripts in control, MCI, and AD groups. A total of 2181 transcripts (of 1912 identified genes) were found to show differential expression between control and AD groups. To visualise distribution of genes, the logFC of transcript expression was plotted against "-log(pvalue)" for all three group comparisons (Figure 3.3.3.1A-C). The number of differentially expressed genes in each group comparison is summarised in a Venn diagram (Figure 3.3.3.1D).



E

Gene name	Gene description
MTCO3P12	mitochondrially encoded cytochrome c oxidase III pseudogene 12
PRKAR1B	protein kinase, cAMP-dependent, regulatory, type I, beta
PCDHGC5	protocadherin gamma subfamily C, 5
PHYHIP	phytanoyl-CoA 2-hydroxylase interacting protein
PARM1	prostate androgen-regulated mucin-like protein 1
MRAS	muscle RAS oncogene homolog
EPB41L3	erythrocyte membrane protein band 4.1-like 3
GALNT17	polypeptide n-acetylgalactosaminyltransferase 17
NCDN	neurochondrin
PLEKHB1	pleckstrin homology domain containing, family B (evectins) 1
MTCO2P12	mitochondrially encoded cytochrome c oxidase II pseudogene 12
RTN1	reticulon 1
MT1L	metallothionein 1L (gene/pseudogene)
FAM107A	family with sequence similarity 107, member A
HERC2P3	hect domain and RLD 2 pseudogene 3
MTCO1P40	mitochondrially encoded cytochrome c oxidase I pseudogene 40
PCSK5	proprotein convertase subtilisin/kexin type 5
CALM3	calmodulin 3 (phosphorylase kinase, delta)
SERPINE1	plasminogen activator inhibitor type 1
DNAJB1	DnaJ (heat shock protein 40) homolog, subfamily B, 1

Figure 3.3.3.1 Differential expression of genes in control, MCI, and AD groups according to clinical diagnosis in ROSMAP dataset. **A** Volcano plot for comparison of transcripts between control and MCI groups. Transcripts that showed significantly differential expression are visualised in red, above threshold line FDR<0.01. The majority of transcripts in MCI have logFC expression within ±1 range of the control group. Labels identify transcripts that have most significantly differential expression. **B** Volcano plot for comparison of transcripts between control and AD groups. Other than pseudogene MTCO3P12, all transcripts in AD show logFC expression with ±1 range of the control group. **C** Volcano plot for comparison of transcripts between MCI and AD groups. **D** Venn diagram for number of genes that show significantly different expression in each of the three group comparisons. Overlap identifies genes that are differentially expressed in two or all three comparisons. **E** List of 20 genes that overlap across all three group comparisons in Venn diagram.

GSEA was used to annotate genes with biological processes related to their function. As previously described, transcripts were filtered for FDR<0.01 to create a subset of differentially expressed transcripts, and then ranked by "-log(q-value)*sign(logFC)". The ranked list was input for GSEA, which identified significant enrichment of biological processes related to synaptic function, including synaptic vesicle cycle, vesicle localisation, vesicle-mediated transport, and regulation of synaptic transmission. Additionally, GO pathways for cognition and adult behaviour were also enriched among genes upregulated in AD compared to control brain. The top 10 significantly enriched GO pathways are listed in Table 3.3.3.1 below, and the corresponding list of upregulated genes can be found in Appendix Table 7.3.10.

GO: gene set	GO: description	Enrichment Score (ES)	Normalised ES	P-value	FDR	Size	Edge Size
0099177	**regulation of trans-synaptic signalling**	0.485	2.539	<1.0E-6	<1.0E-4 (*)	98	49
0099504	**synaptic vesicle cycle**	0.551	2.514	<1.0E-6	<1.0E-4 (*)	51	34
0051648	**vesicle localization**	0.522	2.451	<1.0E-6	<1.0E-4 (*)	58	40
0050890	**cognition**	0.487	2.409	<1.0E-5	0.001 (*)	63	28
0099003	**vesicle-mediated transport in synapse**	0.527	2.411	<1.0E-5	0.001 (*)	53	33
0017156	**calcium ion regulated exocytosis**	0.542	2.303	<1.0E-5	0.003 (*)	39	22
0140029	**exocytic process**	0.621	2.206	<1.0E-5	0.007 (*)	20	12
0051656	**establishment of organelle localization**	0.429	2.185	<1.0E-5	0.008 (*)	79	44
0035249	**synaptic transmission, glutamatergic**	0.586	2.111	<1.0E-4	0.016 (*)	20	13
0030534	**adult behaviour**	0.570	2.074	<1.0E-4	0.021 (*)	21	14
0050886	endocrine process	-0.777	-2.257	<1.0E-3	0.117	9	4
0061614	pri-miRNA transcription by RNA polymerase II	-0.849	-2.143	<1.0E-3	0.186	6	4
0043062	extracellular structure organization	-0.381	-1.936	0.002	0.394	61	41
0030856	regulation of epithelial cell differentiation	-0.515	-1.867	0.005	0.357	18	12
0007162	negative regulation of cell adhesion	-0.397	-1.765	0.009	0.431	34	15

Table 3.3.3.1 Top 10 upregulated and 5 downregulated GO pathways identified from genes differentially expressed between NCI and AD groups in the ROSMAP dataset (grouped by clinical diagnosis). Genes were filtered for FDR adjusted p<0.01 prior to GSEA using WebGestalt. Significantly enriched pathways in Biological processes database are shown with FDR (*) and in description in **bold** (normalised enrichment q<0.05).

To better understand protein networks implicated in clinical AD dementia, the subset of genes which showed differential expression in AD compared to both control and MCI groups were input to STRING database. This created a visual representation of the interactome of AD-specific genes than may provide insight to processes relevant to pathogenesis. The parameters included connections based on co-expression and physical co-occurrence. As seen in Figure 3.3.3.2, this analysis highlighted a number of connections between clusters of heat shock proteins and cell adhesion molecules. This indicates that these protein networks show impairment specifically in AD but not in MCI, and thus may be involved in the conversion to late-stage pathology based on the AD continuum model.

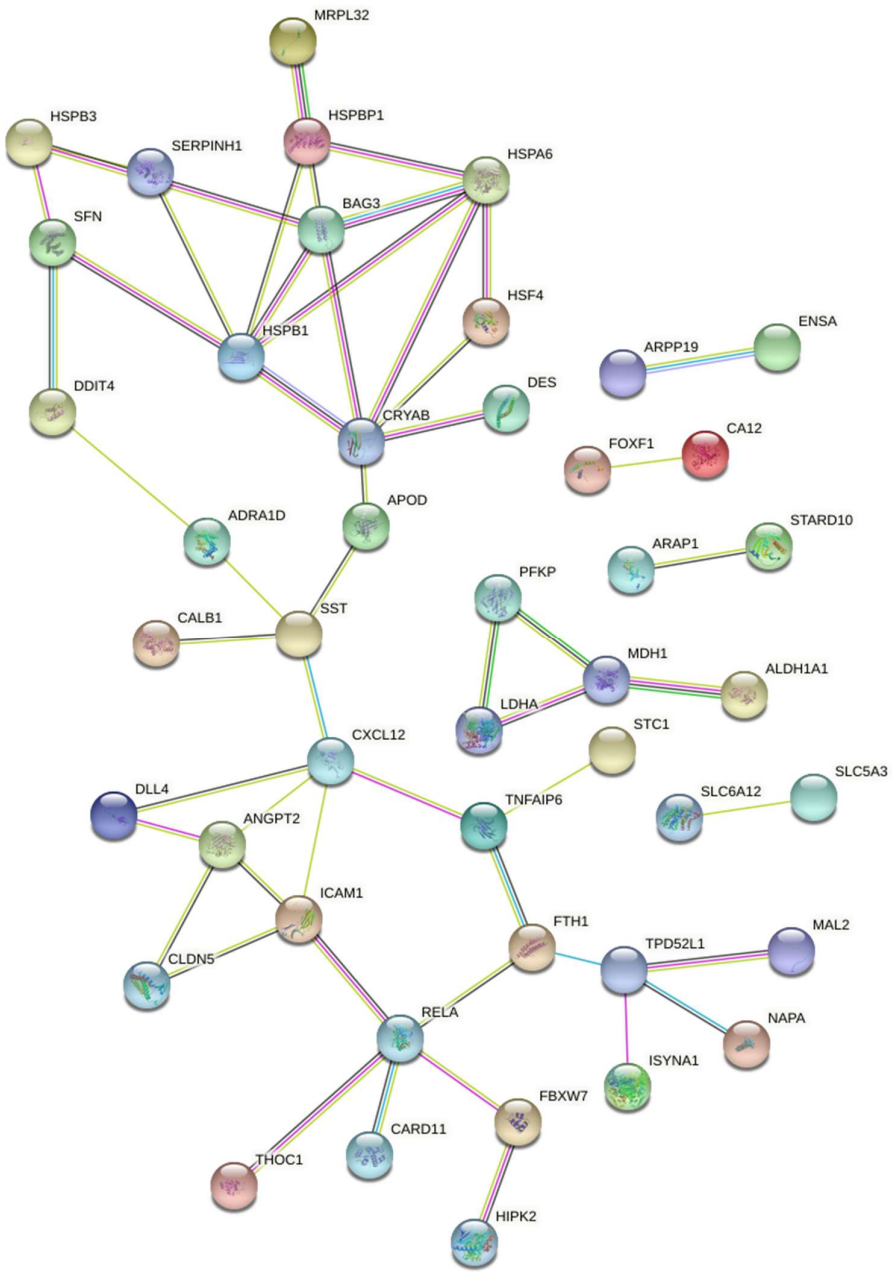
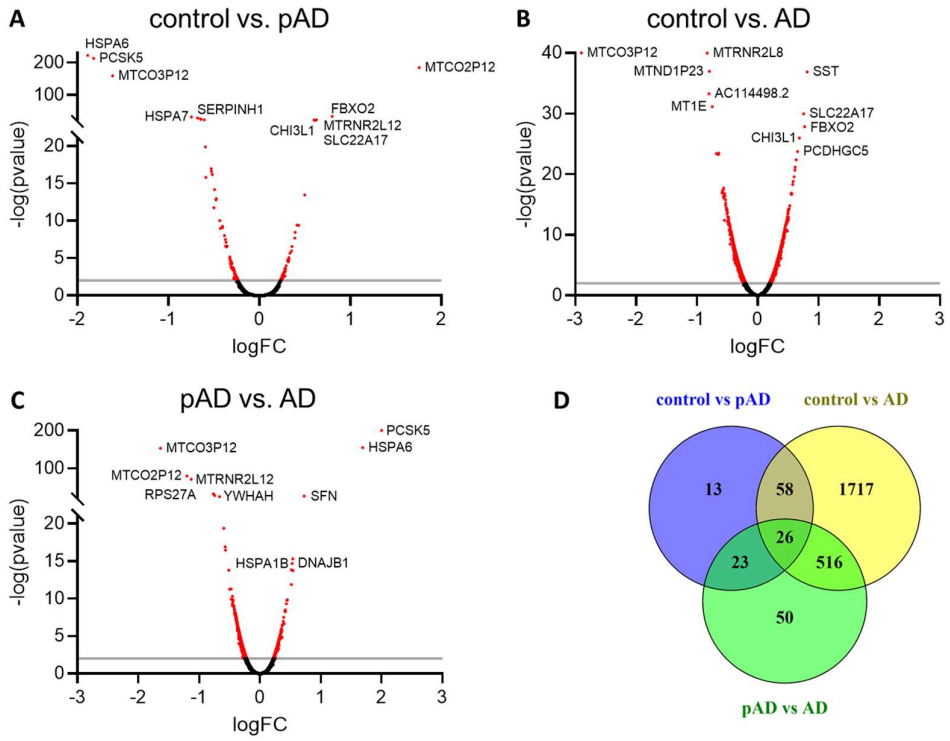


Figure 3.3.3.2 Protein interactions produced from genes which are differentially expressed in AD compared to both control and MCI groups. Colour of edges relates to type of interaction sourced by STRING: cyan = from curated databases, magenta = experimentally determined, green = gene neighbourhood (i.e. related transcription), blue = co-occurrence, black = co-expression, yellow = text-mining.

To further characterise AD-related differential expression, transcript counts from ROSMAP dataset were also split into groups according to CERAD score. This is a pathological assessment of AD based on neuritic plaque distribution and density. As before, transcripts were filtered for expression in all individuals and EgdeR was run to compare three groups: no AD, probable AD, or definite AD. Volcano plots of logFC of transcript expression vs. -log(pvalue) for each comparison are shown in Figure 3.3.3.3 below. Comparison of no and definite AD groups revealed a total of 2617 transcripts (of 2317 identified genes) with differential expression. 516 of these genes were also differentially expressed between probable and definite AD groups.



E

Gene name	Gene description
MTCO3P12	mitochondrially encoded cytochrome c oxidase III pseudogene 12
MTRNR2L8	MT-RNR2-like 8
MTND1P23	MT-ND1 pseudogene 23
SST	somatostatin
PCDHGC5	protocadherin gamma subfamily C, 5
FXYD6	FXYD domain containing ion transport regulator 6
NPTX2	neuronal pentraxin II
PARM1	prostate androgen-regulated mucin-like protein 1
EPB41L3	erythrocyte membrane protein band 4.1-like 3
PFKP	phosphofructokinase, platelet
STXBP1	syntaxin binding protein 1
MTCO2P12	mitochondrially encoded cytochrome c oxidase II pseudogene 12
NTM	neurotrimin
NCAM1	neural cell adhesion molecule 1
MTRNR2L12	MT-RNR2-like 12 (pseudogene)
SARS	seryl-tRNA synthetase
SNAP25	synaptosomal-associated protein, 25kDa
FAM131A	family with sequence similarity 131, member A
ABCA2	ATP-binding cassette, sub-family A (ABC1), member 2
CALM3	calmodulin 3 (phosphorylase kinase, delta)
CRYAB	crystallin, alpha B
ATOH8	atonal homolog 8
FTH1	ferritin, heavy polypeptide 1
SERPINH1	serpin peptidase inhibitor 1 (heat shock protein 47)

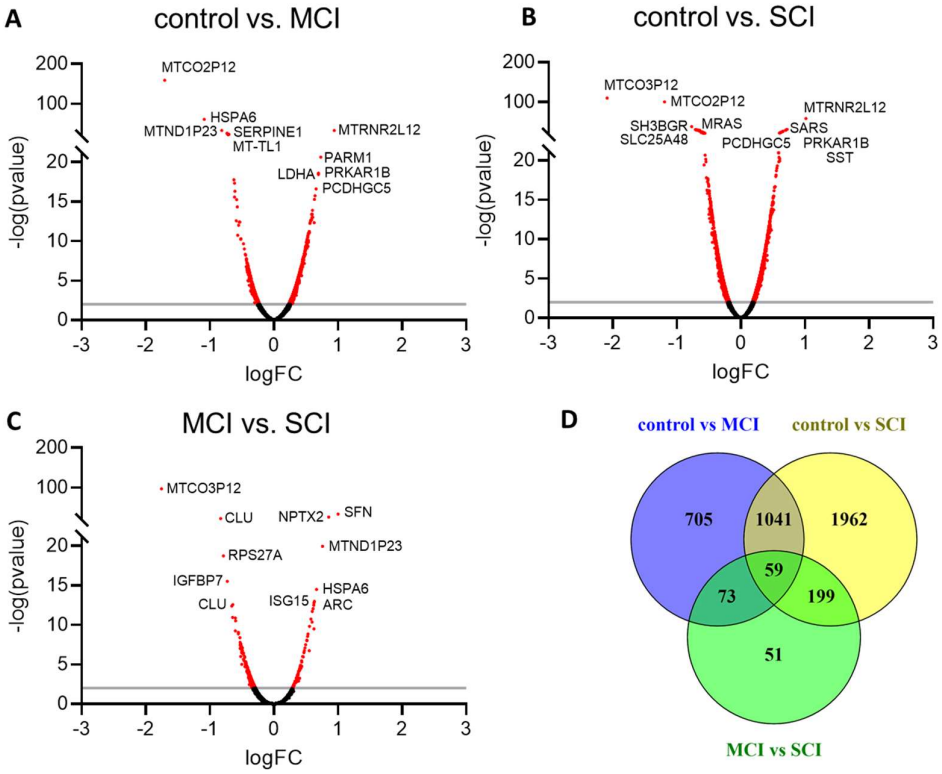
Figure 3.3.3.3 Differential expression of genes in control (no AD), predicted AD, and definite AD groups according to CERAD score in the ROSMAP dataset. **A** Volcano plot for comparison of transcripts between control and probable AD groups. Transcripts that showed significantly differential expression are visualised in red, above threshold line FDR<0.01. The majority of transcripts in probable AD have logFC expression within ±1 range of the control group. Labels identify transcripts that have most significantly differential expression. **B** Volcano plot for comparison of transcripts between control and definite AD groups. As before, labels identify most differentially expressed transcripts. **C** Volcano plot for comparison of transcripts between probable AD and definite AD groups. **D** Venn diagram for number of transcripts that show significantly different expression in each of the three group comparisons. Overlap identifies transcripts that are differentially expressed in two or all three comparisons. **E** List of genes that overlap across all three group comparisons in Venn diagram.

Transcripts were filtered for FDR<0.01 to create a subset of differentially expressed transcripts between groups assessed to have no AD and definite AD, as determined by CERAD score. These genes were ranked by "-log(q-value)*sign(logFC)" to input for GSEA. Similar to the results described from clinical diagnosis of AD, GSEA found significant enrichment of GO pathways for cognition and synaptic function in pathological assessment of AD. This included synaptic vesicle cycle, vesicle localisation, vesicle-mediated transport, and synapse organisation. The top 10 significantly enriched GO pathways are listed in Table 3.3.3.2 below, and the corresponding list of upregulated genes can be found in Appendix Table 7.3.11.

GO: gene set	GO: description	Enrichment Score (ES)	Normalised ES	P-value	FDR	Size	Edge Size
0099504	**synaptic vesicle cycle**	0.549	2.611	<1.0E-6	<1.0E-4 (*)	52	24
0099003	**vesicle-mediated transport in synapse**	0.519	2.488	<1.0E-6	<1.0E-4 (*)	53	32
0051648	**vesicle localization**	0.494	2.471	<1.0E-6	<1.0E-4 (*)	63	35
0099177	**regulation of trans-synaptic signalling**	0.431	2.346	<1.0E-5	0.003 (*)	101	58
0050890	**cognition**	0.466	2.271	<1.0E-5	0.006 (*)	60	28
0017156	**calcium ion regulated exocytosis**	0.493	2.247	<1.0E-5	0.007 (*)	42	32
0050905	**neuromuscular process**	0.620	2.220	<1.0E-5	0.008 (*)	19	14
0035418	**protein localization to synapse**	0.581	2.176	<1.0E-4	0.012 (*)	22	13
0051656	**establishment of organelle localization**	0.395	2.083	<1.0E-4	0.029 (*)	85	36
0050808	**synapse organization**	0.395	2.032	<1.0E-4	0.044 (*)	76	37
0043062	extracellular structure organization	-0.435	-2.155	<1.0E-4	0.087	65	32
0097194	execution phase of apoptosis	-0.764	-2.125	<1.0E-4	0.090	9	4
0002526	acute inflammatory response	-0.673	-2.181	<1.0E-3	0.135	13	5
0090305	nucleic acid phosphodiester bond hydrolysis	-0.562	-1.833	0.015	0.391	15	3
0006413	translational initiation	-0.468	-1.740	0.020	0.434	23	10

Table 3.3.3.2 Top 10 upregulated and 5 downregulated GO pathways identified from genes differentially expressed between control and AD groups in from the ROSMAP dataset (grouped by CERAD score). Genes were filtered for FDR adjusted p<0.01 prior to GSEA using WebGestalt. Significantly enriched pathways in Biological processes database are shown with FDR (*) and in description in **bold** (normalised enrichment q<0.05).

To closely capture genes implicated with cognitive decline, the ROSMAP dataset was also grouped according to Mini-Mental Stare Exam (MMSE) score. Transcript counts were filtered for expression in all individuals and EgdeR was run to compare three groups: no CI, mild CI, or severe CI. Volcano plots of logFC of transcript expression vs. -log(pvalue) for each comparison are presented in Figure 3.3.3.4 below. Out of a total 27,268 transcripts (of 17,444 identified genes), 3,815 transcripts (of 3,261 identified genes) were differentially expressed between no CI and severe CI groups (FDR adjusted p<0.01). The Venn diagram in Figure 3.3.3.4D illustrates that 199 of these genes were also differentially expressed between mild CI and severe CI groups.



E

Gene name	Gene description
MTCO3P12	mitochondrially encoded cytochrome c oxidase III pseudogene 12
SFN	stratifin
NPTX2	neuronal pentraxin II
CLU	clusterin
RPS27A	ribosomal protein S27a
HSPA6	heat shock 70kDa protein 6
ARC	activity-regulated cytoskeleton-associated protein
ISG15	ISG15 ubiquitin-like modifier
CHI3L1	chitinase 3-like 1 (cartilage glycoprotein-39)
PLEKHB1	pleckstrin homology domain containing, family B, member 1
NDRG2	NDRG family member 2
NR4A1	nuclear receptor subfamily 4, group A, member 1
MTCO2P12	mitochondrially encoded cytochrome c oxidase II pseudogene 12
ICAM1	intercellular adhesion molecule 1
SEMA3D	sema domain, immunoglobulin domain (Ig), semaphorin 3D
TPD52L1	tumour protein D52-like 1
ATP1A2	ATPase, Na+/K+ transporting, alpha 2 polypeptide
GLUL	glutamate-ammonia ligase
SLC1A3	solute carrier family 1 (glial high affinity glutamate transporter) 3
CDC16	cell division cycle 16
SERPINE1	plasminogen activator inhibitor type 1
LAMP2	lysosomal-associated membrane protein 2
FTH1	ferritin, heavy polypeptide 1
CXCL2	chemokine (C-X-C motif) ligand 2
ARAP1	ArfGAP with RhoGAP domain, ankyrin repeat and PH domain 1
PFKP	phosphofructokinase, platelet
CRYAB	crystallin, alpha B
PCNP	PEST proteolytic signal containing nuclear protein
YWHAH	tryptophan 5-monooxygenase activation protein, eta
GAREM2	GRB2-associated and regulator of MAPK subtype 2
SLC25A48	solute carrier family 25, member 48
G0S2	G0/G1switch 2
GRASP	GRP1 (general receptor for phosphoinositides 1)-associated scaffold protein
ATP6V1C1	ATPase, H+ transporting, lysosomal 42kDa, V1 subunit C1
SIK1B	salt inducible kinase 1B
APLN	apelin
SLC25A18	solute carrier family 25 (glutamate carrier), member 18
DLG4	discs, large homolog 4
SPAG9	sperm associated antigen 9
MT1E	metallothionein 1E
CSRP1	cysteine and glycine-rich protein 1
SYT1	synaptotagmin I
HERC2P2	hect domain and RLD 2 pseudogene 2
LDHA	lactate dehydrogenase A
ITPRID2	ITPR (inositol trisphosphate receptor) interacting domain containing 2
ARHGEF17	Rho guanine nucleotide exchange factor (GEF) 17
PLXNB1	plexin B1
CLIP2	CAP-GLY domain containing linker protein 2
ISYNA1	inositol-3-phosphate synthase 1
SLC6A12	solute carrier family 6 (neurotransmitter transporter), member 12
NDUFV1	NADH dehydrogenase (ubiquinone) flavoprotein 1, 51kDa
TMEM219	transmembrane protein 219
KCNE4	potassium voltage-gated channel, subfamily E, member 4
NFE2L1	nuclear factor, erythroid 2-like 1
NAPG	N-ethylmaleimide-sensitive factor attachment protein, gamma
SNHG14	small nucleolar RNA host gene 14 (non-protein coding)
MYL6	myosin, light chain 6, smooth muscle and non-muscle
STC1	stanniocalcin 1

Figure 3.3.3.4 Differential expression of genes in control (no CI), MCI, and severe CI groups according to MMSE score in the ROSMAP dataset. **A** Volcano plot for comparison of transcripts between control and MCI groups. Transcripts that showed significantly differential expression are visualised in red, above threshold line FDR<0.01. The majority of transcripts in probable AD have logFC expression within ±1 range of the control group. Labels identify transcripts that have most significantly differential expression. **B** Volcano plot for comparison of transcripts between control and SCI groups. As before, labels identify most differentially expressed transcripts. **C** Volcano plot for comparison of transcripts between MCI and SCI groups. **D** Venn diagram for number of transcripts that show significantly different expression in each of the three group comparisons. Overlap identifies transcripts that are differentially expressed in two or all three comparisons. **E** List of genes that overlap across all three group comparisons in Venn diagram.

A subset of differentially expressed genes was input to GSEA after being ranked by "-log(pvalue)*sign(logFC)" for enrichment of biological processes related to cognitive decline. As seen previously with clinical diagnosis and CERAD score, GO pathways for synaptic function were significantly enriched among genes differentially expressed between MMSE groups. In addition, severe CI was significantly associated with upregulation of genes related to amine transport, whilst the control group was associated with upregulation of epithelial cell adhesion molecules. The top 10 significantly enriched GO pathways are listed in Table 3.3.3.3 below, and the corresponding list of upregulated genes can be found in Appendix Table 7.3.12.

GO: gene set	GO: description	Enrichment Score (ES)	Normalised ES	P-value	FDR	Size	Edge Size
0099504	**synaptic vesicle cycle**	0.579	2.785	<1.0E-6	<1.0E-4 (*)	65	42
0099003	**vesicle-mediated transport in synapse**	0.546	2.689	<1.0E-6	<1.0E-4 (*)	70	47
0017156	**calcium ion regulated exocytosis**	0.528	2.458	<1.0E-5	0.001 (*)	54	34
0051648	**vesicle localization**	0.475	2.421	<1.0E-5	0.001 (*)	83	53
0050890	**cognition**	0.465	2.428	<1.0E-5	0.001 (*)	81	36
0099177	**regulation of trans-synaptic signalling**	0.444	2.438	<1.0E-5	0.001 (*)	133	65
0015837	**amine transport**	0.630	2.256	<1.0E-5	0.006 (*)	19	15
0015844	**monoamine transport**	0.651	2.202	<1.0E-4	0.011 (*)	17	14
0140029	**exocytic process**	0.555	2.175	<1.0E-4	0.014 (*)	28	16
0051656	**establishment of organelle localization**	0.388	2.118	<1.0E-4	0.022 (*)	116	53
0042063	gliogenesis	-0.279	-1.358	0.110	0.591	80	44
0007265	Ras protein signal transduction	-0.266	-1.363	0.100	0.594	109	45
0007389	pattern specification process	-0.291	-1.336	0.144	0.596	58	26
0045785	positive regulation of cell adhesion	-0.280	-1.370	0.125	0.603	82	41
0002064	epithelial cell development	-0.329	-1.368	0.137	0.602	41	31

Table 3.3.3.3 Top 10 upregulated and 5 downregulated GO pathways identified from genes differentially expressed between individuals with NCI and SCI from the ROSMAP dataset (grouped by MMSE score). Genes were filtered for FDR adjusted p<0.01 prior to GSEA using WebGestalt. Significantly enriched pathways in Biological processes database are shown with FDR (*) and in description in **bold** (normalised enrichment q<0.05).

3.3.4 Characterisation of splicing transcripts and splicing kinases in AD brain

So far, the ROSMAP dataset provided insight to differential expression in AD, but with considerably low logFC, so it is unclear whether these expressional changes would have real biological impact, despite statistical significance. To initially characterise splicing levels in AD, the number of transcripts produced for all genes was compared across clinical diagnosis groups: control (no CI), MCI, and AD. Referring to Figure 3.3.4.1, about 80% genes only had one measured transcript, and the remaining genes showed alternative splicing. It should be noted that these only include known transcripts identifiable by ensembl number and not all splicing variants.

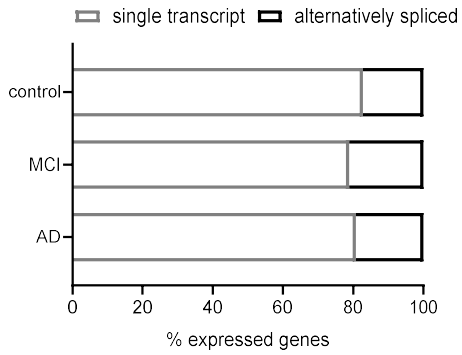


Figure 3.3.4.1 Percent of genes expressed in control, MCI, and AD groups with a single transcript or multiple known transcripts produced through alternative splicing. Individuals were grouped by clinical diagnosis.

The subset of alternatively spliced genes was ranked for the total number of transcripts present in each group. Compared to control, MCI and AD groups had a higher number of transcripts per gene, which suggests there is increased AS in disease. As labelled in Figure 3.3.4.2, there were some genes where higher numbers of transcripts were only expressed in MCI and AD, including *NDRG2*, *SERF2*, and *FXYD1*. In their study of the ROSMAP dataset, Raj et al also reported *NDRG2* to be alternatively spliced in AD. Reproducing this finding supports the use of ROSMAP dataset as a tool to investigate AS in AD.

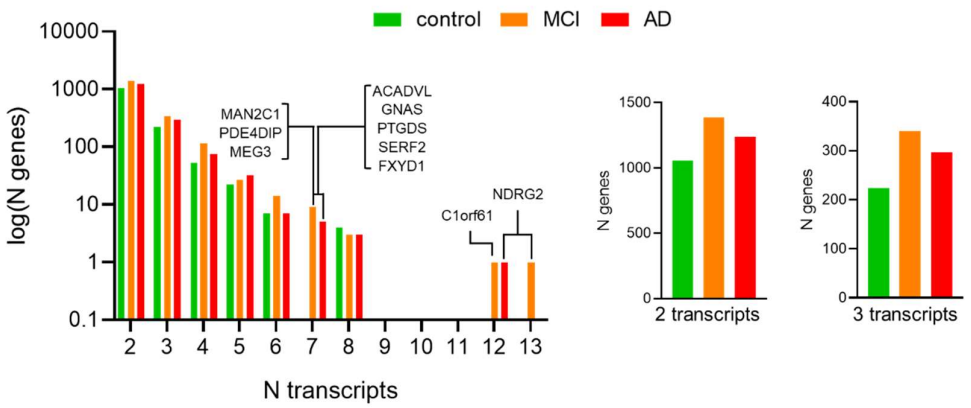
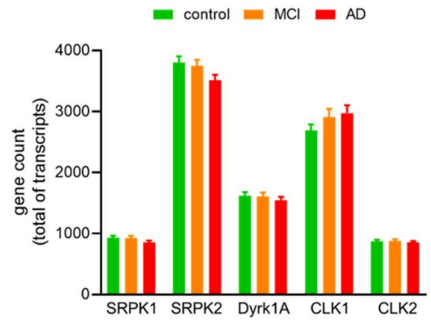


Figure 3.3.4.2 Increased alternative splicing in MCI and AD. Histogram for log number of genes which have expression of 2-13 known splicing transcripts in the ROSMAP dataset. N genes for 2 and 3 transcripts are also displayed on linear axes for easier group comparison. Groups determined by clinical diagnosis.

Due to the magnitude of the ROSMAP dataset, the MATS pipeline is not an appropriate method to investigate alternative splicing. Instead, I decided to characterise the expression of splicing kinases, which are known to regulate splicing events, and establish if they play a role in AD pathology. As seen in Figure 3.3.4.3A below, SRPK2 and CLK1 showed the highest transcript levels in the brain. Overall, clinical groups (control, MCI and AD) had similar expression of splicing kinases SRPK1, CLK2 and Dyrk1A. ANCOVA was used to test for significant effect of kinase expression on clinical group. Although there was a slight trend for higher CLK1 with cognitive impairment, this was not significant when adjusting for sex and age [$F(1,632) = 0.3$, $p > 0.05$] which were included as covariates since they are known to impact clinical outcome and thus account for variability in diagnosis. On the other hand, SRPK2 did differ between clinical groups, with significantly higher expression in individuals with cognitive impairment and AD dementia [$F(1,632) = 6.1$, $p = 0.01$].

A



B

	df	SS	*F*	Pr (>*F*)
Intercept	1	8.61	4.36	0.0370
SRPK2	1	12.0	6.01	**0.0138**
Sex	1	1.50	0.76	0.384
Age	1	72.1	36.5	**<0.0001**
Residuals	632	1250		

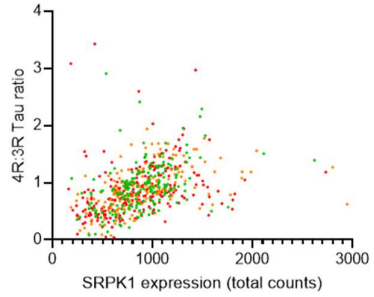
C

	df	SS	*F*	Pr (>*F*)
Intercept	1	15.4	7.75	0.00554
CLK1	1	0.60	0.30	0.582
Sex	1	1.28	0.64	0.423
Age	1	74.7	37.5	**<0.0001**
Residuals	632	1260		

Figure 3.3.4.3 Expression of splicing kinases (sum of all transcripts) in control, MCI and AD groups, as determined by clinical diagnosis. **A** Total expression of splicing kinases, plotted bar = mean and error bars = SD. **B** ANCOVA results show that SRPK1 expression is significantly related to differential clinical diagnosis (p=0.01). **C** ANCOVA results show that CLK1 expression does not account for significant change in clinical diagnosis (p>0.05). Column titles: df = degrees of freedom, SS = sum of squares, *F* = *F* value, Pr(>*F*) = p-value. **Bold** values indicate significance.

Tau pathology is a hallmark of AD and its gene *MAPT* is well-known to be alternatively spliced in AD. Studies have previously shown that these splicing kinases regulate exon 10 inclusion in *MAPT* (Hartmann *et al.*, 2001), so I compared their expression to the ratio of 4R and 3R tau transcripts in matched individuals using ANCOVA. As shown in Figure 3.3.4.4, 4R:3R tau ratio is significantly related to splicing kinase expression, as determined by the sum expression of protein-coding transcripts, and whilst adjusting for covariates (p<0.0001). Interestingly, clinical diagnosis was related to the effect of CLK1 expression on 4R:3R ratio (p<0.05) but it was not significantly related to the expression of other kinases (Figure 3.3.4.4H). As before, covariates sex and age were included in the analysis as they impact differential gene expression and risk for AD. According to *F* statistic, which is calculated by division of the explained variance between groups by the unexplained variance within groups, Dyrk1A expression (Figure 3.3.4.4F) accounts for the most variability in 4R:3R tau ratio [$F(1,631) = 99.4$, $p < 0.0001$] followed by SRPK1 (Figure 3.3.4.4B) and CLK2 (Figure 3.3.4.4J) expression, where [$F(1,631) = 64.3$, $p < 0.0001$] and [$F(1,631) = 49.1$, $p < 0.0001$], respectively.

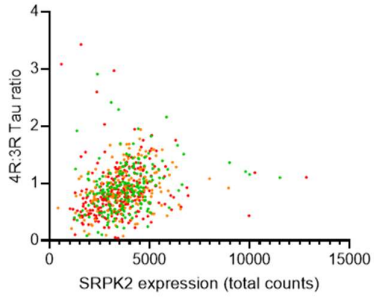
A



B

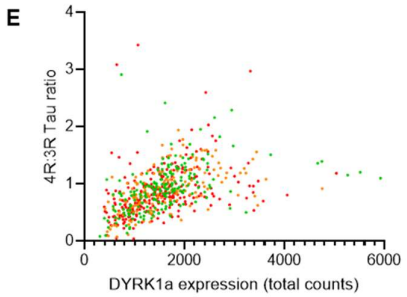
	df	SS	*F*	Pr (>*F*)
Intercept	1	0.497	2.627	0.106
SRPK1	1	12.15	64.28	**<0.0001**
Sex	1	0.059	0.312	0.577
Age	1	0.202	1.070	0.301
Diagnosis	1	0.403	2.130	0.145
Residuals	631	119.3		

C



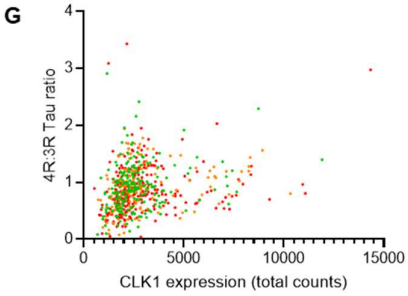
D

	df	SS	*F*	Pr (>*F*)
Intercept	1	0.751	3.701	0.0548
SRPK2	1	3.457	17.05	**<0.0001**
Sex	1	0.058	0.287	0.592
Age	1	0.202	0.996	0.319
Diagnosis	1	0.492	2.428	0.120
Residuals	631	128.0		



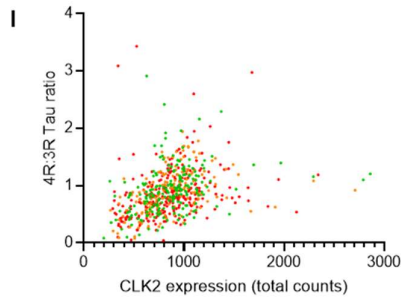
F

	df	SS	*F*	Pr (>*F*)
Intercept	1	0.691	3.839	0.0505
Dyrk1A	1	17.88	99.35	**<0.0001**
Sex	1	0.008	0.044	0.834
Age	1	0.068	0.379	0.538
Diagnosis	1	0.430	2.390	0.123
Residuals	631	113.5		



H

	df	SS	*F*	Pr (>*F*)
Intercept	1	1.557	7.893	0.00512
CLK1	1	6.977	35.38	**<0.0001**
Sex	1	0.182	0.922	0.337
Age	1	0.028	0.142	0.707
Diagnosis	1	0.894	4.532	**0.0337**
Residuals	631	124.4		



J

	df	SS	*F*	Pr (>*F*)
Intercept	1	0.552	2.859	0.0914
CLK2	1	9.483	49.07	**<0.0001**
Sex	1	0.120	0.621	0.431
Age	1	0.134	0.694	0.405
Diagnosis	1	0.675	3.493	0.0621
Residuals	631	121.9		

Figure 3.3.4.4 Expression of splicing kinases is related to 4R:3R tau ratio. **A** There is weak positive correlation between SRPK1 expression and 4R:3R tau ratio. Kinase expression in ROSMAP dataset was calculated by a sum of protein-coding transcripts for *SRPK1*. The tau ratio was calculated from the most abundant 4R and 3R tau transcripts. Green plots = no cognitive impairment, orange plots = MCI, red plots = clinical AD. **B** ANCOVA results show there is significant difference in 4R:3R tau ratio with differential SRPK1 expression ($p<0.0001$). Other confounding factors did not show significant difference ($p>0.05$). Column titles: df = degrees of freedom, SS = sum of squares, *F* = *F* value, Pr(>*F*) = p-value. **Bold** values indicate significance. **C E G I** There is weak positive correlation between the expression of SRPK2, Dyrk1A, CLK1 and CLK2 with 4R:3R tau ratio. **D F H J** ANCOVA results show there is significant difference in 4R:3R ratio with differential kinase expression. Clinical diagnosis only shows significant difference with CLK1 expression (see **H**).

3.3.5 The relationship between splicing kinase expression and the occurrence of AD

To determine effect on clinical and pathological outcomes, expression of splicing kinases was investigated further in the ROSMAP dataset. Beforehand, to control for covariates age and sex, the data was split into males and females, and individuals within 20% of the median age were selected for analysis.

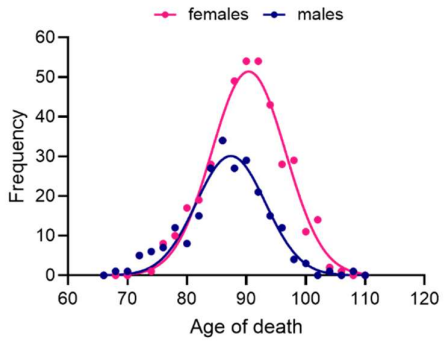


Figure 3.3.5.1 Normal distribution of age and sex in ROSMAP cohort. There are a total of 407 females and 229 males in the dataset.

Next, individuals were ranked based on expression of a selected full-length transcript for SRPK1, SRPK2, Dyrk1A, CLK1, and CLK2. Once filtered for age and sex, subgroups were split into quintiles: the first and fifth quintile were considered to have low and high expression of each splicing kinase. The median ± SD expression level of each kinase in male and female groups are shown in Table 3.3.5.1 below.

Splicing kinase (isoform)		Expression (median transcript count ± SD)					
		Bottom 20%	Top 20%	Total females	Bottom 20%	Top 20%	Total males
SRPK1	(001)	103 ± 44	423 ± 98	254 ± 135	112 ± 41	461 ± 238	260 ± 197
SRPK2	(001)	539 ± 195	2729 ± 337	1365 ± 808	633 ± 229	2620 ± 1338	1558 ± 1088
Dyrk1A	(001)	670 ± 176	2129 ± 335	1281 ± 605	657 ± 130	2835 ± 892	1347 ± 864
CLK1	(007)	13 ± 5	82 ± 38	37 ± 33	13 ± 7	72 ± 21	39 ± 25
CLK2	(003)	7 ± 6	102 ± 21	40 ± 36	13 ± 7	109 ± 40	46 ± 44

Table 3.3.5.1 The relative expression of full-length transcript for splicing kinases in subgroup of females and males investigated in the following analysis. Reported figure for total is median of transcript counts for each named isoform ± SD.

Following these steps, a mix of clinical and pathological markers were used to determine if the likelihood of AD is related to expression of splicing kinases. The first, SRPK1, was found to be related to increased likelihood of AD in the female subgroup. As shown in Figure 3.3.5.2, females with high expression of SRPK1 had a significantly lower proportion of AD clinical diagnosis compared to the low expression group (Chi-square test, $p<0.05$). This effect was supported by CERAD score, which indicated reduced neuritic plaques, as well as reduced tau burden, as determined by pathological scoring of NFTs in the brain. CERAD score predicted 77.8% of the low SRPK1 group to have probable or definite AD, which was significantly higher than 51.9% of the high expression group. The NFT fractional area scores were an average of 2.4 ± 0.3 and 1.6 ± 0.3 in low and high SRPK1 groups, respectively (unpaired t-test, $p<0.05$).

In males, however, there was no significant difference in occurrence of AD between high and low SRPK1 expression groups (Chi-square test, $p>0.05$), as shown in Figure 3.3.5.3. By clinical diagnosis, 30.8% and 46.2% of the low SRPK1 group had MCI and AD, respectively. This is comparable to 23.1% and 30.8% individuals in the high SRPK1 group who fell into these categories. MMSE scores indicated that 46.2% and 15.4% of low and high SRPK1 groups had severe CI, respectively. This was not a significant difference but gave some indication that low SRPK1 could be related to CI in males if the sample size was larger. However, pathological outcomes did not show the same trends: CERAD score predicted very similar proportion of individuals (61.5% and 69.2%) to have probable or definite AD in low and high SRPK1 expression groups. Similarly, NFT fractional area scores were 1.7 ± 0.4 and 1.1 ± 0.2, respectively. Altogether, this evidence suggests that the link between low SRPK1 and AD occurs exclusively in the female subgroup.

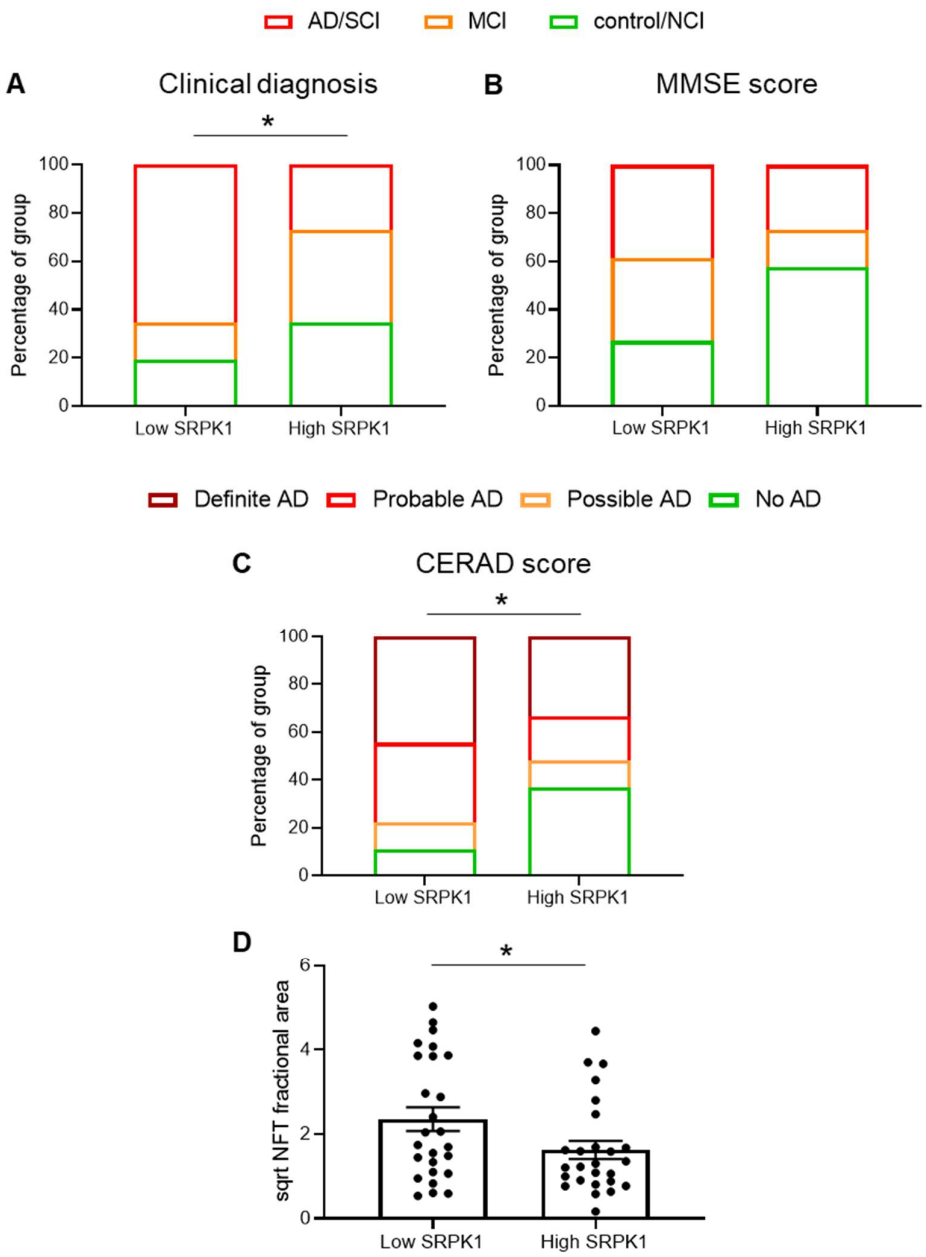


Figure 3.3.5.2 Low SRPK1 expression in females is related to AD phenotype in ROSMAP dataset. **A** Comparison of clinical diagnosis for individuals in low and high SRPK1 groups shows significantly less AD with high SRPK1 expression (Chi-square test, $p<0.05$). **B** According to MMSE score, high SPPK1 group have fewer proportion of individuals with moderate to severe cognitive impairment compared to the low SRPK1 group. **C** Similarly, comparison of CERAD scores in low and high SRPK1 groups identifies significantly more cases of AD with low SRPK1 expression (Chi-square test on binary data i.e., no/possible AD against probable/definite AD, $p<0.05$). **D** Significantly lower tau burden in the high SRPK1 group compared to the low SRPK1 group, as determined by fractional area of NFTs in the brain (unpaired t-test, $p<0.05$).

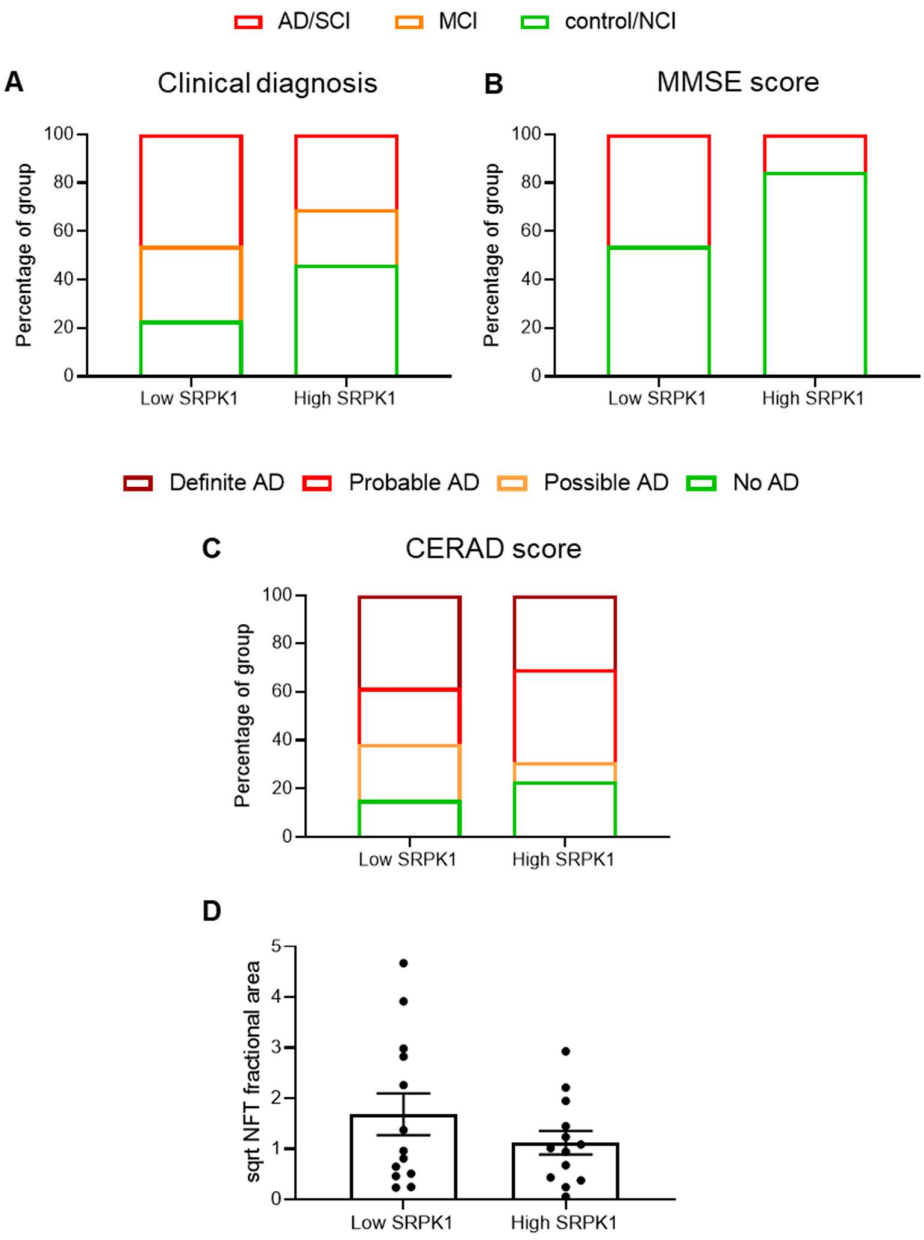


Figure 3.3.5.3 SRPK1 expression in males is not significantly related to AD phenotype in ROSMAP dataset. **A** Comparison of clinical diagnosis in low and high SRPK1 groups: control, MCI and AD. **B** Comparison of MMSE score in low and high SRPK1 groups: no CI, mild CI, and severe CI. **C** Prediction of AD based on pathological study of neuritic (amyloid) plaques produces CERAD score: there was no significant difference between low and high SRPK1 groups. **D** Comparison of tau burden by fractional area of NFTs in the brain showed no significant difference with SRPK1 expression (unpaired t-test, $p>0.05$).

The same analysis was repeated for splicing kinase SRPK2 and I found that low SRPK2 expression is related to the AD phenotype (see Figure 3.3.5.4). In the female subgroup, 59.3% of individuals with low SRPK2 expression had AD diagnoses, which is significantly higher than the 25.9% individuals with high SRPK2 expression (Chi-square test, $p<0.05$). MMSE scores showed corresponding cognitive impairment, with 37.0% and 14.8% of the low and high SRPK2 groups assessed to have severe CI, respectively. However, this difference was not statistically significant. Nonetheless, the relation between low SRPK2 and AD was supported by histopathological data, which indicated that the low SRPK2 group had significantly more neuritic plaques (therefore higher CERAD score) and greater tau burden. CERAD score predicted 77.8% and 48.1% of low and high SRPK2 groups to have probable or definite AD. The NFT fractional area in the brain scored an average 2.2 ± 0.3 in the low expression group but only 1.4 ± 0.2 in the high expression group (unpaired t-test, $p<0.05$).

As seen previously with SRPK1, the link between SRPK2 and AD was observed in females but not males from the ROSMAP cohort. In males, there was no consistent or significant difference in frequency of AD cases between SRPK2 expression groups. This may be due to differing biology or based on the smaller sample size (roughly half the female dataset) which did not provide sufficient power to replicate the effect of SRPK2 expression. For example, an equal number of individuals in low and high SRPK2 groups had no CI, and a similar proportion had clinical diagnosis of AD (46.1% and 30.8% in low and high SRPK2 groups, respectively). CERAD score predicted 69.2% and 76.9% of these groups to have probable to definite AD based on Aβ pathology, which did not constitute significantly different likelihood for disease. Similarly, tau pathology, measured by NFT fractional area scores of 1.6 ± 0.4 and 1.4 ± 0.3, did not differ between low and high SRPK2 groups. Refer to Figure 3.3.5.5 for more details.

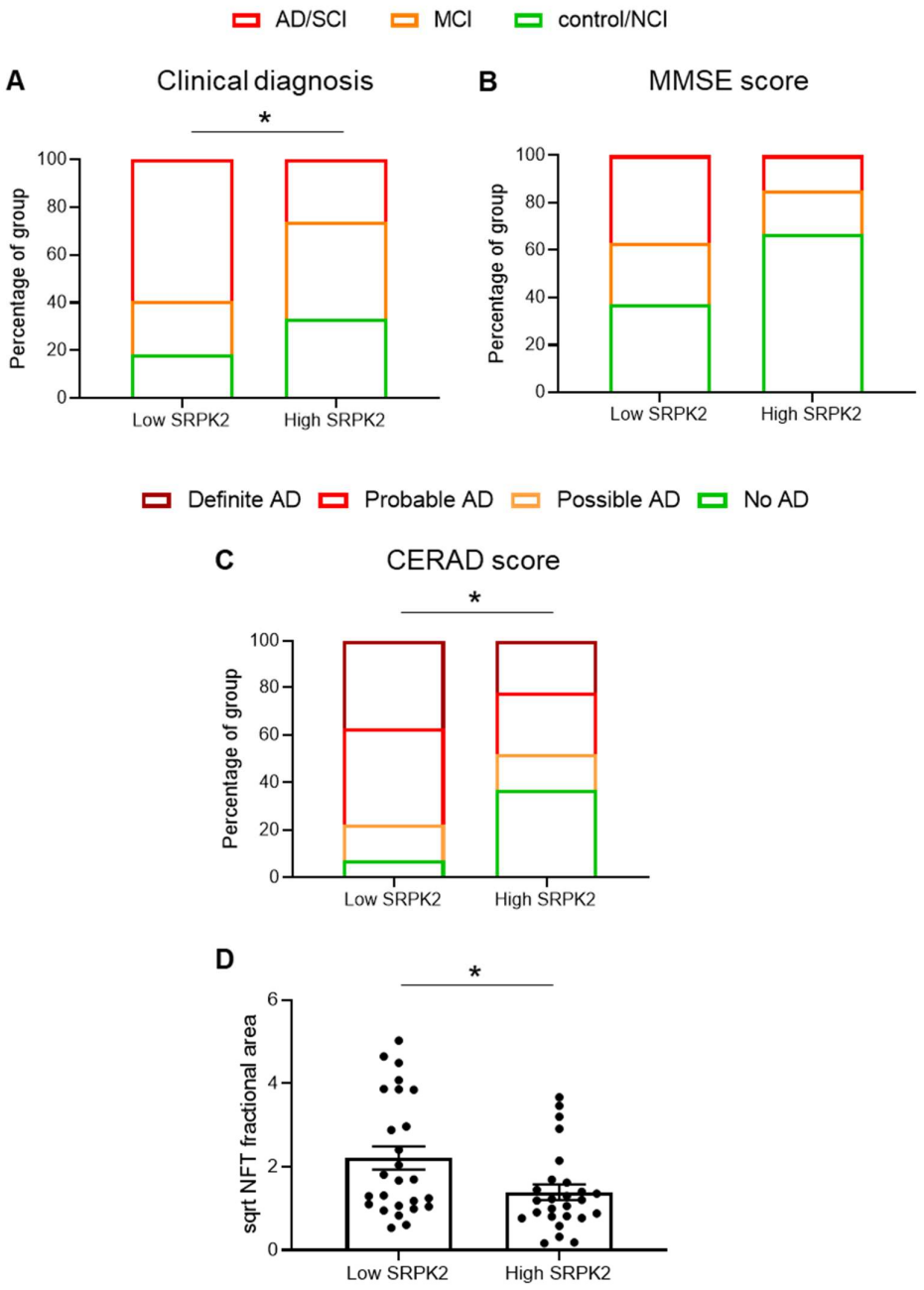


Figure 3.3.5.4 Low SRPK2 expression in females is related to AD phenotype in ROSMAP dataset. **A** Comparison of clinical diagnosis for individuals with low and high SRPK1 expression shows significantly less AD in high SRPK2 group (Chi-square test, $p<0.05$). **B** According to MMSE score, the high SPPK2 group have fewer proportion of individuals with moderate to severe cognitive impairment compared to the low SRPK2 group. **C** Similarly, comparison of CERAD scores in low and high SRPK2 groups identifies significantly more cases of AD with low SRPK2 expression (Chi-square test on binary data i.e., no/possible AD against probable/definite AD, $p<0.05$). **D** Significantly lower tau burden in the high SRPK2 group compared to the low SRPK2 group, as determined by fractional area of NFTs in the brain (unpaired t-test, $p<0.05$).

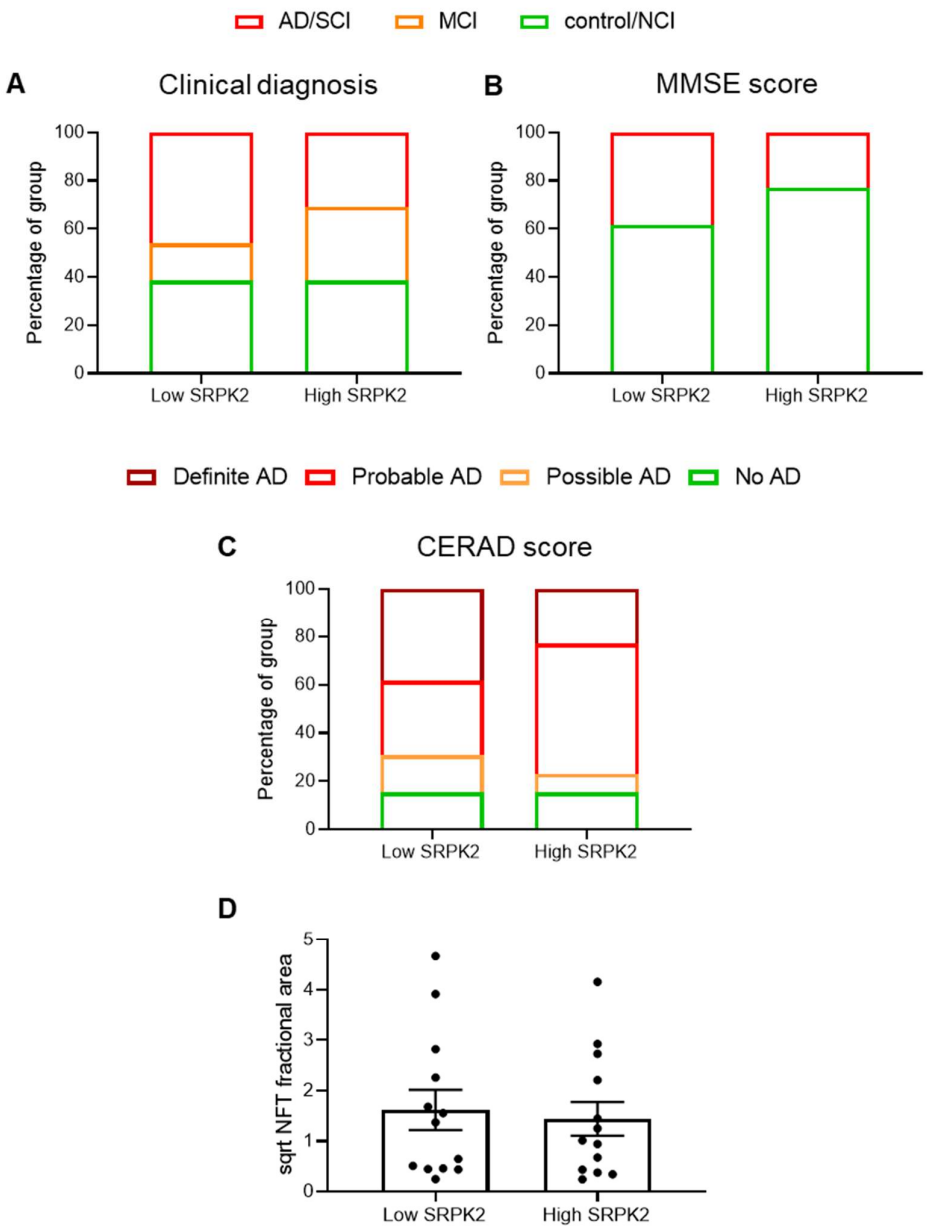


Figure 3.3.5.5 SRPK2 expression in males is not significantly related to AD phenotype in ROSMAP dataset. **A** Comparison of clinical diagnosis in low and high SRPK2 groups: control, MCI and AD. **B** Comparison of MMSE score in low and high SRPK2 groups: no CI, mild CI, and severe CI. **C** No significant difference between CERAD score in low and high SRPK2 groups (Chi-square test on binary data i.e., no/possible AD against probable/definite AD, $p>0.05$). **D** Comparison of tau burden by fractional area of NFTs in the brain showed no significant difference with SRPK2 expression (unpaired t-test, $p>0.05$).

Next, the ROSMAP dataset was interrogated for differential expression of Dyrk1A, as shown in Figure 3.3.5.6, and it was found that females with low Dyrk1A had significantly greater proportion of AD diagnosis (Chi-square test, $p<0.001$). However, this group did not show a significant degree of corresponding changes in amyloid and tau pathology. Nonetheless, CERAD score (Figure 3.3.5.6C) indicated that 77% of the low Dryk1A group had probable or definite AD based on distribution of moderate or frequent neuritic plaques, respectively. In comparison, 57% of individuals with high Dyrk1A expression were categorised for probable/definite AD; although not significantly different (Chi-square test, $p>0.05$) it is important to note that data on amyloid-related pathology does match clinical diagnosis, and there is high representation of both assessments for AD in the low Dyrk1A group. The relation with tau pathology is less unclear; on average, the low and high Dyrk1A groups had a score of 2.3 ± 0.3 and 1.8 ± 0.2, respectively. Although tau burden is slightly higher in the low Dyrk1A group, this could be random variability since it was not found to be statistically significant (unpaired t-test, $p>0.05$).

In males, Dyrk1A expression was not related to AD diagnosis or AD-related pathology. As shown in Figure 3.3.5.7, the low Dryrk1A group had relatively equal proportion of individuals with no CI, mild CI, and clinical AD diagnosis. Interestingly, CERAD score indicated that both groups had a high proportion of amyloid pathology, but pathological diagnosis of AD was greater in individuals with high Dyrk1A expression (86% compared to 64% in the low Dryk1A group). However, this was not a significant difference (Chi-square test, $p>0.05$) and it was not related to degree of cognitive impairment, as determined by MMSE score. In fact, both high and low Dyrk1A groups had a high proportion of individuals with no CI, and an equally smaller proportion (36%) of moderate to severe CI. Tau burden, determined by fractional area of NFTs, was equal between Dyrk1A expression groups, with score of 1.5 ± 0.3 (mean ± SEM).

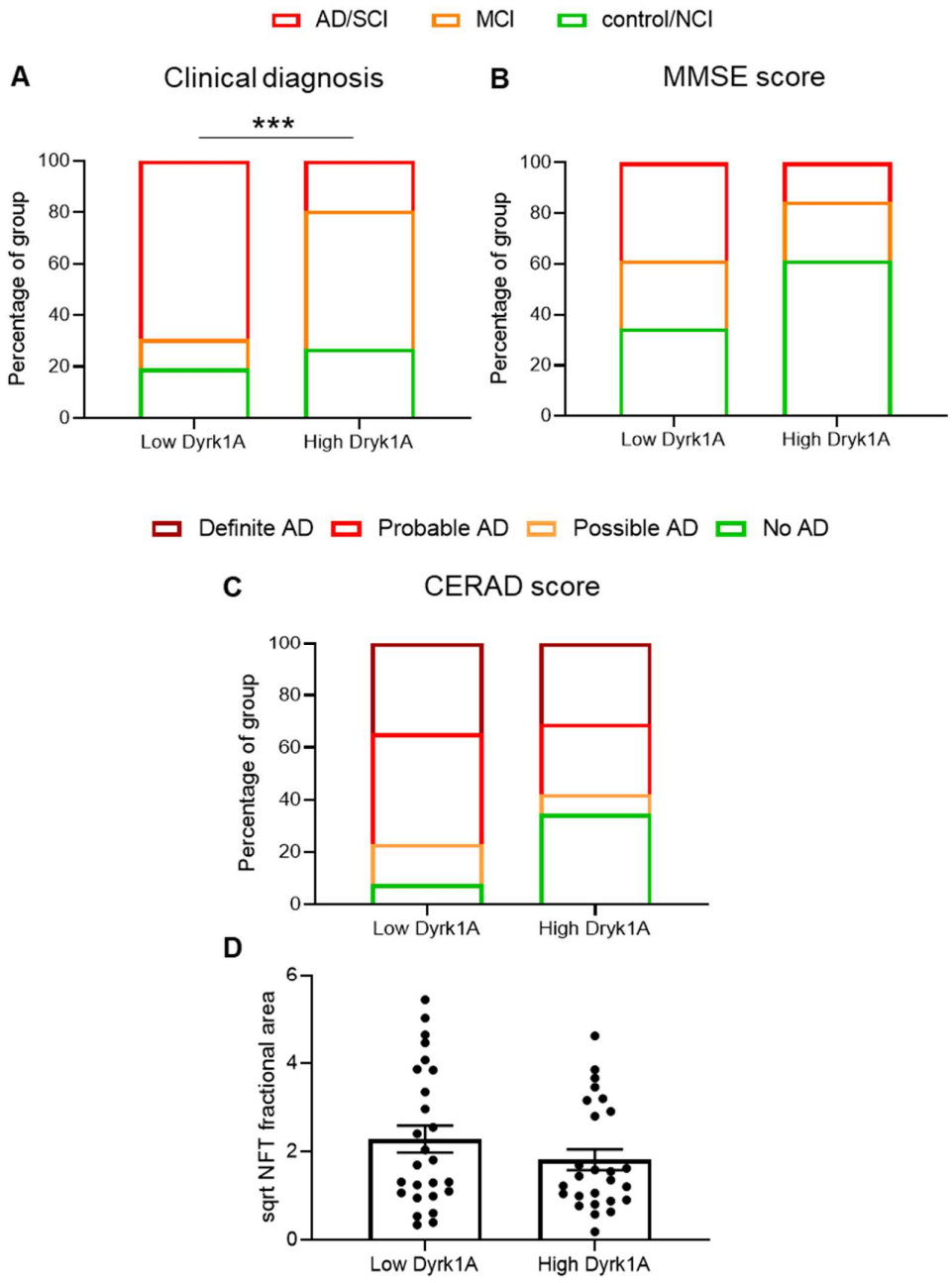


Figure 3.3.5.6 Low Dyrk1A expression in females is related to clinical diagnosis of AD. **A** Comparison of clinical diagnosis in low and high Dyrk1A groups shows that both have similar proportion of individuals with no cognitive impairment but low Dryk1A is related to AD diagnosis whilst the high Dyrk1A group has significantly greater number of individuals with MCI (Chi-square test, $p<0.001$). **B** MMSE scores correspondingly show greater cognitive impairment in the low Dyrk1A group but not to a significant degree (Chi-square test, $p>0.05$). **C** No significant difference between CERAD score in low and high Dyrk1A groups (Chi-square test on binary data i.e. no/possible AD against probable/definite AD, $p>0.05$). **D** Comparison of tau burden by fractional area of NFTs in the brain showed no significant difference with Dyrk1A expression.

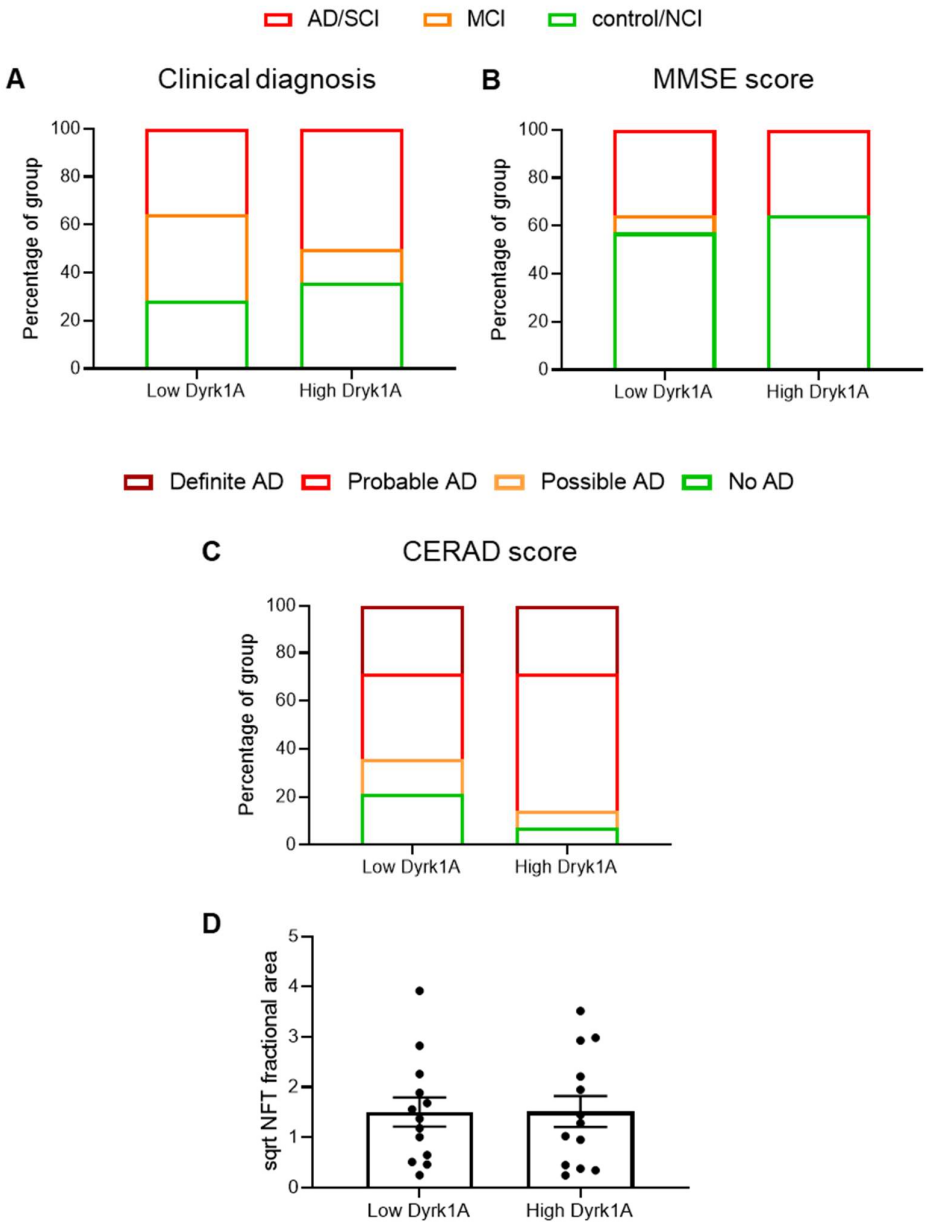


Figure 3.3.5.7 Dyrk1A expression in males is not significantly related to AD phenotype in ROSMAP dataset. **A** Comparison of clinical diagnosis in low and high Dyrk1A groups: control, MCI and AD. **B** Comparison of MMSE score in low and high Dyrk1A groups: no CI, mild CI, and severe CI. **C** No significant difference between CERAD score in low and high Dyrk1A groups, although both had large proportion of probable/definite AD based on neuritic plaque pathology (Chi-square test, $p>0.05$). **D** Comparison of tau burden by fractional area of NFTs in the brain showed no significant difference with Dyrk1A expression (unpaired t-test, $p>0.05$).

Next, I investigated the potential link between CLK1 and AD. In the female subgroup, there was no significant difference in clinical or pathological diagnosis of AD in individuals with low and high CLK1 expression (Chi-square test, $p>0.05$). In the low CLK1 group, there was roughly equal representation of all three clinical groups; 30.7%, 34.6% and 34.6% of females were clinically diagnosed to have no cognitive impairment, mild cognitive impairment, and AD, respectively. In the high CLK1 group, half the females had a diagnosis of AD, and the other half had either no or mild cognitive impairment. According to MMSE score, roughly half (50.0% and 53.8%) of both low and high CLK1 groups had no cognitive impairment, indicating that neither group are associated with higher likelihood of AD. Furthermore, tau burden, measured by fractional area of NFTs, did not show a difference with CLK1 expression. Refer to Figure 3.3.5.8 for more details.

However, in males, it was found that the low CLK1 group had significantly greater diagnoses of AD compared to the high CLK1 group. As presented in Figure 3.3.5.9, only 15.4% of the low CLK1 group had no cognitive impairment, while 61.5% had an AD diagnosis. Inversely, 61.5% of the high CLK1 group had no cognitive impairment and 23.1% had AD. Similarly, CERAD score indicated more individuals with amyloid pathology, as 92% men in the low CLK1 group were categorised to have probable or definite AD. This was not significantly different but comparatively higher than 62% of the high CLK1 group. Histopathological measure of NFTs indicated greater tau pathology, at an average score of 1.99 ± 0.39 in the low CLK1 group and 1.01 ± 0.22 in the high CLK1 group (unpaired t-test, $p<0.05$). This may indicate that tau pathology is more closely related to CLK1-mediated risk for AD diagnosis than amyloid pathology.

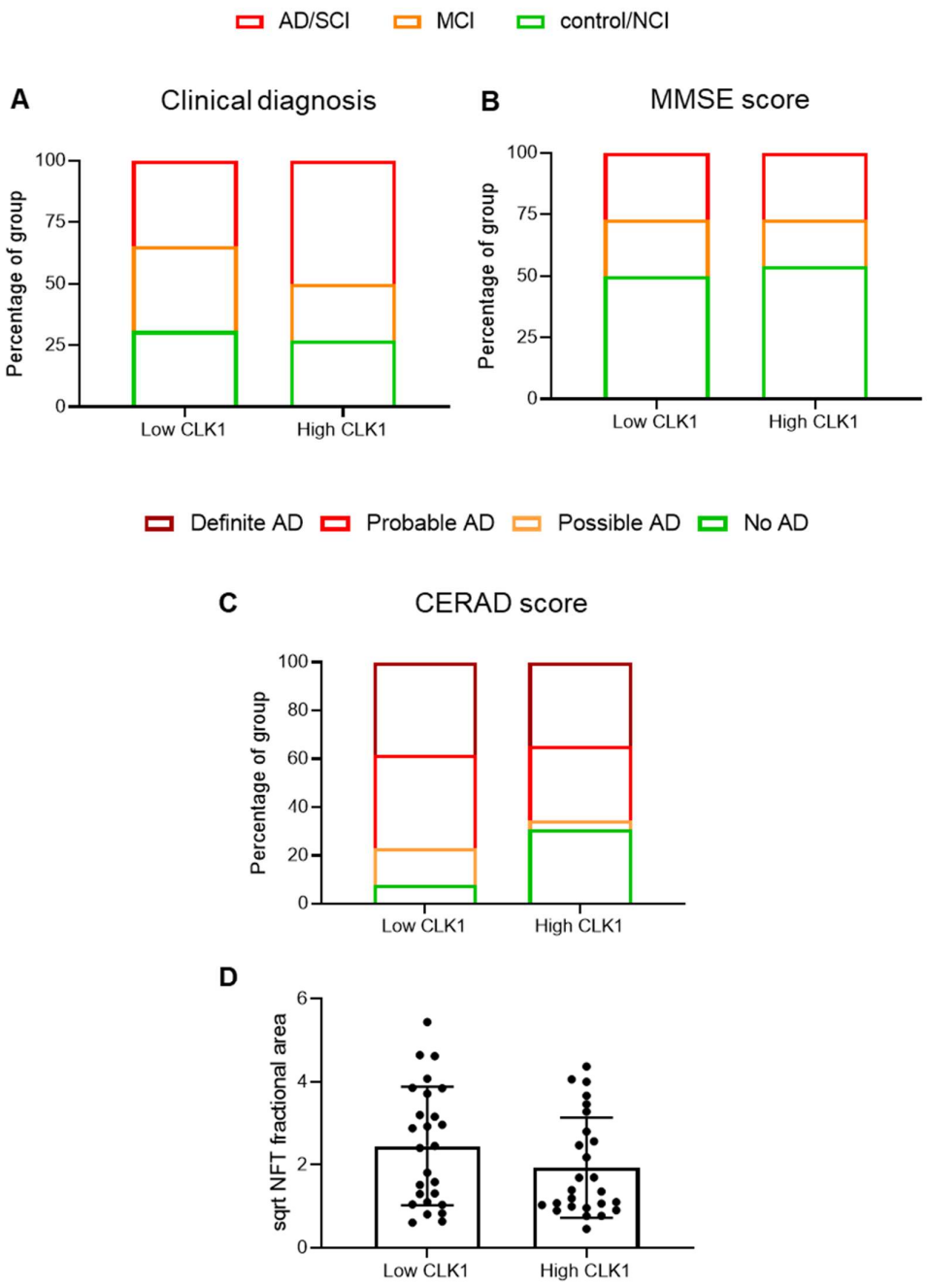


Figure 3.3.5.8 CLK1 expression in females is not significantly related to AD phenotype in ROSMAP dataset. **A** Comparison of clinical diagnosis in low and high CLK1 groups: control, MCI and AD. **B** Comparison of MMSE score in low and high CLK1 groups: no CI, mild CI, and severe CI. **C** No significant difference between CERAD score in low and high CLK1 groups, although a large majority (92%) of the low CLK1 group were quantified to at least have the possibility of AD based on amyloid plaque pathology (Chi-square test, $p>0.05$). **D** Comparison of tau burden by fractional area of NFTs in the brain showed no significant difference with CLK1 expression (unpaired t-test, $p>0.05$).

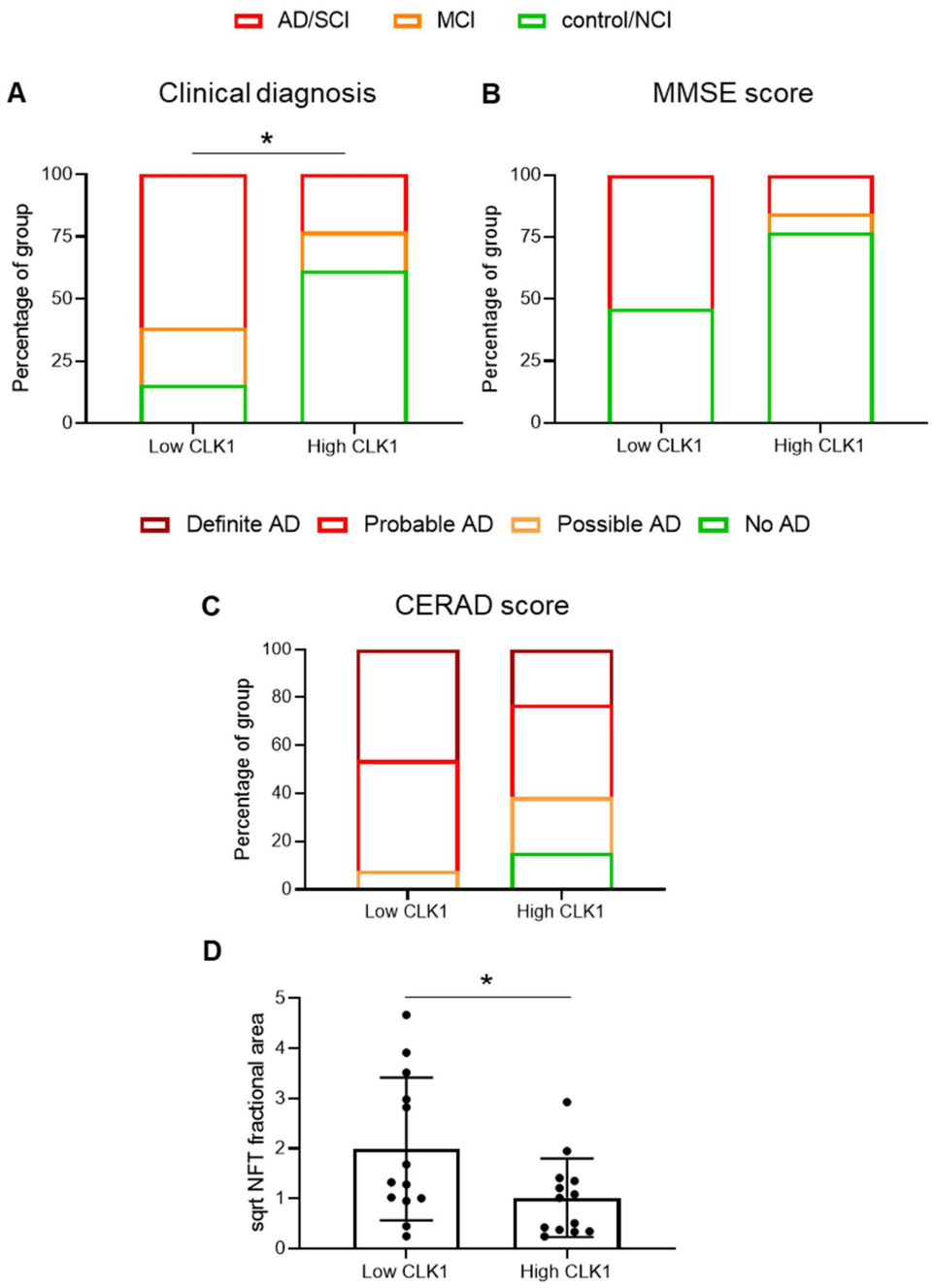


Figure 3.3.5.9 Low CLK1 expression in males is related to clinical diagnosis of AD. **A** Comparison of clinical diagnosis in low and high CLK1 groups shows that the majority of males with high CLK1 expression have no CI whilst the majority of males in the low CLK1 group have AD diagnosis (Chi-square test, $p<0.05$). **B** MMSE scores correspondingly show greater cognitive impairment in the low CLK1 group. The Chi-square test could not be accurately performed as there are no males with MCI in the low CLK1 group, and a Fisher's exact test returned non-significant result ($p>0.05$). **C** CERAD score of males in low CLK1 group all indicated at least the possibility of AD, and the large majority had probable/definite AD based on amyloid plaque pathology. In comparison, fewer males in the high CLK1 group had a positive score for AD, but this difference was not significant (Chi-square test on binary data i.e. no/possible AD against probable/definite AD, $p>0.05$). **D** Comparison of tau burden

by fractional area of NFTs in the brain showed that males in low CLK1 group had significantly greater tau burden (unpaired t-test, $p<0.05$).

Lastly, the ROSMAP dataset was interrogated for differential CLK2 expression. In the female subgroup (Figure 3.3.5.10), there was no significant difference in frequency of AD clinical diagnosis between individuals with low and high CLK2 expression. In the low CLK2 group, 23.1% of females had no CI and 42.3% were diagnosed with AD. To compare, 38.5% and 30.8% of the high CLK2 group fell into these clinical groups respectively, indicating higher likelihood of AD in low CLK2 group. This relatively small difference could equally be attributed to random chance, but amyloid and tau pathology suggest otherwise: CERAD score predicted 88.5% of the low CLK2 group but significantly smaller 52.8% of the high CLK2 group to have probable or definite AD (Chi-square test, $p<0.01$). In addition, NFT fractional area was significantly higher in the low CLK2 group, at an average score of 2.33 ± 0.29, compared to 1.46 ± 0.20 in the high CLK2 group (unpaired t-test, $p<0.05$). Altogether this suggests that low CLK2 expression increases the likelihood of AD pathology but does not translate to significantly increased diagnosis.

In contrast, the male subgroup did not demonstrate a significant link between CLK2 expression and AD. The low CLK2 group had an equal number of individuals with no CI and AD. Clinical groups were similarly distributed in the high CLK2 group, with 30.8% of males having no CI and 46.2% of males having diagnosis of AD. Furthermore, MMSE scores did not show significant difference between CLK2 expression groups: 30.8% and 23.1% of males had moderate to severe CI in low and high CLK1 groups, respectively. CERAD score for Aβ pathology actually predicted the opposite trend, with 61.5% of low CLK2 group but 84.6% of the high CLK2 group having probable or definite AD. However, this difference was not statistically significant, and did not match other AD outcomes, including measure of tau pathology (unpaired t-test, $p>0.05$). Overall, the male subgroup did have a clear link between CLK2 expression and likelihood of AD (see Figure 3.3.5.11). As discussed in previous analyses, this may be a sex-dependent difference in AD pathology or attributable to the sample size disparity between female and male datasets.

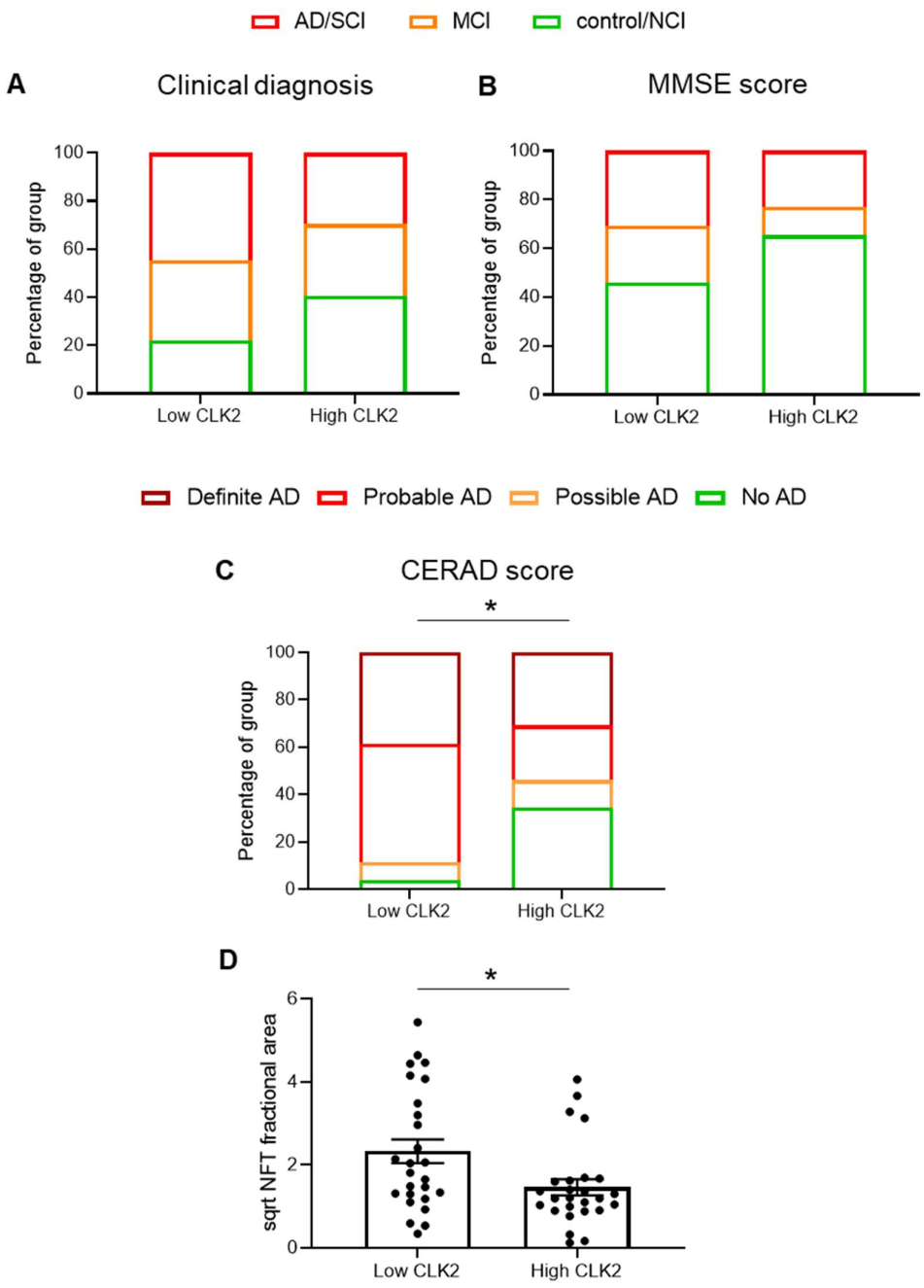


Figure 3.3.5.10 Low CLK2 is related to AD pathology in females but not significantly implicated in clinical outcome. **A** Comparison of clinical diagnosis in low and high CLK2 groups: control, MCI and AD. The low CLK2 group has comparatively higher number of AD cases but is not significantly different to the high CLK2 group (Chi-square test, $p>0.05$). **B** Comparison of MMSE score in low and high CLK2 groups: no CI, mild CI, and severe CI. There is comparatively more CI in low CLK2 group, but this is not statistically significant. **C** Pathological estimation of AD based on CERAD score identifies significantly more cases of AD in low CLK2 group compared to high CLK2 group (Chi-square test on binary data i.e. no/possible AD against probable/definite AD, $p<0.05$). **D** Significantly lower tau burden in the high CLK2 group compared to females with high CLK2 expression, as determined by fractional area of NFTs in the brain (unpaired t-test, $p<0.05$).

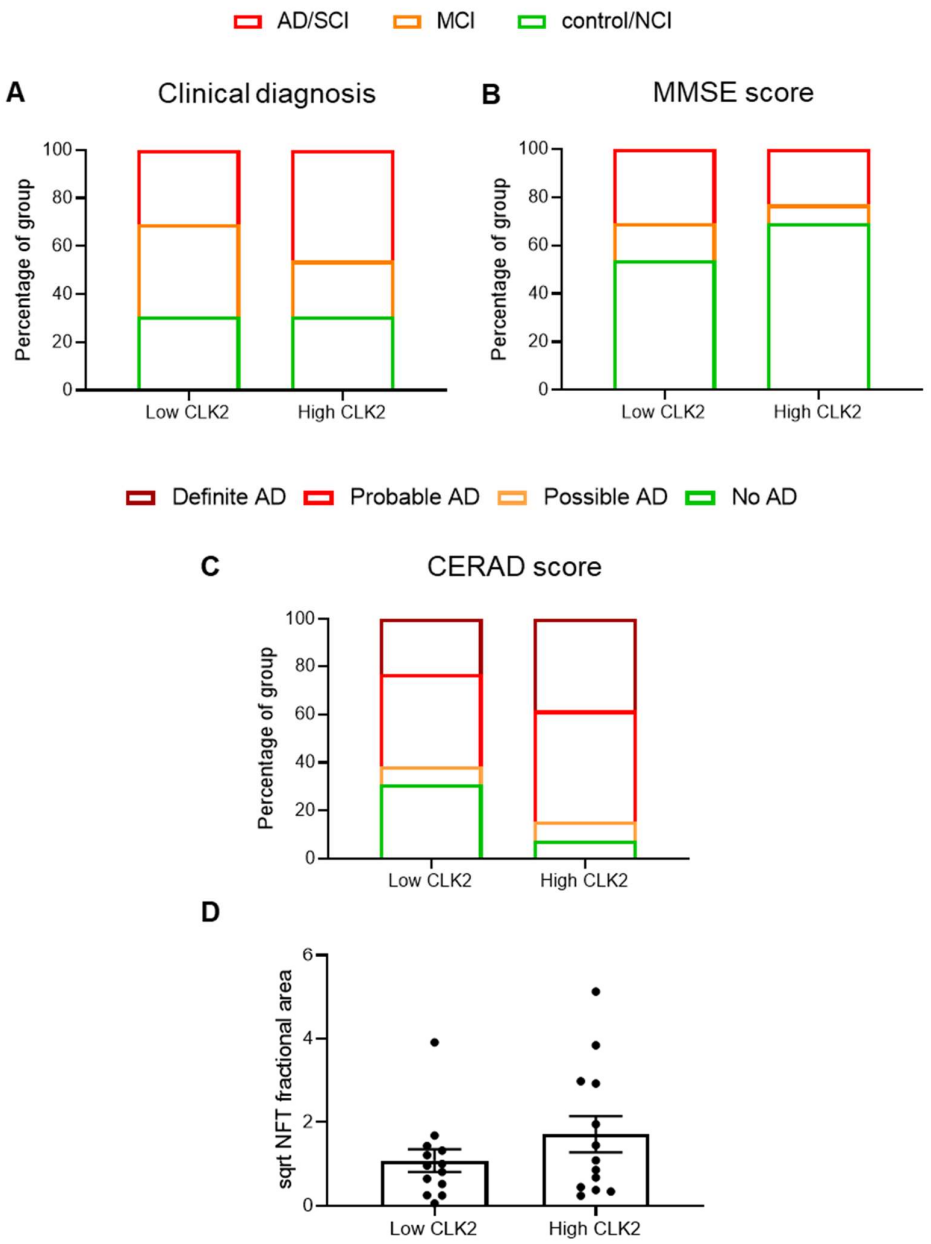


Figure 3.3.5.11 CLK2 expression in males is not significantly related to AD phenotype in ROSMAP dataset. **A** Comparison of clinical diagnosis in low and high CLK2 groups: control, MCI and AD. **B** Comparison of MMSE score in low and high CLK2 groups: no CI, mild CI, and severe CI. **C** No significant difference between CERAD score in low and high CLK2 groups, although males with high CLK2 expression had large proportion of probable/definite AD based on amyloid plaque pathology (Chi-square test, $p>0.05$). **D** Comparison of tau burden by fractional area of NFTs in the brain showed no significant difference with CLK2 expression (unpaired t-test, $p>0.05$).

3.4 Discussion

In this chapter, I investigated gene expression and mRNA splicing in brain regions that are differentially affected by AD to identify what factors may impact vulnerability to disease. Following this, I identified transcriptional differences in the dorsofrontal precortex between individuals with no CI, MCI, and AD. Finally, I interrogated the relationship between expression of splicing kinases and occurrence of AD, determined by both clinical and pathological outcomes. Ultimately, the data collected in this chapter led to the proposition for targeting splicing kinases as a novel therapeutic strategy for AD.

3.4.1 Differential expression in the frontal cortex and cerebellum

The cerebellum presented a differential expression profile compared to the frontal cortex, including significantly lower expression of genes relating to cognition and GPCR signalling pathways. Considering the relative functions of these brain regions, it is unsurprising that genes related to cognition have lower expression in the cerebellum. As seen in Table 3.3.1 and Appendix Table 7.3.2, GPCR signalling pathways were enriched in the frontal cortex by high expression of Neuropeptide Y, serotonin receptors, metabotropic glutamate receptors, and muscarinic cholinergic receptors. Hence, it is likely that the cerebellum has reduced sensitivity to GPCR activation compared to the frontal cortex, and its overall expression profile suggests lower neuronal excitability. Previous transcriptome analysis of the cerebellum and cortical regions has been published to show the cerebellum has a lower density of neurones but increased long-term potentiation (Chappell *et al.*, 2018). As a result, it was suggested that the cerebellum may have relatively stronger synaptic connections which are protective against development of AD. In addition, expression of some AD-related genes, including *CLU* and *BIN1*, were found to be significantly lower in the cerebellum compared to cortices (Chappell *et al.*, 2018). The results presented in this thesis align with published findings, as the GSEA identified GO pathways for the regulation of postsynaptic receptors to be enriched among genes with significantly lower expression in the cerebellum.

There are other examples of AD-related genes that demonstrate region-specific differences. For example, I found *SERPINF1* (regulator of vascular function and inhibitor of angiogenesis) to have higher expression in the frontal cortex compared to the cerebellum (see Appendix Table 7.3.2). This can be considered in parallel to reported evidence that *SERPINE1* is upregulated in AD brain in hippocampi, but not in the cerebellum (Magistri *et al.*, 2015). *SERPINE1* and other senescence-

associated genes have also shown significantly higher expression in prefrontal cortex micro-vessels with exhibition of tau pathology (advanced Braak stage), even after adjustment for cerebrovascular pathology, sex and age (Bryant *et al.*, 2020). Lower expression in the cerebellum may therefore contribute to a protective phenotype. *SERPINE1* is known to facilitate clearance of Aβ (Zhao & Pei, 2008), and thus *SERPINE1* overexpression in hippocampi may constitute a cellular response to region-specific Aβ accumulation, but end up having a negative effect on cerebral vasculature and Aβ degradation (Magistri *et al.*, 2015). Microglia also show regional differences in gene expression, both in normal and AD brain (Mastroeni *et al.*, 2018). Interestingly, the most significant changes in expression were related to neuro-inflammation, which is considered the primary function of microglia, but rather genes involved in neuronal development, plasticity, and neurogenesis. This highlights the importance of brain area selection to avoid variability in results and cell-dependent changes in expression. Furthermore, it suggests that we require characterisation of brain regions, as performed in this chapter, to understand why certain areas are more vulnerable than others.

It is pertinent to note that AD brain also shows differential expression of splicing factors such as hnRNPA2/B1 (Berson *et al.*, 2012). Through hierarchical clustering, it was revealed that splicing factors also have differential expression profiles between the cerebellum and frontal cortex, indicating that alternative splicing may also play a role in the cerebellar phenotype. Specifically, SRSF1, 3, 5, 6, 10 and 11 had higher expression in the cerebellum relative to the frontal cortex, as shown in Figure 3.3.1.2. From these factors, SRSF1 and 6 are involved in the regulation of the spliceosome itself, as they promote binding of U1 and U2 snRNPs to 5' and 3' splice sites, respectively (Howard & Sanford, 2015). Based on this evidence, and our hypothesis that the cerebellum has neuroprotective measures against the onset of AD, rMATS was used to further characterise differential splicing in this brain region.

3.4.2 Differential splicing of AD-related genes in frontal cortex and cerebellum

In section 3.3.2, I found that synaptic genes were differentially spliced in the frontal cortex compared to the cerebellum. The regulation of synapses is vital to normal brain function, and synaptic loss is considered a key pathological feature of AD (Li *et al.*, 2018). The *NRXN2* gene is a member of the neurexin family; β-neurexins are integral to the synapse as they encode pre-synaptic cell adhesion molecules which interact with neuroligins, located on the post-synaptic membrane, forming a connection between the two neurones (Scheiffele *et al.*, 2000; Rowen *et al.*, 2002).

Interestingly, alternative splicing of exon 20 is crucial to the synaptic function of β-neurexins, since protein translated from *NRXN* transcripts without exon 20 do not interact with neuroligins, and consequently inhibit neuroligin-induced differentiation of the presynaptic cell (Scheiffele *et al.*, 2000). Comparing splicing of neurexins in brain regions, it was found that exon 20 skipping was significantly more common in the frontal cortex than in the cerebellum (presented in Figure 3.3.2.2). This indicates that synaptic function may be protected in cerebellum through splicing of neurexins. There is little evidence directly linking *NRXN2* to pathology of AD, but it is known that neurexins are proteolytically processed by presenilins, and familial AD-linked presenilin mutations differentially affect neurexin processing (Saura *et al.*, 2011). Therefore, it has been suggested that neurexins contribute to synaptic dysfunction and memory deficits in the AD brain, particularly because single nucleotide polymorphisms in *NRXN* genes may increase susceptibility for AD (Martinez *et al.*, 2013). Furthermore, reduced *NRXN3* expression in AD brain has been inversely correlated with neuronal inflammation marker *NLRP3*, indicating that dysregulation of neurexin function may increase in neuroinflammation in AD (Hishimoto *et al.*, 2019).

In their study of brain gene expression patterns in MCI, Berchtold et al. found that MCI was not an intermediate between normal ageing and AD, but rather constituted a significant upregulation of synaptic genes, including genes for vesicle fusion and trafficking, neurotransmitter release, and stabilisation of the synapse itself (Berchtold *et al.*, 2014). Interestingly, the expression of synaptic genes, including *NRXN1* and *NRXN2*, were positively correlated with cognitive impairment, as determined by MMSE score. Berchtold et al. noted that genes which regulate synaptic excitability or plasticity had the most significant association with cognitive function as they showed the strongest correlation with MMSE score. This suggests that excitability of the cortex, especially in the vulnerable limbic region, leads to quicker progression of neurodegeneration, and ultimately AD. Independent component analysis of gene expression in AD has also identified the role of neurexins and neuroligins in AD, but found them to be down-regulated, in addition to other genes related to neurotransmitter relay, including *EXOC1* (Kong *et al.*, 2012). The *EXOC1* gene, which encodes a core component of the exocyst complex, is known to help regulate the activity of IP_3R, and *EXOC1* knockdown increases calcium release (Park *et al.*, 2015). In this thesis, it was identified in Figure 3.3.2.4 to be differentially spliced in the cerebellum compared to the frontal cortex. *EXOC1* is a member of the GO pathway for “vesicle-mediated transport to the plasma membrane”, and among other

genes suggest that calcium signalling is differentially regulated in these brain regions through alternative splicing.

The gene *ITPR1* encodes the intracellular receptor IP_3R, which mediates the release of calcium from the endoplasmic reticulum, and consequently modulated the activity of enzymes, either directly or through calmodulin (Mikoshiba *et al.*, 1994). The disruption of calcium homeostasis and dysregulation of calcium signalling is another hallmark of AD (LaFerla, 2002) and IP_3R itself has previously been implicated in AD pathology as single nucleotide variants in *ITPR1* were significantly associated with amyloid deposition and increased AD susceptibility (Seo *et al.*, 2020). The regulation of *ITPR1* expression has been investigated in 3xTg mice, which have three mutations associated with familiar AD (specifically in *APP*, *MAPT* and *PSEN1*) and reliably demonstrate both plaque and tangle pathology. Reduced IP_3R, expression was reported to successfully protect against amyloid accumulation, tau hyperphosphorylation, and memory loss (Shilling *et al.*, 2014). As seen in Figure 3.3.2.5, the cerebellum has more exon 10 skipping compared to the frontal cortex; this "S1" alternatively spliced region has been previously identified in the literature and translates to a 15aa sequence in the binding domain of IP_3R (Nakagawa *et al.*, 1991). Functionally, this has been related to greatly reduced binding of IP_3 to the receptor (Miyawaki *et al.*, 1991). Therefore, relatively lower IP_3 function in the cerebellum resulting from preferential exon splicing could be considered protective against aberrant calcium signalling that occurs in AD. Some studies have found decreased IP_3R in the temporal cortices of AD brain (Haug *et al.*, 1996) and significantly reduced IP_3 binding in regions of the brain with severe NFT pathology (based on Braak staging) or greater amyloid deposition (Kurumatani *et al.*, 1998). Despite this, it is unclear whether IP_3R loss results in a directional change of intracellular calcium levels, so it unlikely to have a straightforward relationship with cortical excitability. Interestingly, Kurumatani also studied IP_3 in the cerebellum, and found no obvious relationship with severity of NFTs; this discrepancy was attributed to the fact this region is less vulnerable to disease and loss of IP_3 would only occur in the end stages of AD. As indicated by results in section 3.3.2, the regulation of splicing (rather than expression) of IP_3 and other mediators of calcium signalling in the cerebellum could play a more important role in providing this neuroprotection.

3.4.3 Differential expression in AD

Transcriptional analysis of the AD brain revealed differential gene expression associated with disease state. I used GSEA to identify biological processes enriched among differentially expressed genes and I found that AD brain could be

distinguished by neurone-specific genes which may be related to cognitive decline through (dys)regulation of synaptic function, vesicle-mediated transport, amine transport, and epithelial cell adhesion molecules.

The dorsolateral prefrontal cortex (DLPFC) of individuals with a clinical diagnosis of AD showed significantly greater expression of synaptic genes compared to individuals with no cognitive impairment. Additionally, GO pathways for synaptic function were enriched with comparisons based on AD pathology (CERAD score) and cognitive impairment (MMSE score), highlighting their importance in the AD phenotype. With transcriptomic stratification of the ROSMAP dataset, Milind et al. also found differential synaptic transmission in AD (Milind *et al.*, 2020). In addition, gene clusters for astrocyte and microglial activation were reported to have opposing differential expression profiles, and related GO inflammatory pathways were enriched among down-regulated genes in my CERAD and MMSE score-based analyses, although not to a significant degree (see Tables 3.3.3.2 and 3.3.3.3, respectively). The GO pathway for "establishment of organelle localisation" organisation was consistently and significantly enriched between control and AD, including structural gene *MYH10* and microtubule-associated proteins *MAP2*, *DCTN2* and *MAPT*. This pathway was also enriched due to upregulation of aforementioned synaptic proteins, such as *RAB*, *CPLX*, and *VAMP* genes, which regulate vesicle transport and membrane docking (see Appendix Table 7.3.10-12). An independent analysis of differential isoform expression in ROSMAP dataset has previously identified enrichment of cell structure regulatory pathways, which are known to be AD-related, and overlap with genes listed in this chapter (Fan *et al.*, 2020). Drawing these parallels from different analysis pipelines validate the findings of this thesis and reinforce the importance of these GO biological processes to the disease state.

To filter for genes with biologically impactful differential expression, RNA-seq studies will often threshold $\log_2$FC>1.5 or >2 rather than p-value alone. However, very few transcripts were identified to show differential expression with these stringent rules, as seen in section 3.3.3. Fan et al. similarly reported a low number of transcripts to be differentially expressed, especially between control and MCI groups, with DEseq2 analysis of the ROSMAP dataset (Fan *et al.*, 2020). This may be attributed to variability in expression profiles, as expected from clinical data collected on a complex disease such as AD. Unfortunately, this makes it rather difficult to find common pathways for AD pathogenesis. The use of transcriptomics has been criticised as an experimental approach to environmental physiology for this same

reason, as it is rare to identify individual genes with large impacts on adaptive responses (Evans, 2015). Nonetheless, physiologically relevant process may be regulated by smaller expressional (1.3- to 1.5-fold) changes and investigated further using an empirical approach. Therefore, genes identified by transcriptional analysis were considered for biological processes that may be altered in AD, and those with statistically significant differences were discussed in this thesis.

Grouping individuals based on MMSE score, a measure of cognitive impairment that is independent of pathological scoring, identified differential expression of *CLU*, known AD-related gene. Clusterin (*CLU*) is the third most significant genetic risk factor identified by GWAS for AD and it has a long-established relationship with β-amyloid; it is thought that clusterin acts to facilitate β-amyloid neurotoxicity, as knockdown of clusterin was shown to be protective *in vitro* and *in vivo* (Killick *et al.*, 2014; Robbins *et al.*, 2018; Foster *et al.*, 2019). This is supported by the ROSMAP dataset, in which *CLU* is among the genes significantly downregulated in severe CI, and may drive conversion from MCI to AD. The severe CI group was also enriched for GO pathways for vesicle-mediated transport in synapse and calcium-regulated exocytosis, which include *VAMP* and *CPLX* genes, as well as *SNAP25*. As previously discussed, synaptic loss is a hallmark of AD, and dysfunction of the synapse is the best correlation between cognitive decline and pathological markers of AD (Li *et al.*, 2018; Chen *et al.*, 2019). Lastly, GO pathways for amine transport were significantly enriched with severe CI. In addition to disruption of the cholinergic system, loss of monoaminergic neurons is known to play a role in AD; long, unmyelinated monoaminergic fibres are particularly vulnerable to aberrant axonal transport, and they are located in many regions of the brain which are affected by neuritic (β-amyloid) plaques and tau pathology (Šimić *et al.*, 2017). In fact, the inter-dependency of cholinergic and monoaminergic neural networks was the basis for proposing the use of multi-modal drugs like ladostigil for the treatment of AD. Ladostigil is a reversable inhibitor of AChE and BuChE (acetyl- and butyryl-cholinesterase) as well as an irreversible monoamine oxidase inhibitor, and was shown to be neuroprotective by enhancing expression of BDNF *in vivo* (Weinreb *et al.*, 2012). The significant enrichment of (mono)amine transporter pathways in the ROSMAP dataset provides further evidence that this group of neurotransmitters are implicated in progression of cognitive impairment and AD. The genes for monoamine transport were upregulated in SCI (listed in Appendix Table 7.3.12), which could be attributed to a compensatory mechanism for possibly reduced monoamine expression and function.

Heat shock proteins *HSPA6* and *HSPA7* were among the genes that showed significantly reduced expression with MCI but not in AD, as highlighted in volcano plots for comparison of CERAD and MMSE scores (see Figures 7.3.11-12). Additionally, functional protein associations were formed between heat shock proteins with STRING enrichment analysis of genes differentially expressed in clinical AD compared to both control and MCI groups (see Figure 3.3.3.2). This is interesting because AD can be characterised by protein misfolding and aggregation, and the primary function of heat shock proteins is to counteract the effects of protein misfolding (Shorbagi & Brown, 2016). Whole transcriptome profiling of AD and Parkinson's disease has previously identified *HSPA6* and *HSPA7* to be differentially expressed compared to control (Annese *et al.*, 2018). This supports findings from the ROSMAP dataset presented in this chapter and suggests that a lack of protection from heat shock proteins contributes to cognitive impairment before progression to AD. Annese et al. also identified dysregulation of *SERPINH1* expression in AD, matching data in section 3.3.3 where *SERPINE1* or related genes were found to be downregulated in individuals with MCI and AD, as determined by cognitive diagnosis, CERAD score, and MMSE score. *SERPINE1* encodes the plasminogen activator inhibitor type-1, which has been previously proposed as an early diagnostic marker for AD because its expression increases with dementia progression (Oh *et al.*, 2014). The inhibitor effectively reduces the production of plasmin, a protease that plays a role in clearance of Aβ (Zhao & Pei, 2008).

Mitochondrially Encoded Cytochrome C Oxidase Psuedogenes (*MTCO*P*) were found to have significantly differential expression in MCI and AD compared to control; since these are long non-coding RNAs, it could be suggested that epigenetic processes are involved in the progression of cognitive impairment. This is supported by the fact GO pathways for regulation of transcription and protein translation were identified to be downregulated, although not to a significant degree (see Tables 3.3.3.1-2). Review of the literature emphasises that non-coding RNAs are implicated in the pathogenesis of AD by altering the expression of various AD risk factors and AD-related genes (Idda *et al.*, 2018).

3.4.4 Differential splicing transcripts in AD brain and splicing kinase expression in relation to 4R:3R tau ratio

In this chapter, the number of known transcripts per gene was used as a general indication of splicing. It was found that individuals with MCI and AD had a greater number of known transcripts per gene, i.e., exhibited increased splicing compared to control. Characterisation of genes by transcript number identified genes with splicing

transcripts exclusively expressed in MCI and AD. Among these genes was NDRG2, which has been previously shown as upregulated in AD pathology (Mitchelmore *et al.*, 2004). In their analysis of splicing of the ROSMAP dataset, Raj et al also identified NDRG2 to be among the 52 genes that show significantly differential splicing in AD. Additionally, MCI and AD groups produced more splicing variants of SERF2, which has been shown regulate amyloid conformation and deposition in both *C elegans* and mouse models (Stroo *et al.*, 2021). Interestingly, splicing of long non-coding RNA gene MEG3 was also identified in cognitive impairment, which further implicates differential epigenetic processes.

The literature reports on differential expression of RNA binding proteins that were not identified in this study but have been previously associated with AD pathology, providing further evidence that regulation of splicing is altered in AD. For example, hnRNPA2/B1 was found to be downregulated as a result of impaired cholinergic signalling in AD (Berson *et al.*, 2012); hnRNPA2/B1 is an important regulator of AS and its activity affects many proteins, among which is β-secretase. Depletion of hnRNPA2/B1 shifts toward the production of more active β-secretase, which in turn causes accumulation of Aβ plaques (Kolisnyk *et al.*, 2017). Additionally, TDP-43 is an RNA-binding protein that has been widely reported as a marker of neurodegenerative diseases, including 20% of AD patients; TDP-43 accumulates and forms inclusions distinct from NFTs, and their wider distribution outside the limbic lobe has been linked to greater severity of AD (Amador-Ortiz *et al.*, 2007). Expression of mutant TDP-43 shows altered alternative splicing of neural genes in a transgenic pig model (Wang *et al.*, 2015a), which emphasises the important role of AS in disease progression.

Dysregulation of tau splicing is known to occur in AD and other tauopathies, as introduced in section 1.4. The 4R:3R tau ratio, based on transcript quantification of two *MAPT* isoforms including and excluding exon 10, was used as an indicator of tau splicing in the ROSMAP dataset. I found that splicing kinase expression was positively correlated with 4R:3R tau ratio (Figure 3.3.4.4), indicating that SRPK, Dyrk1A and CLK are related to AS events which regulate tau function and directly impact tau pathology. Restoring equimolar expression of 4R and 3R isoforms is important for normal brain physiology and has been shown to protect against aggregation of tau, neuronal dysfunction, and cognitive decline (Espindola *et al.*, 2018). As a result, splicing kinases could be targeted to modulate AS of tau and protect against NFT pathology.

AS in AD is also known to impact synaptic function, previously discussed to be central in the process of neurodegeneration. For example, splice-junction microarray identified AD-specific changes in AS that were distinct from age-related differences, including alternative exon inclusion in cell adhesion molecule genes *NEO1*, *CHL1* and *NRCAM*, as well as synaptic assembly gene *GPHN* (Tollervey *et al.*, 2011). Many of these AD-related exons were found to be regulated by NOVA1/2, neuronal-specific RNA-binding proteins, which are known regulators of synapse formation and function (Ruggiu *et al.*, 2009). In this study, AD-related AS of NOVA-regulated genes was associated with decreased nuclear abundance in NOVA proteins (Tollervey *et al.*, 2011), suggesting that many AD splicing events are dependent on NOVA activity. Examination of exon skipping events in the ROSMAP dataset (in addition to data repositories from MSBB and Mayo clinic) similarly revealed enrichment of synaptic processes in differentially spliced genes; this included vesicle-mediated transport and protein localisation to membrane (Yang *et al.*, 2021). These were among GO processes enriched in the differential transcript expression analyses performed for this thesis, highlighting their importance in the AD phenotype. Yang et al. identified significant downregulation of RNA-binding Motif 3 (*RBM3*) to be positively correlated with 107 reported exon skipping events, including exon skipping in cell adhesion molecule gene *CHL1*. Interestingly, the knockdown of *RBM3* has been previously investigated in 5xFAD mice, which express human *APP* and *PSEN1* with three, and two, pathogenic mutations respectively, causing relatively early and aggressive presentation of amyloid pathology, neuronal loss, and cognitive deficits. It was reported that knockdown of *RBM3* exacerbated synapse loss and accelerated neurodegeneration in this model (Peretti *et al.*, 2015), making *RBM3* another noteworthy regulator of AS in AD. The transcript levels of further RNA-binding proteins and splicing kinases are also reported in dementia, so it is likely interplay of multiple mechanisms are involved in AS of synaptic genes and other AD-relevant processes.

3.4.5 Relation between low SRPK expression and AD pathology

Splicing kinases are known to regulate phosphorylation and function of splicing factors, thus targeting splicing kinases can be therapeutic by modifying alternative splicing of downstream targets. The ROSMAP dataset was used to investigate relationship between expression of splicing kinases and occurrence of AD. In women, the top quintile for SRPK1 and SRPK2 expression had a significantly lower number of AD diagnoses than bottom quintiles (see section 3.3.5). This was supported by significantly reduced neuritic (Aβ) plaques, measured by CERAD

score, as well as tau burden, measured by density and distribution of NFT pathology. Altogether, this suggests that low expression of SRPK1 and SRPK2 can be associated with AD in women. Since this has not been empirically tested, there is no evidence for causation, nor is it obvious whether low SRPK1/2 expression increases risk for AD, or rather SRPK1/2 expression is downregulated as a result of AD pathology. Indeed, downregulation of SRPK1/2 expression could be adopted as a compensatory mechanism, albeit insufficient to provide neuroprotection against AD. There is very little published information on SRPK1 in AD pathology, but elevated auto-antibodies against SRPK1 have been reported in AD patients (Daniilidou *et al.*, 2011), which could consequently lead to reduced SRPK1 expression. SRPK2, however, is known to regulate tau function through splicing and direct phosphorylation, and so elevated SRPK2 activity has been tied to NFT formation and dysfunction of synaptic function, crucial steps in the pathogenesis of AD (Hong *et al.*, 2012; Wang *et al.*, 2018). SRPK2 has been investigated in APP/PS1 mice, a double transgenic line with mutations in *APP* and *PSEN1*, causing accelerated plaque pathology, neuroinflammation, and cognitive impairment. Depletion of SRPK2 was proven to inhibit tau phosphorylation and alleviate cognitive impairment (Hong *et al.*, 2012), which appears to contradict data reported here. Having said that, Wang et al. reported AEP-mediated cleavage of SRPK2 to increase its nuclear localisation and kinetic activity i.e., a functional increase in SRPK2 rather than transcriptional upregulation. As a result, SRPK2 expression may be downregulated as a compensatory response to its increased activity in AD, which could possibly explain the higher proportion of AD observed in women with low SRPK2. Further investigation of the dynamics of SRPK2 function is necessary to draw more precise conclusions, but it clear that SRPK function contributes to AD pathology and cognitive decline.

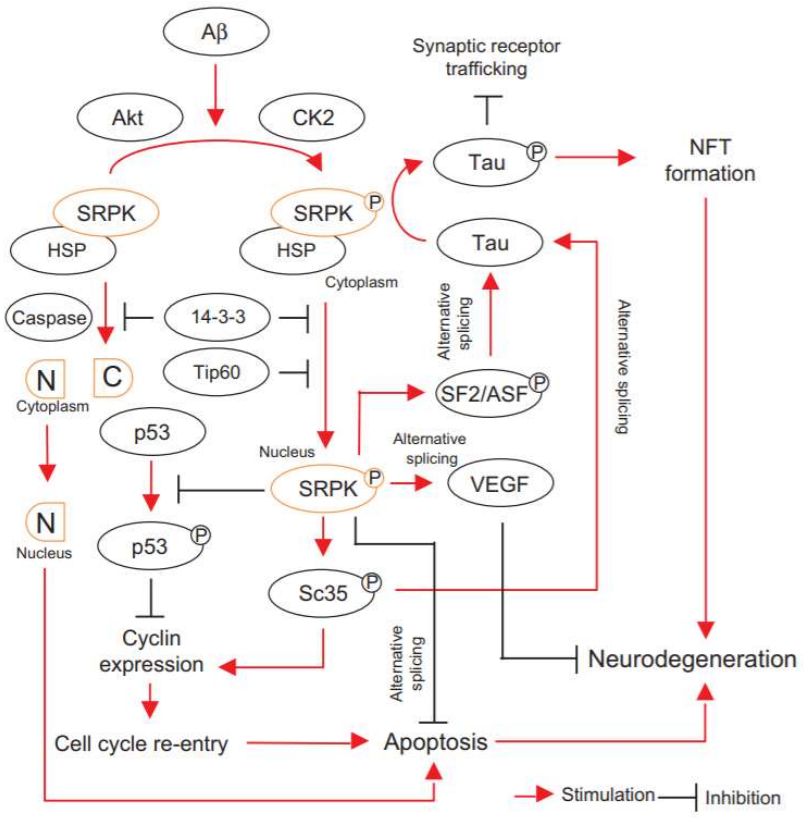


Figure 3.4.5.1 Schematic diagram of potential SRPK mediated regulatory mechanisms in neurodegeneration, presented by (Chan & Ye, 2013).

Sex-dependent differences are well documented to impact disease risk and often involve a combination of biological and environment factors. Unfortunately, AD is known to disproportionately affect women (Mielke *et al.*, 2014). Sex-dependent risk is likely to have played a role in the ROSMAP dataset since differential AD occurrence was observed in females but not replicated in males. However, it is noteworthy that there are roughly double the number of females than males, and so the sample size of males may have been insufficient to observe an effect, particularly after being sorted for age (there was a total of 26 women and 13 men per quintile). This is reflected by post-hoc power analysis (Faul *et al.*, 2007) of NFT pathology data. In females, 1-β = 0.65 and 0.78 for SRPK1 and SRPK2, whilst in males, 1-β = 0.31 and 0.09, respectively. As β is the probability of making a type II error, 1-β is used as an indicator of power; 0.8 is generally accepted as adequate power because it indicates low probability of error. Therefore, a larger age-matched dataset may be necessary for the conduction of the analysis of AD occurrence in

males in order to determine with confidence if splicing kinases are related to diagnosis and/or pathology.

SRPKs can be characterised by a spacer sequence that splits their catalytic domain in two; the spacer has no direct effect on kinase activity (Ngo *et al.*, 2005) but rather determines subcellular localisation through a cytoplasmic retention signal. This effectively acts as a negative regulator of SRPKs by reducing interaction with the spliceosome (Zhong *et al.*, 2009). SRPK1, the ubiquitously expressed member of the family, has been proposed to be a constitutively active kinase that does not require any post-translational modification to optimise function: While other splicing kinases require phosphorylation to be activated, SRPK1 has a relatively short activation loop that is readily accessible (Ghosh & Adams, 2011). This makes its subcellular localisation more important to the regulation of SRPK1 function compared to phosphorylation and other factors (Gonçalves & Jordan, 2015). When in the nucleus, SRPK1 phosphorylates the RS domain of SR proteins to control alternative splicing of downstream targets (Aubol *et al.*, 2013). SRPK2 is highly enriched in the brain but co-expressed with SRPK1 in other human tissues and cell lines (Wang *et al.*, 1998). SRPK2 isoforms differ by selection of an alternative start exon, encoding different N-terminal sequences; the full length 'a' isoform of SRPK2 is 10aa longer than the 'b' isoform and differs by the first 24aa sequence, after which the remaining protein sequence is conserved (determined from Ensembl and NCBI databases). Interestingly, SRPK1 has only one protein-coding isoform with RefSeq on the NCBI database, which encodes the full-length protein. The other listed isoform uses an alternative 5' splice site which results in a novel exon and contains an early stop codon, making it a candidate for nonsense-mediated mRNA decay.

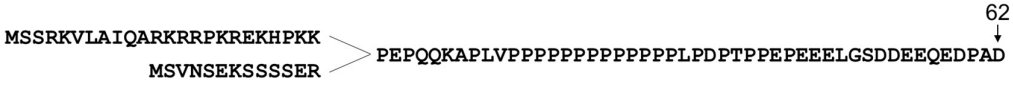


Figure 3.4.5.2 Amino-acid sequence for N-terminus of SRPK2 in 'a' and 'b' isoforms which have alternative start exons, encoding full-length and short version respectively.

The removal of the SRPK2 N-terminus was shown to have deleterious effects on its activity, indicating that it is necessary for SRPK2 function (Liang *et al.*, 2014); this is a unique regulatory feature, since deletion of the SRPK1 N-terminus does not block substrate binding or kinetic activity (Ngo *et al.*, 2005; Ngo *et al.*, 2007). Targeting the N-terminus provides a potential method for regulation of SRPK activity, which may be neuroprotective against AD and other tauopathies. For the purposes of this

thesis, expression of full-length isoform of SRPK2 was investigated in the ROSMAP dataset. However, if truncation of SRPK2 N-terminal blocks kinetic activity, exploiting endogenous regulation of SRPK2 could effectively control its function and potentially attenuate SRPK2-mediated tau pathology.

3.4.6 Relation between Dryk1A expression and AD

The *DYRK1A* gene is localised in the Down syndrome (DS) critical region of chromosome 21 and is associated with many aspects of DS, including mental retardation (Song *et al.*, 1996). Overexpression of *DYRK1A* in a transgenic mouse model replicates key symptoms of DS such as cognition deficit, learning difficulties, motor abnormalities, and memory loss (Altafaj *et al.*, 2001). Interestingly, individuals with DS develop AD-type pathology very early in life, creating a link between the two pathologies (Wisniewski *et al.*, 1985). Indeed, *DYRK1A* expression was found to be dysregulated in AD and other neurodegenerative conditions (Arbones *et al.*, 2019), suggesting that Dyrk1A activity may be driving these pathologies and inhibition of Dryk1A could alleviate shared symptoms. This hypothesis has been tested using *in vivo* models, where pharmacological Dryk1A inhibition significantly reduced effects of pathological tau overexpression and neuroinflammation (Melchior *et al.*, 2019) as well as amyloid plaque levels, which effectively recovers cognitive decline (Lee *et al.*, 2020).

In the ROSMAP dataset, there was no clear relationship between Dyrk1A expression and AD (see Figures 3.3.5.6-7). In a subgroup of women, the bottom quintile for Dyrk1A expression had significantly higher proportion of AD diagnoses compared to the top quintile, suggesting a relationship between low Dyrk1A expression and occurrence of AD. In addition, 86% of the low Dyrk1A group had considerable neuritic (Aβ) plaques required for pathological assessment of probable or definite AD. However, CERAD score and tau burden did not significantly differ between low and high Dyrk1A groups. Since Dyrk1A expression was not consistently associated with pathology of AD, it is reasonable to suggest that Dyrk1A is more relevant to DS dementia, and although high Dyrk1A may increase risk for AD, it is not necessary for pathogenesis. It could also be argued that Dyrk1A plays a less important role in AD than SRPK1/2, as low SRPK groups were significantly associated with AD pathology. However, it may in fact be the case that AD diagnosis is over-represented in individuals with both low and high Dyrk1A expression. However, this somewhat contradicts evidence in the literature for elevated Dyrk1A in AD (Arbones *et al.*, 2019). As I previously discussed with relation to SRPK, it is not possible to conclude causation or definitively determine if

expressional changes occur as a consequence of disease without empirical evidence.

At least two alternative promoters of the *DYRK1A* gene regulate transcription with different 5'- untranslated regions; cassette exon 1-containing isoforms are only found in skeletal muscle and heart whereas exon 2-containing isoforms are ubiquitously expressed in the human body (Guimera *et al.*, 1999). The remaining N-terminal domain encodes a unique nuclear targeting sequence (which confines Dyrk1A to the nucleus), and followed by the kinase domain, PEST region, and finally a C-terminal domain with histidine repeats and serine/threonine repeats (Kentrup *et al.*, 1996; Becker *et al.*, 1998). Conserved tyrosine residue 321 is a key site in the activation loop found within the kinase domain; Y321 is auto-phosphorylated in an intermediate form of Dyrk1A during translation, hence the final form of Dyrk1A is constitutively active (Kentrup *et al.*, 1996). Dyrk1A activity is therefore assumed to be directly related to its expression, known as "dosage effect"; significantly altered expression, such as dramatically higher Dyrk1A observed in DS with an extra gene copy, results in significantly higher kinase activity and leads to pathological processes (Abbassi *et al.*, 2015). In light of this, individuals with low Dyrk1A expression in ROSMAP dataset can be assumed to have reduced Dyrk1A activity, indicating that the association with AD diagnosis does not occur as compensation for increased activity. However, it may be that increased Dyrk1A expression is phenotypic for early development of AD but is not sustained in end-stage dementia. In support of this, plasma Dyrk1A has reported to be significantly decreased in AD patients compared to control, while individuals with negative Aβ status actually showed a rise in Dryk1A expression with age (Delabar *et al.*, 2020). Indeed, low Dyrk1A was more closely related to amyloid status than clusterin, which is a known risk factor for AD, further evidence for its involvement in AD pathology. It was therefore proposed that decreased Dyrk1A could be a biomarker for AD, which altogether agrees with findings from ROSMAP cohort. However, it remains unclear why low Dyrk1A is related to the occurrence of AD.

There is little known about upstream regulation of Dyrk1A, but transcription factor E2FI has been identified to increase *DRYK1* gene expression (Maenz *et al.*, 2008). Additionally, studies on bone homeostasis have suggested that NFATc1 can induce Dyrk1A expression, although NFATc1 itself is inhibited by Dryk1A though a negative feedback loop (Lee *et al.*, 2009). Investigation of these factors may expand our understanding of Dyrk1A regulation, and how its expression may change during AD pathogenesis.

3.4.7 Relation between low CLK expression and AD pathology

The CLKs are dual-specificity kinases; with relation to AD, CLKs have been established to regulate *MAPT* exon 10 splicing (Jain *et al.*, 2014) but otherwise have not been associated with AD risk or pathology. In the ROSMAP dataset, it was found that men with low expression of full-length CLK1 had significantly greater number of AD cases than men with relatively high CLK1 expression (see Figure 3.3.5.9). Although this effect was not supported by CERAD score, the low CLK1 group did have significantly greater tau burden, which indicates that CLK1 expression may be closer related to NFT formation than amyloid pathology. Interestingly, this effect was not seen replicated in the female subgroup, indicating further sex-dependent differences in the roles of kinases in AD. However, women with low and high CLK2 expression did show differences in AD-related outcomes (see Figure 3.3.5.10). In particular, the low CLK2 group had significantly greater pathological assessment of probable or definite AD, as well as greater tau burden (determined by NFT fractional area). Although this group did also have more clinical diagnoses of AD, this was not statistically significant. Nonetheless, low expression of CLK can be associated with greater AD pathology, suggesting that regulating CLK expression could manipulate disease progression.

The CLK kinase domain is located in the C-terminus, highly conserved in the CLK family, and containing a signature amino acid motif ‘EHLAMMER ILG’. The N-terminal domain is poorly conserved between isoforms, but it is considered intrinsically disordered due to enrichment of serine/arginine residues, which enable the N-terminus to readily interact with the RS domains of SR proteins (Colwill *et al.*, 1996). It has been proposed to regulate CLK function through presence of a nuclear localisation signal; when deleted, there is a significant switch to cytoplasmic localisation (Duncan *et al.*, 1997). Additionally, truncation of the N-terminus has been shown to significantly increase CLK-1 activity, specifically the rate of reaction, suggesting that the N-terminus domain negatively regulates CLK1 (Menegay *et al.*, 2000). It was proposed that the N-terminus may “conformationally constrain catalysis” but the mechanism behind its regulatory function remains unclear. More recent studies have shown that the N-terminus is important in facilitating SR protein phosphorylation; while CLK1 is able to incorporate a total of 18 phosphates into the RS domain of SRSF1, CLK1ΔN (without N-terminus) is only able to add 6 phosphates (Aubol *et al.*, 2014). Crucially, Aubol et al also reported that (a) full-length CLK1 bound to SRSF1 with an affinity 15-fold greater than CLK1ΔN, and (b) the N-terminus directly interacts with CLK1 kinase domain as well as SR proteins.

Based on these collective findings, it was proposed that the N-terminus may act as a bridge connecting the CLK1 kinase domain to the RS domain of SR proteins, or bind RS domains to draw them closer the CLK active site.

Interestingly, all four human CLKs are alternatively spliced to produce a full-length protein or a truncated protein lacking the kinase domain. The latter occurs when 91bp exon 4 is skipped, leading to a frameshift and introducing a pre-mature stop codon (Johnson & Smith, 1991; Duncan *et al.*, 1995). These isoforms were reported to have near 1:1 expressed ratio in most tissues, but it was noted that hindbrain (among others) showed much higher levels of the full-length isoform (Menegay *et al.*, 2000). The presence of truncated protein is thought to regulate CLK activity, perhaps through interactions with full-length CLK and/or SR proteins (Aubol *et al.*, 2014). Interrogation of the ROSMAP dataset was based on the full-length CLK transcripts which were selected for "normal" kinase activity. Manipulating CLK activity with truncated isoforms could have an effect on tau pathology, as well as other CLK-regulated pathways.

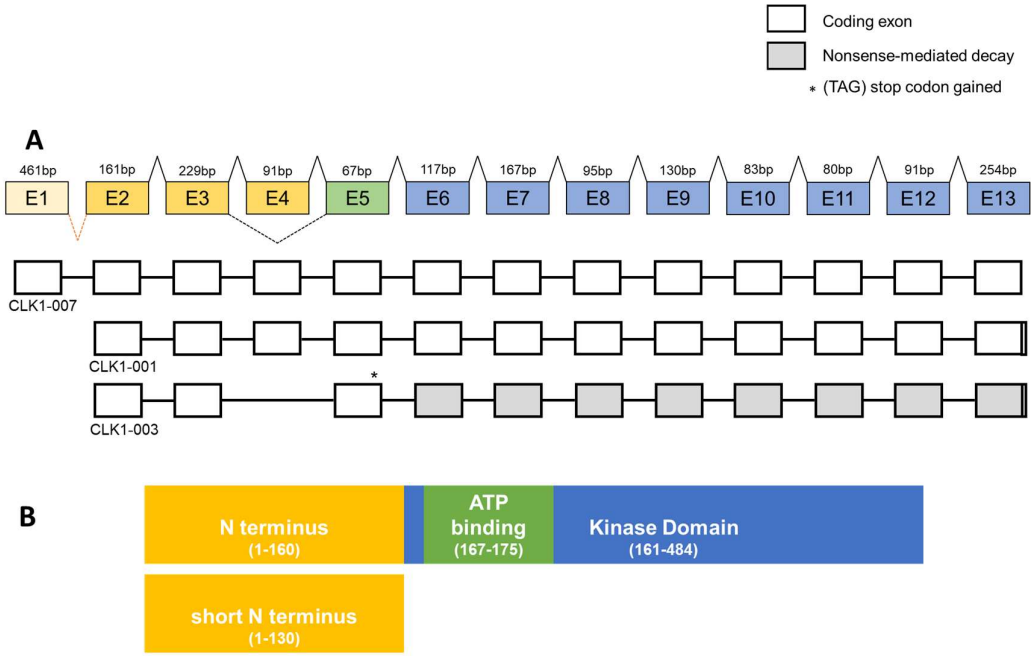


Figure 3.4.7 Alternatively spliced isoforms of CLK1 protein. **A** Exons (length in bp) coding CLK1 found in three different isoforms from NCBI database. The CLK1-003 transcript skips exon 4 and frameshift results in stop codon and nonsense-mediated decay. **B** Full-length protein translated from CLK1 transcripts 007 and 001 and truncated transcript lacking kinase domain translated from CLK1-003 transcript.

With regard to AD pathology, CLKs have been shown to increase *MAPT* exon 10 skipping (Hartmann *et al.*, 2001); if this were the case, low CLK groups could be

assumed to have greater exon 10 inclusion and therefore increased 4R tau relative to 3R tau expression. However, the expression of CLK and other splicing kinases was positively related to 4R:3R tau ratio. As the correlation was weak, it is not necessarily in contradiction with previous findings, especially considering that ANCOVA was conducted on sum of all transcripts, some of which may be regulatory (e.g., nonsense-mediated decay) and not a reliable indicator of kinase function. Even so, it is clear that splicing kinases can be related to *MAPT* exon 10 splicing. The imbalance in 4R:3R tau ratio is known to occur in AD and is thought to contribute to NFT pathology (Park *et al.*, 2016). Indeed, it has been previously reported that AD can be characterised by excess of 4R tau (Spires-Jones *et al.*, 2011; Kopeikina *et al.*, 2012). As many other kinases regulate tau splicing, this cannot be wholly dependent on CLK, but it can nonetheless be postulated that CLK expression modulates risk of AD through 4R:3R tau ratio and related pathology.

3.4.8 Targeting splicing kinases as a therapeutic strategy for AD

SRPK inhibition is being investigated as a novel approach to the treatment of numerous conditions, including cancers (Mavrou *et al.*, 2015) and age-related macular degeneration (Gammons *et al.*, 2013), through AS of VEGF-A. Since the data presented in this chapter relates SRPK expression to the occurrence of AD, I was led to the hypothesis that modulation of SRPK activity may affect AD pathology. Indeed, VEGF-A is already established to play an important role in AD, particularly through its effect on vascular risk, as previously introduced in section 1.6. This provides a potential mechanism through which SRPK activity may affect pathogenesis in AD brain and targeting SRPK may prove neuroprotective. This hypothesis is explored in Chapter 4 through use of SPHINX31, a novel SRPK1 inhibitor, which is known to alter VEGF-A splicing.

Both CLK1 and CLK2 expression was also related to the occurrence of AD. CLK has been previously proposed as a therapeutic target for AD because CLKs can be linked to aberrant splicing in AD, particularly in tau-related pathology (Jain *et al.*, 2014). This led me to the hypothesis that CLK inhibitors may be used to modulate *MAPT* exon 10 splicing and protect against AD pathology. In Chapter 5, I explore the potential use of novel small-molecule CLK inhibitors to shift 4R:3R tau ratio and ameliorate AD-related neurotoxicity.

3.4.9 Concluding remarks

First, I investigated AS in the cerebellum and frontal cortex of normal human brain to identify differences that may make the cortex more susceptible to AD pathology.

This primarily identified AS of genes relating to synaptic function, which highlights the importance of synaptic regulation to providing protection against AD. Indeed, differential expression analyses of the ROSMAP dataset also revealed significant enrichment of synaptic genes with AD diagnosis, pathology, and cognitive decline. Synaptic loss in AD is driven by accumulation of tau and NFT pathology (Gratuze & Holtzman, 2021) which further implicates tau as a key driver of AD pathogenesis.

In this chapter, I also examined the relationship between splicing kinases and occurrence of AD, and I found that groups with low expression of SRPK and CLK transcripts have significantly higher proportion of AD pathology and diagnoses than high expression groups. This was mostly observed in female groups; sex-dependent differences may be dependent on differing biology and/or statistical effect size since the male cohort had half the sample size of women in the ROSMAP dataset. Although this analysis does not indicate causation, it does relate splicing kinases to AD, and suggests that modulation of SRPK and CLK activity could contribute AD pathogenesis. To further characterise the role of splicing kinases in AD, *in vitro* models for Aβ and tau hyperphosphorylation related neurotoxicity were used in Chapters 4 and 5 to experimentally assess AS of VEGF-A and tau, splicing targets of SRPK and CLK, respectively.

Chapter 4: The effect of VEGF-A on AD-related neurotoxicity

4.1 Introduction

The neurovascular unit (NVU) controls blood-brain barrier (BBB) permeability and cerebral blood flow, maintaining the chemical composition of cerebral tissue required for its proper function (Zlokovic, 2011). The NVU unit comprises vascular cells (endothelium, pericytes and smooth muscle), glial cells and neurones. Dysfunction of the NVU, and resulting disruption to the BBB, is associated with the accumulation of neurotoxins, including β-amyloid, as well as a reduction in cerebral blood flow and hypoxia. Cerebrovascular deficits are common in AD: >50% of patients have ischaemic white matter damage and >90% of patients have cerebral amyloid angiopathy, characterised by the deposition of Aβ in vessel walls (Thomas *et al.*, 2015). Furthermore, vascular risk factors, such as atherosclerosis and diabetes mellitus, also increase risk of developing AD (Yang *et al.*, 2004).

4.1.1 Amyloid and VEGF-A

There is growing evidence that amyloid production and cerebral hypoperfusion are inherently linked to each other in AD pathology. VEGF-A, a key regulator of angiogenesis, is known to bind to amyloid peptides with high affinity and specificity. In addition, it has been found to co-localise with neuritic (Aβ) plaques in the AD brain (Yang *et al.*, 2004). Aβ treatment has been shown to alter angiogenesis in a concentration dependent manner: At lower concentrations, amyloid can result in the stimulation of microvessel formation whereas higher concentrations significantly inhibit the angiogenic process in endothelial cells (Paris *et al.*, 2004). Investigation of amyloid's anti-angiogenic activity found that it can inhibit VEGFR2 activation by directly binding and acting as an antagonist of the receptor (Patel *et al.*, 2010). Furthermore, amyloid treatment of endothelial cells can reverse a VEGF-A induced increase in permeability. Considering VEGF-A is a very potent permeability factor, these studies put forward strong evidence of amyloid's ability to antagonise VEGF-A related activity.

Interestingly, levels of VEGF-A are increased in the AD brain, specifically in the frontal cortex and para-hippocampus (Thomas *et al.*, 2015). In addition, the total level of VEGFR1, a negative regulator of VEGF-A expression, is reduced in AD despite being upregulated by hypoxia (Harris *et al.*, 2018). However, this may be offset by the fact the ratio of membrane bound to soluble VEGFR1 is also reduced, since soluble VEGFR1 is inactive and can sequester VEGF-A by acting as a

competitive inhibitor of its ligand. Ultimately, this suggests that inhibition of VEGF-A binding at VEGFR2, and related VEGF-A mediated activity, may be driving upregulation of its expression. Indeed, Thomas et al. suggested that overproduction of VEGF-A in AD may be a compensatory mechanism for reduced cerebral perfusion associated with Aβ accumulation. This is supported by evidence that VEGF-A expression positively correlates with disease severity (Thomas *et al.*, 2015). Since cerebral hypoperfusion persists as a symptom of AD, endogenous upregulation of VEGF-A may be an insufficient response to NVU dysfunction. Exogenous VEGF-A can oppose the effect of high Aβ concentrations and partially restore angiogenic activity *in vitro* (Patel *et al.*, 2010) suggesting that stimulation of VEGF-A activity could be relevant to neuroprotection. However, it is important to elucidate the direct effect on neurones as the majority of studies so far have only characterised role of VEGF-A in the endothelial cell component of the NVU.

4.1.2 Neurofibrillary tangles and VEGF-A

As a hallmark of AD pathology, neurofibrillary tangles (NFTs) are the second key driver of cognitive decline. NFTs are mainly comprised of hyperphosphorylated tau, a protein particularly abundant in neurones, and lead to cell dysfunction and death (Theofilas *et al.*, 2018). Compared with amyloid, there is less literature linking NFTs to VEGF-A biology, but diminished VEGF-A has been correlated with the presence of NFTs in AD cortices (Provias & Jeynes, 2008). Furthermore, the ratio of phosphorylated tau to amyloid is considered a strong positive predictor of cognitive decline and has been used to identify other CSF biomarkers for AD (Harari *et al.*, 2014). The use of lentiviral VEGF-A treatment was tested in apoE4-driven AD pathology (using mice expressing the ε4 allele) and VEGF-A was found to reverse apoE4-associated increase in hyperphosphorylated tau as well as amyloid accumulation (Salomon-Zimri *et al.*, 2016). Considering this evidence for crosstalk between amyloid, tau and VEGF-A, it is necessary to account for both amyloid and tau hypotheses in order to properly understand the role of VEGF-A in AD pathology.

4.1.3 AD-related neurotoxicity *in vitro*

The accumulation of Aβ leads to cell death through generation of reactive oxygen species (ROS) and mitochondrial dysfunction in the AD brain (Cheignon *et al.*, 2018). To create a pathologically relevant *in vitro* model, oxidative species and exogenous Aβ can be used to induce concentration-dependent toxicity in neuronal cell lines. Introduction of Aβ in a cell assay has been previously reported to be problematic since Aβ can rapidly assemble in different aggregation states, leading to

different physiological effects and inconsistency between assays (Faller & Hureau, 2020). Naturally, Aβ in the AD brain is also found to assemble by different mechanisms, but *in vitro* this creates an obstacle to building a robust assay. However, investigation of the relative toxicity of aggregation states could perhaps shed light on which mechanisms are linked to pathogenesis of AD. “Amyloids” are the most stable form of Aβ assembly, defined as fibrillar aggregates with a high content of β-sheet structures, whilst amorphous aggregates are larger assemblies of mainly unstructured peptides. There are also Aβ oligomers, which usually refers to soluble Aβ aggregates with a limited size, and are now thought to be the most toxic form of amyloid (Lee *et al.*, 2017). In this chapter, all Aβ treatments were conducted immediately after suspension of DMSO stock in ice-cold water, which is recommended for an unaggregated state (Stine *et al.*, 2011). In this instance, Aβ treatment of Neuro2a cells was shown to cause a concentration-dependent decrease in cell survival but was less severely toxic than oligomeric and fibrillar forms.

In order to model tau-related neuronal dysfunction, okadaic acid (OA) was selected as a neurotoxin that is known to cause hyperphosphorylation and abnormal aggregation of tau. A neurite outgrowth assay was developed to provide a functional measure of OA-induced toxicity *in vitro*; this was achieved by using βIII-tubulin as a neuronal-specific marker that is also linked to AD pathophysiology. Together, α- and β-tubulins make up heterodimers that polymerise into microtubules, and the function of microtubules is known to be disrupted in AD (Nasu *et al.*, 2020). This is perhaps unsurprising since tau is a microtubule associated protein, but it also has wider implications on pathophysiology, since microtubules are required for cell morphology and axon stability, as well as maintenance of cell cycle and division. Critically, if co-treatments are able to protect and stabilise microtubules, as indicated by maintenance of βIII-tubulin and neurite outgrowth, they could also significantly reduce downstream effects of microtubule dysfunction, including cell death, and therefore offer real therapeutic options for AD.

4.1.4 Hypotheses

Central to this work is the notion that VEGF-A is not limited to its original discovery as a vascular protein but rather a pleiotropic protein that exerts cytoprotective effects in the nervous system (Greenberg & Jin, 2005). It has thus been proposed to act as an neuroprotective agent implicated in a number of neurodegenerative conditions, including AD (Storkebaum *et al.*, 2004). In cases of ischemic injury, VEGF-A not only protects neural tissue by reperfusion but also directly exerts

neurotrophic (survival) and neurotropic (neurogenesis) actions (Hobson *et al.*, 2000). I wanted to investigate the use of VEGF-A as a neuroprotective agent using *in vitro* models relevant to AD pathology. In addition to this, I aimed to look at the effects of alternative splicing isoform VEGF-A_{165}b, which has previously been shown to protect against sensory neuronal degeneration in a model of diabetes (Hulse *et al.*, 2015) but had not yet been studied in AD. The SRPK1 inhibitor SPHINX31, which can shift VEGF-A splicing from VEGF-A_{165}a to VEGF-A_{165}b isoforms, had never been used in the context of AD either. I initially established a neuronal cell assay based on oxidative stress since ROS production is widely accepted to be crucial to amyloid plaque toxicity (Cheignon *et al.*, 2018). I then proceeded to use amyloid as a direct neurotoxin. Metabolic activity was used as a proxy for cell viability to quantify neuronal insult and investigate the potential protective effect of VEGF-A_{165} isoforms. Finally, I investigated the effect of VEGF-A and SPHINX31 treatments in a neuronal outgrowth assay based on the induction of tau hyperphosphorylation (Metin-Armagan *et al.*, 2018).

The hypotheses for this chapter are:

1. NGF and VEGF-A_{165} isoforms will increase viability of SHSY5Y cells and N2a cells.

2. NGF and VEGF-A_{165} isoforms will protect against H_2O_2-induced reduction in neuronal viability.

3. VEGF-A_{165} isoforms will protect against amyloid-induced reduction in neuronal viability.

4. VEGF-A_{165} isoforms will ameliorate reduction in neuronal outgrowth induced by okadaic acid.

5. SRPK1 inhibition with SPHINX31 treatment of SHSY5Y cells will shift VEGF-A splicing toward VEGF-A_{165}b isoform.

6. SPHINX31 treatment will replicate the neuroprotective effect of VEGF-A_{165}b in the neuronal outgrowth assay.

4.2 Methods

Human SHSY5Y cells and mouse N2a cells were cultured for use *in vitro*. Cells were treated with neurotoxic agents hydrogen peroxide, β-amyloid or okadaic acid for 24h with and without 2.5nM (100ng/mL) VEGF-A co-treatment. Neuroprotective agent NGF was used as a positive control. For SRPK1 inhibition, cells were treated with SPHINX31 for 24-72h (depending on assay) at a range of 1-10μM. Cells were assayed for cell viability with WST-1 reagent. After 0.5-1h incubation, Magellan microplate reader was used at 480nm wavelength with 620nm reference. Cells were assayed for neurite outgrowth with βIII tubulin immunofluorescence. Images were taken with Leica confocal microscope at 20x and 40x magnification. The VEGF-A_{165}a and VEGF-A_{165}b ELISA were performed on whole cell lysates collected from SHSY5Y cell culture. Unless stated otherwise, all replicates are experimental (technical) replicates. All methods are described in detail in Chapter 2.

4.3 Results

4.3.1 VEGF-A isoforms are neuroprotective against oxidative stress

To establish an assay of neuronal toxicity, SHSY5Y and N2a cells were treated with hydrogen peroxide, a strong reactive oxygen species that can induce oxidative stress *in vitro* (Bonello *et al.*, 2007). The WST-1 assay showed a decrease cell viability at 150-250μM and 25-100μM H_2O_2 in SHSY5Y cells (Figure 4.3.1.1A) and N2a cells (Figure 4.3.1.1B), respectively. These concentrations were selected based on the published work in SHSY5Y cells (Ossola *et al.*, 2012; Garcimartin *et al.*, 2017) and my own optimisation of culture conditions. Co-treatment with neuroprotective agent NGF was used as a positive assay control since it is known to consistently increase neuronal cell survival (Bogetti *et al.*, 2018). WST-1 assay quantified a significant increase in viability of both cell lines (two-way ANOVA, $p<0.01$), validating the use of the assay to investigate the effect of VEGF-A isoforms in this *in vitro* model of oxidative stress.

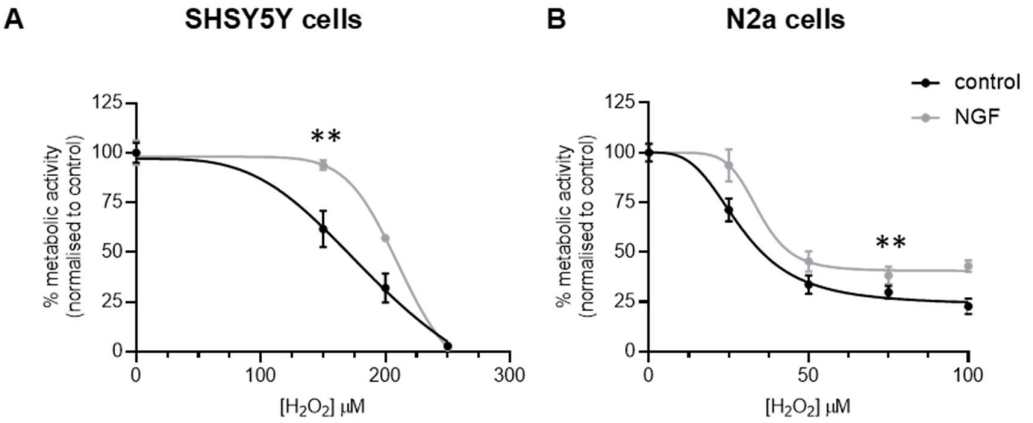


Figure 4.3.1.1 NGF increases metabolic activity of SHSY5Y cells and N2a cells co-treated with hydrogen peroxide. SHSY5Y cells and N2a cells were treated with H_2O_2 alone or with NGF for 24h and a WST-1 assay was performed to measure metabolic activity. Readings were normalised against an assay control (media + WST-1 reagent) and experimental control (cells treated with PBS or NGF alone + WST-1 reagent). **A** Concentration-dependent decrease in percent metabolic activity of SHSY5Y cells with H_2O_2. NGF treatment significantly increased metabolic activity compared to control group (two-way ANOVA, $p<0.01$). **B** Concentration-dependent decrease in percent metabolic activity of N2a cells with H_2O_2. NGF treatment significantly increased metabolic activity compared to control group (two-way ANOVA, $p<0.01$). N=3-4 replicates.

In SHSY5Y cells, treatment with 100ng/mL recombinant VEGF-A_{165}a acted against increasing concentrations of hydrogen peroxide and significantly increased cell viability (two-way ANOVA, $p<0.01$) in a similar manner to NGF. There is an upward shift in cell metabolic activity where the drop in the control group induced by 150μM H_2O_2 (62% ±9.8% of control) is completely recovered by 100ng/mL VEGF-A_{165}a (shown in Figure 4.3.1.2A below). In N2a cells, there was no significant difference in the viability with VEGF-A_{165}a treatment (see Figure 4.3.1.2B) but measured slightly higher under 50-100μM H_2O_2.

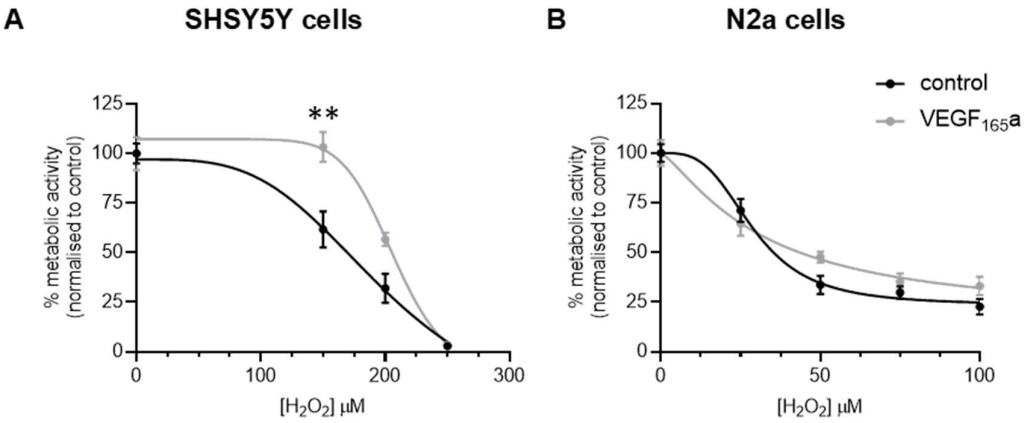


Figure 4.3.1.2 VEGF-A_{165}a increases metabolic activity of SHSY5Y cells and N2a cells co-treated with hydrogen peroxide. SHSY5Y cells and N2a cells were treated with H_2O_2 alone or with 100ng/mL VEGF-A_{165}a for 24h and a WST-1 assay was performed to measure metabolic activity. **A** Concentration-dependent decrease in percent metabolic activity of SHSY5Y cells with H_2O_2. VEGF-A_{165} treatment consistently and significantly increased metabolic activity compared to control group (two-way ANOVA, $p<0.01$). **B** Concentration-dependent decrease in percent metabolic activity of N2a cells with H_2O_2. VEGF-A_{165} treatment slightly increased metabolic activity compared to control but not to a significant degree (two-way ANOVA, $p>0.05$). N=3-4 replicates.

Recombinant VEGF-A_{165}b has previously demonstrated cytoprotective properties in the retina (Magnussen *et al.*, 2010), as measured by the same WST-1 assay used in this study. In SHSY5Y cells, 100ng/mL VEGF-A_{165}b treatment induced a similar effect. Figure 4.3.1.3 shows an upward shift in cell metabolic activity where VEGF-A_{165}b completely recovered the decrease in the control group at 150μM H_2O_2 (62% ±9.8% of control). As previously seen with VEGF-A_{165}a, there was no significant difference in the viability of N2a cells with 100ng/mL VEGF-A_{165}b treatment, but it measured slightly higher under 50-100μM H_2O_2.

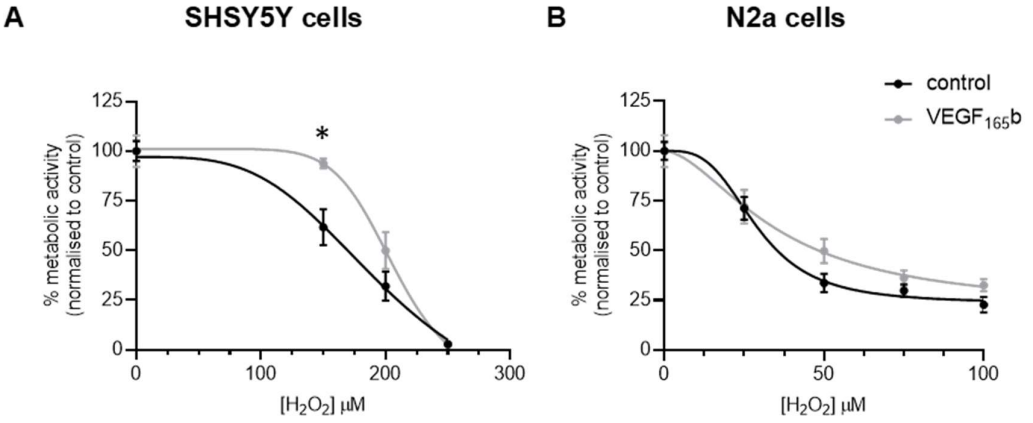


Figure 4.3.1.3 VEGF-A_{165}b increases metabolic activity of SHSY5Y cells and N2a cells co-treated with hydrogen peroxide. SHSY5Y cells and N2a cells were treated with H_2O_2 alone or with 100ng/mL VEGF-A_{165}b for 24h and a WST-1 assay was performed to measure metabolic activity. **A** Concentration-dependent decrease in percent metabolic activity of SHSY5Y cells with H_2O_2. VEGF-A_{165}b treatment consistently and significantly increased metabolic activity compared to control group (two-way ANOVA, $p<0.05$). **B** Concentration-dependent decrease in percent metabolic activity of N2a cells with H_2O_2. VEGF-A_{165}b treatment slightly increased metabolic activity compared to control but not to a significant degree (two-way ANOVA, $p>0.05$). N=3-4 replicates.

4.3.2 VEGF-A isoforms are neuroprotective against Aβ-induced neurotoxicity

In the development of the amyloid *in vitro* model, increasing concentrations were used to reduce cell viability in accordance to guidance from the literature, particularly methods chapter detailing how to prepare amyloid in unaggregated, oligomeric and fibrillar states (Stine *et al.*, 2011). Since amyloid has a tendency to aggregate *in vitro* and its unaggregated form had been shown to reduce viability of N2a cells, this method was selected for my study. In SHSY5Y cells, 10-100nM amyloid did not have any effect on cell viability after both 24h and 48h treatment. However, 1μM amyloid significantly decreased viability to 80% ±3% of control after 24h, as presented in Figure 4.3.2.1A. As 48h treatment produced a very similar response, the remainder of assays were carried out after 24h incubation. The same optimisation was repeated in N2a cells: although viability decreased to 69% ±8% of control with 24h 1μM amyloid treatment, the assay did not produce a consistent decrease in viability (see Figure 4.3.2.1B). To validate the use of WST-1 as a measure of cell viability, both SHSY5Y and N2a cells were treated with chemotherapy agent cisplatin: 24h treatment produced a decrease to 35% ±4% and 40% ±2% of control viability, shown in Figure 4.3.2.1C and D, respectively.

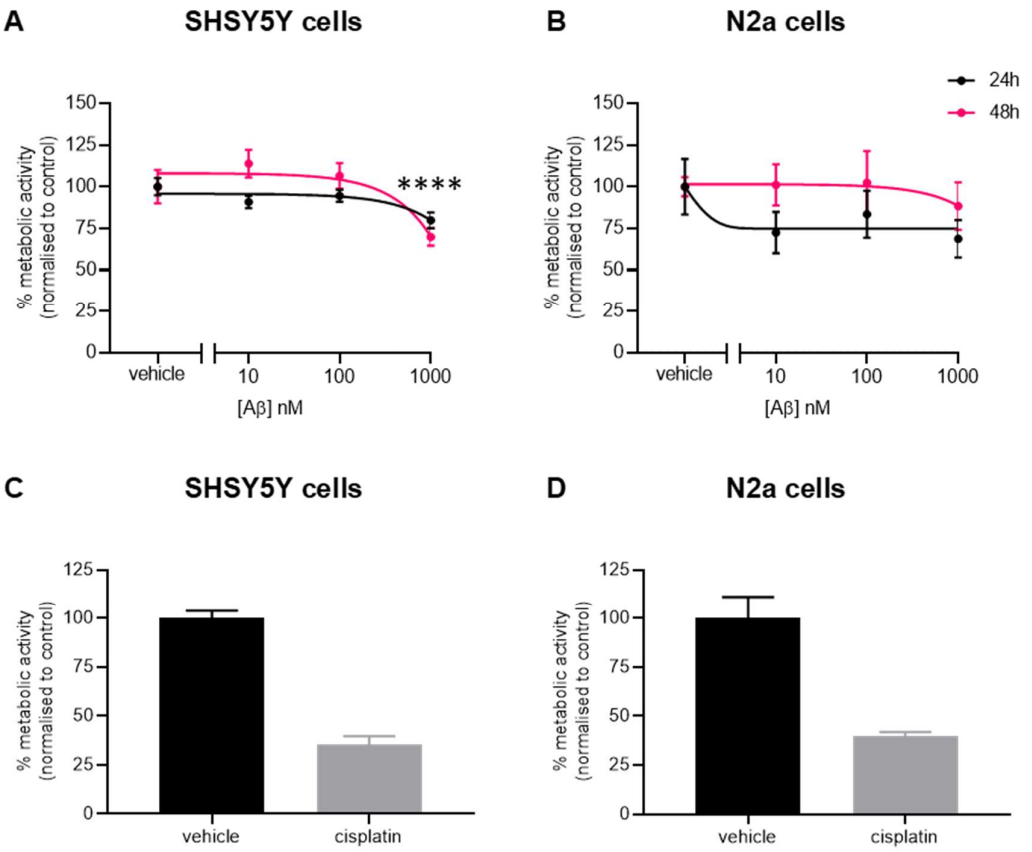


Figure 4.3.2.1 β-amyloid (Aβ) caused modest decrease in metabolic activity of SHSY5Y cells and N2a cells. SHSY5Y cells and N2a cells were treated with increasing concentrations of Aβ for 24h and 48h. WST-1 assay was performed to measure metabolic activity and readings were normalised against an assay control (media + WST-1 reagent) and experimental control (cells treated with vehicle alone + WST-1 reagent). N=3 replicates. **A** After both 24h and 48h treatment, SHSY5Y cells were not affected by 10-100nM Aβ but percent metabolic activity was significantly decreased with 1μM Aβ (two-way ANOVA, $p<0.0001$). **B** N2a cells had a variable response to different concentrations of Aβ. Metabolic activity was reduced but not to a significant degree (two-way ANOVA, $p>0.05$). **C D** Normalised to control, cisplatin decreased metabolic activity in both SHSY5Y cells and N2a cells.

In this model, SHSY5Y cells were treated with 100ng/mL recombinant VEGF-A_{165}a and VEGF-A_{165}b to identify whether they could rescue amyloid-induced reduction in cell viability. Treatment with 100ng/mL VEGF-A_{165}a and VEGF-A_{165}b recombinant protein alone did not significantly alter metabolic activity compared to vehicle control ($p>0.05$). Treatment with 1μM amyloid alone significantly decreased cell viability to 63% ±5% of control (one-way ANOVA, $p<0.05$), but when co-treated with either VEGF-A_{165}a (in Figure 4.3.2.2A) or VEGF-A_{165}b (in Figure 4.3.2.2B), there was no significant drop in cell viability between with 1μM amyloid ($p>0.05$). Comparing amyloid treatment groups, Tukey's multiple comparisons test revealed that SHSY5Y cells with Aβ + VEGF-A_{165}a treatment were not significantly to Aβ alone, viability measured at 81% ±7% of control ($p>0.05$). VEGF-A_{165}b co-treated cells had similar metabolic activity, measured at 84% ±5% of control, but this was significantly higher than Aβ alone ($p<0.05$).

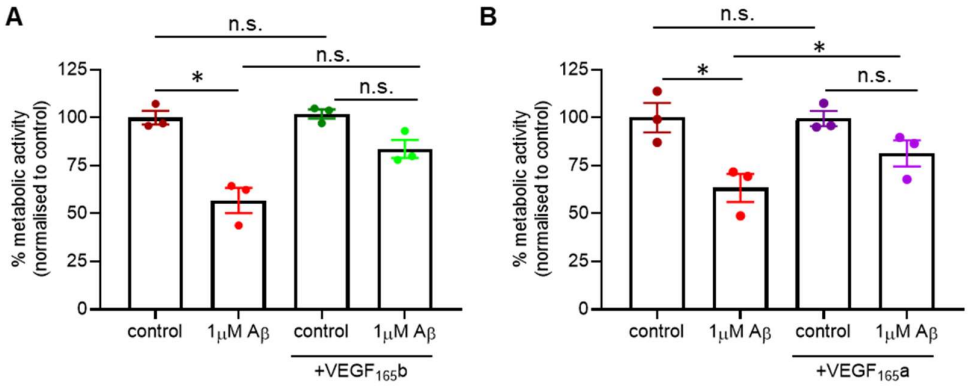


Figure 4.3.2.2 VEGF-A_{165}a or VEGF-A_{165}b treatment recovers Aβ-induced decrease in metabolic activity in SHSY5Y cells. **A** Normalised metabolic activity showed decrease with 1μM Aβ (one-way ANOVA, $p<0.05$) and was recovered with co-treatment of VEGF-A_{165}a. Treatment with 100ng/mL VEGF-A_{165}a alone did not significantly change metabolic activity. **B** Similarly, 100ng/mL VEGF-A_{165}b alone did not change metabolic activity but protected against Aβ-induced reduction. N=3 replicates.

As previously demonstrated in Figure 4.3.2.1, 1μM amyloid did not cause a significant decrease in N2a cell viability, measured at an average 92% ±8% of control. Co-treatment with 100ng/mL VEGF-A_{165}a and VEGF-A_{165}b maintained a similar level of cell viability, at 82% ±9% and 80% ±4% of control, seen in Figure 4.3.2.3A and B, respectively.

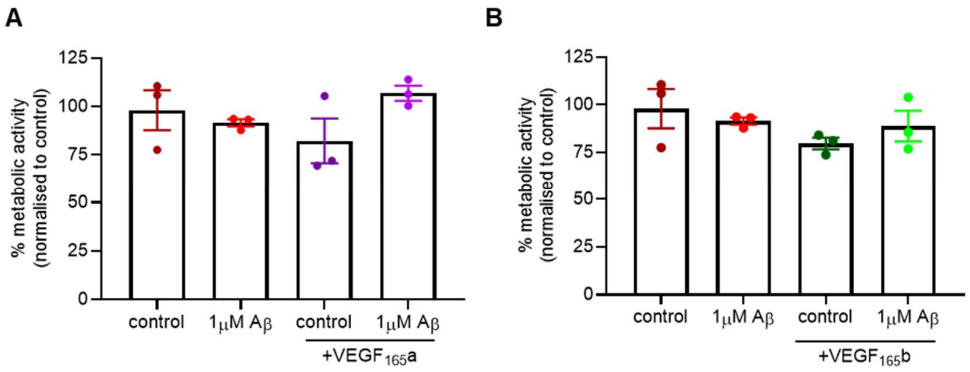


Figure 4.3.2.3 Aβ treatment did not replicate decreased in metabolic activity in N2a cells. **A** No consistent change in metabolic activity of N2a cells was measured with WST-1 assay with 1μM Aβ nor 100ng/mL VEGF-A_{165}a. **B** Furthermore, co-treatment with 100ng/mL VEGF-A_{165}b did not produce a measurable change in metabolic activity by WST-1 assay of N2a cells. N=3 replicates.

4.3.3 VEGF-A isoforms are protective in neuronal outgrowth assay

Okadaic acid (OA) is a neurotoxic agent that has been established to cause hyperphosphorylation and aggregation of tau in SHSY5Y cells (Boban *et al.*, 2019). I used OA to develop a neurite outgrowth assay, which was selected to be a basic measure of neuronal viability and function that is closely related to the primary role of tau as a microtubule-associated protein. Tau stabilises the neuronal cytoskeleton by copolymerising with tubulin for microtubule formation. However, an increase in its phosphorylation reduces its interaction with microtubules, causing destabilisation of the cytoskeleton and neurodegeneration (Lindwall & Cole, 1984; Iqbal *et al.*, 2010). βIII tubulin antibody was selected as a neuronal specific marker (Draberova *et al.*, 1998) and used to probe SHSY5Y cells treated with increasing concentration of OA, as presented in Figure 4.3.3.1A. Quantification showed a concentration-dependent decrease in cell number (Figure 4.3.3.1B) and normalised neurite outgrowth length (Figure 4.3.3.1C). At 3nM OA, SHSY5Y cells decreased to 60% ±9% of control cell number and 56% ±9% of control neurite outgrowth length. Based on these findings, the outgrowth assay was taken forward to interrogate the neuroprotective effect of VEGF-A isoforms.

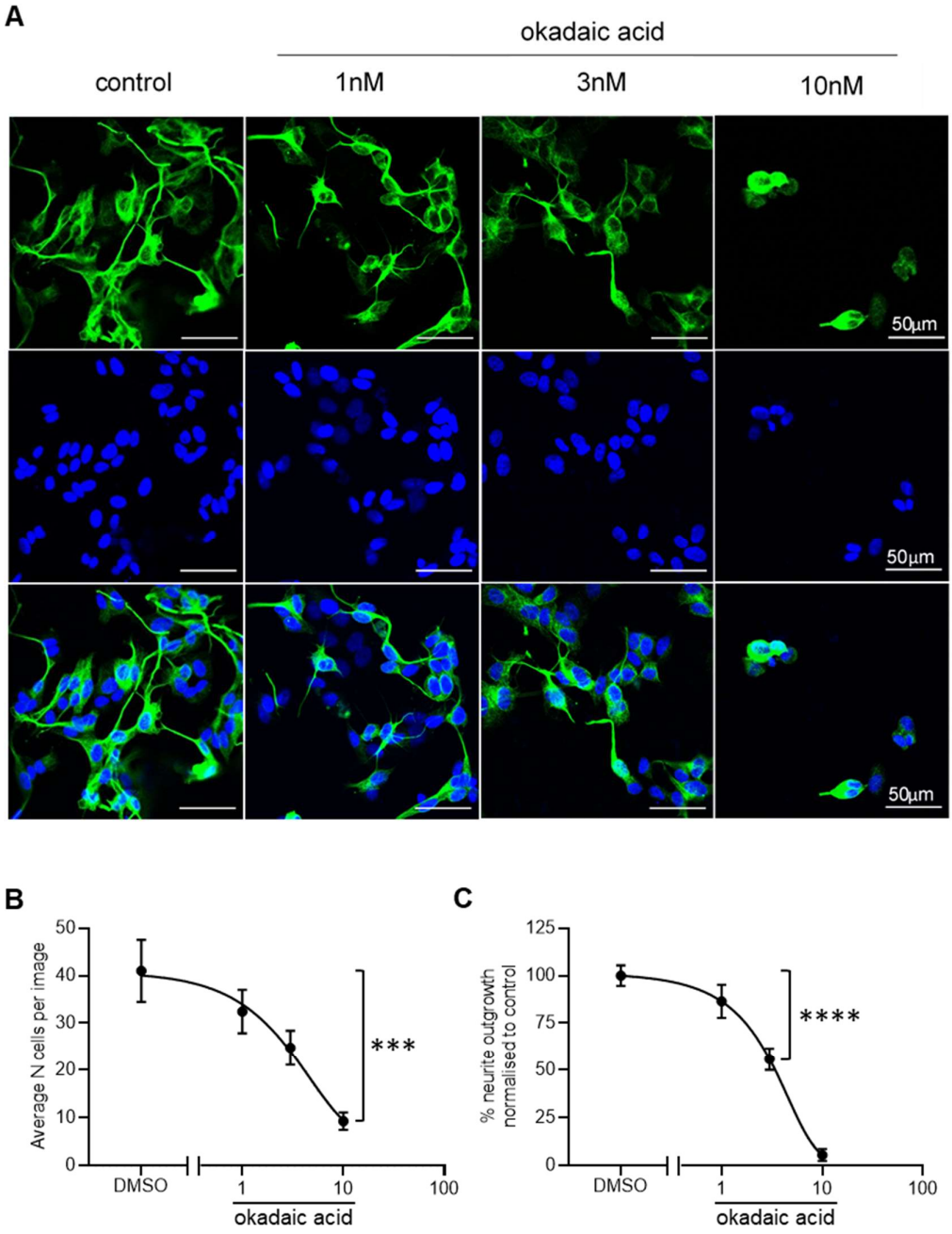


Figure 4.3.3.1 Reduced neurite outgrowth with increased concentration of OA. **A** Neurone-specific marker βIII tubulin identified neurites in SHSY5Y cells shown in green. Cell nuclei stained with Hoechst shown in blue. Merged images in final row. N=3 replicates (18 images) per condition. **B** Decreased number of live cells with increased concentration of OA. Nuclei automatically counted on FIJI software with a macro **C** Neurite length was quantified using simple tracer and the sum neurite length was divided by number of nuclei. The outgrowth in SHSY5Y cells treated with OA was plotted as percentage of DMSO control. Points = mean, error bars = SEM.

SHSY5Y cells co-treated with OA and 100ng/mL recombinant VEGF-A_{165}a (as shown in the second panel of Figure 4.3.3.2A) had significantly increased neurite outgrowth compared with vehicle and with OA alone (two-way ANOVA, $p<0.05$). There is an upward shift in neurite length, where in the absence of OA, the average neurite length per cell increased from 22µm ±1µm to 30µm ±2µm (see Figure 4.3.3.2B). With up to 3nM OA, 100ng/mL VEGF-A_{165}a maintained higher neurite outgrowth in SHSY5Y cells, as seen by the increase from 12µm ±1µm to 18µm ±1µm. When neurite outgrowth was normalised to the -OA control in each group, there was overlap between two curves with and without VEGF-A_{165}a (see Figure 4.3.3.2C), indicating that VEGF-A_{165}a increased baseline neurite outgrowth but did not counteract the OA-induced decrease. For example, with 3nM OA, PBS and VEGF-A_{165}a treated cells had an average 56% ±5% and 59% ±3% of their -OA controls, respectively.

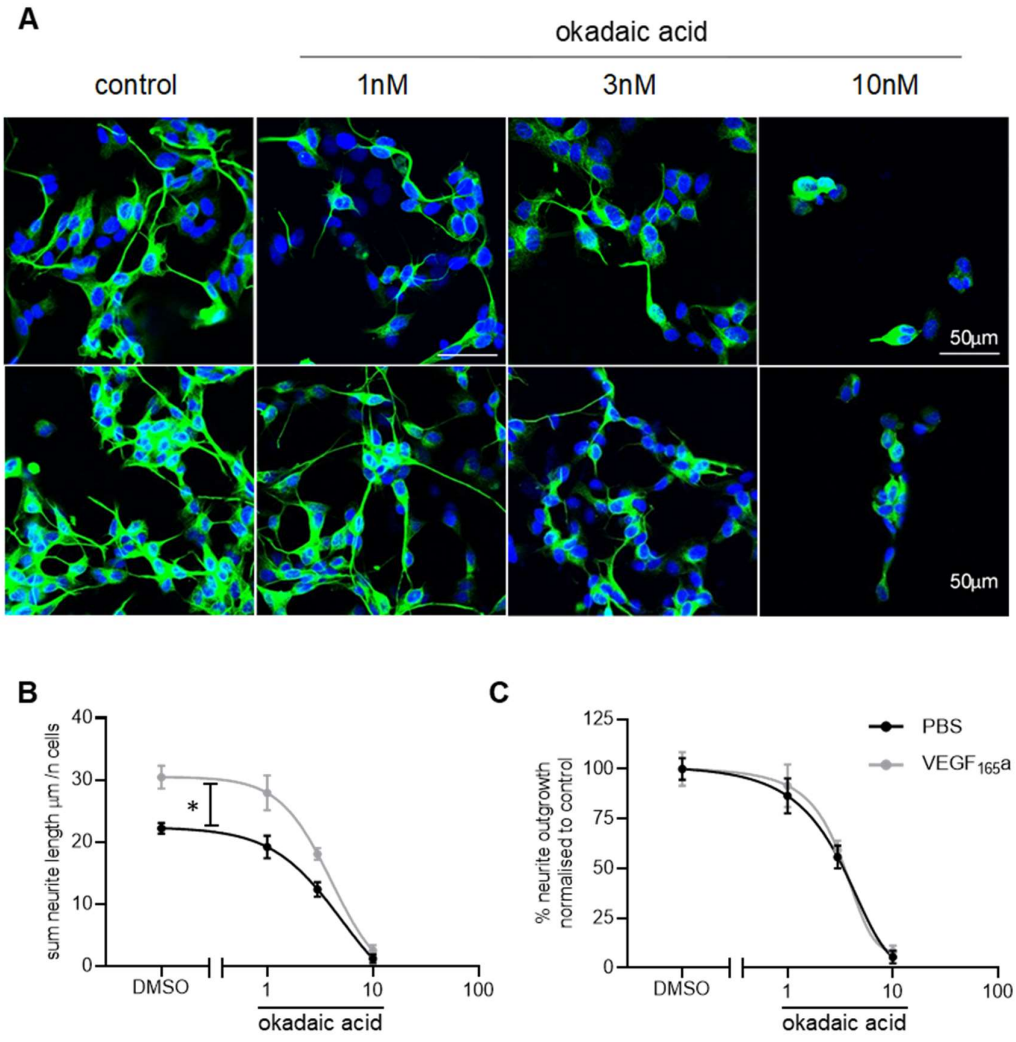
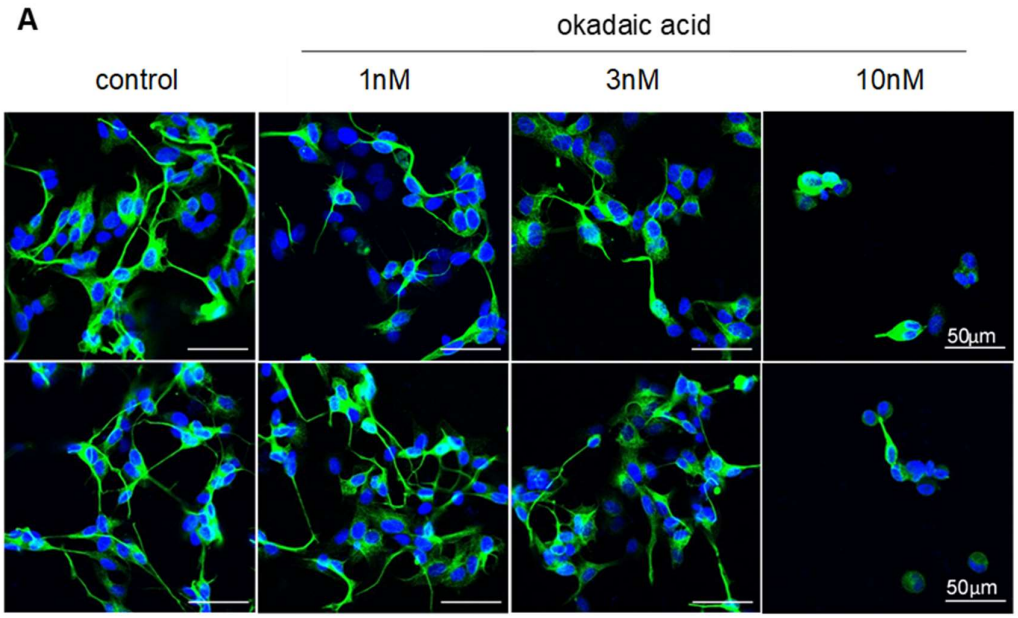


Figure 4.3.3.2 VEGF-A_{165}a increased neurite outgrowth in SHSY5Y cells co-treated with OA. **A** Neurone-specific marker βIII tubulin identified neurites in green. Cell nuclei stained with Hoechst shown in blue. N=3 replicates (18 images) per condition. **B** Using FIJI software, neurite length was quantified using simple tracer and the sum neurite length was divided by number of nuclei counted with a macro. Plot showed that average neurite length is significantly and consistently higher with 100ng/mL VEGF-A_{165} in control, 1nM and 3nM OA treatments (two-way ANOVA, $p<0.05$). With 10nM OA, VEGF-A_{165} did not have an effect. **C** Neurite outgrowth was plotted as percentage of DMSO control with and without VEGF-A_{165} treatment. Points = mean, error bars = SEM.

In comparison, 100ng/mL recombinant VEGF-A_{165}b alone did not induce an increase in neurite outgrowth in vehicle treated neurones (as shown in the second panel of Figure 4.3.3.3A). However, VEGF-A_{165}b treated SHSY5Y cells did maintain significantly higher sum neurite outgrowth when treated with OA (two-way ANOVA, $p<0.01$). While 3nM OA decreased neurite outgrowth from 22μm ±1 μm to 12μm ±1μm in the control group, VEGF-A_{165}b treated cells had average neurite length of 22μm ±2 μm and 21μm ±1μm, respectively (see Figure 4.3.3.3B). This equated to maintaining 97% ±6 of -OA control with 100ng/mL VEGF-A_{165}b treatment and resulted in a rightward shift in the normalised curve, as shown in Figure 4.3.3.3C.



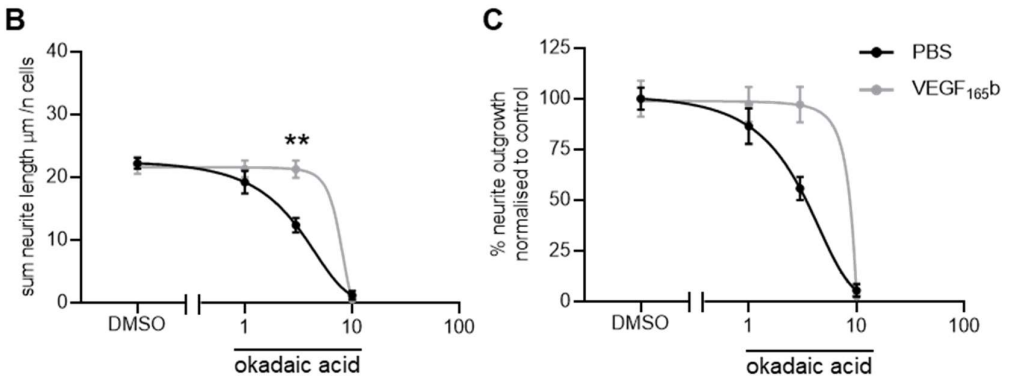


Figure 4.3.3.3 VEGF-A$_{165}$b recovered OA-induced decrease in neurite outgrowth. **A** Neurone-specific marker βIII tubulin identified neurites in green. Cell nuclei stained with Hoechst shown in blue. N=3 replicates (18 images) per condition. **B** Using FIJI software, neurite length was quantified using simple tracer and the sum neurite length was divided by number of nuclei counted with a macro. Plot showed that 100ng/mL VEGF-A$_{165}$b treatment alone did not increase average neurite length but maintained outgrowth in SHSY5Y cells co-treated with 1nM and 3nM OA where average length was significantly higher than PBS control (two-way ANOVA, $p<0.01$). With 10nM OA, 100ng/mL VEGF-A$_{165}$b did not have an effect. **C** Neurite outgrowth was plotted as percentage of DMSO control with and without VEGF-A$_{165}$b treatment. Points = mean, error bars = SEM.

To quantify the effect of VEGF-A isoforms on OA-induced decrease in neurite outgrowth, the half maximal inhibitory concentration (IC50) of OA on sum outgrowth (per cell) was compared between groups co-treated with vehicle only, VEGF-A$_{165}$a or VEGF-A$_{165}$b. Using log inhibitor vs response curves on GraphPad Prism, I found that VEGF-A$_{165}$a treatment caused a modest increase in IC50 from 3.0µM to 3.4µM whilst VEGF-A$_{165}$b treatment caused a greater increase to 5.1µM. This suggests that VEGF-A$_{165}$b treatment exerts a stronger protective effect on outgrowth as higher concentration of OA is required to produce the same level of "dieback", i.e., decline in neuritic outgrowth.

Co-treatment	PBS (vehicle)	VEGF-A$_{165}$a	VEGF-A$_{165}$b
Bottom	Constrained ≥ 0		
Top	24.18	33.36	24.83
LogIC50	0.479	0.534	0.710
IC50	3.011	3.423	5.133

Table 4.3.3: Summary of the effect size and IC50 of VEGF-A isoforms on OA-induced neurite "dieback" in SHSY5Y cells. Values based on N=3 biological replicates per condition and quantification of sum neurite outgrowth normalised to the number of cells in field of view.

4.3.4 SRPK1 inhibition can shift splicing of VEGF-A in SHSY5Y cells

SPHINX31 is a SRPK1 inhibitor that has been shown to switch splicing from VEGF-A_{165}a to VEGF-A_{165}b in endothelial cells, as well as DRG. Consequentially, SPHINX31 is a powerful investigatory tool for alternative splicing of VEGF-A and other genes regulated by SRPK1. However, SPHINX31 has not been previously used on SHSY5Y cells. Since recombinant VEGF-A_{165}b was shown to have neuroprotective effects in SHSY5Y cells, I wanted to determine whether use of SPHINX31 could increase endogenous expression of VEGF-A_{165}b, and potentially replicate the same physiological results. To quantify relative expression of VEGF-A isoforms, competitive RT-PCR primers were used to produce bands for VEGF-A_{165}a and VEGF-A_{165}b respectively, with the forward primer in exon 7a and the reverse primer in exon 8b/3' UTR. However, VEGF-A_{165}b expression was not detectable in control or SPHINX31-treated samples. To validate use (and specificity) of the primers, plasmids for VEGF-A_{165}a and VEGF-A_{165}b were run together with SHSY5Y samples and demonstrated distinct bands for expression of both isoforms, as seen in Figure 4.3.4.1. Lack of VEGF-A_{165}b detection could be due to the fact it is expressed comparatively lower than VEGF-A_{165}a, causing its amplicon to be out-competed by the other isoform.

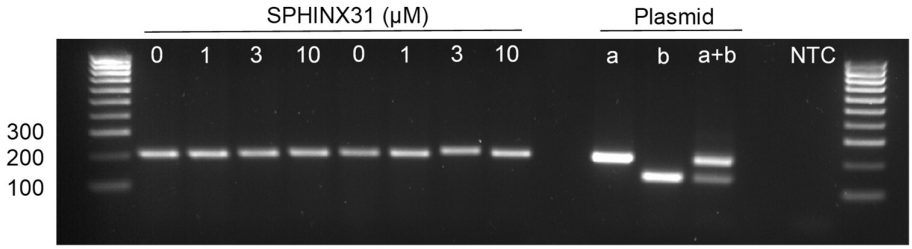


Figure 4.3.4.1 VEGF-A_{165}b bands are not detectable by conventional RT-PCR in SPHINX31 treated SHSY5Y samples. Cells were treated with 1μM, 3μM, and 10μM SPHINX31 and RT-PCR was conducted to quantify VEGF-A isoform expression. Positive control plasmids for VEGF-A_{165}a and VEGF-A_{165}b expression selectively showed detection of each isoform. NTC = no template control for cDNA and PCR reaction.

As an alternative and highly sensitive measure of expression, ELISA was used to detect relative expression of VEGF-A_{165}a and VEGF-A_{165}b isoforms in SHSY5Y cells. Optimisation of this ELISA is described in section 2.5.4, and the standard curves used for relative protein quantification are shown in Figure 4.3.4.2 below (minus "blank" i.e., OD measured from 1% BSA only). All values were then normalised to vehicle control group VEGF-A isoform expression.

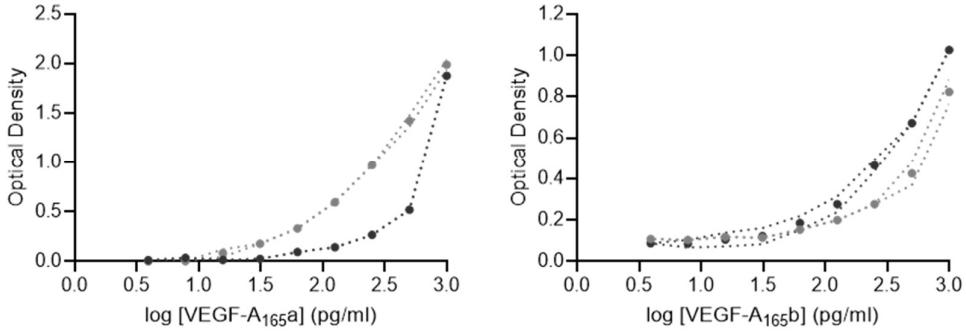


Figure 4.3.4.2 Standard curves for VEGF-A_{165}a and VEGF-A_{165}b ELISA show detection window for protein expression. Two standard curves are shown on each graph for two independent ELISA plates, run for SHSY5Y cell lysates and media samples. Quantification of VEGF-A_{165}a has a larger window than VEGF-A_{165}b. Dots indicate mean values (from duplicate) and dashed lines indicate SD.

Expression of both isoforms was detectable in both cell lysate and media collected from SHSY5Y samples. In the cell lysate, VEGF-A_{165}a expression did not change with SPHINX31 treatment (Figure 4.3.4.3A) but VEGF-A_{165}b significantly increased 82.6% ± 7.7% above vehicle control with 1μM SPHINX31 (Figure 4.3.4.3C, one-way ANOVA, $p<0.001$). The ratio of VEGF-A_{165}a:VEGF-A_{165}b in cell lysate was calculated to show a significant decrease with both 1μM and 10μM SPHINX31 treatment (shown in Figure 4.3.4.3E, $p<0.001$ and $p<0.05$, respectively). However, this effect was not concentration-dependent, suggesting that lowest concentration 1μM SPHINX31 was sufficient to induce shift in VEGF-A splicing toward the VEGF-A_{165}b isoform, and this was the maximal effect observable in SHSY5Y cells through SRPK1 inhibition.

In cell media, VEGF-A_{165}a expression significantly reduced with 10μM SPHINX31 treatment to 63.5% ± 1.1% of vehicle control, as shown in Figure 4.3.4.3B ($p<0.0001$, one-way ANOVA). VEGF-A_{165}b expression showed a general increase, albeit variable, in Figure 4.3.4.3D. At 3μM and 10μM SPHINX31, VEGF-A_{165}b expression was measured to be 97.3% ± 12.2% and 66.6% ± 26.1% higher than

vehicle control, respectively ($p<0.05$ at 3μM treatment, one-way ANOVA), This caused a significant decrease in the ratio of VEGF-A_{165}a:VEGF-A_{165}b in cell media at both 3μM and 10μM SPHINX31 treatment (see Figure 4.3.4.3E). This is a measure of secreted protein and confirms that altered splicing of VEGF-A in SPHINX31-treated SHSY5Y cells can be quantified in both intracellular and extracellular protein.

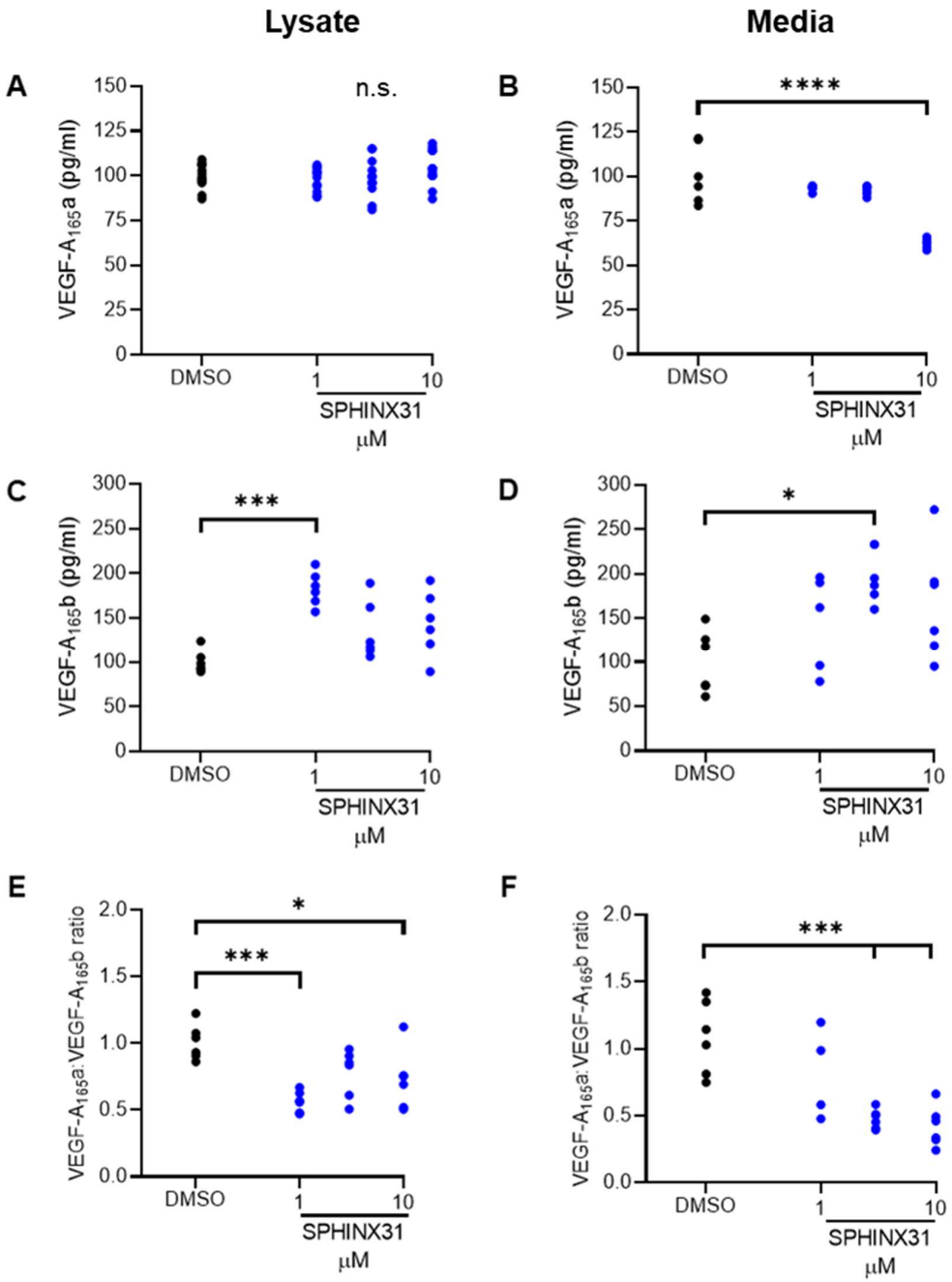


Figure 4.3.4.3 SPHINX31 treatment significantly reduces VEGF-A_{165}a:VEGF-A_{165}b ratio expression in SHSY5Y cells. **A** SPHINX31 does not produce measurable change in VEGF-A_{165}a expression in cell lysate. **B** Similarly, VEGF-A_{165}a in cell media remains stable with 1-3μM SPHINX31 but is significantly reduced with 10μM treatment ($p<0.0001$, one-way ANOVA). **C** Cell lysate shows a significant increase in VEGF-A_{165}b with 1μM SPHINX31 ($p<0.001$) and there is also a trend of higher VEGF-A_{165}b expression with 3μM and 10μM SPHINX31 treatment. **D** Cell media shows measured increase in VEGF-A_{165}b with 3μM and 10μM SPHINX31 treatment. Measured increase with 3μM is statistically significant ($p<0.05$, one-way ANOVA). **E F** The ratio of VEGF-A_{165}a:VEGF-A_{165}b is significantly reduced in both cell lysate and media with SPHINX31 treatment, but this does not occur in a concentration-dependent manner ($p<0.001$ and $p<0.05$, one-way ANOVA). N=3 biological replicates and N=2 technical replicates.

4.3.5 SRPK1 inhibition is protective of neuronal outgrowth through a VEGF-A_{165}b mediated mechanism

Based on the findings that VEGF-A_{165}b can increase outgrowth of SHSY5Y cells and SPHINX31 can shift splicing from VEGF-A_{165}a toward VEGF-A_{165}b, the next logical step was to determine whether SPHINX31 treatment would have comparable effects on neurite outgrowth to recombinant VEGF-A_{165}b. Using the OA neurotoxicity model (with DMSO vehicle control, representative images shown in Figure 4.3.5.1A), I found that SPHINX31 treatment protected against OA-induced decline in SHSY5Y cell outgrowth. As shown in Figure 4.3.5.1B, OA significantly reduces outgrowth in a concentration-dependant manner, while SPHINX31 ameliorates OA-induced neurite “dieback”. At 1nM, SPHINX31-treated cells showed higher neurite outgrowth at an average of 18.4μm ± 1.1μm compared to 14.8μm ± 0.6μm but this was not significantly different (two-way ANOVA, $p>0.05$). At 3nM OA, SPHINX31 treatment increased outgrowth from an average of 16.7μm ± 1.3μm to 8.9μm ± 1.0μm (two-way ANOVA, $p<0.0001$). At 10nM OA, SPHINX31 treatment was no longer neuroprotective. In fact, outgrowth was effectively ablated with this treatment combination, as very few cells were observed compared to the control group (Figure 4.3.5.1A). Similar results were seen in previous iterations of this assay with PBS vehicle control, which could imply that DMSO alone may affect outgrowth. However, higher cell survival could equally be due to inter-plate variance in seeding densities and cell passage, etc. As vehicles were independently controlled in each experiment, any vehicle effect should have no bearing on the experimental results.

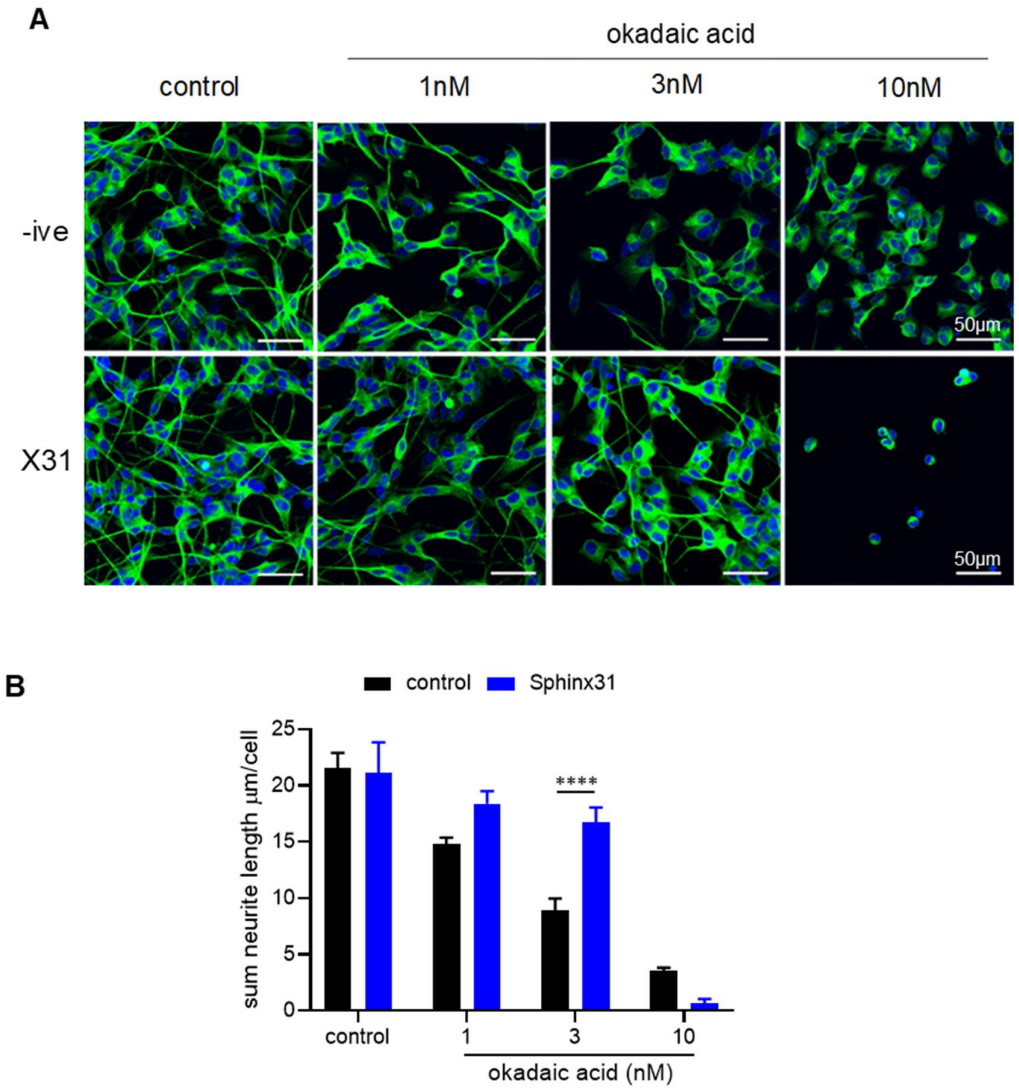


Figure 4.3.5.1 SPHINX31 significantly ameliorates OA-induced decline in neurite outgrowth from SHSY5Y cells. **A** Neurone-specific marker βIII tubulin identified neurites in green. Cell nuclei stained with Hoechst shown in blue. Neurite outgrowth was calculated by tracing neurites on Image J and dividing the sum length per image by the number of cells. **B** SPHINX31 co-treatment significantly ameliorates decline in neurite outgrowth induced by 3nM OA (two-way ANOVA, $p<0.0001$). N=3-5 biological replicates per condition.

OA was used in this thesis to model AD-related neurotoxicity, since OA is known to induce hyperphosphorylation of tau (Martin *et al.*, 2011). However, the relative expression of 4R and 3R tau isoforms (see section 1.4) is also important to AD pathology (Espindola *et al.*, 2018). Since SRPK1 is a splicing kinase, and SPHINX31 is a selective and potent SRPK1 inhibitor, I wanted to determine whether SPHINX31 and OA co-treatment caused a shift in the 4R:3R tau ratio. Tau splicing

will be discussed in greater detail in Chapter 5, but for the purpose of this experiment, it is important to note that although SHSY5Y cells preferentially express 3R tau, they do endogenously express both 4R and 3R tau isoforms. SPHINX31 treatment showed slightly increased 4R:3R tau ratio, quantified to be 32% ± 7% higher than control group (see Figure 4.3.5.2 below). However, this change was not statistically significant, and 3nM OA treatment did not induce a significant shift in the 4R:3R tau ratio either (one-way ANOVA, $p>0.05$). This indicates that the observed physiological effect of SPHINX31 on outgrowth is not dependent on alternative splicing of the *MAPT* gene. The vehicle for both OA and SPHINX31 is DMSO, thus all values were normalised to 0.02% DMSO treated control group.

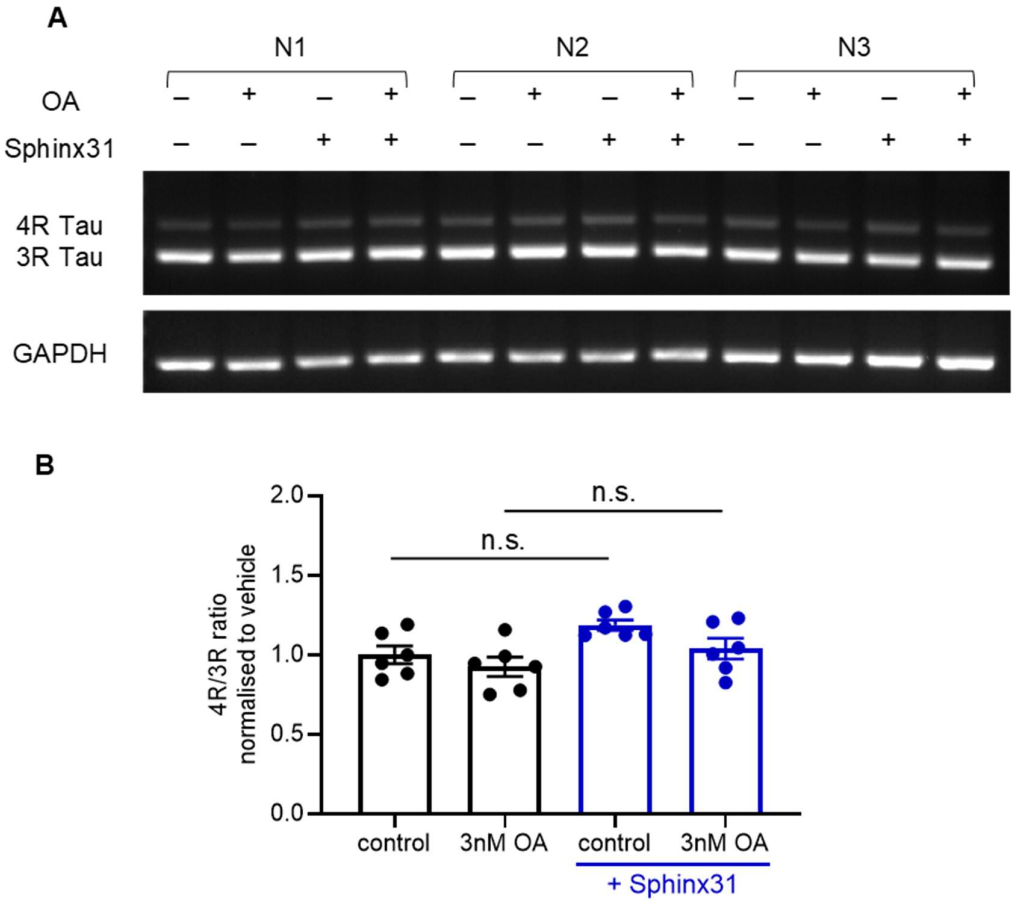
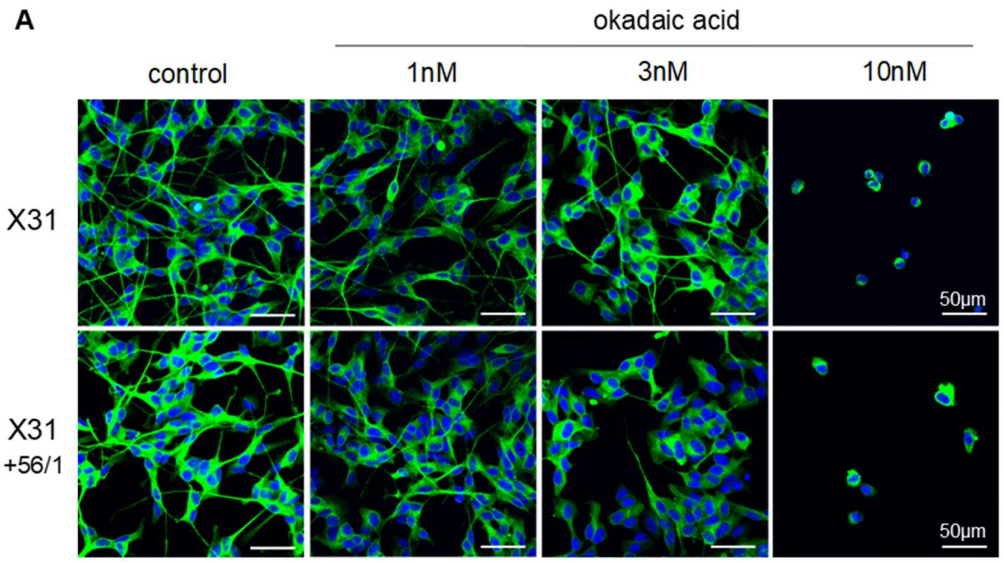


Figure 4.3.5.2 OA and SPHINX31 treatments do not significantly alter the 4R:3R tau ratio in SHSY5Y cells. **A** SHSY5Y cells were treated with 3nM OA and/or 3μM Sphinx31 for 24h. *MAPT* PCR was carried out using primers spanning exon 10 (forward primer in exon 9, reverse primer in exon 11) to quantify relative expression of 4R and 3R tau isoforms. Images show tau isoform expression and housekeeping gene *GAPDH* matched to each sample. **B** Sphinx31 treatment does not significantly alter 4R:3R tau ratio (one-way ANOVA, $p>0.05$). All presented 4R:3R tau ratios are normalised to the control group. The variability of control group itself is shown by normalisation to its own average. N=4, error bars show SEM.

To determine whether the neuroprotective effect of SPHINX31 is dependent on alternative splicing of VEGF-A, the outgrowth assay was repeated with 56/1 antibody co-treatment, which neutralises the VEGF-A_{165}b isoform (presented in Figure 4.3.5.3A). Compared to the SPHINX31 group, SHSY5Y cells treated with SPHINX31 + 56/1 showed significantly reduced outgrowth (Figure 4.3.5.3B), indicating that amelioration of outgrowth with SPHINX31 does in fact occur through increased VEGF-A_{165}b expression. In the presence of 1nM OA and 3nM OA respectively, SPHINX31 treated cells were quantified to have average sum outgrowth of 18.4μm ± 1.1μm and 16.8μm ± 1.2μm, which was higher than averages 14.8μm ± 0.6μm and 8.9μm ± 1.0μm in vehicle control (two-way ANOVA, $p>0.05$ and $p<0.0001$, respectively). When co-treated with both SPHINX31 and 56/1 antibody, there was a significant reduction in neurite outgrowth compared to SPHINX31 alone, at an average sum length of 12.5μm ± 0.4μm (two-way ANOVA, $p<0.001$). This was not significantly different to the control group at 3nM OA (two-way ANOVA, $p>0.05$).



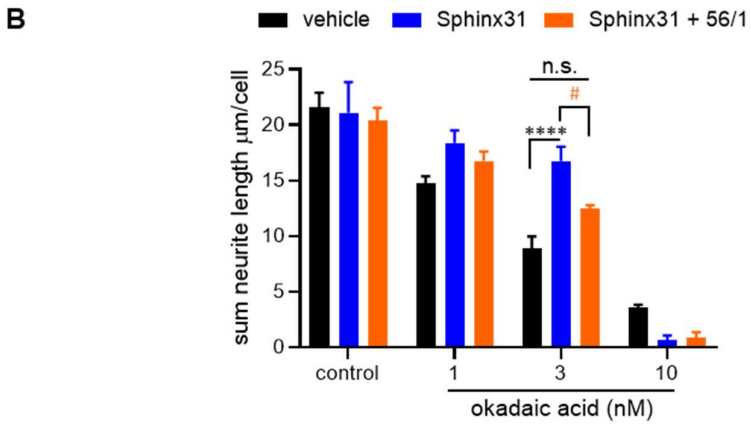


Figure 4.3.5.3 VEGF-A_{165}b neutralisation with 56/1 antibody significantly reduces the neuroprotective effect of SPHINX31 treatment. **A** SHSY5Y cells were treated for 24h with 1-10nM OA and a combination of 3µM Sphinx31 + 56/1 co-treatments. Neurone-specific marker βIII tubulin identified neurites shown in green. Cell nuclei stained with Hoechst shown in blue. Using FIJI software, neurite length was quantified using simple tracer and the sum neurite length was divided by number of nuclei counted with a macro. **B** Compared to control, SPHINX31 treatment significantly ameliorates decline in outgrowth at 3nM OA (two-way ANOVA, $p<0.0001$). Co-treatment with 56/1 in addition to Sphinx31 reduces the protective effect of Sphinx31, significantly reducing outgrowth again ($p<0.05$, indicated by #). Neuronal outgrowth in this treatment group was not significantly different to 3nM OA alone ($p>0.05$). N=3-5 replicates per condition, error bars show SEM.

4.4 Discussion

There are numerous *in vitro* models for AD that incorporate different aspects of its pathology. To investigate the neuroprotective properties of VEGF-A isoforms, it was necessary to develop a robust neurotoxicity assay that consistently presented concentration-dependent cell death within a reasonable range and that could be rescued by neuroprotective agents.

4.4.1 VEGF-A_{165} isoforms increase viability of SHSY5Y cells in oxidative stress *in vitro* model

For optimisation of the oxidative stress model, H_2O_2 was used at a range of concentrations alongside a positive assay control, NGF. In both SHSY5Y and N2a cell lines, NGF treatment evoked a significant and dependable increase in cell viability. It is worth noting that there was not a significant increase in cell viability with NGF treatment compared to the no treatment control, indicating good cell maintenance in its absence. When treated with either VEGF-A_{165}a or VEGF-A_{165}b, SHSY5Y cells demonstrated a similar increase in metabolic activity normalised to -H_2O_2 control. This is in alignment with other studies which have demonstrated VEGF-A dependent neuroprotection (Beazley-Long *et al.*, 2013) and supports the hypothesis that VEGF-A treatment can increase neuronal viability in the presence of oxidative stress. There wasn't an observable difference in the effect of alternative splicing isoforms which suggests that despite having opposing effects on angiogenesis (Nowak *et al.*, 2010) both splicing families maintain neuroprotective effects in these cell lines.

However, VEGF-A induced increase in cell viability was not reproduced in N2a cells. This could be attributed, at least in part, to the smaller cell viability window where relatively low concentrations of hydrogen peroxide (e.g. 50μM) reduced cell viability to less than half of control. There is limited literature surrounding VEGF-A function in N2a cells, but it has been reported that inhibition of VEGF-A with a neutralising antibody increases N2a cellular viability under hypoxic conditions (Saraswat *et al.*, 2015). This finding was related to maintaining normal levels of VEGF-A since it is upregulated by hypoxia via hypoxia-inducible factor-1 (HIF-1). Since HIF-1 is also known to be upregulated by reactive oxygen species, including H_2O_2 (Bonello *et al.*, 2007) it could be postulated that VEGF-A was already upregulated and no longer exerting cytoprotective effects, explaining why I could not measure a significant change in N2a viability. The VEGF-A_{165}b isoform did not significantly affect N2a viability either, despite evidence that VEGF-A_{165}b can negatively regulate VEGFR2

expression (Ballmer-Hofer *et al.*, 2011) which would arguably counteract HIF-1 induced VEGF-A activity. However, VEGF-A_{165}b remains a partial agonist of VEGFR2 (Kawamura *et al.*, 2008) and is dependent on VEGFR2 to elicit neuroprotection (Beazley-Long *et al.*, 2013). Therefore, it is not appropriate to compare VEGF-A_{165}b mediated neuroprotection with that related to VEGF-A neutralisation. It is also important to note that Saraswat et al. did not measure VEGFR2 expression or activation, and it is likely that blocking VEGF-A activity would have caused upregulation of VEGFR2 through the clathrin-mediated pathway (Bruns *et al.*, 2010). VEGFR2 trafficking could also explain the lack of response seen in N2a cells if HIF-1 induced VEGF-A expression resulted in VEGFR2 internalisation. For future work, and more comprehensive understanding of neuronal VEGF-A signalling, treatment with recombinant VEGF-A isoforms could be repeated in the presence of an VEGFR2 inhibitor.

4.4.2 VEGF-A_{165} isoforms increase viability of SHSY5Y cells in amyloid *in vitro* model

The amyloid *in vitro* model was less consistent in its cell viability results, particularly at lower concentrations, but at 1μM it was able to induce some loss of viability in N2a cells and a significant reduction in SHSY5Y cells. This observation was consistent with the literature, particularly with a study optimising treatment methods of amyloid in various states (Stine *et al.*, 2011). In its unaggregated state, 1μM amyloid was found to decrease N2a cell survival whilst lower concentrations (0.01μM and 0.1μM) actually increased survival by ~20% over control. In other studies carried out in SHSY5Y cells, amyloid treatment between 1 μM and 10 μM was successfully used to induce neurotoxicity (Stine *et al.*, 2011; Hettiarachchi *et al.*, 2014; Zheng *et al.*, 2014). Taking into account these findings, the assay was taken forward at 1μM to determine the effects of VEGF-A co-treatment.

As seen in Figure 4.3.2.2, both VEGF-A_{165}a and VEGF-A_{165}b completely rescued the amyloid-induced decrease in SHSY5Y cell viability. This complements results from the oxidative stress *in vitro* model and confirms that both splicing isoforms are able to rescue neurotoxic effects associated with the accumulation of amyloid. In N2a cells, amyloid treatment did not reliably produce a significant decrease in viability, despite several rounds of assay optimisation. As a result, it was not possible to conclusively characterise the effect of VEGF-A in this cell line other than to observe that VEGF-A maintained control-level cell viability.

4.4.3 VEGF-A_{165}a increases neurite outgrowth of SHSY5Y cells

In AD and many other tauopathies, NFTs result from the hyperphosphorylation of tau and its aggregation within neurones (Bancher *et al.*, 1989). Regulation of tau function is dependent on glycogen synthase kinase 3β (GSK-3β) and protein phosphatase 2A (PP2A) enzymes which play a role in tau phosphorylation and dephosphorylation respectively (Gong & Iqbal, 2008). In fact, PP2A activity is decreased by ~30% in AD brain (Gong *et al.*, 1995), highlighting its importance in the regulation of normal tau function. Okadaic acid (OA) has been used a potent inhibitor of PP2A to induce tau hyperphosphorylation *in vitro* (Martin *et al.*, 2011). In the development of this neurotoxicity model (Figure 4.3.3.1), I demonstrated that OA decreases neurite outgrowth of SHSY5Y cells in a concentration-dependent manner. This neurotoxic effect of OA is in alignment with observations from similar studies using OA in SHSY5Y cells (Metin-Armagan *et al.*, 2018; Boban *et al.*, 2019).

OA treatment has also been shown to upregulate VEGF-A expression (Wakiya & Shibuya, 1999) which is closely related to increased activity of HIF-1 activated by the mTOR pathway (Kim *et al.*, 2009). While PP2A inhibits ribosomal protein S6 kinase (S6K) activity, VEGFR2 promotes mTOR signalling and PKC activation which positively regulates S6K. Therefore, OA inhibition of PP2A significantly increases VEGF-A mediated PKC activation and S6K activity (Edelstein *et al.*, 2011) which is yet further augmented by treatment with recombinant VEGF-A. As well as controlling protein synthesis, S6K activity is known to signal cell survival (Harada *et al.*, 2001) which may account (or at least contribute toward) the cytoprotective properties of VEGF-A. In this study, VEGF-A_{165}a treatment amplified neurite outgrowth in the absence and presence of OA; this can be observed in Figure 4.3.3.2, which shows a general increase in SHSY5Y neurite outgrowth in cells treated with 0-3nM OA. This could be mediated by an upregulation of S6K activity, suggesting that VEGF-A could compensate for loss of neuronal function related to tau hyperphosphorylation. When coupled with previous experiments that showed recovery of amyloid-induced decrease in cell viability, it can be concluded that VEGF-A is protective against both forms of AD-related neurotoxicity.

4.4.4 VEGF-A_{165}b recovers the decrease in neurite outgrowth of SHSY5Y cells

As opposed to VEGF-A_{165}a, a full agonist of endothelial VEGFR2 that stabilises its interaction with NP-1, VEGF-A_{165}b is a partial agonist of endothelial VEGFR2 that is unable to bind NP-1 and promotes internalisation and degradation of VEGFR2 (Ballmer-Hofer *et al.*, 2011). Consequentially, VEGF-A_{165}a binding leads to PKC activation while VEGF-A_{165}b binding does not (Kisko *et al.*, 2011; Hulse *et al.*, 2014). Since PKC is a negative regulator of Akt, its inhibition has been shown to increase Akt phosphorylation (Edelstein *et al.*, 2011). Akt is known to inhibit GSK-3β activity (Hermida *et al.*, 2017), which in turn phosphorylates tau (Gong & Iqbal, 2008). If VEGF-A_{165}b is able to downregulate neuronal VEGFR2 in a similar way to endothelial VEGFR2, I would postulate that resulting Akt inhibition of GSK-3β protects against tau hyperphosphorylation and could therefore have knock-on effects on tau function.

In this study, VEGF-A_{165}b co-treatment alone did not increase neurite outgrowth of SHSY5Y cells. However, VEGF-A_{165}b protected against the decrease in neurite outgrowth seen with 1nM and 3nM OA (Figure 4.3.3.3) wherein sum neurite outgrowth was significantly greater than vehicle treated cells. This indicates that VEGF-A_{165}b is not ubiquitously increasing neurite outgrowth but acting directly against the effect of OA. This could potentially occur via the PI3/Akt pathway: if VEGF-A_{165}b causes downregulation of VEGFR2 and attenuates PKC activation, it may lead to increased Akt phosphorylation, greater inhibition of GSK-3β activity and thus reduced phosphorylation of tau. If sufficient to counter-act OA inhibition of PP2A, this could prevent the hyperphosphorylation of tau and thus protect against downstream effects, including decrease in neurite outgrowth.

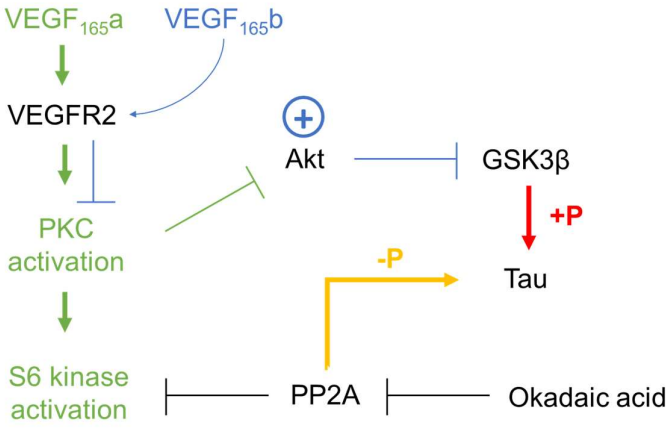


Figure 4.4.4 Schematic summarising proposed action of VEGF-A_{165}a and VEGF-A_{165}b via VEGFR2 binding and full or partial agonism, respectively. Green path displays VEGF-A_{165}a activation, blue path displays VEGF-A_{165}b activation.

4.4.5 SRPK1 inhibitor SPHINX31 significantly decreases VEGF-A_{165}a:VEGF-A_{165}b ratio in SHSY5Y cells

SRPK1 is related to alternative splicing of VEGF-A through phosphorylation of SRSF1 (Harper & Bates, 2008). As introduced in sections 1.9-10, SRPK1 activity drives nuclear localisation of SRSF1 and promotes selection of the proximal splice site in exon 8, producing VEGF-A_{165}a (Nowak *et al.*, 2008). SRPK1 inhibition reduces phosphorylation of SRSF1 and consequentially increases selection of the distal splice site in exon 8, producing VEGF-A_{165}b (Nowak *et al.*, 2010). This has been established through use of SRPK1 inhibiting compounds SRPN340 and SPHINX31 in a variety of tissues, including the kidney (Amin *et al.*, 2011), retinal epithelium (Gammons *et al.*, 2013; Batson *et al.*, 2017), peripheral neurones (Hulse *et al.*, 2014), prostate cancer (Mavrou & Oltean, 2016) and acute myeloid leukaemia (Tzelepis *et al.*, 2018). Consequently, alternative VEGF-A splicing has been related to a number of pathological conditions, including Denys Drash Syndrome, diabetic retinopathy, age-related wet macular degeneration (AMD), neuropathic pain, and cancer. However, SPHINX31 (or SRPK1 inhibition) had not been previously investigated in SHSY5Y cells, used in this thesis as a neuronal model. As shown in Figure 4.3.4.3, SRPK1 inhibition does modulate VEGF-A exon 8 splicing in SHSY5Y cells, making them a viable model to investigate the neuroprotective role of VEGF-A isoforms in AD-related neurotoxicity. Consistent with the effect observed in other tissues, both intracellular and extracellular VEGF-A showed a proportional shift toward the VEGF-A_{165}b isoform and significant decrease in VEGF-A_{165}a:VEGF-A_{165}b ratio.

4.4.6 SRPK1 inhibition recovers OA-induced decrease in neurite outgrowth and recovery is dependent on endogenous VEGF-A_{165}b

Similar to observed effects of recombinant VEGF-A_{165}b, SPHINX31 treatment was shown to protect against OA-induced decrease in neurite outgrowth. In the presence of 1nM and 3nM OA, SPHINX31 co-treatment significantly increased outgrowth to a level comparable to vehicle control (see Figure 4.3.5.1). This is a novel finding which suggests SRPK1 inhibition is neuroprotective in the OA model for tau hyperphosphorylation. When SHSY5Y cells were co-treated with SPHINX31 and VEGF-A_{165}b-neutralising antibody 56/1 (Figure 4.3.5.3), amelioration of neurite outgrowth was significantly reduced. As a result, it can be concluded that the neuroprotective effect of SPHINX31 is dependent on VEGF-A_{165}b expression, which increases relative to VEGF-A_{165}a with SRPK1 inhibition. However, it remains

possible that SPHINX31 is neuroprotective through other mechanisms in addition to VEGF-A alternative splicing.

In the literature, recombinant VEGF-A_{165}b has been reported as a neuroprotective agent in response to numerous insults, including glutamatergic excitotoxicity in hippocampal neurones, chemotherapy-induced cytotoxicity of dorsal root ganglia, and ischaemia-reperfusion injury in retina (Beazley-Long *et al.*, 2013). Therefore, the main findings in this chapter are in keeping with previous work and confirm that SPHINX31 can be used as a tool to switch VEGF-A splicing and replicate the protective effect of VEGF-A_{165}b for neurite outgrowth. Beazley-Long et al reported that the neuroprotective action of VEGF-A_{165}b in hippocampal neurones was mediated through VEGFR2, as it was blocked by VEGFR2 inhibitors but maintained with selective R1 inhibition. It was also found that hippocampal neuroprotection was unaffected by inhibition of PI3K or p38 MAPK, supporting the previously discussed hypothesis that VEGF-A_{165}b acts as a partial agonist at VEGFR2 and does not activate the mTOR pathway (Ballmer-Hofer *et al.*, 2011). Similarly, SPHINX31-mediated VEGF-A_{165}b expression seems to act against canonical VEGF-A_{165}a signalling, preventing activation of PKC and phosphorylation of PI3K (Harper & Bates, 2008). Therefore, SPHINX31 is likely to exert neuroprotection through another pathway. Beazley-Long et al. suggest involvement of MEK1/2 pathway because VEGF-A_{165}b was shown to induce Erk1/2 phosphorylation, which has been independently shown to ameliorate neuronal damage (Bhowmick *et al.*, 2019). However, activation of Erk1/2 is thought to be altered in AD pathology and has been related to hyperphosphorylation of tau and increased NFT burden (Pei *et al.*, 2002; Veeranna *et al.*, 2004). Considering OA-induced neurotoxicity is based on tau phosphorylation, it would be contradictory to suggest that VEGF-A_{165}b-mediated neuroprotection occurred through a mechanism that is known to further phosphorylate tau. As a result, I would postulate that VEGF-A_{165}b (and by extension SPHINX31) dependent neuroprotection occurs through aforementioned inhibition of GSK-3β activity. As this hypothesis is mostly based on evidence from endothelial cells, it is necessary to empirically test VEGF-A_{165}b binding to neuronal VEGFR2 and activation of downstream targets, most notable GSK-3β, to definitively conclude how neuronal VEGF-A_{165}b functions.

Future work on SPHINX31 could focus on investigating its effect against other insults used by Beazley-Long et al., because SPHINX31 has not been proven as neuroprotective in these contexts. The most closely related data published on the effect of SPHINX31 in nervous tissue identified its use for analgesia: Treatment of

primary afferents and resultant shift toward VEGF-A_{165}b expression was found to lower VEGF-A_{165}a mediated sensitisation of mechanical nociceptors to stimulation (Hulse *et al.*, 2014). Together with data presented in this chapter, this identifies SRPK1 inhibition as an interesting therapeutic target in both the CNS and PNS, with potential applications in neuroprotection and nociception. With regards to AD, it would be interesting to explore the effect of SPHINX31 on other aspects of its pathology, perhaps using a mouse model for AD, and determine whether *in vitro* results translate *in vivo*. The 3xTg mouse model would be particularly useful in this instance, with mutations in *APP*, *MAPT* and *PSEN1*, since it reliably demonstrates both plaque and tangle pathology, as well as modelling aspects of behavioural and psychological symptoms seen in dementia (Kosel *et al.*, 2020).

4.4.7 Concluding remarks

Amyloid and tau-related *in vitro* models caused measurable decrease in cell viability and neurite outgrowth. In SHSY5Y cells, VEGF-A_{165}a treatment ameliorated amyloid- and tau-related damage suggesting that VEGF-A mediated signalling can act against the progression of AD pathology. By comparison, VEGF-A_{165}b exerted similar neuroprotective effects in the amyloid model and acted directly against OA-induced toxicity in the neurite outgrowth assay. This identified VEGF-A_{165}b as a more ideal therapeutic agent for nervous tissue. Furthermore, SRPK1 inhibition with SPHINX31 was able to reproduce the neuroprotective effect of recombinant VEGF-A_{165}b. This validated the use of small-molecule compounds to inhibit splicing kinases and modulate neuronal function. Naturally, kinase inhibition would not only affect VEGF-A splicing but also shift splicing of other genes involved in neuronal survival and function. In the next chapter, novel splicing kinase inhibitors are used to regulate splicing of AD-related gene *MAPT* and determine whether this could protect against tau-related neurotoxicity.

Chapter 5: The regulation of *MAPT* splicing

5.1 Introduction

The *MAPT* gene is alternatively spliced at exon 10, resulting in the production of 4R or 3R tau based on the inclusion or exclusion of exon 10, respectively. There are a number of cis-acting elements that modulate splicing of *MAPT* (Park et al., 2016). These are short sequences located either within the exon or intron, including a purine-rich sequence within exon 10 and various sequences further downstream of exon 10, which have been identified to alter the ratio of 4R:3R tau ratio (Andreadis, 2005). The mutation of these cis-acting elements has been linked with Frontotemporal Dementia (FTD) and other tauopathies. Most known intronic mutations are clustered around the boundary of exon 10 and intron 10, which is thought to form a stem-loop structure as illustrated in Figure 5.1 below (McCarthy *et al.*, 2015). The presence of stem-loop structures can inactivate 5' splice sites (Eperon *et al.*, 1988) by competing with the U1 snRNP for binding (Grover *et al.*, 1999). Therefore, a mutation in this region can disrupt the secondary structure, effectively protecting the 5' splice site and increasing exon 10 inclusion (Niblock & Gallo, 2012). For example, the pathogenic exon 10 mutations G272V and P301L in select families with familial FTD has been associated with tangles that are almost exclusively 4R tau (Hutton *et al.*, 1998; Malkani *et al.*, 2006). Since missense mutations at the 5' splice site are related to mis-splicing and can clinically manifest as FTD, alternative splicing of *MAPT* exon 10 could also be implicated in other tauopathies, including AD.

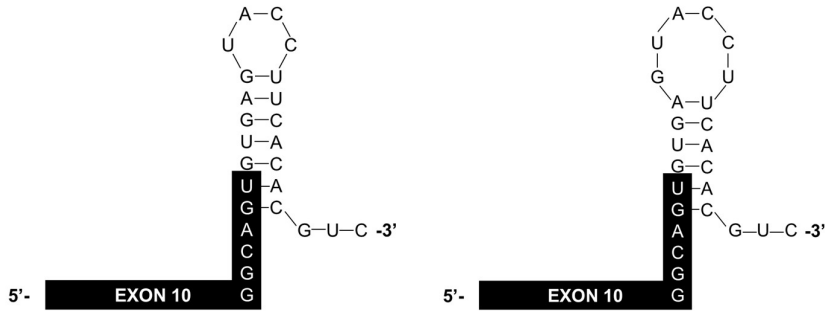


Figure 5.1 The sequence of the stem-loop located immediately after exon 10 of MAPT gene; proposed 6-8bp loop structures adapted from (Grover *et al.*, 1999; Donahue *et al.*, 2006).

Interacting with cis-acting elements are trans-acting factors that regulate alternative splicing of *MAPT* pre-mRNA. These include RBM4, which was shown *in vitro* to bind at a pyrimidine-rich element located 100 nucleotides downstream of the 5' splice site of exon 10 and consequently increase exon 10 inclusion. Additionally, splicing factors TRA2-β and SRSF1 have been found to bind to exonic splicing enhancer (ESE) motifs in the 5' end of *MAPT* exon 10 and promote exon 10 inclusion, acting together with SRSF9 (Kondo *et al.*, 2004). In fact, there is evidence for involvement of many splicing factors in regulation of exon 10 splicing, but some of the literature is contradictory. For example, co-transfection of COS cells with a Tau minigene and SRSF1 or SRSF9 (in addition to other splicing factors) showed inhibition of exon 10 inclusion and decreased the 4R:3R tau ratio expression (Gao *et al.*, 2000; Wang *et al.*, 2004). Based on these findings, it is not clear how these trans-acting factors regulate *MAPT* splicing. SRSF2, however, has been consistently shown to promote inclusion of exon 10 as well as tau expression in general through stabilisation of its mRNA (Hernández *et al.*, 2004; Qian *et al.*, 2011a; Qian *et al.*, 2011b; Chen *et al.*, 2014).

5.1.1 Role of regulatory splicing kinases

The activity of splicing factors is dependent on their phosphorylation state, and therefore is dependent on regulatory kinases. For example, the CLKs play a key role phosphorylation of SR proteins and their subcellular redistribution (Jain *et al.*, 2014). In relation of *MAPT* isoform expression, CLK activity (murine CLK1-4) has been shown to increase exon 10 skipping *in vitro*, therefore causing a decrease in the 4R:3R tau ratio (Hartmann *et al.*, 2001). CLK2 was highlighted to have the strongest effect (compared to CLK1, 2 and 4) on exon 10 skipping and counteract the effect of FTD mutations which enhance exon 10 usage. Otherwise, SRPK1 is known to phosphorylate SRSF1 and facilitate its translocation to the nucleus (Ma *et al.*, 2008), and SRSF1 has been shown to promote exon 10 inclusion (Kondo *et al.*, 2004). Therefore, one could postulate that SRPK1 promotes a shift towards 4R tau isoform expression. However, studies have shown that it causes exon 10 skipping instead (Hartmann *et al.*, 2001; Nikolakaki *et al.*, 2001). As of yet, there is no empirical evidence that SRPK1 exerts its effect on *MAPT* splicing through either SRSF1, so it may promote exon skipping through regulation of other splicing factors instead.

Another splicing kinase that regulates *MAPT* exon 10 inclusion is Dyrk1A. As a gene encoded by the region of chromosome 21 critical to Down Syndrome, its activity has been long established as critical to the condition. Individuals with Down Syndrome develop AD-type tau pathology very early in life (Wisniewski *et al.*, 1985),

so it is perhaps unsurprising that Dyrk1A is also been linked to AD. In both *in vitro* studies and AD patients, it was found that Dyrk1A inhibits exon 10 inclusion, shifting toward 3R tau isoform expression (Shi *et al.*, 2008; Jin *et al.*, 2015a). In particular, the AD brain showed increased truncation of Dyrk1A through calpain I, which was positively correlated with Dyrk1A activity (Jin *et al.*, 2015a). Downstream, it has been proposed that Dyrk1A phosphorylates SRSF1 at serine residues 227, 234 and 238, which drives it into nuclear speckles and prevents SRSF1-mediated inclusion of exon 10 (Shi *et al.*, 2008). Dyrk1A is also known to target SRSF2, and similarly inhibits SRSF2 mediated exon 10 inclusion in a concentration dependent manner (Qian *et al.*, 2011b).

5.1.2 Splicing models

Splicing of *MAPT* exon 10 in humans and rodents is constitutively different; where there is equal expression of 4R:3R tau in adult human brain (Gao *et al.*, 2000), the adult mouse brain almost exclusively expresses 4R tau (Kosik *et al.*, 1989). Interestingly, the 5' splice site of exon 10 is only partially conserved between human and mouse, differing after position +8 (Grover *et al.*, 1999) where a number of mutants are known to affect regulation of exon 10 splicing and cause FTD. It has therefore been suggested that failure of rodent models to reproduce neurofibrillary tangles may be related to their constitutive splicing of exon 10 (Gao *et al.*, 2000). The difference in *MAPT* splicing between species is also observed in SHSY5Y and Neuro2a cell lines: while the former human line preferentially expresses 3R tau, the latter murine line expresses 4R tau at a much higher level. From a technical standpoint, this was advantageous because combined use of these cell lines created a large window for measuring change in splicing with novel compound treatments.

Considering the endogenous expression of tau isoforms in SHSY5Y and Neuro2a cell lines, I sought to investigate the inhibition of splicing factors, which was hypothesised to cause exon skipping, in Neuro2a cells. However, the inhibition of splicing kinases, which was hypothesised to increase exon inclusion, was predominately conducted in SHSY5Y cells. I then proceeded to examine the physiological impact of selective CLK inhibition on neurite outgrowth using a previously established *in vitro* model for tau hyperphosphorylation (Metin-Armagan *et al.*, 2018).

5.1.3 Hypotheses

In this chapter, I tested the following hypotheses:

1. SRSF1 and SRSF2 promote exon 10 inclusion and knockdown of these splicing factors will increase relative expression of 3R tau through exon 10 skipping.

2. Inhibition of splicing kinases with novel compounds will significantly increase exon 10 inclusion by blocking kinase-mediated exon 10 skipping.

3. Selective CLK inhibition can decrease phosphorylation of SR proteins

4. Selective CLK inhibition can ameliorate OA-induced neurotoxicity and significantly increase neurite outgrowth.

5.2 Methods

Compound treatments and siRNA experiments were conducted in serum-free media and the absence of any inducing factors, unless otherwise stated. The VEGF-A_{165}a and VEGF-A_{165}b ELISA were performed on whole cell lysates collected from SHSY5Y cell culture. In the OA assay, SHSY5Y cells were assayed for neurite outgrowth with βIII tubulin immunofluorescence. Images were taken with Leica confocal microscope at 20x and 40x magnification. All replicates are experimental (technical) replicates unless otherwise stated. All methods are described in detail in Chapter 2.

5.2.1 GRIFFIN compounds

The GRIFFINs used in this chapter were a gift from our collaborator Prof Jonathan Morris in the University of New South Wales. The data on percent remaining kinase activity and IC50 values were reported by the Morris lab. Structures for the GRIFFIN compounds can be found in the Figure 5.2.1 below.

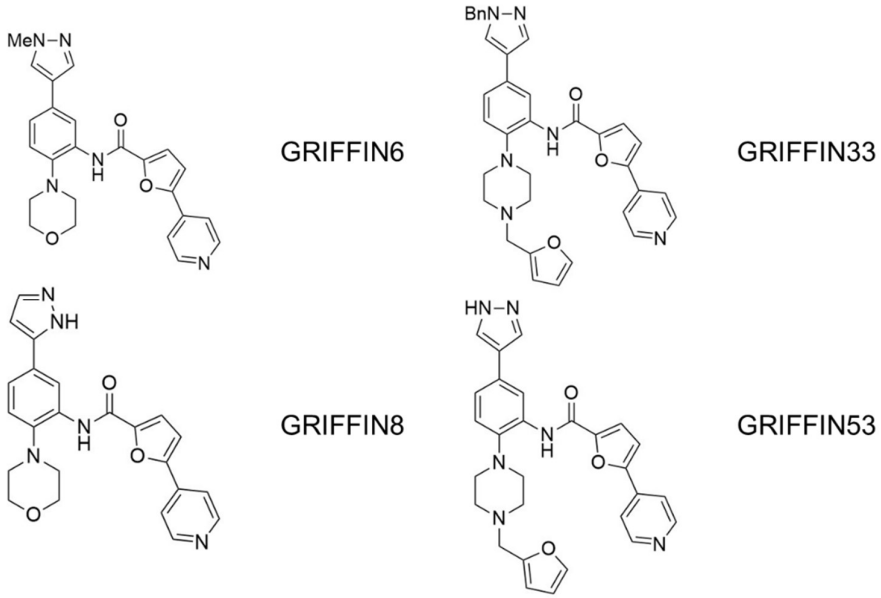


Figure 5.2.1: Chemical structures for GRIFFIN compounds gifted by the Morris lab.

5.2.2 The *MAPT* RT-PCR

To assess alternative splicing of exon 10, the MAPT RT-PCR was carried out using forward and reverse primers in exons 9 and 11, producing two competitive products for 4R and 3R tau isoforms, with and without inclusion of exon 10 (93bp). In Neuro2a cells these products were 168bp (excluding exon 10) and 261bp (including exon 10) in length. In SHSY5Y cells, these products were 297bp (excluding exon 10) and 390bp (including exon 10) in length. PCR products from Neuro2a and SHSY5Y cells were run in 2% agarose gel and imaged using Gel Doc EZ.

5.3 Results

Neuro2a and SHSY5Y cells are used in this chapter to investigate the regulation of *MAPT* exon 10 splicing. Untreated Neuro2a cells were found to preferentially express 4R tau, whilst SHSY5Y cells expressed relatively higher levels of 3R tau, as shown in Figure 5.3.1 below. Neuro2a cells transfected with tau minigene (refer to section 2.6) maintained the same splicing pattern of relatively greater 4R tau expression, indicating preference for exon 10 inclusion in human *MAPT* as well as endogenous mouse *MAPT*. Moving forward, endogenous expression was quantified after siRNA and compound treatment.

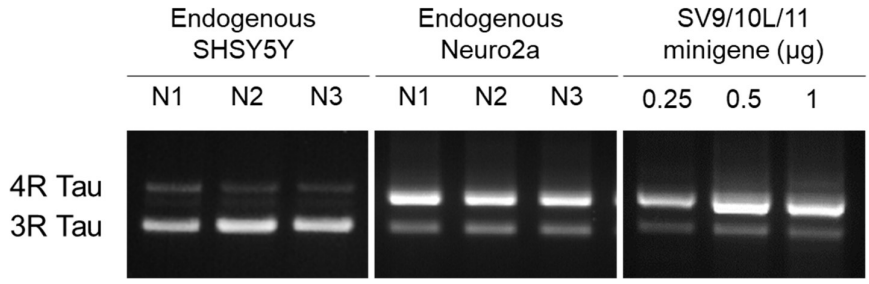


Figure 5.3.1 Expression of 4R and 3R tau isoforms in SHSY5Y and Neuro2a cells. Human *MAPT* RT-PCR was carried out on RNA samples collected from SHSY5Y cells and Neuro2a cells transfected with SV9/10L/11 construct. Mouse *MAPT* RT-PCR was carried out on RNA samples from untreated Neuro2a cells. There is relatively higher expression of 3R tau in SHSY5Y cells and higher expression of 4R tau (both murine and human) in Neuro2a cells.

5.3.1 Knockdown of SRSF1 and SRSF2 promotes *MAPT* exon 10 skipping

To characterise the endogenous control of *MAPT* exon 10 splicing in neuronal cells, I confirmed the role of splicing factors SRSF1 and SRSF2. This provided a basis to postulate whether splicing kinases regulate exon 10 inclusion through phosphorylation of these SR proteins. Knockdown of SRSF2 was hypothesised to increase exon 10 skipping, since SRSF2 has been consistently reported to promote exon 10 inclusion (Hernández *et al.*, 2004; Qian *et al.*, 2011a; Qian *et al.*, 2011b; Chen *et al.*, 2014). The effect of SRSF1 knockdown was under contention since there is evidence for SRSF1 activity promoting *MAPT* exon 10 inclusion (Kondo *et al.*, 2004) and contradictory evidence for exon 10 skipping (Gao *et al.*, 2000; Wang *et al.*, 2004). Neuro2a cells were treated with siRNA targeting SRSF1 and SRSF2 for an optimised length of 48h and 72h respectively, after which RNA was collected for RT-PCR. As shown in Figure 5.3.1.1, SRSF1 and SRSF2 expression was significantly reduced (densitometry values normalised to GAPDH expression and lipofectamine control), confirming the knockdown.

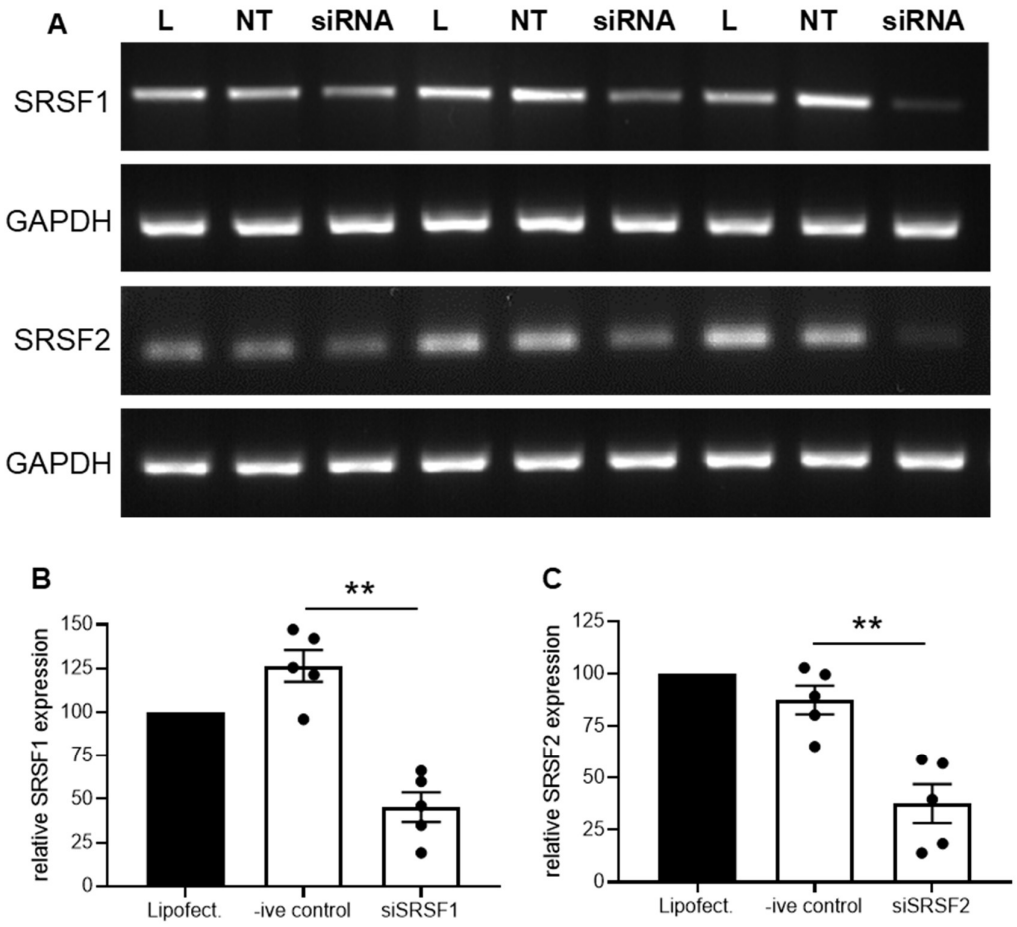


Figure 5.3.1.1 Transient knockdown of SRSF1 and SRSF2 in Neuro2a cells with targeted siRNA confirmed by RT-PCR and densitometry. **A** Images show level of SRSF1 and SRSF2 expression with respective siRNA treatments, relative to expression of housekeeping gene *GAPDH* displayed directly under each sample. Labelling with L = lipofectamine only, NT = control siRNA, siRNA = targeting SRSF1/2. **B C** Quantification of SRSF1 and SRSF2 demonstrates significantly reduced expression with respective siRNA treatment (one-way ANOVA, $p<0.01$), values normalised to *GAPDH* expression and experimental control (Lipofectamine-only) N=5, error bars show SEM.

Next, tau isoform expression was quantified to determine the effect of SRSF1 on *MAPT* exon 10 inclusion. As hypothesised, knockdown of SRSF2 caused both a significant decrease in 4R tau and an increase in 3R tau, as presented in Figure 5.3.1.2 below ($p<0.01$, one-way ANOVA). N2a cells treated with SRSF2 targeting siRNA showed 4R tau expression at an average 70.3% ± 3.9% of Lipofectamine control whilst 3R tau was 139.7% ± 20.9% higher. This shift to exon 10 skipping is consistent with previously cited literature, where SRSF2 was reported to promote exon 10 inclusion. Quantification of 4R and 3R tau isoform expression translated to

a significant change in 4R:3R tau ratio. Non-selective “scramble” siRNA treatment caused an average decrease in 4R:3R ratio to 65% ± 5% of lipofectamine control. SRSF2 knockdown cells showed significantly greater reduction in 4R:3R tau ratio ($p<0.0001$, one-way ANOVA) measuring 31% ± 5% of lipofectamine control.

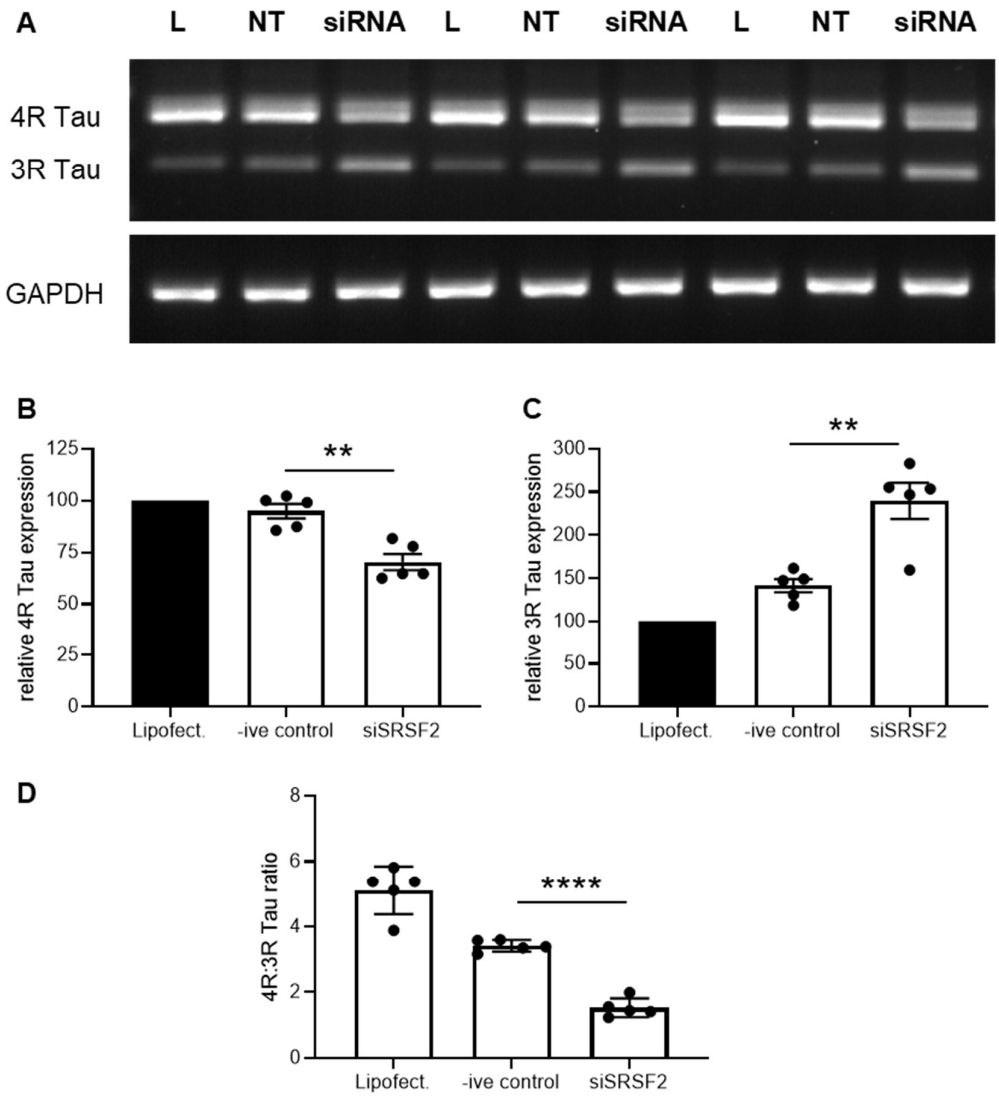


Figure 5.3.1.2 SRSF2 knockdown with targeted siRNA treatment of Neuro2a cells increases MAPT exon 10 skipping and decreases 4R:3R tau ratio. **A** Images show relative expression of 4R and 3R tau, in addition to housekeeping gene *GAPDH*, for samples treated with L= lipofectamine only, NT= scramble siRNA, siRNA= targeting SRSF2. **B** Quantification of 4R tau shows significant reduction with SRSF2 knockdown (one-way ANOVA, $p<0.01$). **C** SRSF2 knockdown induces two-fold increase in 3R tau expression due to significantly more exon 10 skipping (one-way ANOVA, $p<0.01$). **D** 4R:3R tau ratio is significantly reduced by SRSF2 knockdown to less than half of experimental (scramble siRNA) control (one-way ANOVA, $p<0.0001$). All values normalised to *GAPDH* expression, N=5, error bars show SEM.

Knockdown of SRSF1 in N2a cells caused a slight decrease in 4R tau and/or a significant increase in 3R tau expression, as shown in Figure 5.3.1.3 below ($p<0.01$, one-way ANOVA). This supports evidence that SRSF1 activity promotes exon 10 inclusion (Kondo *et al.*, 2004) and opposes findings which suggest SRSF1 promotes exon skipping (Gao *et al.*, 2000; Wang *et al.*, 2004). It can be concluded that the latter does not occur in the Neuro2a cell line. The decrease in 4R tau expression in N2a cells treated with SRSF1 targeting siRNA was not significant but averaged 68.2% ± 12.8% of Lipofectamine control. 3R tau showed significantly higher expression with SRSF1 knockdown and ranged from 29.8% to 547.2% higher than Lipofectamine control (one-way ANOVA, $p<0.05$). This translated to a significant decrease in 4R:3R tau ratio with SRSF1 knockdown (one-way ANOVA, $p<0.01$), which measured at 23% ± 2% of Lipofectamine control.

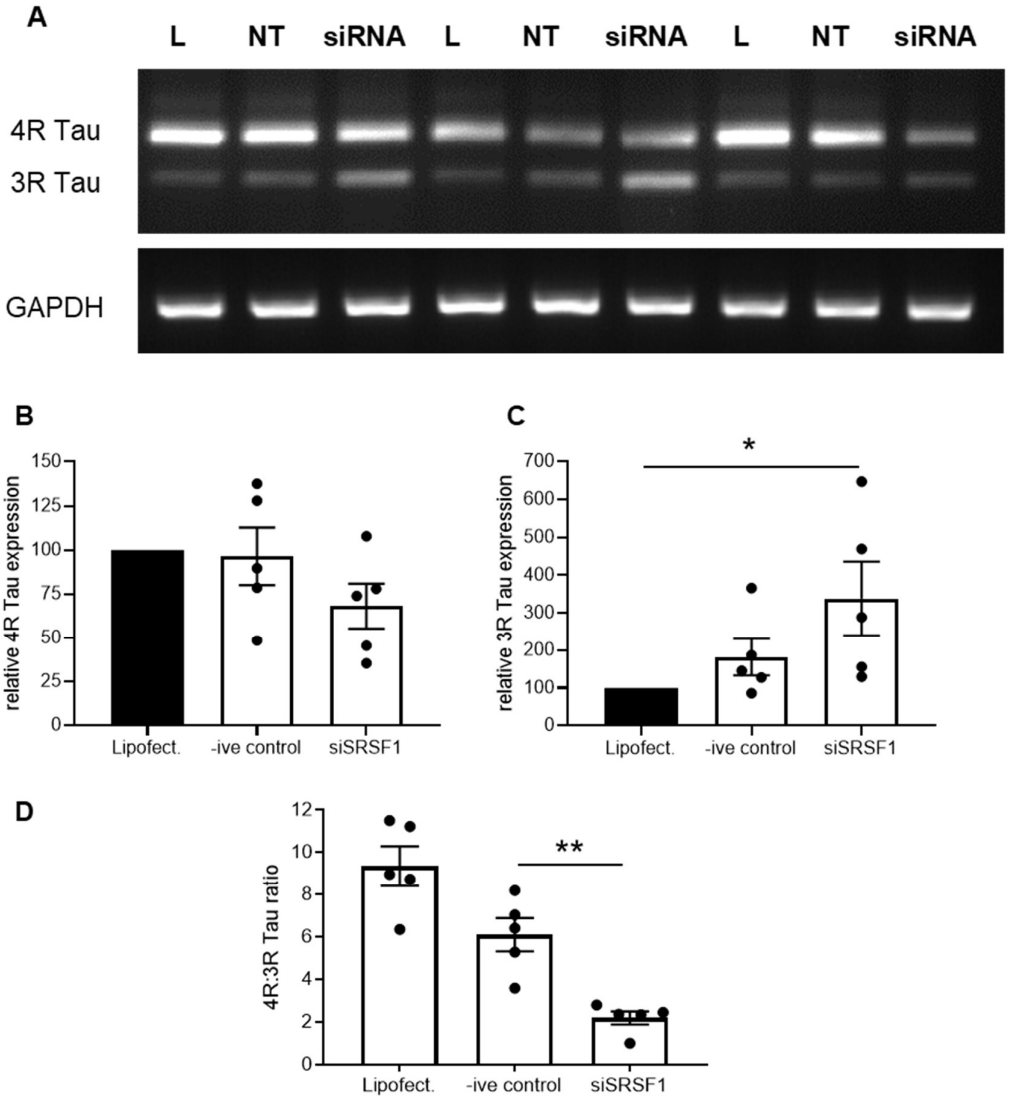


Figure 5.3.1.3 SRSF1 knockdown with targeted siRNA treatment of Neuro2a cells increases MAPT exon 10 skipping and decreases 4R:3R tau ratio. **A** Images show relative expression of 4R and 3R tau, in addition to housekeeping gene *GAPDH*, for samples treated with L= lipofectamine only, NT= scramble siRNA, siRNA= targeting SRSF1. **B** Quantification of 4R tau shows slight reduction with SRSF1 knockdown (ns, one-way ANOVA, $p>0.05$). **C** Quantification of 3R tau shows variable increase with SRSF1 knockdown due to significantly more exon 10 skipping (one-way ANOVA, $p<0.05$). **D** 4R:3R tau ratio is significantly reduced by SRSF1 knockdown to less than half of experimental (scramble siRNA) control (one-way ANOVA, $p<0.01$). All values normalised to *GAPDH* expression, N=5, error bars show SEM.

5.3.2 Selective inhibition of SRPK1 does not conclusively increase *MAPT* exon 10 inclusion

In contrast with Neuro2a cells that preferentially include *MAPT* exon 10, SHSY5Y cells exclude exon 10 and so constitutively express 3R tau at a much higher level. Because of this, SHSY5Y cells were used as a model to test the hypothesis that inhibition of splicing kinases can also alter *MAPT* splicing through altered phosphorylation of SR proteins. SPHINX31 is a known SRPK1 inhibitor that has been previously shown to change splicing of VEGF-A in endothelial cells (Batson *et al.*, 2017). SRPK1 inhibition with other compounds has also been shown to regulate VEGF-A splicing in neuronal cells (Hulse *et al.*, 2014). In the previous chapter, I demonstrated that SPHINX31 treatment of SHSY5Y cells can reproduce similar results, shifting expression from VEGF-A_{165}a to VEGF-A_{165}b isoforms. Since SRPK1 has been found to increase *MAPT* exon 10 skipping (Hartmann *et al.*, 2001), SPHINX31 was used to inhibit SRPK1 in SHSY5Y cells to determine if there was a shift towards exon 10 inclusion (and increase in the 4R:3R tau ratio). Cell treatment was carried out between 10nM and 10μM (as shown in Figure 5.3.2.1), and no significant change in 4R tau expression was measured until the highest concentration 10μM SPHINX31 (see 5.3.2.1C), which may be no longer specific to SRPK1 inhibition.

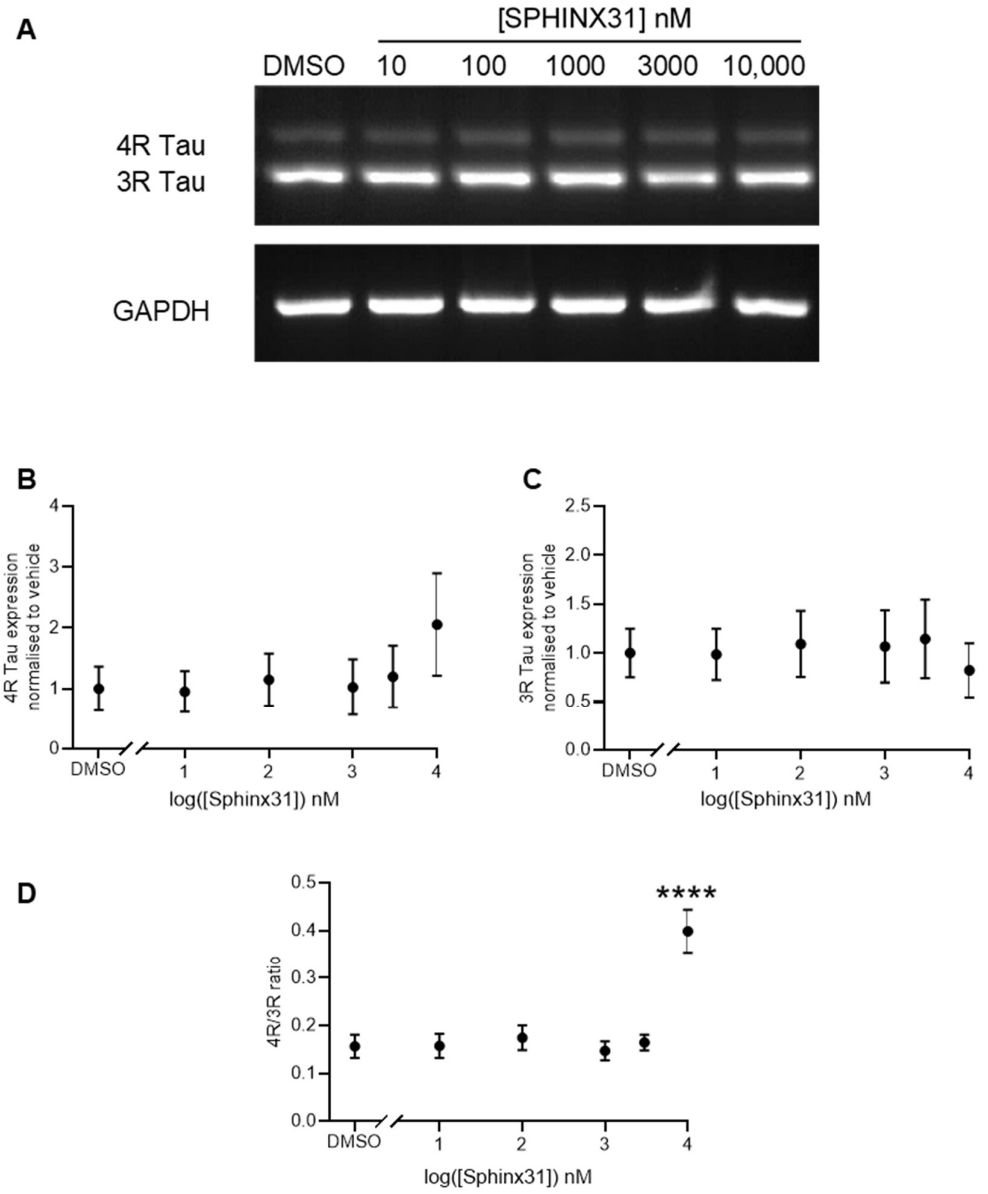


Figure 5.3.2.1 SPHINX31 treatment of SHSY5Y cells for 24h does not significantly alter 4R:3R tau ratio in concentration range 10-3000nM. **A** Images show relative expression of 4R and 3R tau, in addition of housekeeping gene *GAPDH*, for samples treated with 10-10,000nM SPHINX31. 4R tau band is noticeably brighter with 10μM SPHINX31. **B C** Quantification of 4R tau and 3R tau does not show a statistically significant change in expression with SPHINX31 treatment. Values normalised to *GAPDH*. **D** Up to 3μM SPHINX31 does not significantly alter 4R:3R tau ratio in SHSY5Y cells (one-way ANOVA, $p>0.05$) but treatment with 10μM SPHINX31 increases 4R:3R ratio by inducing exon 10 inclusion (one-way ANOVA, $p<0.0001$). N=4, error bars show SEM.

SRPN56 is a novel compound that has not been previously used in neuronal cells nor any physiological assay to investigate alternative splicing. Preliminary *in vitro* data (cell-free) shows that SRPN56 inhibits SRPK1 at 25nM but its selectivity is unknown. Here, I investigated the effect of SRPN56 on *MAPT* exon 10 splicing. From 1-10μM, SRPN56 treated SHSY5Y cells showed significantly increased 4R tau expression (Figure 5.3.2.2), suggesting increased exon 10 inclusion (one-way ANOVA, $p<0.05$ and $p<0.0001$ with 1-3μM and 10μM, respectively). This led to a shift in the ratio of 4R:3R tau isoforms from an average of 0.11 with vehicle (DMSO) only to 0.17 with 10μM SRPN56 treatment (see Figure 5.3.2.2C). This is a small but consistent and significant increase (one-way ANOVA, $p<0.01$ and $p<0.0001$), as the standard deviation of 4R:3R tau ratio for all concentrations was ≤0.01.

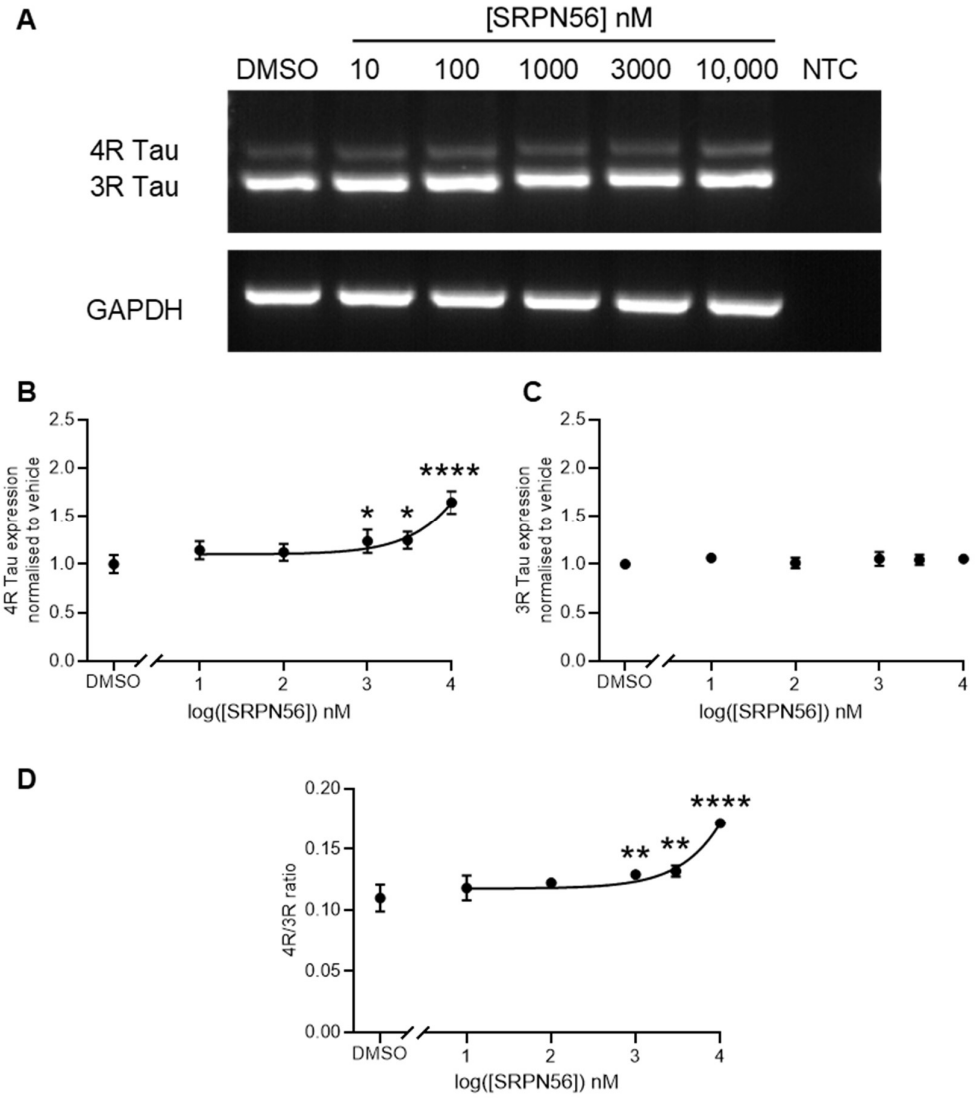
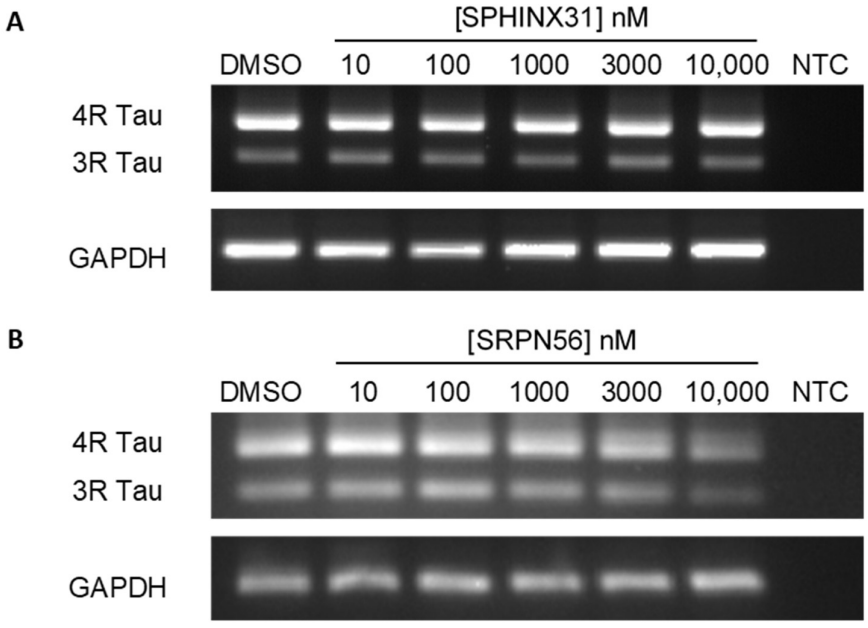


Figure 5.3.2.2 SRPN56 treatment significantly increases 4R:3R tau ratio in SHSY5Y cells. **A** *MAPT* PCR was carried out on samples treated with 10-10,000nM SRPN56 for 24h. Images show relative expression of 4R and 3R tau, in addition of housekeeping gene *GAPDH*. **B** 4R tau expression significantly increases with 1μM, 3μM, and 10μM SRPN56 treatment (one-way ANOVA, *p<0.05 and ****p<0.0001), values normalised to *GAPDH*. **C** Quantification of 3R tau revealed no significant change in expression. **D** 4R:3R tau ratio was significantly increased with 1μM, 3μM and 10μM SRPN56 treatment indicating increased exon 10 inclusion (one-way ANOVA, **p<0.01 and ****p<0.0001 respectively). N=4, error bars show SEM.

To further characterise the role of SRPKs in *MAPT* exon 10 splicing, SRPK1 inhibitors SPHINX31 and SRPN56 were also used in Neuro2a cells. Similar to concentration-response presented in SHSY5Y cells, 1-10,000nM SPHINX31 treatment did not induce a significant change in 4R:3R tau ratio in Neuro2a cells (Figure 5.3.2.3A and C). Interestingly, 100nM SRPN56 treatment showed slightly higher expression of 3R tau (as seen in Figure 5.3.2.3B) which significantly decreased 4R:3R tau ratio below vehicle control, from an average of 1.8 ± 0.1 to 1.2 ± 0.1 (one-way ANOVA, p<0.05). However, 1-10μM SRPN56 treatment returned ratio back to control levels (Figure 5.3.2.3C, p>005). The latter concentration range produced an increase in 4R:3R tau ratio of SHSY5Y cells, which indicates that SRPN56 treatment may have different effects on exon 10 inclusion through inhibition of different splicing kinases.



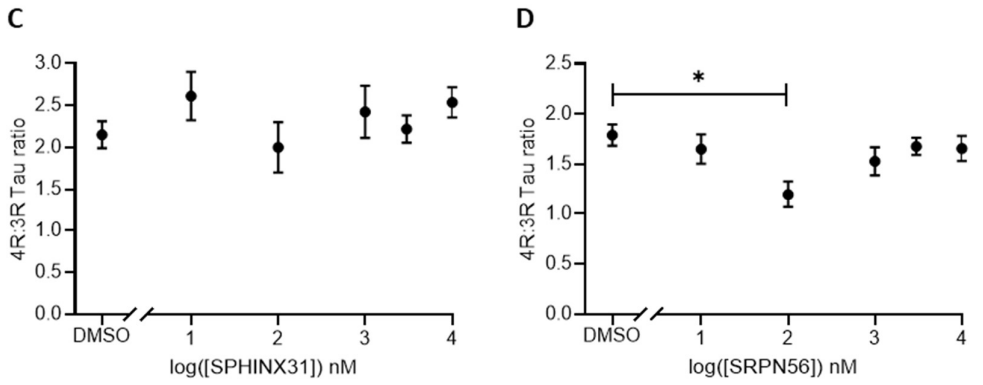


Figure 5.3.2.3 SPHINX31 and SRPN56 treatment of Neuro2a cells does not significantly increase 4R:3R tau ratio. **A B** *MAPT* PCR was carried out on samples treated with 10-10,000nM SPHINX31 and SRPN56 for 24h. Images show relative expression of 4R and 3R tau, in addition of housekeeping gene *GAPDH*. **C** There is no significant change in 4R:3R tau ratio in Neuro2a cells treated with SPHINX31. **D** Neuro2a cells show significant decrease in 4R:3R tau ratio with 100nM SRPN56 but higher concentrations 1-10μM SRPN56 do not have a significant effect. N=3-6, error bars show SEM.

5.3.3 GRIFFIN treatment of SHSY5Y cells increases *MAPT* exon 10 inclusion

The GRIFFINs are novel compounds that have not been published in cell-based assays. Based on preliminary data, they are potent inhibitors of CLKs, and cause varying inhibition of other splicing kinases (summarised in Tables 5.3.3.1-2). Whilst Griffin6 and Griffin8 are selective for CLK1 and CLK2, Griffin33 strongly inhibits SRPK1 and SRPK2 as well as the CLKs. Comparative use of these compounds, alongside SPHINX31, creates a powerful tool for investigating the individual and combined effect of these splicing kinases on *MAPT* exon 10 inclusion.

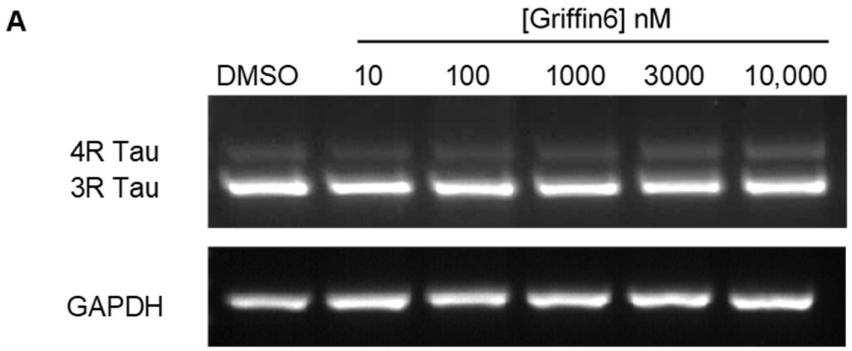
GRIFFIN	% activity remaining at 1μM				
	CLK1	CLK2	DYRK1A	SRPK1	SRPK2
6	2	3	42	26	70
8	4	5	27	27	54
33	4	6	22	2	9

Table 5.3.3.1 The percent remaining activity of splicing kinases with 1μM GRIFFIN treatment in a cell-free in vitro assay. GRIFFIN6 and 8 are more selective for CLK inhibition, whilst GRIFFIN33 is a pan-inhibitor for CLK1/2 and SRPK1/2.

GRIFFIN	IC50 (nM)				
	CLK1	CLK2	DYRK1A	SRPK1	SRPK2
6	6	4	350	199	1400
33	15	17	125	5	45

Table 5.3.3.2 The half maximal inhibitory concentration (IC50) for GRIFFINs for splicing kinases based on a cell-free in vitro assay. IC50 data for GRIFFIN8 is not currently available.

SHSY5Y cells were treated with Griffin6 and Griffin8 to investigate the effect of CLK inhibition on endogenous *MAPT* exon 10 expression in a neuronal model. These compounds were used between 10nM and 10μM, and as shown in Figure 5.3.3.1, treatment with 3-10 μM Griffin6 induced a significant increase in 4R tau expression through exon 10 inclusion (one-way ANOVA, $p<0.05$ and $p<0.01$ respectively). 3R tau expression did not change, so this caused a significant shift in the 4R:3R tau ratio from an average of 0.11 with vehicle (DMSO) only to 0.17 with 10μM Griffin6 (one-way ANOVA, $p<0.05$ and $p<0.001$, respectively).



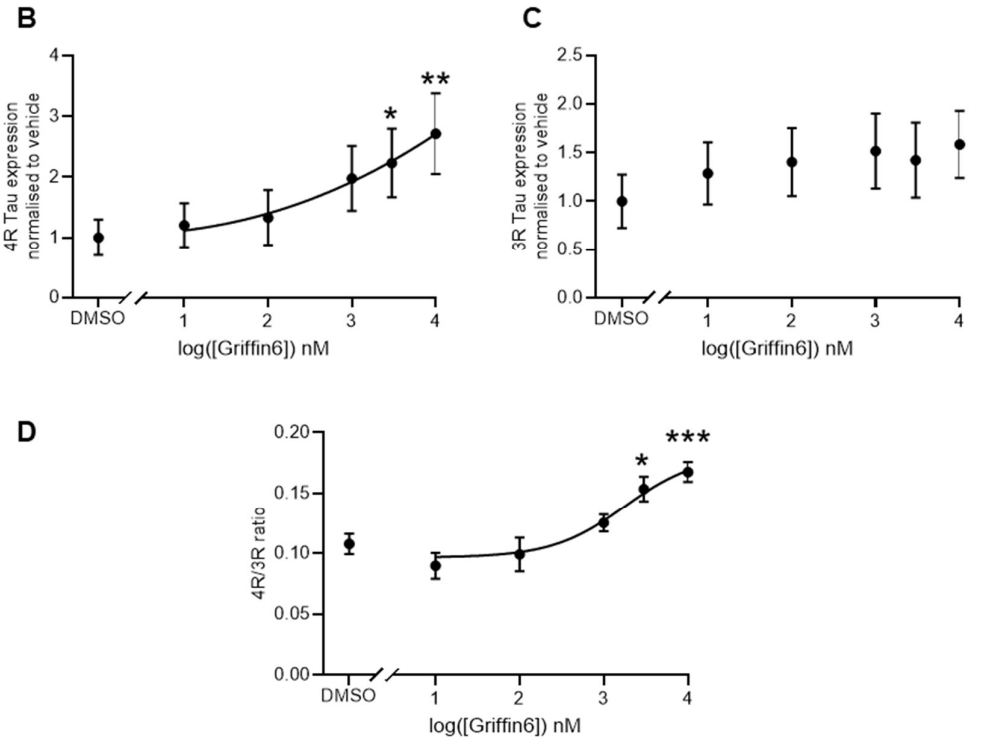


Figure 5.3.3.1 GRIFFIN6 treatment significantly increases 4R:3R tau ratio in SHSY5Y cells. **A** *MAPT* PCR was carried out on samples treated with 10-10,000nM GRIFFIN6 for 24h. Images show relative expression of 4R and 3R tau, in addition of housekeeping gene *GAPDH*. **B** 4R tau expression significantly increases with 3μM and 10μM GRIFFIN6 treatment (one-way ANOVA, $p<0.05$ and $p<0.001$ respectively), values normalised to *GAPDH*. **C** Quantification of 3R tau revealed no significant change in expression. **D** 4R:3R tau ratio is significantly increased with 3μM and 10μM GRIFFIN6 treatment indicating increased exon 10 inclusion (one-way ANOVA, $p<0.05$ and $p<0.001$ respectively). N=4, error bars show SEM.

Griffin8 treatment similarly induced a concentration-dependent increase in 4R:3R tau ratio between 1-10μM (summarised in Figure 5.3.3.2). Cells treated with 10μM Griffin8 showed 2.7 ± 0.6 times greater expression of 4R tau than vehicle control (one-way ANOVA, $p<0.01$). However, 10μM Griffin8 treatment also induced a concentration-dependent increase in 3R tau expression (Figure 5.3.3.2C), albeit to a smaller degree, which measured at 1.5 ± 0.2 times greater than vehicle control ($p<0.01$). These changes in tau expression translated to a limited but significant increase in 4R:3R tau ratio from 0.031 with vehicle only to 0.047-0.052 with 1-10μM Griffin8 (Figure 5.3.3.2D, $p<0.05$ and $p<0.01$). Compared to Griffin6, it could be concluded that Giffin8 had a more potent effect, where 1μM was sufficient to shift toward exon 10 inclusion. However, it may also increase total tau expression. As indicated by Table 5.3.3.1, Griffin8 has similar activity on CLK but differs by greater

inhibition of Dyrk1A. Since CLKs and Dyrk1A have been shown to increase exon 10 skipping (Hartmann *et al.*, 2001; Qian *et al.*, 2011b), these results are consistent with published data.

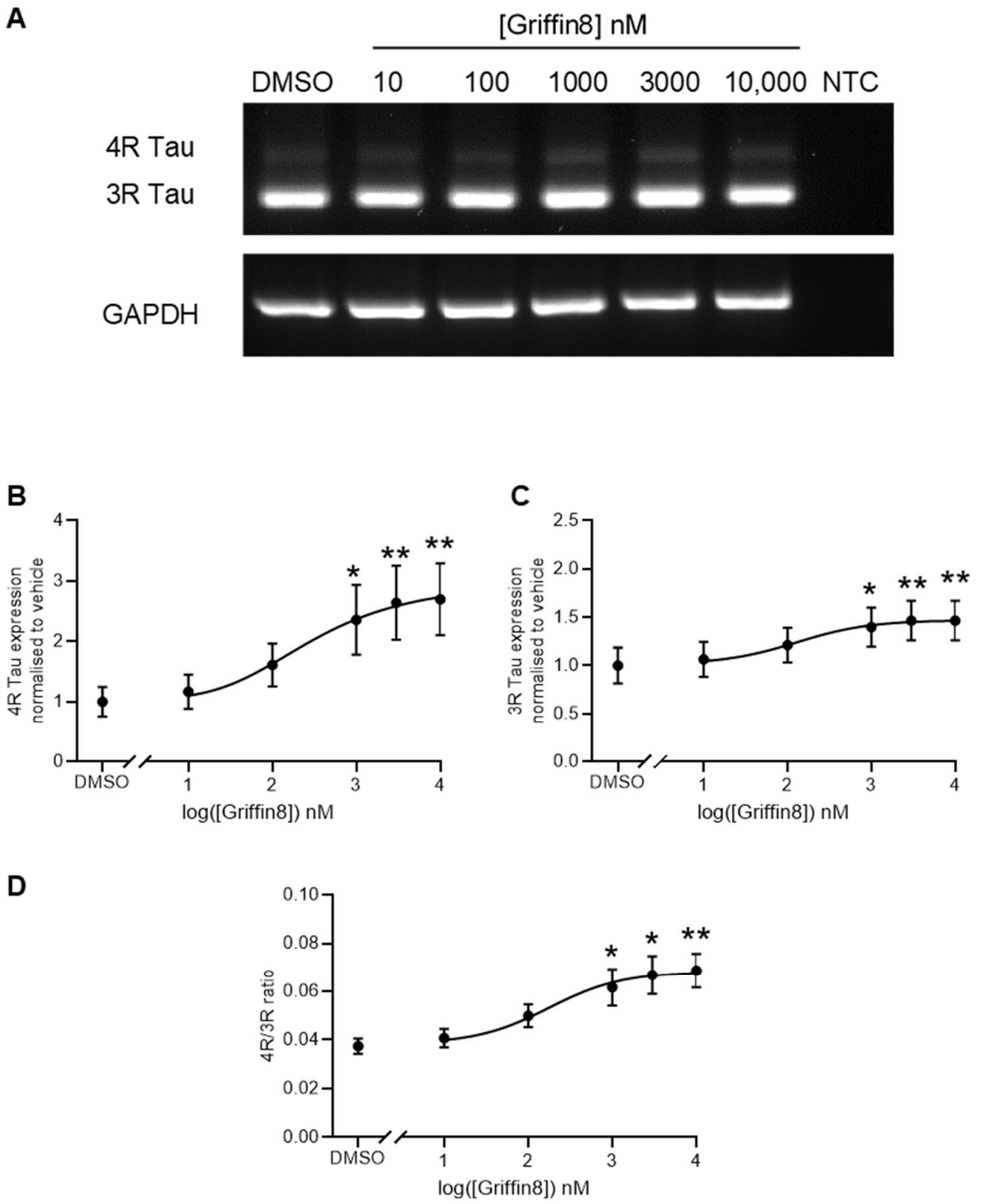
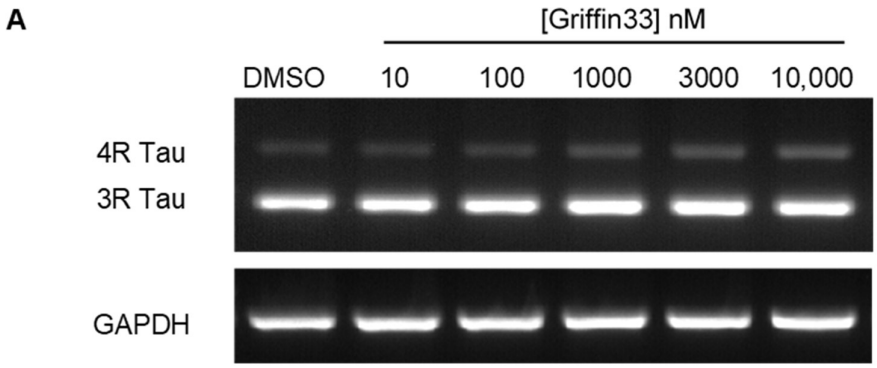


Figure 5.3.3.2 GRIFFIN8 treatment significantly increases 4R:3R tau ratio in SHSY5Y cells. **A** *MAPT* PCR was carried out on samples treated with 10-10,000nM GRIFFIN8 for 24h. Images show relative expression of 4R and 3R tau, in addition of housekeeping gene *GAPDH*. **B** 4R tau expression significantly increases with 1μM, 3μM and 10μM GRIFFIN8 treatment (one-way ANOVA, *p<0.05 and **p<0.01), values normalised to *GAPDH*. **C** GRIFFIN8 also induced an increase in 3R tau but to a smaller degree than 4R tau (one-way ANOVA, *p<0.05 and **p<0.01) indicating a rise in overall tau expression **D** 4R:3R tau ratio is significantly increased with 1μM, 3μM and 10μM GRIFFIN8 treatment indicating increased exon 10 inclusion (one-way ANOVA, *p<0.05 and **p<0.01). N=4, error bars show SEM.

Griffin33 could be considered a pan-inhibitor as it non-selectively inhibits CLK1, CLK2, SRPK1, SRPK2 and to a lower degree Dyrk1A. As demonstrated in Figure 5.3.3.3, SHSY5Y treatment with 3-10μM Griffin33 induced a significant increase in 4R tau expression and 4R:3R tau ratio (refer to B and D for respective quantification; one-way ANOVA, p<0.05). Cells treated with 10μM Griffin33 had 1.6-fold higher expression of 4R tau compared to vehicle control, which caused an increase in 4R:3R tau ratio from 0.075 with vehicle only to 0.129. This is somewhat similar to the effect measured from Griffin6 treatment. When considered alongside results from SPHINX31 inhibition of SRPK1, these data suggest that CLK is the main regulator of *MAPT* exon 10 splicing in SHSY5Y cells.



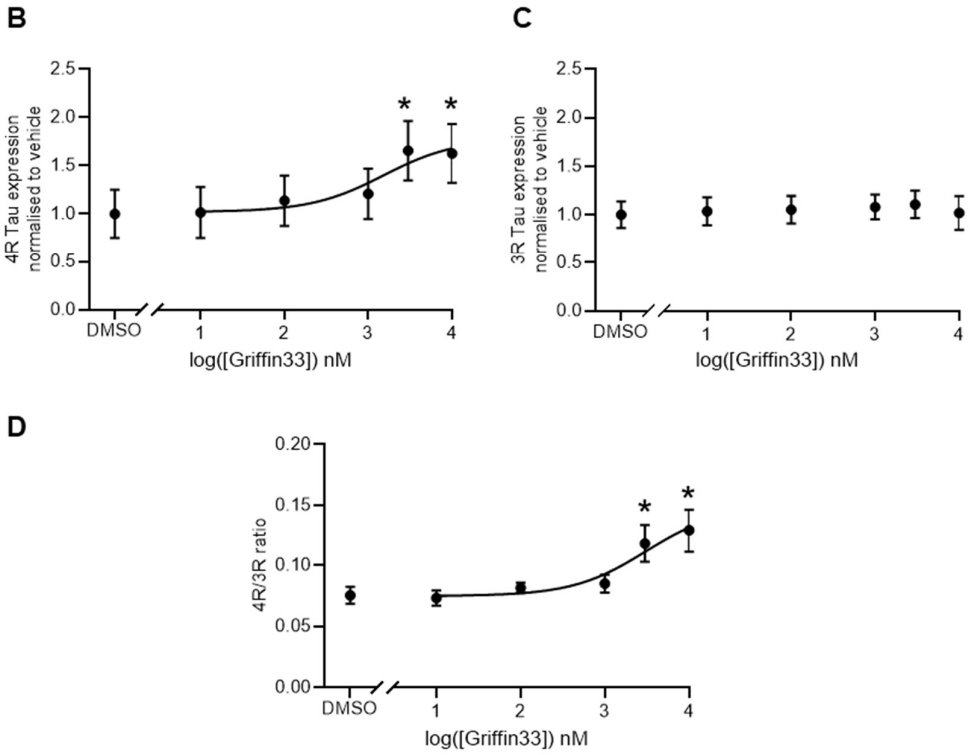


Figure 5.3.3.3 GRIFFIN33 treatment significantly increases 4R:3R tau ratio in SHSY5Y cells. **A** *MAPT* PCR was carried out on samples treated with 10-10,000nM GRIFFIN33 for 24h. Images show relative expression of 4R and 3R tau, in addition of housekeeping gene *GAPDH*. **B** 4R tau expression significantly increases with 3μM and 10μM GRIFFIN33 treatment (one-way ANOVA, $p<0.05$), values normalised to *GAPDH*. **C** Quantification of 3R tau revealed no significant change in expression. **D** 4R:3R tau ratio is significantly increased by 3μM and 10μM GRIFFIN33 treatment indicating increased exon 10 inclusion (one-way ANOVA, $p<0.05$). N=4, error bars show SEM.

To compare the effect of GRIFFINs 6, 8 and 33 on 4R:3R tau ratio, EC50 values were calculated from non-linear curve fit (log agonist v.s. response on GraphPad Prism). These values are summarised in Figure 5.3.3.4 below. Out of the three compounds, GRIFFIN33 had the least potent effect (3μM), and GRIFFIN8 had the most potent effect (177nM) on *MAPT* exon 10 inclusion.

Compound	GRIFFIN6	GRIFFIN8	GRIFFIN33
Bottom	0.097	0.038	0.075
Top	0.182	0.068	0.148
LogEC50	3.249	2.248	3.484
EC50	1775	176.9	3048

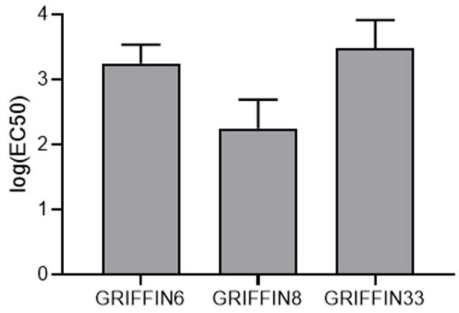


Figure 5.3.3.4 Summary of the effect size and EC50 of GRIFFINs 6, 8 and 33 increasing 4R:3R tau ratio in SHSY5Y cells. N=4-6, error bars show SEM.

Alternative splicing of *MAPT* was further investigated with Griffins 42 and 53. As summarised in Tables 5.3.3.3-4, Griffin42 is more selective for CLK1 compared to CLK2, but is otherwise similar to Griffin6 in terms of Dyrk1A inhibition and Griffin8 in terms of SRPK inhibition. In contrast, Griffin53 exerts greater inhibition of CLK2 and Dyrk1A, and so is most similar to pan-inhibitor Griffin33. One notable difference is that Griffin53 does not inhibit SRPK2, which has been demonstrated to promote *MAPT* exon 10 inclusion (Wang *et al.*, 2018).

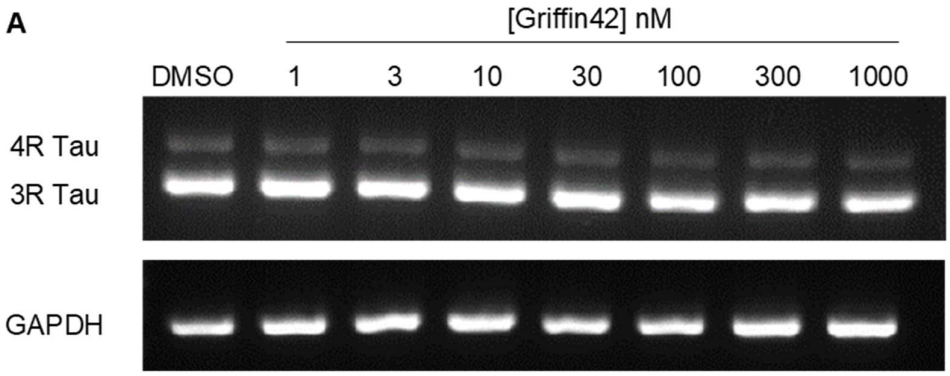
GRIFFIN	**% activity remaining at 1μM**				
	CLK1	**CLK2**	**DYRK1A**	**SRPK1**	**SRPK2**
42	1	25	48	9	53
53	1	12	17	11	58

Table 5.3.3.3 The percent remaining activity of splicing kinases with 1μM GRIFFIN42 and 53 treatment in a cell-free in vitro assay. Both GRIFFINs inhibit CLK and SRPK1 but GRIFFIN53 causes relatively more inhibition of Dyrk1A.

GRIFFIN	IC50 (nM)				
	CLK1	CLK2	DYRK1A	SRPK1	SRPK2
42	14			110.2	
53	8		97	122.6	

Table 5.3.3.4 The half maximal inhibitory concentration (IC50) for GRIFFINs for splicing kinases based on a cell-free in vitro assay. Missing data points because some IC50 values are not currently available.

SHSY5Y cells were treated with 1nM to 1μM Griffin42 for 24h and RNA was collected for RT-PCR. Measured expression of 4R and 3R tau showed no significant change in *MAPT* exon 10 splicing nor 4R:3R tau ratio (Figure 5.3.3.5). Since Griffin42 is a less potent inhibitor of CLK2 compared to Griffin8, this could suggest that increased exon 10 inclusion at 1μM Griffin8 (seen in Figure 5.3.3.2B and D) was related to CLK2 rather than CLK1. Indeed, Hartmann et al. found that CLK2 activity had a stronger effect on *MAPT* splicing compared to other CLKs. However, Griffin8 also differs to Griffin42 by its more potent inhibition of Dyrk1A. Thus, it is equally plausible that discrepancy between compounds is dependent on Dyrk1A inhibition. This theory is further supported by the fact Griffin6, which selectively and potently inhibits CLK1 and CLK2, does not shift 4R:3R at 1μM either, with significant effect measured at 3μM and 10μM Griffin6 treatment.



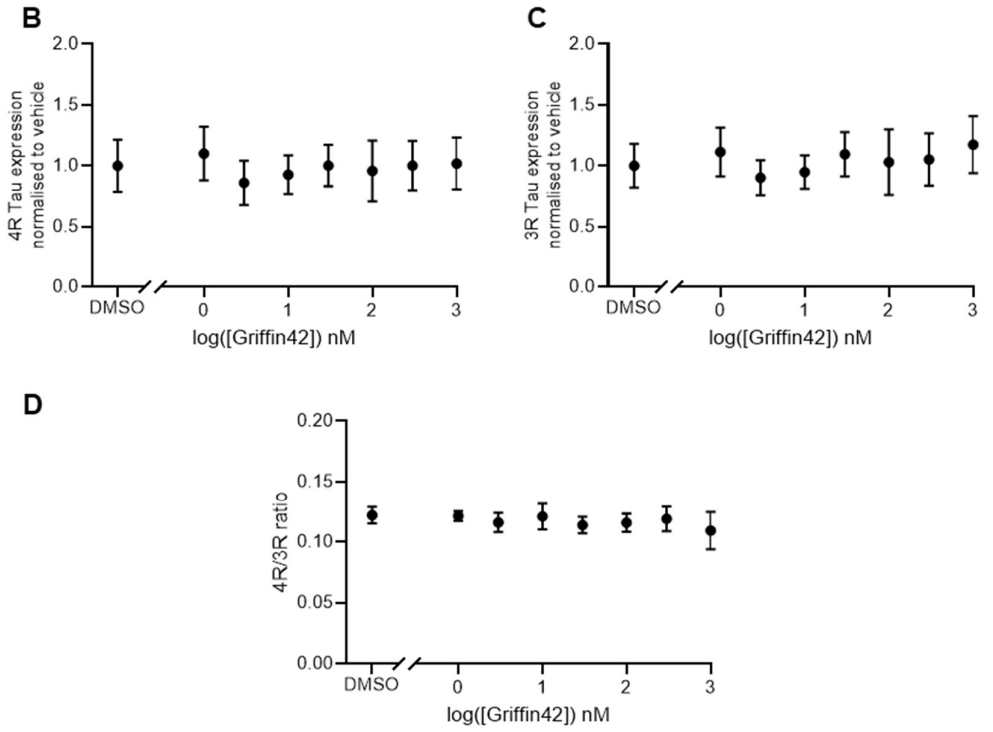


Figure 5.3.3.5 GRIFFIN42 treatment does not significantly change 4R:3R tau ratio in SHSY5Y cells. **A** *MAPT* PCR was carried out on samples treated with 1-1000nM GRIFFIN42 for 24h. Images show relative expression of 4R and 3R tau, in addition of housekeeping gene *GAPDH*. **B C** Quantification of 4R and 3R tau expression revealed no significant change with GRIFFIN42 treatment, values normalised to GAPDH. **D** 4R:3R tau ratio remains unchanged in the presence of up to 1μM GRIFFIN42 (one-way ANOVA, $p>0.05$). N=3, error bars show SEM.

To further elucidate the role of CLK1 in regulation of *MAPT* exon 10 splicing, SHSY5Y cells were treated with siRNA targeting CLK1 and expression of 4R:3R tau ratio was quantified by RT-PCR. As shown in Figure 5.3.3.5A and B, *CLK1* knockdown was confirmed to an average of 65% ±3.6% of experimental control (one-way ANOVA, $p<0.001$). However, this did not induce a significant change in *MAPT* exon 10 splicing: the expression of 4R and 3R tau remained unchanged, as did the 4R:3R tau ratio (refer to 5.3.3.6C; one-way ANOVA, $p>0.05$). Unfortunately, protein quantification of CLK1 was not possible due to time constraints caused by the COVID pandemic. Nonetheless, this evidence indicates that 65% knockdown of *CLK1* gene expression alone is insufficient to change *MAPT* exon 10 splicing.

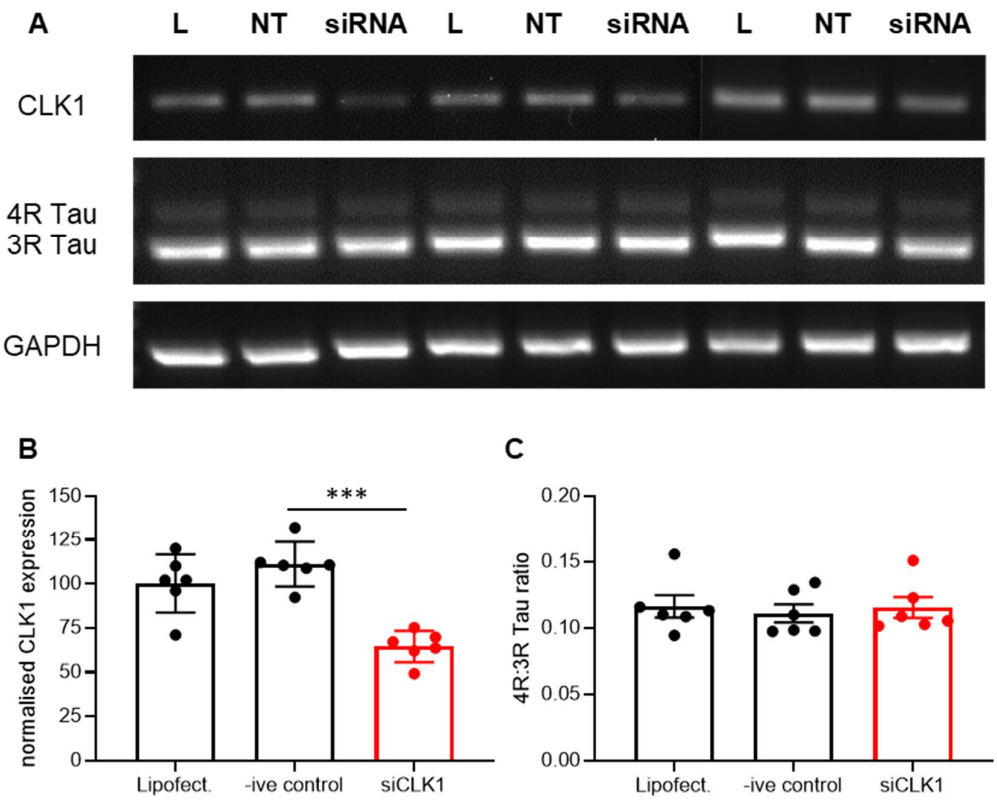


Figure 5.3.3.6 CLK1 knockdown (65%) is insufficient to change MAPT exon 10 splicing in SHSY5Y cells. **A** *CLK1* and *MAPT* RT-PCR were carried out on samples from SHSY5Y cells treated with siRNA targeting CLK1. Images show expression of *CLK1*, both 4R and 3R tau isoforms, and the housekeeping gene *GAPDH*. Samples labelled L= lipofectamine only, NT= control (scramble) siRNA, siRNA= targeting CLK1. **B** Quantification of *CLK1* expression shows significant decrease to an average 65% ± 3.6% of Lipofectamine control (one-way ANOVA, $p<0.001$). All values normalised to sample *GAPDH* expression and then Lipofectamine control. **C** Quantification of 4R and 3R tau expression indicated that 4R:3R tau ratio remains unchanged by CLK1 knockdown (one-way ANOVA, $p>0.05$). N=6, error bars display SEM within each treatment group.

Griffin53, a pan-inhibitor, was found to induce greater exon 10 inclusion in SHSY5Y cell, as shown in Figure 5.3.3.7 below. Cells treated with 1μM Griffin53 showed 1.9-fold increase in 4R tau expression compared to vehicle control (Figure 5.3.3.7B). 3R tau expression was not significantly altered (Figure 5.3.3.7C), which led to a modest but significant shift in the 4R:3R tau ratio from an average of 0.11 to 0.16 with 1μM Griffin53 treatment (Figure 5.3.3.7D). This effect is comparable to 3μM Griffin33 seen in Figure 5.3.3.3D. Considering IC50 values in Table 5.3.3.4, the stronger effect of 1μM Griffin53 may be dependent on less potent inhibition of SRPK2 activity. Selective SRPK1 inhibition with SPHINX31 did not significantly shift 4R:3R

ratio, but strong CLK inhibition combined with weaker SRPK2 inhibition seems to promote exon 10 inclusion more than CLK inhibition alone.

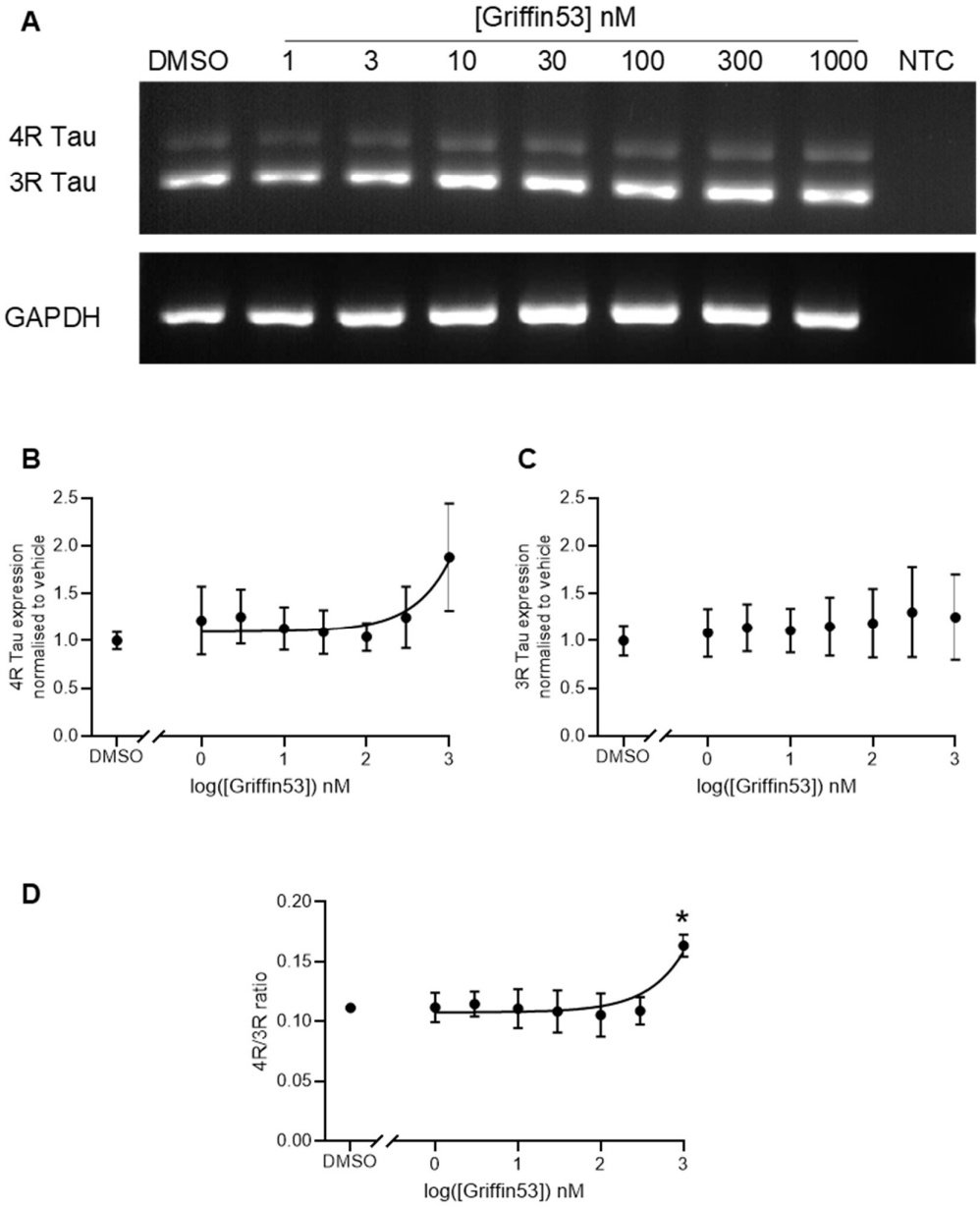


Figure 5.3.3.7 1μM GRIFFIN53 treatment significantly increases 4R:3R tau ratio in SHSY5Y cells. **A** *MAPT* PCR was carried out on samples treated with 1-1000nM GRIFFIN53 for 24h. Images show relative expression of 4R and 3R tau, in addition of housekeeping gene *GAPDH*. **B** 4R tau quantification shows upward trend with GRIFFIN53 treatment, but expression is variable, and change is not statistically significant (one-way ANOVA, $p>0.05$). All values normalised to *GAPDH*. **C** Quantification of 3R tau revealed no significant change in expression. **D** 4R:3R tau ratio is significantly increased by 1μM GRIFFIN53 treatment, indicating increased exon 10 inclusion (one-way ANOVA, $p<0.05$). N=3, error bars show SEM.

5.3.4 Griffin6 treatment of SHSY5Y cells reduces SR protein phosphorylation

The GRIFFINs are splicing kinase inhibitors and splicing kinases are known to phosphorylate SR proteins, but the direct effect of GRIFFINs on SR phosphorylation has not been previously investigated. In this experiment, I sought to empirically measure SR phosphorylation in Griffin6-treated SHSY5Y cells to test the hypothesis that Griffin6 inhibition of CLK would cause a decrease in SR phosphorylation. For comparison, SHSY5Y cells were also treated with SPHINX31, which operated in part as a positive control, since it has been previously published to decrease SR phosphorylation but not specifically in SHSY5Y cells. After 48h treatment, cell lysate was collected and 50µg protein per sample was used for Western blot, then probed for phosphorylated-SR protein and SRSF1 expression. As shown in Figure 5.3.4.1, both SPHINX31 and Griffin6 treatment caused a significant decrease in phosphorylation of SRSF1 (one-way ANOVA, $p<0.05$).

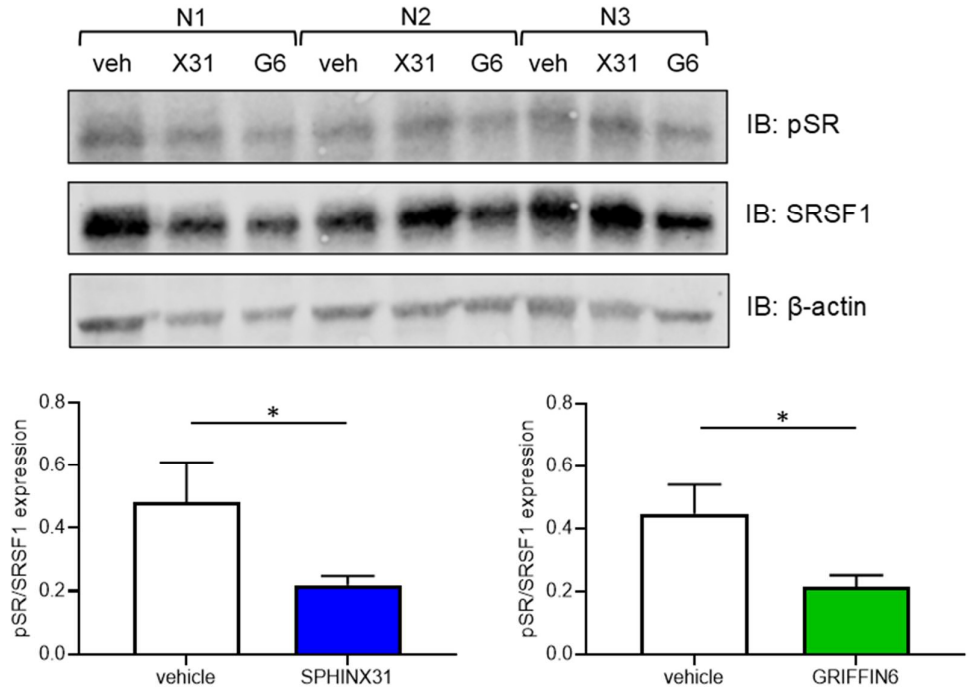


Figure 5.3.4.1 GRIFFIN6 and SPHINX31 treatment of SHSY5Y cells induces a significant decrease in SRSF1 phosphorylation. **A** Western blot was carried out on SHSY5Y cell lysates after 48h treatment with 10µM SPHINX31 and GRIFFIN6. Blots were probed with mouse phospho-SR antibody, rabbit SRSF1 antibody and goat β-actin antibody. Expression was quantified on a dual-colour blot by densitometry using Licor Image Studio software. **B** Quantification of pSR band at 28kDa relative to SRSF1 band shows significant decrease with SPHINX31 treatment compared to vehicle control (one-way ANOVA, $p<0.05$). **C** The relative expression of pSR to SRSF1 also decreases with GRIFFIN6 treatment (one-way ANOVA, $p<0.05$). Total N=5, error bars show SEM.

The expression of other phosphorylated-SR proteins observed on the same blot also changed with treatment of SHSY5Y cells with splicing kinase inhibitors. For example, faint pSR bands at 55kDa and 75kDa, relating to SRSF6 and SRSF4 respectively, seemed to decrease with Griffin6 treatment (as demonstrated in Figure 5.3.4.2). Although phosphorylated SRSF4 bands could not be reliably quantified (due to lack of clarity), SRSF6 was expressed at higher levels and could be more easily assessed. Based on densitometry, Griffin6 treatment significantly decreased phosphorylation of SRSF6 (Figure 5.3.4.2C; one-way ANOVA, $p<0.05$). Since CLK1 is known to phosphorylate SRSF6, this effect is likely through Griffin6 dependent CLK inhibition (Hartmann *et al.*, 2001). On average, SPHINX31 treatment also might decrease phosphorylation of SRSF6, but not to a statistically significant degree within current sample size (Figure 5.3.4.2B; one-way ANOVA, $p>0.05$).

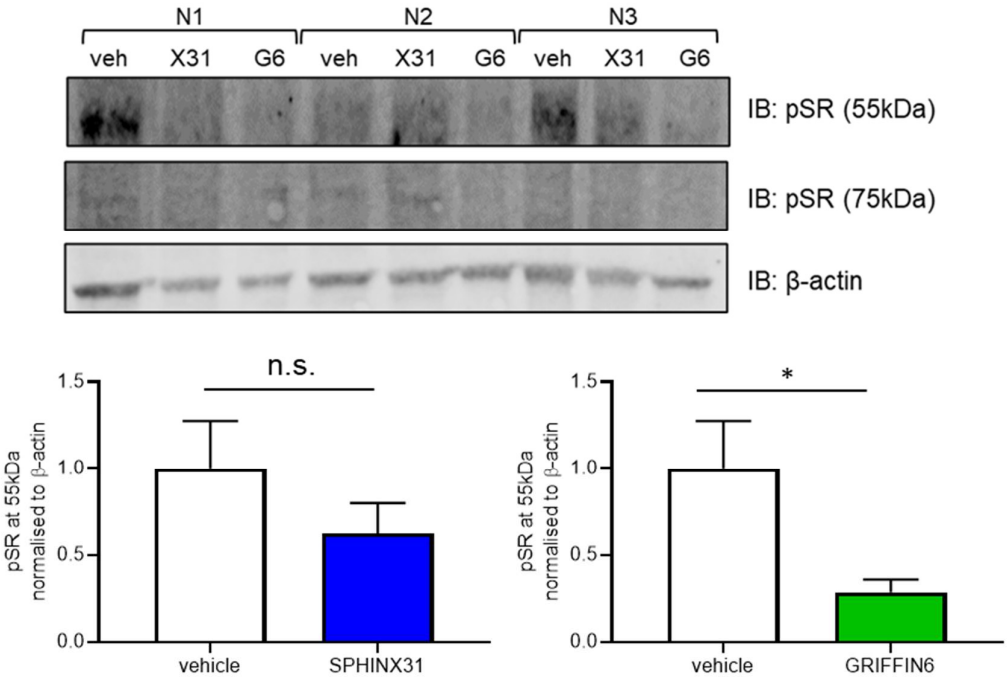
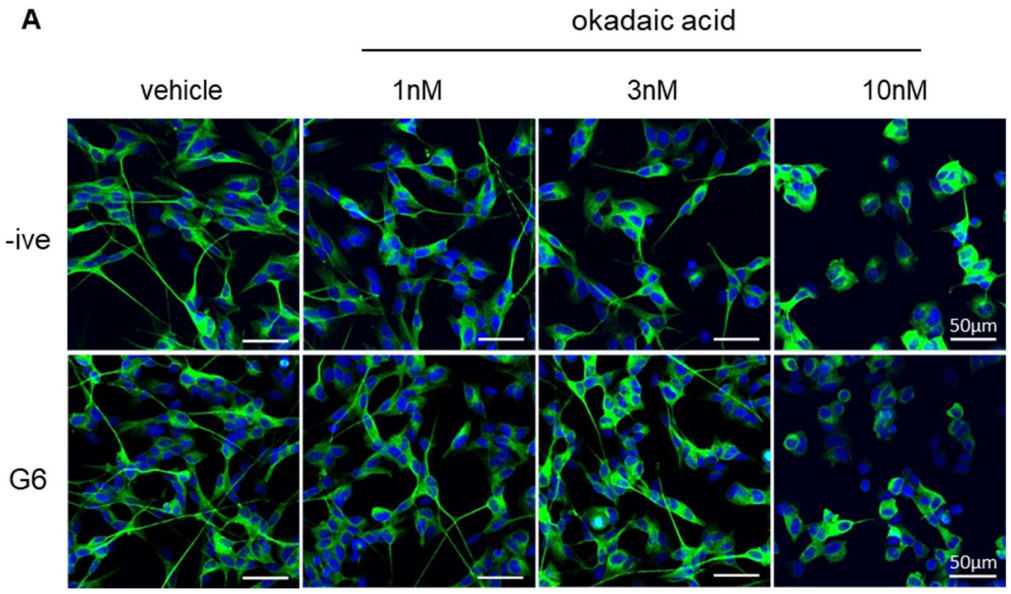


Figure 5.3.4.2 GRIFFIN6 treatment of SHSY5Y cells induces a significant decrease in pSR at 55kDa. **A** Western blot was carried out on SHSY5Y cell lysates after 48h treatment with 10μM SPHINX31 and GRIFFIN6. Blots were probed with mouse phospho-SR antibody and goat β-actin antibody. Expression was quantified on a dual-colour blot by densitometry using Licor Image Studio software. **B** Quantification of pSR band at 55kDa relative to housekeeping protein β-actin band does not show a significant change with SPHINX31 treatment (one-way ANOVA, $p>0.05$). **C** GRIFFIN6 treatment does induce significant decrease in 55kDa pSR relative to β-actin expression (one-way ANOVA, $p<0.05$). Total N=4, error bars show SEM.

5.3.5 Griffin6 treatment of SHSY5Y cells ameliorates OA-induced decrease in neurite outgrowth

As an indicator of how altered splicing relates to cell physiology, I investigated the effect of Griffin6, selective CLK inhibitor, on neurite outgrowth. Within the OA model introduced in Chapter 4, Griffin6 was found to recover neurite outgrowth. SHSY5Y cells were probed with βIII-tubulin (shown in green) and outgrowth was calculated by tracing neurites on Image J and dividing the sum length per image by the number of cells. OA treatment induced a concentration-dependent decrease in neurite outgrowth (see Figure 5.3.5.1A and B). 1nM and 3nM OA significantly inhibited outgrowth (Figure 5.3.5.1C), as determined by decrease in control group values from 21.6μm ± 1.3μm (vehicle only) to 14.8μm ± 0.6μm and 8.9μm ± 1.0μm, respectively. With Griffin6 co-treatment, I measured higher average 15.4μm ± 0.8μm outgrowth in the presence of 3nM OA. Using two-way ANOVA to compare all experimental groups, Griffin6 was determined to have a significant effect on sum neurite length ($p<0.001$), indicating that Griffin6 is protective of neuronal outgrowth.



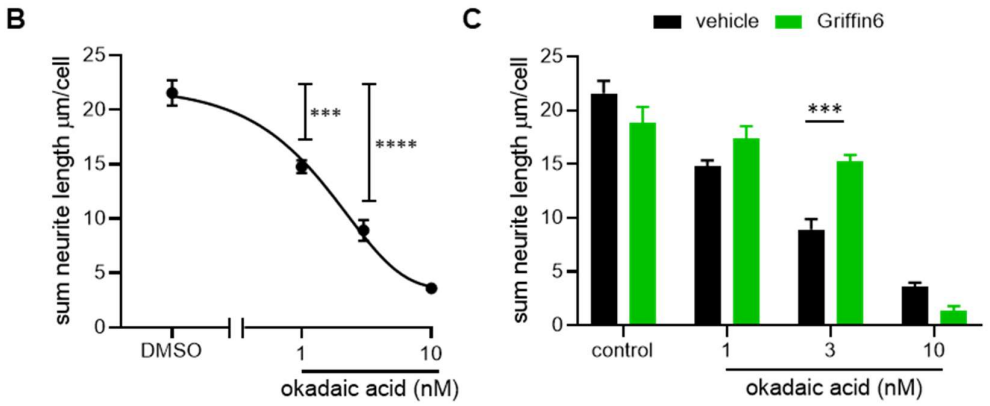


Figure 5.3.5.1 Griffin6 treatment protects against OA-induced decline in neurite outgrowth. **A** SHSY5Y cells were treated for 24h with 1-10nM OA with or without 3µM Griffin6. Neurone-specific marker βIII tubulin identified neurites shown in green. Cell nuclei stained with Hoechst shown in blue. Using FIJI software, neurite length was quantified using simple tracer and the sum neurite length was divided by number of nuclei counted with a macro. **B** Quantification shows that 1nM and 3nM OA significantly inhibits outgrowth of SHSY5Y cells (one-way ANOVA, $p<0.001$ and $p<0.0001$ respectively). **C** Griffin6 co-treatment significantly ameliorates decline in neurite outgrowth induced by 3nM OA (two-way ANOVA, $p<0.0001$). N=3 replicates per condition, error bars show SEM.

Since Griffin6 can have neuroprotective effects in SHSY5Y cells, RT-PCR was used to further investigate whether (a) OA treatment, used to reduce neurite outgrowth *in vitro*, significantly changes *MAPT* exon 10 inclusion, and (b) measured neuroprotection is dependent on the increase in 4R:3R tau ratio previously demonstrated with 3µM Griffin6 treatment. As presented in Figure 5.3.5.2, OA alone did not significantly affect 4R:3R tau ratio, but Griffin6 treatment reproduced a significant increase in exon 10 inclusion and 4R:3R tau ratio (one-way ANOVA, $p<0.01$). SHSY5Y cells co-treated with OA and Griffin6 seemed to show lower average 4R:3R tau ratio relative to Griffin6 treatment alone (not significant) but statistically higher 4R:3R tau ratio than OA treatment alone (one-way ANOVA, $p<0.05$). This suggests that Griffin6 treatment can still increase exon 10 inclusion in the presence of OA, and it may exert (at least part) of its neuroprotective effect through regulation of *MAPT* splicing.

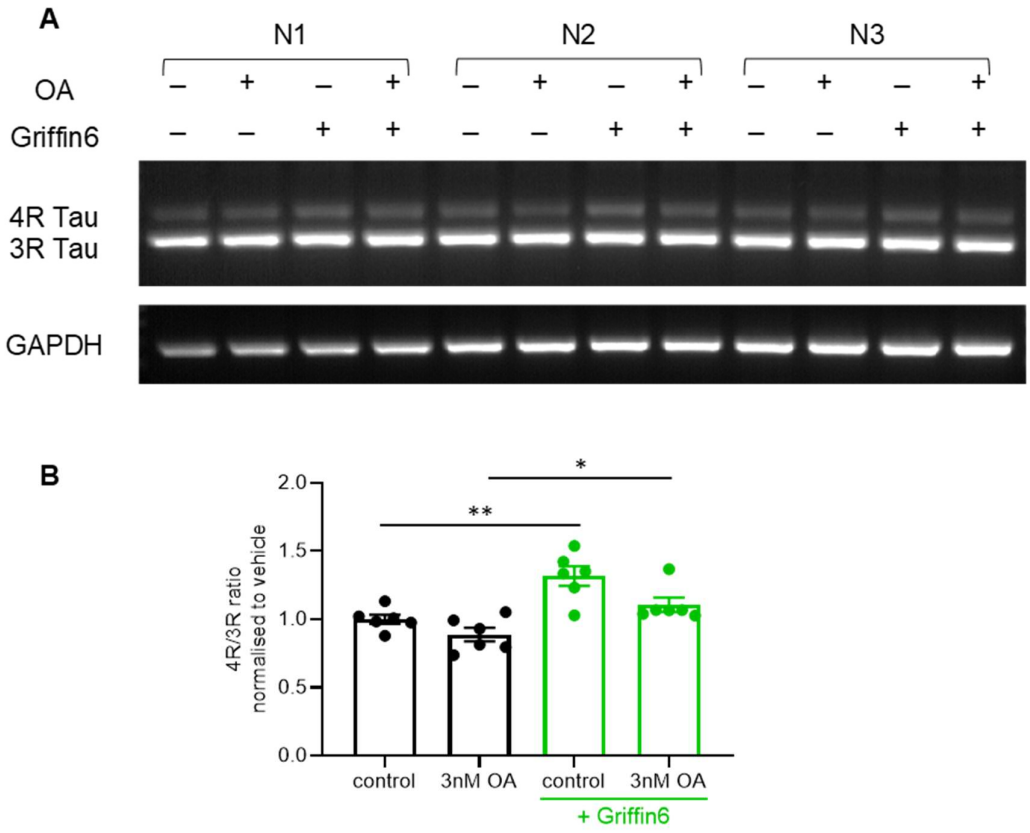


Figure 5.3.5.2 Griffin6 treatment of SHSY5Y cells increases 4R:3R tau ratio in both absence and presence of OA. **A** SHSY5Y cells were treated with 3nM OA and/or 3μM Griffin6 for 24h. *MAPT* PCR was carried out using primers spanning exon 10 (forward primer in exon 9, reverse primer in exon 11) to quantify relative expression of 4R and 3R tau isoforms. Images show tau isoform expression and housekeeping gene *GAPDH* matched to each sample **B** Griffin6 treatment induces a significant increase in 4R:3R tau ratio (one-way ANOVA, $p<0.01$). Additionally, combination of OA and Griffin6 treatment shows significantly higher 4R:3R tau ratio than OA treatment alone (one-way ANOVA, $p<0.05$). The 4R:3R tau ratio of experimental groups was normalised to vehicle-only control group, and variability within control group is produced by normalisation to its own average. N=4, error bars show SEM.

As a CLK inhibitor, Griffin6 treatment could shift alternative splicing of many other genes, which are likely contributing to measured neuroprotection and other physiological effects. Since VEGF-A isoforms were demonstrated to be an important player in this neuronal model (see Chapter 4), alternative splicing of VEGF-A was investigated in Griffin6-treated SHSY5Y cells. As seen with RT-PCR of SPHINX31-treated cells (see Figure 5.3.5.3), VEGF-A_{165}b isoforms could not be detected. As previously discussed, lack of VEGF-A_{165}b detection could be due to the fact it is expressed comparatively lower than VEGF-A_{165}a, causing its amplicon to be out-competed by the other isoform.

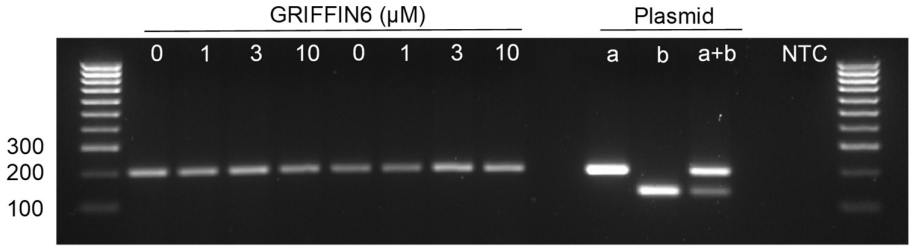


Figure 5.3.5.3 VEGF-A_{165}b bands are not detectable by conventional RT-PCR in GRIFFIN6 treated SHSY5Y samples. Cells were treated with 1μM, 3μM, and 10μM Griffin6 and RT-PCR was conducted to quantify VEGF-A isoform expression. Positive control plasmids for VEGF-A_{165}a and VEGF-A_{165}b expression selectively showed detection of each isoform. NTC= no template control for cDNA and PCR reaction

Using ELISA, it was possible to quantify both VEGF-A isoforms and measure relative expression against standard curves produced by serial dilution of VEGF-A_{165}a and VEGF-A_{165}b recombinant proteins (see section 2.5.4 for optimisation and Figure 4.3.4.2 for standard curves). All values were then normalised to vehicle control group VEGF-A isoform expression. In SHSY5Y samples, I did not measure a significant change in expression of either VEGF-A isoform with Griffin6 treatment (see Figure 5.3.5.4). In cell lysate, VEGF-A_{165}a measured at an average of 105% ± 4.7%, 99.1% ± 6.4%, and 103.7% ± 9.1% of vehicle control with 1μM, 3μM and 10μM Griffin6, respectively (Figure 5.3.5.4A). Similarly, in cell media, VEGF-A_{165}a remained at 102.9% ± 5.2% of vehicle control with highest concentration 10μM Griffin6 (Figure 5.3.5.4B). In both cell lysate and media, VEGF-A_{165}b showed a downward trend but this change was insignificant, as shown in Figure 5.3.5.4C and D, respectively. With 10μM Griffin6 treatment, VEGF-A_{165}b expression was calculated to be 109.6 ± 6.6% and 121.4% ± 8.9% of vehicle control, respectively ($p>0.05$, one-way ANOVA). When isoforms are expressed as a ratio VEGF-A_{165}a:VEGF-A_{165}b, there is no concentration-dependent change with Griffin6

treatment (see Figure 5.3.5.4E and F). In cells treated with 10μM Griffin6, the ratio measured from lysate and media remained at 98.2% ± 12.7% and 91.5% ± 8.2% of vehicle control, respectively ($p>0.05$, one-way ANOVA). I should be noted that quantification of expression, particularly of VEGF-A_{165}b, was variable even in the control group suggesting that a larger sample size could have produced more reliable results. Nonetheless, these results suggest that CLK does not play as important a role in neuronal VEGF-A alternative splicing compared to SRPK1 (refer to Figure 4.3.4.3).

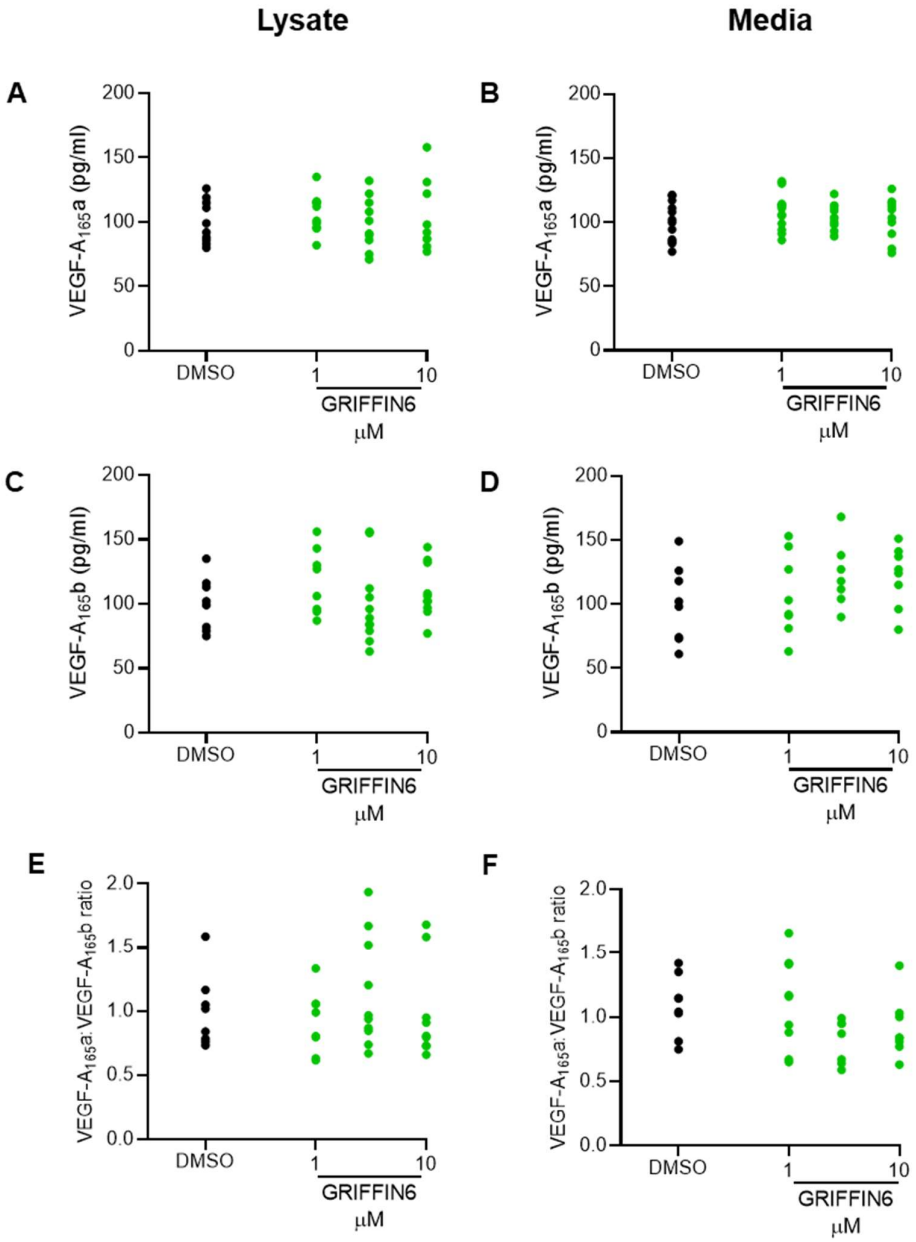
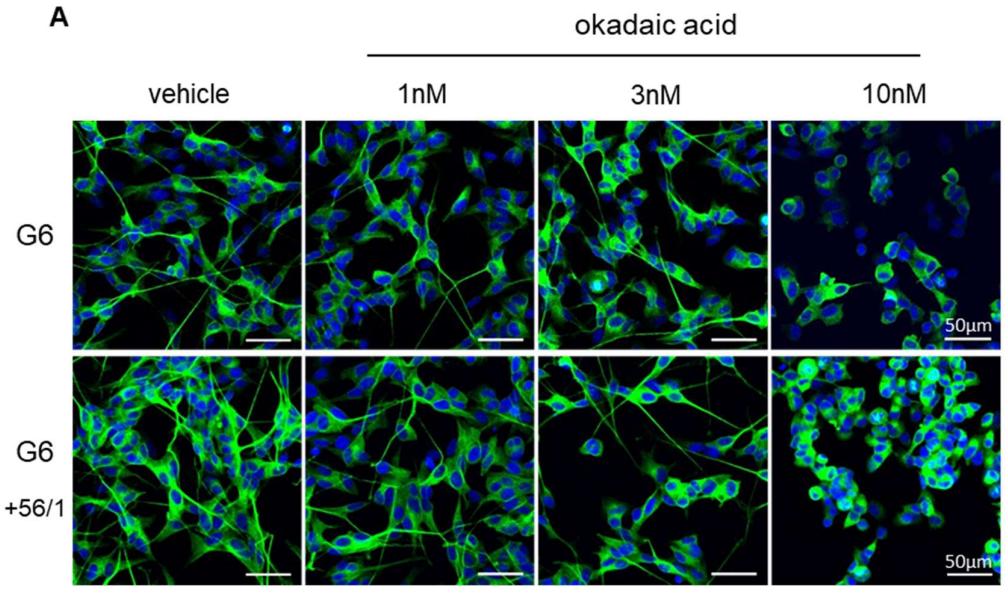


Figure 5.3.5.4 Griffin6 treatment does not significantly change VEGF-A_{165}a:VEGF-A_{165}b ratio in SHSY5Y cells. **A B** SHSY5Y cells were treated with 1-10μM GRIFFIN6 for 72h and ELISA was used to quantify relative expression of VEGF-A isoforms against respective standard curves. Quantification of VEGF-A_{165}a expression in cell lysate and media showed no significant difference between vehicle and Griffin6 treated samples. **C D** Similarly, VEGF-A_{165}b quantification did not show significantly differential expression in either cell lysate or media (one-way ANOVA, $p>0.05$). **E F** Finally, measured ratio of VEGF-A_{165}a:VEGF-A_{165}b in cell lysate and media does not show a significant effect of Griffin6 treatment on SHSY5Y cells. However, there is a downward trend in some samples, e.g., 3μM GRIFFIN6 treated cell media. N=3 biological replicates and N=2 technical replicates.

To confirm that Griffin6 is not acting through alternative splicing of VEGF-A, the neurite outgrowth assay was repeated to include tertiary treatment with 56/1, a neutralising antibody for VEGF-A_{165}b, as presented in Figure 5.3.5.5 below. I found that blocking action of VEGF-A_{165}b did not significantly change the neuroprotective effect of Griffin6 (Figure 5.3.5.5B; two-way ANOVA, $p>0.05$). Compared to control, Griffin6 treatment significantly increases outgrowth from SHSY5Y cells in the presence of 3nM OA, from an average of 15.4μm ± 0.8μm to 8.9μm ± 1.0μm (two-way ANOVA, $p<0.001$). When also treated with 56/1 antibody, there is no significant difference to Griffin6 treatment alone: Cells treated with Griffin6 + 56/1 + 3nM OA showed an average sum outgrowth of 14.7μm ± 1.3μm (two-way ANOVA, $p>0.05$).



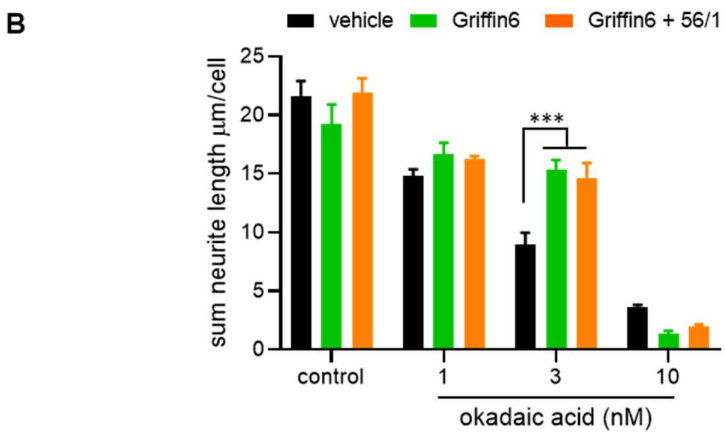


Figure 5.3.5.5 Griffin6 amelioration of OA-induced decline in neurite outgrowth is not dependent on VEGF-A_{165}b expression. **A** SHSY5Y cells were treated for 24h with 1-10nM OA and a combination of 3µM Griffin6 + 56/1 co-treatments. Neurone-specific marker βIII tubulin identified neurites shown in green. Cell nuclei stained with Hoechst shown in blue. Using FIJI software, neurite length was quantified using simple tracer and the sum neurite length was divided by number of nuclei counted with a macro. **B** Quantification of neurite outgrowth shows that Griffin6 co-treatment significantly ameliorates decline in neurite outgrowth induced by 3nM OA (two-way ANOVA, $p<0.001$). Co-treatment of SHSY5Y cells with 56/1 in addition to Griffin6 does not significantly change neurite outgrowth (two-way ANOVA, $p>0.05$) which remains greater than vehicle + OA group (two-way ANOVA, $p<0.001$). N=3-5 replicates per condition, error bars show SEM.

5.4 Discussion

In this chapter, SHSY5Y cells were successfully used as a neuronal model to investigate endogenous alternative splicing of *MAPT* exon 10. Novel compounds acting as splicing kinase inhibitors were used to alter splicing of exon 10 and elucidate their role in tau function.

5.4.1 Knockdown of SRSF1 and SRSF2 in Neuro2a cells confirmed to increase *MAPT* exon 10 skipping

Transient knockdown of SRSF1 and SRSF2 caused a significant decrease in 4R:3R tau ratio through *MAPT* exon 10 skipping (see section 5.3.1). This suggests that both SRSF1 and SRSF2 are necessary for exon 10 inclusion, and inhibition of either splicing factor cannot be compensated by the other. As previously discussed, this is in keeping with the literature, where SRSF1 and SRSF2 have both been shown to promote *MAPT* exon 10 inclusion (Kondo *et al.*, 2004; Qian *et al.*, 2011b). SR proteins, including SRSF1, are known to bind to AG-rich region at the 5' splice site of exon 10, AATAAGAAG, which acts as an exonic enhancer element (Kondo *et al.*, 2004). FTD mutation of this sequence, known to cause an increase exon 10 inclusion, was associated with greater SR protein binding (compared to wildtype). This implicates SR protein regulation in tauopathies and suggests that control of SR protein binding could ameliorate mis-splicing of tau. To further investigate the control of *MAPT* splicing, site-directed mutagenesis of the SV9/10L/11 tau construct could be conducted to ascertain essential SR protein binding sites around the exon 10 sequence. The activity of splicing factors is dependent on their phosphorylation state, which is in turn regulated by splicing kinases (Ghosh & Adams, 2011). The inhibition of splicing kinases using novel compounds was therefore hypothesised to shift *MAPT* exon 10 splicing through modulation of SR proteins, including SRSF1 and SRSF2.

5.4.2 Selective SRPK1 inhibition does not conclusively promote *MAPT* exon 10 inclusion

As a potent SRPK1 inhibitor and best-characterised compound used in this thesis, SPHINX31 treatment of SHSY5Y cells was used to investigate the role of SRPK1 in splicing of *MAPT* exon 10. SPHINX31 has not been previously studied in SHSY5Y cells or any models of AD, but it has been published in peripheral neurones (Hulse *et al.*, 2014) and most commonly in endothelial cells (Gammons *et al.*, 2013; Allen *et al.*, 2017). Validated as a highly selective inhibitor, 1μM SPHINX31 was shown to decrease SRPK1 activity without significantly affecting 50 key enzymes representing

the human kinome (Batson *et al.*, 2017). Since kinase assays are carried out in a cell-free environment, remaining activity and IC50 values do not translate to experimental design but rather provide information on relative selectivity and potency. For this reason, a concentration range of SPHINX31 (and all other compounds) was used to study its effect in SHSY5Y cells. As seen in section 5.3.2, 10nM-3μM SPHINX31 did not significantly change 4R:3R tau ratio but 10μM SPHINX31 did cause a significant increase in exon 10 inclusion. It is unclear whether SPHINX31 remains highly selective for SRPK1 at this higher concentration, so it is not possible to determine that SRPK1 activity is necessary for *MAPT* exon 10 splicing based on this result alone. In Neuro2a cells, the whole concentration range, including 10μM SPHINX31, did not have any significant effect on 4R:3R tau ratio. Novel compound SRPN56 did show a significant increase in exon 10 inclusion between 1μM-10μM treatment range. As a potent SRPK inhibitor, this provides some evidence that SRPKs may be necessary for *MAPT* exon 10 skipping. However, Neuro2a cells treated with 100nM SRPN56 showed significantly lower 4R:3R tau ratio, and higher concentrations (1-10μM) returned the ratio back to control levels. Since profiling of SRPN56 is incomplete, I do not have data on its selectivity. Related compound SRPN340 has been published as a SRPK inhibitor (Gammons *et al.*, 2013; Siqueira *et al.*, 2015) but it remains impossible to make conclusions about SRPN56 with great confidence. Nonetheless, one could postulate that SRPK inhibition with SRPN56 can reduce 4R:3R tau ratio, and higher concentrations of SRPN56 may increase 4R:3R tau ratio in SHSY5Y cells through inhibition of other splicing kinases. Further investigation is necessary to elucidate its concentration dependent effects.

SRPK1 activity was once reported to promote exon 10 skipping (Hartmann *et al.*, 2001) but there is little evidence elsewhere in the literature linking SRPK1 to *MAPT* splicing. Hartmann et al. did not reverse SRPK1-mediated exon skipping, and their study involved co-transfection of a tau minigene and SRPK1 expression vector, thus it cannot be directly compared to modulation of endogenous *MAPT* splicing with SPHINX31 and SRPN56 treatment. Because SPHINX31 did not exert an effect between 1μM-3μM, it could be postulated that other kinases are able to compensate for SRPK1 activity. To consolidate the role of SRPK1 in *MAPT* splicing, it would be interesting to determine which splicing factors, phosphorylated by SRPK1, mediate its effect on exon 10 skipping. This would reveal more about the regulatory mechanisms at play.

One mediator could be SRSF1, as SRSF1 activity is dependent on SRPK1 phosphorylation, which drives its nuclear localisation (Harper & Bates, 2008). Following this, phosphorylated SRSF1 can remain within nuclear speckles, therefore requires further phosphorylation from CLK1 for its release and access to splicing machinery (Aubol *et al.*, 2014). However, this model is likely over-simplistic. In actuality, evidence suggests that SRPK1 and CLK1 act synergistically rather than sequentially; SRPK1 has been found to form a complex with CLK1 within the nucleus that leads to hyperphosphorylation of SRSF1 and more efficient splice-site selection (Aubol *et al.*, 2016). When acting alone, it was found that CLK1 lacks the mechanism to release phosphorylated SR proteins, effectively inhibiting the function of SR proteins. Taking this into consideration, it can be postulated that even if inhibition of CLK1 and SRPK1 is highly selective, it could impact that activity of the other kinase and phosphorylation state of SR proteins, particularly SRSF1, that is required for their function. With regard to *MAPT* exon 10 splicing, this model suggests that SRPK1 mediated effects could be blocked by CLK1 inhibition if splicing factors required further phosphorylation by CLK1 to be released from nuclear speckles. Equally, SRPK1 inhibition could mean that CLK1 activity is dampened, as it lacks the mechanism to release splicing factors when operating alone. This hypothesis was not investigated in this thesis but creates very interesting future directions. For example, augmentation effects in AS could be investigated by comparison of joint SPHINX31 and Griffin6 treatment, or transient knockdown of SRPK1 and CLK1, with the effect of treatments alone. Furthermore, it would be possible to test whether inhibition of CLK1 or SRPK1 could be partially recovered by activity of the other kinase, or if they are both necessary for regulation of target splicing factors.

5.4.3 Selective CLK inhibitor promotes *MAPT* exon 10 inclusion and reduces SRSF1/6 phosphorylation

SRSF1 promotes *MAPT* exon 10 inclusion (Kondo *et al.*, 2004), and Griffin6 treatment of SHSY5Y cells was shown to have the same effect. As Griffin6 inhibits CLK, and CLK1 phosphorylation increases activity of SRSF1 (via release from nuclear speckles), these results are somewhat conflicting. Nonetheless, CLK activity has been reported to promote exon skipping (Hartmann *et al.*, 2001), based on which one could logically hypothesise that CLK inhibition can increase exon 10 inclusion, as observed with Griffin6 treatment of SHSY5Y cells. Search of the literature could not find any other data on the effect of CLK inhibition on exon 10 splicing; hence, it can be concluded for the first time that CLK is (in part) necessary

for exon 10 skipping, and its inhibition increases 4R tau isoform expression. It remains unclear how CLK has this effect but understanding the function of CLK phosphorylated splicing factors can put forward potential mechanisms for investigation. At this point, it would be important to assess (a) co-localisation of CLK and the splicing factor, (b) interaction between the splicing factor and *MAPT* exon 10, and (c) the effect of constituently phosphorylated splicing factor (e.g. phosphorylated-SRSF1) on exon 10 inclusion. Furthermore, using kinase-dead CLK would further validate findings presented in this chapter.

To help elucidate the targets of CLK in SHSY5Y cells, SR protein phosphorylation was quantified with Griffin6 treatment (and SPHIINX31 treatment as a positive control, see section 5.3.4). Phosphorylated SRSF1 was significantly reduced with Griffin6, but as discussed, it is unlikely that CLK inhibition increases exon 10 inclusion through SRSF1 because knockdown of SRSF1 had the opposite effect on *MAPT* splicing. Considering other mediators, Griffin6 caused an equally significant decrease in phosphorylated SRSF6 and the literature reports that SRSF6 activity can also modulate exon 10 inclusion (Gao *et al.*, 2000; Wang *et al.*, 2004). More specifically, these studies found that co-transfection of SRSF6 with a tau minigene results in an increase of 3R tau expression. If selective CLK inhibition through Griffin6 treatment reduces phosphorylation of SRSF6, this could theoretically block SRSF6-mediated exon 10 skipping, and ultimately increase exon 10 inclusion. However, there is conflicting evidence that SRSF6 increases exon 10 inclusion in a number of cell lines, including SHSY5Y cells (Yin *et al.*, 2012). This effect was validated for both endogenously expressed tau and transfected tau minigene, as siRNA targeting SRSF6 lead to inhibition of exon 10 inclusion in both instances. Having been observed in the same cell line, these data are more compelling and relevant to the splicing of *MAPT* quantified in this chapter.

Toward an alternative hypothesis, we must consider the role of other splicing factors. Although not quantified in Griffin6-treated SHSY5Y cells, CLK is known to phosphorylate SRSF7 (originally named 9G8) and CLK inhibitor TG003 has been shown to reduce phosphorylation of SRSF7 (Ding *et al.*, 2012). In this same study, SRSF7 was shown to block *MAPT* exon 10 inclusion, promoting exon skipping and 3R tau isoform expression. SRSF7 activity was inhibited by Dyrk1A phosphorylation, which led to its translocation to the cytoplasm and increased exon 10 inclusion. Similarly, PKA phosphorylation has been demonstrated to prevent SRSF7 from blocking exon 10 inclusion (Gu *et al.*, 2012). If CLK phosphorylation counteracts these kinases and can instead increase SRSF7-mediated exon skipping, then

SRSF7 activity may explain how CLK inhibition increases exon 10 inclusion. For future work, this would be a crucial hypothesis to investigate. Ultimately, more research is necessary to comprehensively interrogate the role of CLK in exon 10 splicing and conclusively determine how inhibition of CLK leads to higher 4R tau expression.

5.4.4 CLK2 is more important in *MAPT* exon 10 splicing than CLK1

Both CLK1 and CLK2 activity have been implicated in exon 10 skipping, but CLK2 has a comparatively stronger effect (Hartmann *et al.*, 2001). Griffin42 was the only compound that showed slightly higher selectivity for CLK1 over CLK2, and it was not able to induce significant increase in exon 10 inclusion (up to 1μM treatment). To determine whether CLK1 inhibition alone was sufficient to increase 4R tau expression, CLK1 was transiently knocked down in SHSY5Y cells (Figure 5.3.3.6), and there was no significant change in exon 10 splicing. This further supports the hypothesis that Griffin-mediated increase in exon 10 inclusion predominately occurs through CLK2 rather than CLK1. However, it should be noted that an average of 65% CLK1 activity remained with siRNA knockdown, which could be sufficient to perform its function and promote exon 10 skipping in SHSY5Y cells. It can still be inferred that shift in 4R:3R ratio quantified with treatment with other Griffins was, at least in part, dependent on CLK2 inhibition rather than CLK1 inhibition. Further investigation of CLKs in SHSY5Y cells would be necessary to validate this hypothesis, including independent knockdown of CLK2 at the protein level. It was not possible to conduct these experiments due to time constraints and adjusted working schedule during the COVID-19 pandemic.

CLK2 mediated exon 10 skipping has been proposed to occur through inhibitory interaction with TRA2-β1, a splicing factor which can bind to a *MAPT* exonic splicing enhancer (ESE) and promote exon 10 inclusion (Jiang *et al.*, 2003). CLK2 phosphorylates TRA2-β1 at its RS domain which triggers TRA2-β1 autoregulation, where its own exons 2 and 3 are skipped, promoting the transcription of TRA2-β3 instead. Since TRA2-β3 lacks a RS domain, it cannot influence TRA2-β splicing, thus phosphorylation of TRA2-β1 can act as powerful negative feedback for expression of TRA2-β1. Consequently, it has been theorised that CLK2 increases *MAPT* exon 10 skipping by reducing TRA2-β1 activity, effectively blocking TRA2-β1-mediated exon 10 inclusion (Glatz *et al.*, 2006). CLK2 is also known to phosphorylate other SR proteins, including SRSF4 and SRSF6, which can also increase exon 10 skipping but not to the same degree as CLK2 (Hartmann *et al.*,

2001). It is therefore likely that CLK2 exerts its effect on *MAPT* exon 10 splicing through phosphorylation of all these splicing factors combined.

5.4.5 SRPK2 inhibition may partially block increased *MAPT* exon 10 inclusion mediated by other kinases

SRPK1 is ubiquitously expressed but SRPK2 is highly enriched in the brain. SRPK2 is known to play an important role in regulation of brain tissue, for instance, it is involved in the control neuronal survival and cell cycle progression (Chan & Ye, 2013). SRPK2 is thought to be activated during the pathological processes of AD, as elevated SRPK2 expression has been associated with NFTs in AD brain (Hong *et al.*, 2012). Additionally, Wang et al have shown that SRPK2 can increase *MAPT* exon 10 inclusion in hTau mice. This is a mouse model for tauopathies that is designed to only human tau isoforms, produced by mating 8c mice, which express a human tau transgene, and tau knock-out mice, which do not express endogenous mouse tau. It was found that γ-secretase cleavage of SRPK2 can escalate its kinase activity, and overexpression of cleaved SRPK2 not only leads to significantly higher 4R tau expression, but also accelerated tau pathology and cognitive impairment (Wang *et al.*, 2018).

Comparing Griffin33 and Griffin53 yields an interesting insight into the role of CLKs and SRPK2 in the alternative splicing of *MAPT* that occurs in SHSY5Y cells. These two compounds are almost identical in their selectivity, except that Griffin53 is a less potent SRPK2 inhibitor. In Figures 5.3.3.3 and 5.3.3.7, it was shown that Griffin53 increased *MAPT* exon 10 inclusion at a lower concentration (1μM) than Griffin33 (3μM). Since SRPK2 increases exon 10 inclusion (Wang *et al.*, 2018), it could be postulated that inhibition of SRPK2 with Griffin33 treatment was partially protecting SHSY5Y endogenous splicing that preferentially skips exon 10. In this case, the comparative ability of Griffin53 to potently increase exon 10 inclusion may be dependent on increased SRPK2 activity. To validate this hypothesis, it would be interesting to selectively inhibit SRPK2, perhaps by siRNA, and determine if there is increased exon 10 skipping in the Neuro2a cell line. It is also important to determine how SRPK2 is exerting its effect. In a similar way to SRPK1, SRPK2 is known to phosphorylate SR proteins and modulate their activity (Wang *et al.*, 1998). For example, SRPK2 can change the nuclear localization of SRSF1 from nuclear speckles to the nucleoplasm, increasing its interaction with the spliceosome (Koizumi *et al.*, 1999). Furthermore, SRPK2 phosphorylation has been shown to improve the stability of SRSF2 and SRSR4 against degradation (Fukuhara *et al.*, 2006). Although its function has not been directly investigated in *MAPT* splicing, it is

reasonable to hypothesis that SRPK2 may increase exon 10 inclusion through phosphorylation of SRSF1 and SRSF2, since both have been independently shown to have the same effect (Kondo *et al.*, 2004; Qian *et al.*, 2011b). To test this hypothesis, it would be necessary to empirically find interactions between the kinase, splicing factors and *MAPT* exon 10.

5.4.6 Combined CLK and Dyrk1A inhibition has a synergistic effect on *MAPT* exon 10 inclusion

Griffin8 and Griffin53 both inhibit Dryk1A as well as CLK and treatment of SHSY5Y cells with these compounds induced a shift in the 4R:3R tau ratio more potently (at 1μM) compared to selective CLK inhibitor Griffin6 (at 3μM). As previously discussed in section 5.1.1, Dyrk1A has been shown to promote exon 10 skipping through phosphorylation of SRSF1 and driving it into nuclear speckles (Shi *et al.*, 2008). Moreover, Dryk1A phosphorylation of SRSF2 and similarly inhibits SRSF2-mediated exon 10 inclusion (Qian *et al.*, 2011b). In the later study, downregulation of Dyrk1A was found to increase exon 10 inclusion, and so the findings reported in this thesis are in keeping with the literature. It can be concluded that both CLK and Dyrk1A are required for exon 10 skipping, and their inhibition causes increased exon 10 inclusion. Dyrk1A constitutes an interesting target in AD because it can directly phosphorylate tau at numerous sites (most notably at threonine residue 212), increasing self-aggregation and priming tau for further phosphorylation by GSK-3β (Liu *et al.*, 2008). Therefore, future investigation of Dyrk1A specific inhibitors could become a novel therapeutic strategy for AD and other tauopathies.

5.4.7 Other kinases also play a role in regulation of MAPT exon 10 inclusion

Although not tested in this chapter, it would be remiss not to mention the role of other kinases known to regulate *MAPT* splicing. One such example is GSK-3β. In addition to its direct interaction with tau (discussed in section 1.4), GSK-3β alters the splicing of *MAPT* exon 10, and promotion of GSK-3β activity through calpain I cleavage is associated with increased 3R tau expression (Jin *et al.*, 2015b). This has been proposed to occur through phosphorylation of SRSF2, a promoter of exon 10 inclusion (Hernández *et al.*, 2004). GSK-3β was found to regulate intranuclear distribution of SRSF2, as GSK-3β inhibition increased SRSF2 localisation in nuclear speckles as well as increasing its own co-localisation with SRSF2 therein. Since SR proteins are released from speckles upon phosphorylation, it was hypothesised that GSK-3β phosphorylation causes SRSF2 release from nuclear speckles. However, GSK-3β inhibition confining SRSF2 within nuclear speckles would reduce SRSF2

interaction with *MAPT* and Hernández et al. incongruently reported greater exon 10 inclusion. Rather than being dependent on SRSF2, this increase in 4R tau could be mediated through other splicing factors. Otherwise, it could be resultant from crosstalk with other regulatory kinases compensating for GSK-3β inhibition, especially because Hernández et al. used lithium which is not highly selective for GSK-3β. As discussed in the paper, measured changes in tau isoform expression are further confounded by GSK-3β phosphorylation of SRSF2 requiring pre-phosphorylation from "priming" kinases at its RS domain, the most likely candidates being CLKs and SRPKs.

MAPT splicing has also been related to cyclic-AMP dependent protein kinase (PKA) activity; SRSF2-mediated exon 10 inclusion was shown to be dependent on PKA phosphorylation of its RS domain (Qian *et al.*, 2011b; Chen *et al.*, 2014). This would act in opposition to GSK-3β and Dyrk1A activity, promoting expression of the 4R tau isoform. It has also been reported that PKA phosphorylation of SRSF1 enhances promotion of exon 10 inclusion (Shi *et al.*, 2008). Interestingly, studies found that SRSF7 promotes skipping of exon 10, shifting isoform expression toward 3R tau, and PKA phosphorylation inhibits SRSF7-mediated change in tau splicing (Shi *et al.*, 2011). Altogether, PKA interactions with SRSF1, SRSF2 and SRSF7 can all lead to increase in 4R tau expression. As with Dyrk1A, PKA has also been shown to directly phosphorylate tau at several sites, priming it for further phosphorylation from GSK-3β (Liu *et al.*, 2006), and strongly implicating PKA in regulation of tau function.

Finally, CDK5 has also been shown to increase exon 10 skipping, but to a much smaller degree (Hartmann *et al.*, 2001). Also known as Neuronal CLK, CDK5 is the major cyclin-dependent kinase constitutively expressed in the brain and significantly elevated in AD (Lee *et al.*, 1999). Functionally, CDK5 is involved in the dynamic organisation of actin cytoskeleton and neurite outgrowth (Nikolic *et al.*, 1998) but has been related to abnormal phosphorylation of tau and formation of paired helical filaments (Paudel *et al.*, 1993). Even so, there is no evidence to suggest it plays as important a role as other splicing kinases discussed in this chapter.

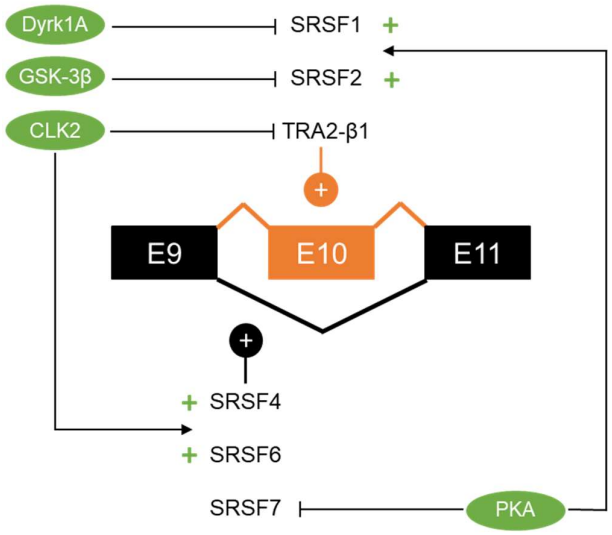


Figure 5.4.7 Summary schematic for the role of regulatory splicing kinases in the inclusion of *MAPT* exon 10.

5.4.8 Griffin6 is neuroprotective against OA-induced neurotoxicity

The OA model for neurotoxicity, introduced in Chapter 4, was used again in this chapter to investigate potential physiological effect of selective CLK inhibitors in section 5.3.5. Griffin6 treatment was found to protect against OA-induced decline in neurite outgrowth, suggesting that CLK inhibition can exert neuroprotective effects in this neuronal model. In the control group, 3mM OA decreased the average length of outgrowth to 41.1% ±4.4% of vehicle treated SHSY5Y cells. With Griffin6 co-treatment, this decline was significantly reduced, where 3nM OA treated cells maintained 81.1% ±3.0% average outgrowth of vehicle control. In this assay, OA causes tau hyperphosphorylation through PP2A inhibition (Metin-Armagan *et al.*, 2018), thus it is possible that Griffin6-mediated CLK inhibition may be neuroprotective, at least in part, by directly or indirectly blocking hyperphosphorylation of tau. However, there is no evidence in the literature that suggests CLK regulates tau phosphorylation, so to validate this hypothesis, it would be necessary to quantify the phosphorylation of tau with OA, Griffin6, and their concurrent treatment.

Since Griffin6-mediated CLK inhibition ameliorated OA-induced “dieback” of SHSY5Y cells but did not increase outgrowth on its own, it could be hypothesised that CLK inhibition is neuroprotective through a mechanism that is specific to OA-induced neurotoxicity, and perhaps directly related to tau function. As established through Griffin6 and Griffin8 treatments, CLK inhibition leads to an increase in 4R:3R tau ratio in SHSY5Y cells, which persists in the presence of 3nM OA (see

Figure 5.3.5.2). Therefore, it is possible that CLK inhibition is neuroprotective through regulation *MAPT* splicing. This is particularly interesting because maintaining an equimolar 4R:3R tau ratio is thought to be crucial in the human brain (Espindola *et al.*, 2018) and SHSY5Y cells preferentially express 3R tau. Therefore, shifting toward exon 10 inclusion brings these cells closer toward equimolar expression of 4R and 3R tau isoforms. The SHSY5Y cell model, however, is limited in its use to determine the physiological effects relating to 4R:3R ratio, because it is not known if SHSY5Y cells have inherently disrupted physiology related to their imbalance of 4R:3R tau isoform expression. Therefore, further studies could focus on investigating the neuroprotective role of shifting 4R:3R tau ratio in primary tissue or another neuronal model that is closer to normal physiology.

A number of studies have otherwise shown CLKs to play a role in neuronal function, such as inducing neuronal-like differentiation of PC12 cells from their adrenal gland origin (Myers *et al.*, 1994), and relating to dendritic spine density in the cerebral cortex (Bidinosti *et al.*, 2016). More specifically, CLK2 negatively regulates Akt, an important mediator of cell growth, survival and metabolism, by phosphorylation of the B56β subunit of PP2A, which triggers (and is required for) PP2A-mediated dephosphorylation of Akt (Rodgers *et al.*, 2011). Activation of Akt by pharmacological CLK2 inhibition reverses neuronal impairments related to Akt deficiency and restores dendritic spine density (Bidinosti *et al.*, 2016). Akt phosphorylation operates within the PI3K/Akt/S6K signalling pathway, which has been shown to promote neuronal survival, differentiation, neurite elongation, and regeneration (Zhang *et al.*, 2017). In addition to regulating Akt phosphorylation, CLKs can also affect the PI3K/Akt/S6K pathway through its role as a splicing regulator. CLK inhibition may affect neuronal survival through regulation of S6K, since CLKs strongly inhibit canonical S6K activity by producing alternatively spliced isoforms of S6K, which effectively block S6-mediated cell growth and survival (Araki *et al.*, 2015). However, in the specific context of neurite outgrowth, it is unclear whether S6 activity is always protective, since the literature supports S6-mediated neuronal sprouting in the CNS (Zhang *et al.*, 2017) while demonstrating that S6 can inhibit axonal regeneration in the periphery (Al-Ali *et al.*, 2017). To further complicate matters, S6 is directly related to tau dysfunction, as intense S6 phosphorylation is associated with NFTs in the AD brain, particularly in the CA1 region of the hippocampus (Sonoda *et al.*, 2016). This highlights that up- or down-regulation of a kinase does not have straightforward results and is likely to affect cell physiology through many mediators, sometimes in contradictory ways. It is therefore crucial to

identify the most influential mechanisms driving neuroprotection and promote them while minimising undesirable side-effects.

Regarding the effects of CLK inhibition on OA-induced neurotoxicity, I would postulate that Griffin6 mediated neuroprotection is not directly dependent on Akt activity, since OA is a PP2A inhibitor, and has been shown to block Akt dephosphorylation (Rodgers *et al.*, 2011). As a result, it is unlikely that OA-induced neurotoxicity occurs through reduced Akt activity. Future work could explore the mTOR pathway and expression of PI3K, Akt and S6K activation markers to determine if they link between CLK activity and neurite outgrowth in this *in vitro* model of tau hyperphosphorylation.

5.4.9 The neuroprotective effect of Griffin6 is not dependent on VEGF-A_{165}b isoform expression

CLK1 phosphorylates SRSF6 which has been shown to promote distal splice site selection of exon 8 in *VEGFA* (Nowak *et al.*, 2008). As a result, this would cause an increase in VEGF-A_{165}b and inhibition of CLK1 could block SRSF6-mediated VEGF-A_{165}b expression. On the other hand, CLK1 is also involved in the regulation of SRSF1 alongside SRPK1, and phosphorylated SRSF1 promotes proximal splice site selection of exon 8 in *VEGFA* (Nowak *et al.*, 2010). Since these effects are conflicting, it was difficult to hypothesise how CLK inhibition would affect *VEGFA* splicing. However, as determined by ELISA, CLK inhibition through Griffin6 treatment of SHSY5Y cells (see Figure 5.3.5.4) did not induce a significant shift in VEGF-A_{165}a:VEGF-A_{165}b ratio. As expression values were variable, using a larger sample size (current N=3 biological samples) could produce more reliable data on VEGF-A isoform expression. Having said that, Griffin6-treated samples were run on the same plates as SPHINX31-treated samples, which did show significant increase in VEGF-A_{165}b isoforms (see Figure 4.3.4.3), acting as an experimental positive control. As previously discussed in Chapter 4, endogenous VEGF-A_{165}b acts as a neuroprotective agent and decreasing the VEGF-A_{165}a:VEGF-A_{165}b ratio can ameliorate damage from various neuronal insults (Beazley-Long *et al.*, 2013). The neuroprotective role of Griffin6 was not dependent on VEGF-A_{165}b since neutralisation of the isoform with antibody 56/1 did not reduce its ability to ameliorate OA-induced “dieback” of SHSY5Y cells. This is in contrast to previous findings that SPHINX31-mediated neuroprotection was significantly reduced by concurrent 56/1 treatment, suggesting that SRPK1 inhibition may primarily act through *VEGFA* splicing but CLK inhibition does not.

5.4.10 Concluding remarks

It was confirmed that SRSF1 and SRSF2 are necessary for *MAPT* exon 10 inclusion and their knockdown significantly increases exon 10 skipping. The inhibition of CLK, SPRK and Dyrk1A with novel small molecule inhibitors significantly increased *MAPT* exon 10 inclusion. Selective CLK inhibitor Griffin6 was also shown to ameliorate OA-induced “die-back”, increasing neurite outgrowth in the presence of 1-3nM OA. Considering that Griffin6 alone did not increase neurite outgrowth, it was suggested that CLK inhibition was selectively blocking OA-induced neurotoxicity. It was also found that Griffin6-mediated neuroprotection was not dependent on AS of VEGF-A. Altogether, this chapter identifies that CLK plays an important role in *MAPT* splicing and that regulating tau expression could be therapeutic in tauopathies. Particularly in cases where *MAPT* mis-splicing has led to pathologically high 3R tau, CLK inhibition could provide neuroprotection through increased exon 10 inclusion.

Chapter 6. Summary and future directions

Globally, there are roughly 47 million people living with dementia, a figure projected to increase to 132 million by the year 2050 (World Health, 2017). As the most common cause of dementia, AD is becoming a public health priority worldwide. Unfortunately, current treatments can only temporarily manage or slow symptoms, and do not effectively halt pathogenesis. For this reason, innovative AD research is critical to identify novel therapeutics and provide a higher standard of patient care. Unfortunately, all clinical trials for disease-modifying drugs have failed (Anderson *et al.*, 2017). A number of explanations have been proposed for their failure, ranging from scepticism of biological drug targets and doses to criticism of participant selection and choice of clinical outcomes. Any combination of these can be argued and disputed, but what remains irrefutable is the need to change our approach to the treatment of AD. In order to affect change, it is necessary to (a) improve early detection of AD, particularly through quantification of polygenic risk (Hannon *et al.*, 2020) to enable effective intervention in the pre-clinical stage, and (b) target drivers of disease that may be upstream of Aβ and tau pathology, rather than more apparent but less instrumental targets which are reactionary to (and may even oppose) AD pathogenesis (Persson *et al.*, 2014). In fulfilment of the latter, I propose targeting splicing factor kinases, known regulators of AS, as a novel therapeutic approach for AD.

6.1 Alternative splicing in AD

Changes in alternative splicing are linked to both normal ageing and ageing-related diseases (Angarola & Anczuków, 2021). This is thought to occur through differential expression of splicing factors, which affects regulation of splicing events and isoform production in older age (Balliu *et al.*, 2019). A larger than average proportion of these splicing events constitute increased intron retention, in both normal physiology (Mazin *et al.*, 2013) and Alzheimer's disease (Adusumalli *et al.*, 2019). Intron retention is reported to be widespread in the human brain and typically leads to nonsense-mediated decay due to inclusion of a premature stop codon. Consequently, intron-retained mRNAs are unlikely to be translated into proteins, and so the role of intron retention in regulating gene expression may be overlooked. Indeed, Adusumalli et al. found that 80 protein isoforms significantly downregulated in AD were encoded by 73 genes showing differential intron retention. In a recent study, intron retention was described to be functionally associated with occurrence of AD and positively correlated with Braak stage, indicating greater disease severity

(Li *et al.*, 2021). These differential splicing events were found to be regulated by components of the spliceosome and major splicing factors, including *SNRNP70*, *HSPA2*, *SRSF6* and *HNRNPH1*.

Exon skipping, however, is the most common type of splicing event and this too has been implicated in AD (Han *et al.*, 2019; Yang *et al.*, 2021). For example, exon skipping in *RELN*, extracellular matrix glycoprotein, was associated with AD whilst exon inclusion was negatively correlated with Aβ burden (Han *et al.*, 2019). Most notable is exon skipping in *APP* and *MAPT* genes, which produce AD hallmarks Aβ and tau, and it is becoming evident that splicing dysregulation can drive pathogenesis (Habekost *et al.*, 2021; Jakubauskienė *et al.*, 2021). In the ROSMAP dataset, AD patients were found to have differential intron usage (Raj *et al.*, 2018) and exon skipping (Yang *et al.*, 2021), emphasising the importance of both splicing events in AD pathology. In this thesis, the expression of splicing kinases was linked to likelihood of AD diagnosis and markers of AD pathology. Low SRPK1/2 expression in females and low CLK1 expression in males were associated with more frequent occurrence of AD compared to high expression groups. This suggests that targeting kinases could be therapeutic by shifting AS and shielding against the AD phenotype.

6.2 Targeting splicing kinases to modulate alternative splicing

Investigation of AD-related protein VEGF-A, which is a known splicing target of SRPK1, found that it could protect against oxidative stress, Aβ-related neurotoxicity, and OA-induced decline in neuronal outgrowth. Interestingly, both VEGF-A_{165}a and VEGF-A_{165}b isoforms were neuroprotective, but it was hypothesised that VEGF-A_{165}b was blocking tau-related toxicity in the neurite outgrowth assay, while VEGF-A_{165}a was causing a general increase in outgrowth. Treatment with SPHINX31, a SRPK1 inhibitor that can switch splicing toward the VEGF-A_{165}b isoform, was also found to neuroprotective against tau-related toxicity in a VEGF-A_{165}b dependent manner. This led us to the conclusion that SRPK1 inhibition ameliorates AD-related neurotoxicity, and our proposal that SRPK1 inhibition may be therapeutic in AD brain through VEGF-A mediated mechanisms.

To explore the role of splicing kinases in regulation of tau splicing, which is implicated in AD and other tauopathies, neuronal cells were treated with a panel of small-molecule inhibitors *in vitro*. I reported that CLK inhibitors significantly increased 4R:3R tau ratio by promoting *MAPT* exon 10 inclusion in SHSY5Y cells, which predominately express 3R tau. Functionally, this was associated with greater

neurite outgrowth despite OA-induced 'die-back', which indicates that CLK-mediated control of tau splicing could be another effective therapeutic strategy for AD. This is particularly noteworthy because CLK1 expression was related to tau pathology in male AD patients in the ROSMAP dataset. In order to elucidate other splicing changes that occur with SRPK1 or CLK1 inhibition, it would be interesting to perform RNA-seq on neuronal cell samples treated with SPHINX31 and GRIFFIN6 respectively. This would ultimately determine other mechanisms which may mediate neuroprotection not explored within this thesis. For example, a number of other factors have been associated with both amyloid and tau related AD pathology, including *MYCN* gene (Ferrer & Blanco, 2000). MYC-c can promote neuronal survival and post-injury axon regeneration (Belin *et al.*, 2015). Although its expression was not found to be in correlation with neuronal loss in AD brain (Ferrer & Blanco, 2000) it could also be considered an important target for neurogenesis.

The regulation of Dyrk1A activity has also been proposed as a novel approach for AD as it directly phosphorylates tau in advance of further phosphorylation from GSK-3β (Ryoo *et al.*, 2007). Dyrk1A is also involved in tau splicing, although research findings conflict on whether Dyrk1A promotes or blocks exon 10 inclusion (Qian *et al.*, 2011b; Ding *et al.*, 2012). In this thesis, co-inhibition of CLK and Dyrk1A increased inclusion of *MAPT* exon 10 with greater potency than selective CLK inhibitor GRIFFIN6, which suggests that Dyrk1A activity mediates exon skipping in SHSY5Y cells. In the ROSMAP dataset, Dyrk1A expression did not show a clear relationship with AD pathology but females with low Dyrk1A did have significantly higher occurrence of AD diagnoses. To further characterise tau related Dyrk1A function, future experiments could include use of a selective Dyrk1A inhibitor in the neurite outgrowth assay to determine whether it has neuroprotective effects *in vitro*.

To interrogate the impact of 4R:3R tau ratio in both directions, it would be interesting to promote CLK and/or Dyrk1A-mediated exon 10 skipping in Neuro2a cells, which predominately express 4R tau, and determine whether this too is neuroprotective against OA-induced toxicity in the neurite outgrowth assay. This would support the hypothesis that imbalance of 4R:3R tau makes cells more susceptible to tau hyperphosphorylation and related neurotoxicity. Working under this assumption, shifting expression of 4R and 3R tau isoforms closed to 1:1 ratio will provide neuroprotection. Since it is more common for tauopathies to be caused by excessive 4R rather than 3R (Spillantini & Goedert, 2013), this could lead to the conclusion that CLK1 inhibition is not an effective therapeutic intervention. It would also indicate that over-representation of AD pathology in males with low CLK1 expression may be

consequential rather than compensatory, i.e. downregulation of CLK1 may contribute to AD pathology. However, this counterargument remains speculative until further investigation. The discrepancy herein lies with use of imperfect cell models since neither cell lines have “normal physiology” with equimolar production of 4R and 3R tau. In the literature, hTau mice (expressing only human tau isoforms) are reported to have high 3R tau expression due to endogenous splicing preference for exon 10 skipping, which causes aged hTau mice to exhibit tau hyperphosphorylation and cognitive deficits (Espindola *et al.*, 2018). Increased exon 10 inclusion to 4R:3R tau ratio ~0.8 by injection of trans-splicing molecules ameliorated both tau pathology and cognitive performance. At the same time, inducing high 4R tau expression in hTau mice has also been shown to cause tau hyperphosphorylation and exacerbation of seizures (Schoch *et al.*, 2016). Considering this evidence altogether, one must conclude that modulation of tau splicing can be neuroprotective in both directions depending on the pre-existing splicing and constituted risk for pathology. Although this does not provide a clear path for therapeutics, it does provide a more comprehensive understanding of the underlying physiology.

6.3 Models to investigate AD pathology

Use of models is integral to AD research, and the lack of accurate and representative AD models is a significant hindrance. Clinical research provides useful insight into disease, but basic scientific research is required for target validation and to empirically test new therapeutic strategies. Since it is impossible to produce a model for all aspects of AD, it is imperative to use a combination of models that integrate AD-related pathologies. Up until now, the lack of success of unidirectional therapeutics, e.g., exclusively targeting Aβ pathology (Doody *et al.*, 2013), has highlighted the heterogeneity of AD and consequently the importance of using a multimodal approach to its treatment.

In this thesis, I was able to establish models for AD to study alternative splicing. Through multivariate analysis of transcript splicing (rMATS), I found that the cerebellum has differential splicing patterns as well as differential gene expression to the frontal cortex. Gene set enrichment analysis revealed that alternative spliced genes are predominately related to vesicle-mediated transport and synaptic function, including *NRXN2* and *EXOC1* which have significantly less skipped exons in the cerebellum. These novel findings suggest that regulation of splicing contributes to the cerebellar phenotype, which may protect against synaptic

dysfunction in AD. Enrichment of GO pathways related calcium signalling were also identified among differentially spliced genes. For example, IP3 receptor gene *ITPR1* was shown to have significantly more skipped exons in the cerebellum, which could cause the cerebellum to have reduced sensitivity to IP_3R-mediated calcium release. Overall, the cerebellar splicing profile can be proposed to protect against (or at the very least delay onset) AD pathogenesis. To validate this hypothesis, future work could involve empirically testing differential splicing of target genes *in vitro* to determine whether replication of the cerebellar phenotype can be neuroprotective.

To produce a model for AD-related pathology *in vitro*, I used a combination of oxidative stress, Aβ-induced neurotoxicity, and tau hyperphosphorylation assays in Chapter 4. This provided unique insight into the neuroprotective effects of VEGF-A_{165}a and VEGF-A_{165}b splicing isoforms. The establishment of this model with SHSY5Y cells provides an accessible model for investigation of other neuroprotective agent; for future work, this model could be used to further investigate use of splicing kinase inhibitors such as the GRIFFINs as therapeutic candidates for AD. Ideally, primary brain cells from the hippocampus or other vulnerable areas would be used for greater physiological relevance, but primary tissue brings its own complications and has considerably more limited supply. One step further would be investigating the use of splicing kinase inhibitors in an animal model, such as hTau mice, which exhibit tau pathology in old age (Espindola *et al.*, 2018).

6.4 Summary

To conclude, inhibition of splicing kinases using selective small-molecule inhibitors is a viable strategy for regulation of aberrant splicing associated with AD pathology. In this thesis, use of SRPK1 inhibitor SPHINX31 and CLK inhibitor GRIFFIN6 were identified to have protective effects on neuronal outgrowth *in vitro.* SPHINX31 neuroprotection was shown to be mediated through alternative splicing of *VEGFA* while GRIFFIN6 was postulated to act through alternative splicing of *MAPT*. Since exclusively targeting either Aβ or tau is insufficient for AD treatment, and I found that expression of splicing factors can be related to occurrence of AD, they constitute an interesting target for modulation alternative splicing in AD and upstream protection against neuropathology. Further investigation into mechanisms of action is necessary to elucidate how inhibition of splicing kinases may be neuroprotective and identify novel splicing targets which also play a role in AD.

Chapter 7. Appendix

7.1 PIPS Review

7.1.1 Introduction

I completed a 3-month internship with the UN Interagency Task Force (UNIATF) on noncommunicable diseases (NCDs) based in the World Health Organisation (WHO) headquarters. The UNIATF acts a platform for the UN system and non-state actors to support governments tackle NCDs and mental health conditions. It primarily focuses providing context-specific technical assistance and policy advice to support national action and build capacity for best practices on the prevention and control of NCDs. In addition, the Task Force advocates at the highest level of governments and works with multi-stakeholder partners to mobilise human and financial resources, which in turn establishes a strong base for sustainable and effective responses to NCDs and mental health conditions. This work has successfully increased integration of NCDs into policy and development plans and continues to promote a whole-of-government and whole-of-society approach to public health.

7.1.2 Outputs and Outcomes

While working within the UNIATF Secretariat, I was able to contribute to a variety of projects by collaborating with other team members and learning from their experience and expertise. We collectively researched for new projects or wrote draft papers for other members of Task Force to edit and publish. For example, my colleagues and I made a series of edits on four briefing papers that can now be found on the UNIATF website. These papers succinctly describe how the strategic priorities and direction of work in the Task Force is aligned with commitments made by the UN Economic and Social Council as well as WHO's general programme of work. Early in my placement, this exercise quickly developed my understanding of the Task Force's work and built confidence in my writing ability.

I was later able to focus on two projects which provided the opportunity to establish broader knowledge of the UN system and its global health priorities. The first project was about developing a methodological guidance tool for national investment in the area of mental health. This would be used by WHO staff working with government bodies to identify best practices and incorporate more mental health interventions to their ongoing work. After showing an interest in this area and familiarising myself with the draft document, I requested and collected notes from technical experts in

different UN organizations; these notes were used by the author for a comprehensive revision of the guidance tool. I secondly took responsibility for liaising between the Task Force and other WHO collaborators in the UN joint global programme on Cervical Cancer Prevention and Control. This role included attending meetings, writing minutes and following up on relevant action points.

Throughout my internship, my most technical task was producing a needs assessment of staff training in NCD prevention and control. This involved collecting and analysing data from a questionnaire sent to country offices across all WHO regions about their staff working experience in NCDs and mental health. In response, my report was sent to all the regional offices to assess their current level of training and to nominate members of staff for participation in NCD seminars. I was also involved in the organisation of these NCD seminars with the University of Lausanne to build greater capacity for NCD-related work. The remainder of my tasks were mainly secretarial; they included organising lists of participants and agendas for Task Force meetings as well as scheduling a timetable of events for the World Health Assembly.

7.1.3 Impact

Overall, my internship at UNIATF was a valuable learning experience in the public health sphere. Although it hasn't drastically changed my career plan, it was a good opportunity to apply my skills outside of the laboratory environment. It revealed how much I enjoy working within a team; my favourite part of the internship was making new acquaintances and growing relationships through collaboration and shared responsibilities. As I became more familiar with the work, I grew more confident in my technical abilities and outspoken in group meetings. I also developed organizational, writing and editing skills which will be particularly useful for my thesis as well as work beyond my PhD.

Since this was my first time working in a global organisation, the UNIATF provided a truly unique perspective on high-level and high-impact work in healthcare. Despite the hurdles of bureaucracy, I really enjoyed seeing the translation of hard work into policy change and progress on sustainable development goals. Outside the traditional route of academia, I discovered that there are many ways of building research skills and engaging with empirical science. As a result, I am more like to seek career opportunities in a wider breadth of workplaces as long as I can maintain a technical or researcher role within the field.

7.2 COVID Statement

The abrupt closure of the university in response to the COVID-19 pandemic had various repercussions on my work. I did not have access to the lab for several months, and consequently I was unable to complete protein validation of SRSF1/2 knockdown experiments. Similarly, due to severe delays in our ordering system and the delivery of lab reagents, I was forced to terminate Tau minigene experiments originally planned between March and June 2020. Lockdown was particularly disruptive for our lab group because it occurred shortly after we moved buildings. This meant I had been previously unable to perform molecular biology experiments between November 2019 and January 2020.

7.3 Supplementary Tables and Figures

Primer	Sequences	Amplicon size (bp)	Anneal temp (°C)
GAPDH	F: AATTCCATGGCACCGTCAAG R: GGTCATGAGTCCTTCCACGA	365	58
mGAPDH	F: CCATCTTCCAGGAGCGAGAC R: GCCCTTCCACAATGCCAAAG	297	55
VEGFR2	F: AAAACCTTTTGTTGCTTTTGGA R: GAAATGGGATTGGTAAGGATGA	237	55
mVEGFR2	F: AGAACACCAAAAGAGAGGAACG R: GCACACAGGCAGAAACCAGTAG	384	57
mSRSF1	F: CGGGTTAAAGTTGATGGGCC R: CCAGTTCACACAAACCAGGG	464	58
mSRSF2	F: GTGCTTGGCTGTTTCCTGTTT R: CACTGTATGCTCCATTATTTATATGC	172	55
CLK1	F: GAACAAGCGCTGCAAATACA R: CTGATACCGGCTTTCATGGT	175	54
MAPT	F: CTCCAAAATCAGGGGATCGC R: CCTTGCTCAGGTCAACTGGT	297 (-E10) 390 (+E10)	54
mMAPT	F: CCCCCTAAGTCACCATCAGCTAGT R: CACTTTGCTCAGGTCCACCGGC	168 (-E10) 261 (+E10)	55
VEGF-A	E7a F: GAGCGGAGAAAGCATTTGTT E8b R: TCAGTCTTTCCTGGTGAGAGAT	201 ($_{165}$a) 135 ($_{165}$b)	60

Table 7.3.1 List of PCR primer sequences.

GO: gene set	GO: description	Leading Edge
0055088	lipid homeostasis	CYP39A1;EHD1;EPHX2;GRAMD1B;LCAT;LDLRAP1;LIMA1;LIPG;PCSK9;ZBTB20
0006289	nucleotide-excision repair	CCNH;CHD1L;ERCC6;FANCC;NEIL1;OGG1;POLA1;POLB;POLD1;POLE;RFC3;SIRT1; SLX4;USP45
0006298	mismatch repair	MSH4;MSH6;MUTYH;SETD2;TP73
0006304	DNA modification	ATF7IP;BEND3;DNMT1;DNMT3B;EZH2;KMT2E;MUTYH;NEIL1;OGG1;PPM1D;PRMT7; TET1
0032200	telomere organization	ATM;BLM;CTC1;DCLRE1B;PKIB;POLA2;PRIM1;PRIM2;RFC3;SLX4;SMC5;SMG1;XRCC3
0007187	**GPCR signalling pathway, coupled to cyclic nucleotide**	ADCY2;ADCY5;ADRA1D;ADRB1;AKAP13;AKAP5;APLP1;ATP2B4;CHGA;CHRM1;CHRM3; CHRM4;DRD1;DRD5;GLP2R;GNA14;GNG2;GPR26;GRM2;GRM7;HRH1;HRH2;HTR1F; HTR2A;HTR2C;HTR4;HTR6;HTR7;LPAR1;NPY;NPY1R;NPY2R;OPRD1;PDE2A;PTGER3; RAPGEF2;RXFP1;SSTR1
0050890	**cognition**	ATP8A1;BTBD9;CCK;CHRM1;CHRNA7;CNTNAP2;CRHBP;CUX2;DRD1;DRD5;EPHB2; FGF13;FOXP2;GABRA5;GPR88;GRIN1;GRIN2A;GRIN2B;GRM5;HRH1;HRH2;HTR2A; JAKMIP1;KALRN;KCNK2;MAP1A;MEF2C;NETO1;NRGN;NTRK2;NTSR1;PDE1B;PLCB1; PLK2;PRKAR1B;PRKAR2B;PTGS2;RGS14;SERPINF1;SHC3;SYNJ1;SYNPO;TBR1;TMOD2
0007210	**serotonin receptor signalling pathway**	CHRM1;CHRM3;CHRM4;HRH1;HRH2;HTR1F;HTR2A;HTR2C;HTR3B;HTR4;HTR6;HTR7
0007200	**PLC-activating GPCR signalling pathway**	ACTN2;CHGA;CHRM1;DRD1;DRD5;GNA14;GRM5;HRH1;HTR2A;HTR2C;LPAR1;OPRD1; PLCE1;PTGER3;TACR1
0099072	postsynaptic membrane neurotransmitter receptor levels	AP2B1;CACNG3;CACNG8;CALY;DLG2;GRASP;GRIP1;GSG1L;HPCA;LRRC7;SYNJ1

Table 7.3.2 List of genes from GSEA analysis that show significant differential expression in cerebellum compared to the frontal cortex. Significantly enriched pathways in Biological processes database are shown with FDR (*) and in description in **bold**.

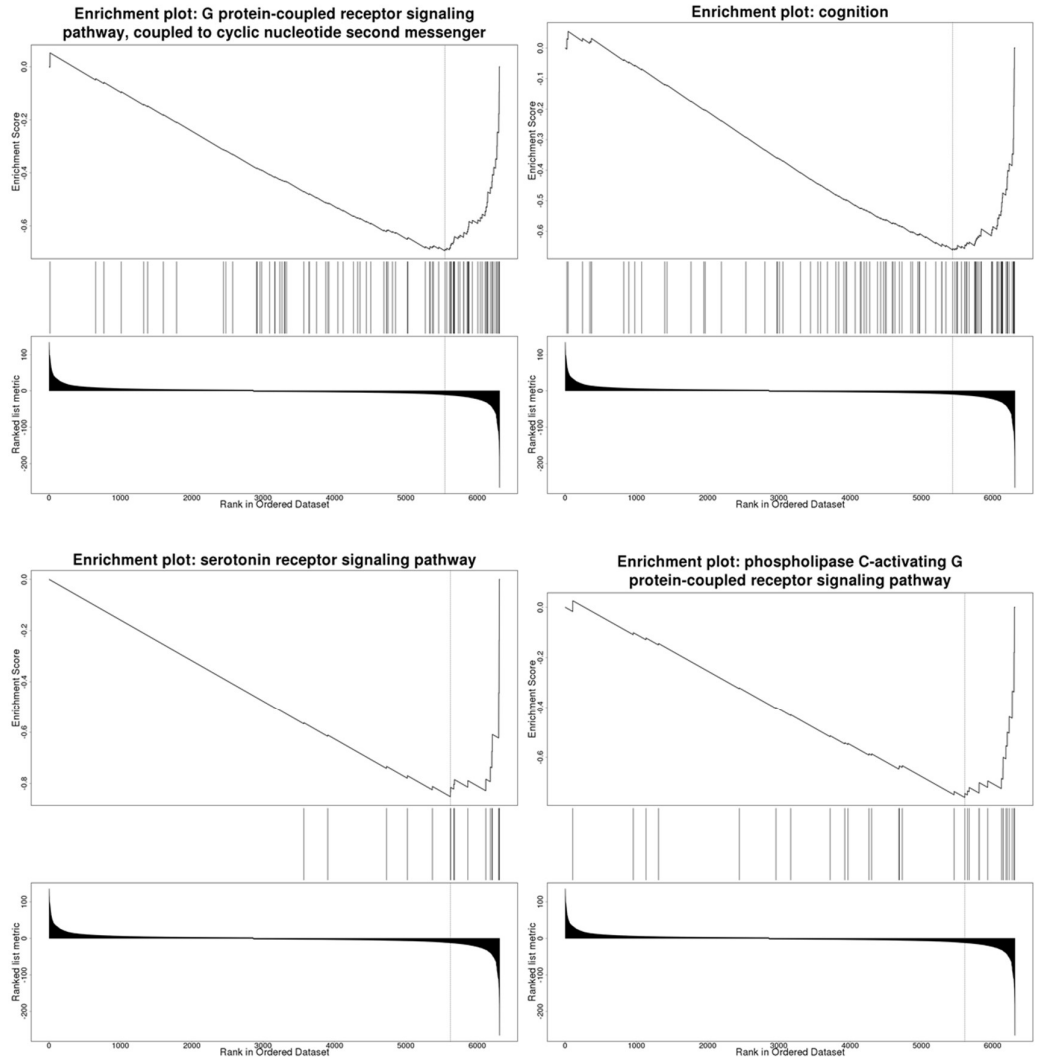


Figure 7.3.1 Enrichment plots for biological processes that are significantly enriched in gene list of differential expression between the cerebellum and frontal cortex. Lines show 'hits' or genes at relevant rank in ordered dataset and resultant enrichment score. Produced by Webgestalt.

GO: gene set	GO: description	Leading Edge
0019932	second-messenger-mediated signaling	ARRDC3;CAMK2D;FIS1;GNAS;GRIN2A;ITPR1;ITPR2;PPP3CA;SLC8A1;TPCN2
0010038	response to metal ion	APP;CACNA1G;CAMK2D;DNMT3A;GSN;IREB2;KCNMA1;MAP1LC3A;MNAT1;NLGN1;PKD2; PPP3CA;SLC25A13;SNCA;SYT7
0007059	chromosome segregation	BAG6;BEX4;CDC26;CTNNB1;HFM1;INO80;MLH1;NTMT1;RAN;TERF1;TPR;TUBG2
0051604	protein maturation	ASRGL1;CYFIP2;GRIN2A;GSN;OGT;OMA1;PMPCB;PRKACB
0007187	GPCR signalling pathway, coupled to cyclic nucleotide	ARRDC3;GNAS;PRKACB
0098876	**vesicle-mediated transport to the plasma membrane**	ANK3;ARF3;CPLX1;EXOC1;EXOC6;GGA1;RABEP1;SNAP25;SPTBN1;TRIM23;VPS35;VPS39
0017156	calcium ion regulated exocytosis	APBA1;APBA2;CADPS2;CALM1;CASK;CPLX1;CPLX2;DNAJC5;DNM1L;DOC2B;GRIK5;PIP5K1C; PREPL;RAB5A;RAPGEF4;RIMS2;SCAMP5;SNAP25;STXBP1;SYT1;SYT12;UNC13C
0009896	positive regulation of catabolic process	ABCD2;ADAM9;AMBRA1;APC;ARNT;C9orf72;CALCOCO2;CBFA2T3;CD81;CNOT8;CPEB3; CSNK1D;CSNK2A1;DCN;DDB1;EDEM2;FAF1;FMR1;FTO;GGA1;GPSM1;HECW1;MAPK9; PACSIN3;PRKCE;PTEN;RBM23;RBX1;RGN;SCOC;SH3GLB1;SIRT1;SORL1;SPTLC1;STK11; SUMO1;TRIM13;TSC2;UBE2V2;VPS13C;VPS35;WAC
0023061	signal release	APBA1;APBA2;CACNA1A;CADPS2;CALM1;CASK;CDK16;CPLX1;CPLX2;DNAJC5;DNM1L; DOC2B;GLUD1;GLUL;GRIK5;HADH;NRXN1;PFKM;PHPT1;PIP5K1C;PNKD;PREPL;PRKCE; PTPRN;PTPRN2;RAB11FIP3;RAB5A;RAPGEF4;RIMS2;SLC25A6;SMAD4;SNAP25;SRI;STXBP1; SYT1;SYT12;UNC13C;VPS35
0048013	ephrin receptor signalling pathway	AP2A2;AP2B1;ARPC2;DNM1;FYN;GRIN1;PAK3;RASA1;RHOA;SDCBP

Table 7.3.3 List of genes from GSEA analysis that show significant increased or decreased exon skipping in cerebellum compared to the frontal cortex.

GO: gene set	GO: description	Overlap
0099003	vesicle-mediated transport in synapse	RIMS2;ROCK1;DNM3;ERC2;SYT7;BLOC1S6;CAMK2A;DGKQ;SNAP23;PREPL;STXBP1;RIMS1;RAP1B; CADPS2;TRIM9;DNAJC6;STXBP5L;SYT12;PCLO;DNM1;STX2;CADPS;DNM1L;EPS15;KIAA1109;RAB5A; UNC13A;CASK;VPS35;GRIK5;FMR1;DGKI;MAP2;SNPH;AMPH;PPFIA2;STX6;NAPA;AP3B1;DENND1A;GAK; PIP5K1C;AP3S1;CACNB2;NLGN1;BRAF;SH3GL1;SNAP47;CTBP2;DOC2B;KIF5C;SNAP25;APBA1;PFN2; DNAJC5;SH3GL2;SPG11;SYNJ1;CTNNB1;APBA2;CPLX1;CPLX2;UNC13C;FCHO2;ATAD1;SNCA;AP2B1; HPCA;PPP3CB;ADCY1;CANX;SYT1;CALM1
0099504	synaptic vesicle cycle	RIMS2;ROCK1;NRXN1;DNM3;ERC2;SYT7;BLOC1S6;CAMK2A;DGKQ;SNAP23;PREPL;STXBP1;RIMS1;RAP1B; GRIPAP1;CADPS2;TRIM9;MAGI2;DNAJC6;STXBP5L;SYT12;PCLO;DNM1;STX2;CADPS;DNM1L;KIAA1109; RAB5A;UNC13A;CASK;GRIK5;FMR1;DGKI;SNPH;AMPH;PPFIA2;STX6;NAPA;AP3B1;DENND1A;GAK;PIP5K1C; CACNB2;NLGN1;BRAF;RAPGEF4;PTEN;SH3GL1;SNAP47;CTBP2;DOC2B;SNAP25;APBA1;PFN2;DNAJC5; SH3GL2;SYNJ1;CTNNB1;APBA2;CPLX1;CPLX2;UNC13C;FCHO2;SNCA;PPP3CB;ADCY1;STXBP5;CANX; SYT1;CALM1
0010975	regulation of neuron projection development	RIMS2;SEMA6D;PTPRF;ASAP1;DBN1;PAK1;FYN;NDRG4;CAPRIN2;DNM3;PTK2;PTPRS;SHANK3;OBSL1; ACAP3;TRAK1;NRCAM;SIPA1L1;SEMA6C;FGFR1;KIDINS220;RIMS1;COBL;RIT2;CAMK2B;ARHGAP33;PTPRD; NSMF;SHTN1;GOLGA4;CRTC1;GPRC5B;SHANK2;NIN;GRIN1;MAGI2;PPP3CA;DNM1L;STK24;SHANK1; MACF1;STK25;PAK3;MAP4K4;TRAK2;CCDC88A;UNC13A;NPTN;SRCIN1;SEMA4F;KDM1A;NTRK3;SEMA4B; CTTN;RYK;MARK2;ZMYND8;FMR1;MYCBP2;RTN4;MAP2;TTL;FBXW8;PDLIM5;SEMA6A;RUFY3;CNTN2; NEURL1;NTRK2;PAFAH1B1;GAK;SSH1;IST1;DENND5A;ATP8A2;CARM1;LRP8;UBE2V2;INPP5J;KANK1; NLGN1;CPEB3;BRAF;PTEN;VLDLR;ULK2;MTOR;MAPT;SCN1B;SNAP25;LRRC4C;DHX36;OPA1;FBXO31; PARP6;SETX;RAP1GAP2;CNTN1;RELN;EFNA5;ROBO1;DGUOK;STK11;ARHGAP44;MEGF8;RAPGEF2; RAPGEF1;SS18L1;PLXNA2;AKT1;CUX1;L1CAM;ADGRB3;TIAM1;HECW1;UST;ADAM10;KNDC1;APBB1; TMEM106B;NEGR1;RHOA;FKBP4;SYT1;CFLAR;PTK2B;YWHAH;PLXNA4
0051648	vesicle localization	RIMS2;CLASP1;DNM3;ERC2;SYT7;BLOC1S6;CAMK2A;SNAP23;TRAK1;PPP6R3;PREPL;STXBP1;RIMS1; RAP1B;SEC16A;GRIPAP1;CADPS2;TRIM9;MAGI2;STXBP5L;SYT12;PCLO;DNM1;STX2;WDR11;KIF1C;CADPS; DNM1L;CLASP2;RAB5A;STARD3NL;TRAK2;UNC13A;CASK;CSNK1D;GRIK5;FMR1;RAB1B;DGKI;DYNC1I1; MAP2;SNPH;CNIH1;PPFIA2;NAPA;PAFAH1B1;AP3B1;TRAPPC10;PIP5K1C;KIF1A;AP3S1;CACNB2;NLGN1; BRAF;PTEN;SNAP47;CTBP2;DOC2B;PRKCZ;KIF3A;KIF5C;SNAP25;ARL6;PPP6R1;USO1;APBA1;PFN2; DNAJC5;SAR1A;CD59;KIF1B;SPG11;SYNJ1;CTNNB1;TRAPPC9;ANKRD28;APBA2;CPLX1;CPLX2;SCFD1; GOSR1;WASL;UNC13C;TFG;SNCA;KIFAP3;STARD3;BBS2;KIF5B;ADCY1;SYT1;DYNC1H1;CALM1
0051656	establishment of organelle localization	RIMS2;CLASP1;DOCK7;DNM3;ERC2;SYT7;PTK2;BLOC1S6;CAMK2A;SNAP23;MYH10;TRAK1;PPP6R3;PREPL; STXBP1;WASF1;RIMS1;RAP1B;TERF1;SEC16A;BICD2;MLH1;GRIPAP1;CADPS2;SYNE2;SNX4;RAN;SUN1; DCTN1;BICD1;TRIM9;PDCD6IP;STXBP5L;SYT12;PCLO;DNM1;STX2;WDR11;KIF1C;CADPS;SUN2;DNM1L; ABCE1;CLASP2;STK25;RAB5A;PINX1;STARD3NL;TRAK2;UNC13A;YWHAZ;XPO1;NUP62;CASK;CSNK1D; TRAPPC12;GRIK5;FMR1;RAB1B;ARHGAP21;DGKI;DLG1;DYNC1I1;MAP2;TTL;SNPH;CNIH1;PPFIA2;RHOT1; NAPA;PAFAH1B1;AP3B1;TRAPPC10;PIP5K1C;KIF1A;AP3S1;CACNB2;NLGN1;BRAF;SNAP47;RHOT2;CTBP2; DOC2B;PRKCZ;KIF3A;MAPT;PCM1;KIF5C;SNAP25;ARL6;PPP6R1;USO1;OPA1;APBA1;NUMA1;PFN2;DNAJC5; NUP88;SAR1A;CD59;KIF1B;SPG11;SYNJ1;CTNNB1;TRAPPC9;SPIRE2;CDK5RAP2;ANKRD28;LRPPRC;APBA2; CPLX1;CPLX2;MAP1S;SCFD1;GOSR1;CEP120;WASL;UNC13C;TFG;SNCA;MAP4;KIFAP3;STARD3;BBS2; HOOK3;KIF5B;ADCY1;SYT1;DYNC1H1;CALM1
0016358	dendrite development	ASAP1;RBFOX2;DBN1;FYN;CAPRIN2;DNM3;PTPRS;SHANK3;CAMK2A;OBSL1;TRAK1;SIPA1L1;KIDINS220; COBL;PICALM;CAMK2B;ARHGAP33;PTPRD;NSMF;MEF2A;CRTC1;SHANK2;GRIN1;PPP3CA;DNM1L;DCLK1; SHANK1;BTBD3;PAK3;TRAK2;SRCIN1;CTNNA2;ABI1;ZMYND8;FMR1;MAP2;APP;FBXW8;PDLIM5;NEURL1; PAFAH1B1;CARM1;LRP8;NLGN1;CPEB3;PTEN;VLDLR;STRN;MTOR;DHX36;OPA1;FBXO31;PARP6;RELN; STK11;ARHGAP44;RERE;RAPGEF2;SS18L1;MAP1S;CUX1;WASL;ADGRB3;TIAM1;HECW1;ADAM10;KNDC1; TMEM106B;RHOA;YWHAH;MAP1A
0099177	regulation of trans-synaptic signalling	RIMS2;SQSTM1;GRM1;DBN1;AKAP9;CACNA1A;FYN;NRXN1;SYT7;PTPRS;SHANK3;CAMK2A;PNKD;NISCH; PREPL;LAMA2;STAU1;SIPA1L1;STXBP1;RIMS1;RAP1B;CAMK2B;ADORA1;NSMF;RNF19A;CACNB3;CRTC1; SHANK2;GRIN1;STXBP5L;SYT12;PPP3CA;MCTP1;DNM1;DNM1L;PACSIN2;SHANK1;SLC8A2;RNF216;RAB5A; UNC13A;CNTNAP4;NPTN;CASK;GRIK5;ZMYND8;FMR1;DGKI;HRAS;IQSEC2;APP;GRIK2;CNTN4;PPFIA2; RHOT1;NF1;NAPA;CNTN2;RASGRF1;NEURL1;NTRK2;SSH1;LRP8;CACNB2;NLGN1;CPEB3;BRAF;PTEN; SH3GL1;SNAP47;MTOR;PRKCZ;MAPT;PTPRA;SYNGR1;SNAP25;LRRC4C;CELF4;APBA1;FLOT1;PFN2; SLC6A1;RELN;GRM3;ARRB2;PXK;RAPGEF2;PRKCE;JPH3;APBA2;CPLX1;CPLX2;GRIN2A;PLCB4;UNC13C; ATAD1;SNCA;RAB26;CLSTN3;NPTXR;PPP3CB;KIF5B;ADCY1;SYT1;PTK2B;JPH4;YWHAH;NCDN;GLUL; MAP1A;FAM107A;CALM1
0031346	positive regulation of cell projection organization	RIMS2;DBN1;PAK1;FYN;NDRG4;CAPRIN2;DNM3;SHANK3;OBSL1;TRAK1;FGFR1;KIDINS220;RIMS1;COBL; RIT2;CAMK2B;PTPRD;SHTN1;DZIP1;GOLGA4;CRTC1;GPRC5B;SHANK2;NAV3;NIN;TGFBR1;MAGI2;GPM6A; DNM1L;SHANK1;MACF1;STK25;PAK3;CCDC88A;DEF8;UNC13A;NPTN;KCTD17;KDM1A;NTRK3;TENM2; MARK2;ZMYND8;FMR1;HRAS;RAC1;APC;FBXW8;RUFY3;CCP110;NEURL1;NTRK2;PAFAH1B1;IST1;ATP8A2; LRP8;UBE2V2;NLGN1;PALM;CPEB3;BRAF;VLDLR;PLEKHM1;MTOR;MAPT;SCN1B;TAPT1;ARPC2;DHX36; OPA1;FBXO31;FUZ;PARP6;SETX;CNTN1;RELN;EFNA5;ROBO1;STK11;ARHGEF7;MEGF8;RAPGEF2; RAPGEF1;SS18L1;PLXNA2;CEP120;CUX1;WASL;L1CAM;TIAM1;APBB1;ANLN;TMEM106B;NEGR1;NCKAP1; RHOA;SYT1;CFLAR;PTK2B;PLXNA4
0050808	synapse organization	NRXN2;ANK3;PTPRF;DBN1;FYN;CAPRIN2;NRXN1;DNM3;ERC2;PTK2;PTPRS;ADGRL1;SHANK3;ADGRL3; MYH10;NRCAM;STAU1;SIPA1L1;WASF1;DLG2;SEZ6L;CAMK2B;ARHGAP33;PTPRD;NFASC;GRIPAP1; DLGAP3;CACNB3;ERBB4;DCTN1;SHANK2;CACNB4;GRIN1;MAGI2;PCLO;GPM6A;DNM1L;CNKSR2;SHANK1; ABHD17A;PAK3;UNC13A;CNTNAP4;YWHAZ;NPTN;SRCIN1;NTRK3;ALS2;VPS35;CTTN;BCAN;RYK;CTNNA2; LHFPL4;ZMYND8;ARHGEF9;FMR1;NFIA;DLG1;APP;PDLIM5;FNTA;RER1;PPFIA2;GPHN;MAPK14;CNTN2; NEURL1;NTRK2;PAFAH1B1;SSH1;LRP8;UBE2V2;CACNB2;NLGN1;PALM;PTEN;CTBP2;MAPT;LRRC4C; ACTN1;DHX36;OPA1;PFN2;RELN;EFNA5;ARHGAP44;CTNNB1;DAG1;LRRC4B;ADD2;WASL;L1CAM;ADGRB3; UNC13C;TIAM1;SNCA;ADAM10;CLSTN3;SPTBN2;IGSF21;RHOA;MDGA1
0061564	axon development	ANK3;CHL1;SEMA6D;PTPRF;NRXN3;PAK1;C9orf72;FYN;DOCK7;EVL;NRXN1;PTK2;PTPRS;SHANK3;MYH10; TRAK1;NRCAM;LAMA2;SIPA1L1;STXBP1;SEMA6C;COBL;PICALM;MAPK8IP3;SPTAN1;NFIB;NFASC;SHTN1; GOLGA4;NIN;GRIN1;UNC5A;NCAM1;ETV1;RAP1GAP;APBB2;CTNNA1;STK24;DCLK1;FGFR2;MACF1;STK25; PAK3;TRAK2;NPTN;PARD3;NUMBL;SEMA4F;PTCH1;NTRK3;ALS2;SEMA4B;FRS2;CTTN;RYK;CTNNA2; MARK2;MYCBP2;RTN4;UNC5D;MAP2;APP;TTL;SEMA6A;RUFY3;CNTN4;CNTN2;RPS6KA5;NTRK2;PAFAH1B1; SSH1;IST1;ATP8A2;BRAF;SPTBN4;PTEN;EPHA5;TCTN1;VLDLR;FEZ2;ULK2;KIF3A;MAPT;SCN1B;PTPRA; KIF5C;PLPPR4;LRRC4C;ENAH;ADARB1;FLOT1;USP33;RELN;EFNA5;ROBO1;STK11;SPG11;NREP;MEGF8; CYFIP2;DAG1;CNTN6;SMAD4;PLXNA2;SPTB;MAP1S;ATL1;GRB10;L1CAM;TIAM1;UST;APBB1;SPTBN2;FEZ1; RHOA;PPP3CB;ADCY1;SPTBN1;BSG;MAP1A;PLXNA4

Table 7.3.4 List of genes from ORA analysis that show significant differential exon skipping between cerebellum and frontal cortex.

GO: gene set	GO: description	Leading Edge
0032103	positive regulation of response to external stimulus	C3;FGFR1;IL17RB;P2RX4;STAT5B;STX4
0048284	organelle fusion	AKT2;CORO1A;OPA1;SNAP23;STOML2;STX4;VPS16
0061025	membrane fusion	AKT2;CORO1A;GCA;NAPA;OPA1;PPIA;SNAP23;STX18;STX4;VPS16
0006638	neutral lipid metabolic process	C3;DGAT1;DGKA;DGKB;DGKZ;SLC27A1
0032606	type I interferon production	FLOT1;IFI16;OTUD5;PCBP2;PQBP1
0007215	glutamate receptor signalling pathway	DLG4;GRIN2C;MINK1
0018209	peptidyl-serine modification	AKT1;CAMK1;CAPRIN2;CSNK1D;CSNK1G2;DMTN;HAX1;MAP2K2;MAP3K10;MAP3K12;NAA10; PARP1;PINK1;PKD1;UHMK1
0006732	coenzyme metabolic process	CYB5A;DCXR;ENO2;FDXR;HK1;MAT2B;MOCS2;MTHFD1L;MVD;PDHB;PFKL;PFKM;SLC2A3; VCP
0043687	post-translational protein modification	COPS5;FBXO9;LRRC41;OBSL1;PSMA1;PSMA4;PSMB4;PSMC1;PSMC5;RBBP7;WDTC1
0006898	receptor-mediated endocytosis	DBNL;DLG4;DNM1;GAK;LRP1;PICK1;SNX17

Table 7.3.5 List of genes from GSEA analysis that show significant increased or decreased intron retention in cerebellum compared to the frontal cortex.

GO: gene set	GO: description	Overlap
0006413	translational initiation	TPR;RPL18;RPL31;RPL3;EIF3D;EIF5;RPS16;EIF3B;RPL28;EIF4G2;EIF2B4;RPS15;COPS5;MIF4GD;ATF4; RPS15A;RPLP1;RPS2;RPS11;RPL13A;RPS27A;EIF2B5;RPL10;RPL7A;EIF3M;UHMK1;RPL30;EIF4A2;RPSA; RPS9;RPS21;RPS6KB2;EIF3K;RPS26;RPL37A;RPL10A
0070972	protein localization to endoplasmic reticulum	RPL18;RPL31;RPL3;PMM1;RPS16;RPL28;RPS15;RPS15A;OS9;RPLP1;SRP14;RPS2;RPS11;RPL13A;RPS27A; RPL10;RPL7A;RPL30;ZFAND2B;RPSA;RPS9;RPS21;PDIA2;RPS26;RPL37A;GPAA1;RPL10A
0010498	proteasomal protein catabolic process	PKD1;POMT2;PSMC4;PSMA4;CUL1;SIRT2;RNF126;PSMC5;ANAPC5;MAEA;PSME1;WAC;PSMC6;PSMA3; PSMC1;PSME2;USP14;RNF40;DVL1;UBE2D3;FBXO9;AUP1;CLU;RBCK1;PSMA1;ARNTL;UBQLN1;OS9; DNAJB2;CSNK1D;AKT1;RPS27A;UBXN4;RMND5B;OGT;ALAD;UCHL1;UBXN11;ZFAND2B;PINK1;CCAR2; FBXW5;PSMD4;PSMB4;UBXN1;SYVN1;VCP;NEMF;HSP90B1;UBXN6;GBA;RAD23A;TMEM259;PCBP2;WWP2
0048193	Golgi vesicle transport	ARF5;AP3D1;KIF22;SNAP23;PICK1;ARFRP1;COG4;GGA2;CSK;AP3B2;NAPA;GORASP1;BBS2;C16orf70;GGA3; MACF1;VPS13C;LLGL1;SORT1;COG2;PREB;ACTR1A;SCAMP2;SGSM2;CSNK1D;SCYL1;HYOU1;ANK3;VCP; YIF1B;RAB26;STX18;KLC2;DCTN2;SEC24C;GAK;TRAPPC6B;NRBP2;LAMP1;BICD2;TRAPPC4;DYNC1H1; PGAP1;HTT;DCTN1;ANKRD28;VPS52;PDCD6
0006605	protein targeting	ACAA1;RPL18;AP3D1;RPL31;TIMM21;GNPTG;HPS4;RPL3;PMM1;NUCB1;RPS16;AKT2;CDC37;PITRM1;RPL28; UBE2D3;RPS15;HTRA2;ITGB1BP1;CLU;RAB3IP;VPS13C;RPS15A;OS9;RPLP1;SRP14;RPS2;NPEPPS;RPS11; RPL13A;HAX1;RPS27A;RPL10;RPL7A;ANK3;RPL30;ZFAND2B;PINK1;DMTN;BAP1;PMPCA;YWHAB;RPSA; RPS9;RPS21;GSTK1;RPS26;RPL37A;ECI2;RPL10A
0042176	regulation of protein catabolic process	PKD1;PSMC4;CTSA;SIRT2;XPO1;PSMC5;PSME1;WAC;SGSM3;PSMC6;PSMC1;PSME2;USP14;RNF40;OAZ1; DVL1;CDK5RAP3;APC2;MAD2L2;CLU;LRP1;GGA3;ARNTL;UBQLN1;OS9;DNAJB2;CSNK1D;AKT1;OGT;ALAD; PINK1;CCAR2;ATP13A2;VPS28;GRIN2C;UBXN1;VCP;RAB26;ATG4B;GBA;RAD23A;TMEM259;WWP2;EGLN2
0022613	ribonucleoprotein complex biogenesis	XAB2;XPO1;CIRBP;DDX17;RPL3;EIF3D;PRMT5;SRSF5;EIF5;NOP56;PIH1D1;SF3A2;RPS16;EIF3B;FTSJ3; RPS15;EXOSC8;EXOSC9;EMG1;AAMP;KRI1;EXOSC2;NOL11;DHX30;RAN;PAN2;DDX56;RPS2;PELP1; RPL13A;RPL10;C9orf72;RPL7A;EIF3M;DCAF13;POP5;RPSA;RPS9;RPS21;DDX23;EIF3K;TBL3;RPS27L;DDX51; DYNC1H1;DDX39B;RPL10A;WDR46;MRPL20
0090150	protein localization to membrane	RPL18;RPL31;RPL3;ARFRP1;GGA2;CSK;RPS16;AKT2;RPL28;GORASP1;RPS15;ITGB1BP1;BBS2;C16orf70; GGA3;RAB3IP;MACF1;RPS15A;RPLP1;SRP14;RPS2;RPS11;RPL13A;RPS27A;RPL10;RPL7A;ANK3;RPL30; ZFAND2B;DMTN;YWHAB;RAB26;RPSA;RPS9;RPS21;RPS26;RPL37A;RPL10A
0006401	RNA catabolic process	RNH1;EDC4;RPL18;RPL31;XPO1;CNOT3;PCBP4;CIRBP;RPL3;APEX1;RPS16;RPL28;DDX5;MAGOHB;RPS15; EXOSC8;EXOSC9;EXOSC2;RPS15A;PAN2;RPLP1;SSB;RPS2;AKT1;RPS11;RPL13A;RPS27A;RPL10;RPL7A; RPL30;YWHAB;RPSA;RPS9;RPS21;RPS26;RPL37A;TTC37;RPL10A;SKIV2L;PPP2R2A
0034976	response to endoplasmic reticulum stress	POMT2;PPP2R5B;ACADVL;UBA5;XBP1;PSMC6;USP14;CDK5RAP3;AUP1;CLU;COPS5;ATF4;UBQLN1;OS9; DNAJB2;FLOT1;PREB;UBXN4;EIF2B5;HYOU1;UBXN1;SYVN1;CREBRF;VCP;TPP1;HSP90B1;UBXN6;GRINA; TMEM259;TSPYL2;PDIA2;OPA1;DCTN1

Table 7.3.6 List of genes from ORA analysis that show significant differential intron retention between cerebellum and the frontal cortex.

GO: gene set	GO: description	Overlap
0050808	synapse organization	FYN;CTNNA2;CACNB1;GRIPAP1;PAK3;DNM1L;NRCAM;ZMYND8;EEF2K;NRXN2;CAPRIN2;DLGAP3;ADGRB2;STAU1;WASF3;EGLN1;DGKB;DAB2IP;NTRK3;PTPRF;SYBU;NTRK2;LRRC4C;CNKSR2;ADGRL3;GPM6A;DLG2;ANK3;HOMER1;PTPRD;TIAM1;NFASC;BSN;LRFN5;CACNB2;PTK2;GPHN;LINGO2;ERBB4;NRXN1;PCLO;SIPA1L1;DNM3;UNC13B;OPA1;NOS1AP;PCDHGC3
0099504	synaptic vesicle cycle	SYT7;APBA2;SYT1;GRIPAP1;AMPH;RIMS1;CADPS2;DNM1L;RAPGEF4;SNPH;BLOC1S6;DNM1;APBA1;DNAJC6;SNAP25;STXBP5L;CACNA1D;DGKI;CADPS;BSN;CACNB2;RIMS2;NRXN1;PIP5K1C;PCLO;DNM3;UNC13B
0050803	regulation of synapse structure or activity	FYN;CTNNA2;GRIPAP1;PAK3;DNM1L;NRCAM;ZMYND8;EEF2K;DNM1;CAPRIN2;ADGRB2;EGLN1;DGKB;DAB2IP;NTRK3;SYBU;NTRK2;ADGRL3;GPM6A;HOMER1;PTPRD;TIAM1;LRFN5;PTK2;LINGO2;NRXN1;SIPA1L1;DNM3;OPA1
0099177	regulation of trans-synaptic signalling	FYN;SYT7;APBA2;RASGRF1;PRKCZ;SYT1;RIMS1;DNM1L;ZMYND8;CELF4;DNM1;APBA1;RAPGEF2;STAU1;GRM4;GFAP;SNAP25;EGLN1;DGKB;ATAD1;CNTN4;STXBP5L;SYBU;NTRK2;LRRC4C;HOMER1;GRIA1;CACNA1D;DGKI;GRIN2C;GRIK2;CACNB2;MCTP1;RIMS2;NRXN1;ABAT;SIPA1L1;UNC13B;GRID2IP
0051648	vesicle localization	SYT7;APBA2;KIF1B;PRKCZ;SYT1;GRIPAP1;CLASP1;RIMS1;CADPS2;DNM1L;SNPH;BLOC1S6;DNM1;APBA1;PPP6R3;ARL6;SNAP25;STXBP5L;SYBU;ARFGAP2;GRIA1;CACNA1D;DGKI;DYNC1I1;CLASP2;CADPS;CACNB2;RIMS2;PIP5K1C;PCLO;DNM3;UNC13B
0010975	regulation of neuron projection development	CFLAR;FYN;CNTN1;SYT1;PAK3;RIMS1;DNM1L;NRCAM;FBXO7;EP300;ZMYND8;NDRG4;FBXO31;EEF2K;RAPGEF2;CAPRIN2;MACF1;CHN1;GFAP;SNAP25;ATP8A2;DAB2IP;SEMA6D;NTRK3;PTPRF;PTPRG;NTRK2;LRRC4C;PAK1;ASAP1;PTPRD;ZFYVE27;TIAM1;ULK4;PTK2;RIMS2;SIPA1L1;DNM3;OPA1;BMPR2
0099003	vesicle-mediated transport in synapse	SYT7;APBA2;SYT1;AMPH;RIMS1;CADPS2;DNM1L;SNPH;BLOC1S6;DNM1;APBA1;DNAJC6;SNAP25;ATAD1;STXBP5L;CACNA1D;DGKI;CADPS;CACNB2;RIMS2;PIP5K1C;PCLO;DNM3;UNC13B
0017156	calcium ion regulated exocytosis	SYT7;APBA2;SYT1;RIMS1;CADPS2;DNM1L;RAPGEF4;SNPH;BLOC1S6;APBA1;SNAP25;STXBP5L;CACNA1D;DGKI;CADPS;CACNB2;RIMS2;PIP5K1C;PCLO;UNC13B
0006836	neurotransmitter transport	SYT7;APBA2;SYT1;RIMS1;CADPS2;DNM1L;SNPH;BLOC1S6;APBA1;NRXN2;SLC25A12;GRM4;GFAP;SNAP25;STXBP5L;CACNA1D;DGKI;CADPS;CACNB2;MCTP1;RIMS2;NRXN1;ABAT;SV2B;PIP5K1C;PCLO;UNC13B
0043087	regulation of GTPase activity	RASGRF1;ARHGAP10;PICALM;SMAP2;DNM1L;DOCK9;ITGA6;TBC1D12;RAPGEF2;RIC8B;ITGB1BP1;CHN1;TBC1D5;ARHGEF11;TBC1D4;LRCH1;DAB2IP;FAM13A;RAP1GDS1;NTRK3;BCAS3;SOD1;PKP4;STXBP5L;NTRK2;ARFGAP2;ASAP1;TIAM1;DGKI;MLST8;PTK2;RALGAPA1;RGS6;SRGAP3;ARHGEF12;TBC1D9B;SIPA1L1;TBC1D8

Table 7.3.7 List of genes from ORA analysis that show significantly differential splicing of mutually exclusive exons in the cerebellum and frontal cortex.

GO: gene set	GO: description	Overlap
0034453	microtubule anchoring	CLASP1;PCM1;CEP350;BICD1;CLASP2;DAG1;DCTN1
0030705	cytoskeleton-dependent intracellular transport	KIF1B;PRKCZ;CDC42;KIFAP3;MAP2;PCM1;TNPO1;SUN2;IFT27;ARHGAP21;IFT43;IFT22;MAPK8IP3;BICD1;WDR19;DYNC1I1;MAPT;IFT140;OPA1;DCTN1
0031023	microtubule organizing center organization	CEP68;PPP1R12A;CLASP1;PCM1;XPO1;ARHGEF10;KAT2B;CHMP1A;ODF2;FBXW5;CLASP2;CTNNB1;CKAP5;KIAA0753;DCTN1
0022406	membrane docking	CAMK2A;CLASP1;PCM1;SNPH;NDRG4;EXOC2;STX16;RAB3IP;TUBA4A;UNC13A;ODF2;STXBP1;SYTL2;RAB15;IQCB1;CKAP5;SFI1;DCTN1
0031503	protein-containing complex localization	AKAP8L;NUP160;PRKCZ;DLG1;KIFAP3;PCM1;XPO1;TNPO1;EXOC1;THOC5;IFT27;CPSF3;IFT43;ENY2;HNRNPA2B1;NUP85;IFT22;FIP1L1;WDR19;SLU7;CPSF2;CLSTN1;DAG1;ANKS1B;IFT140;DNM3
0006401	RNA catabolic process	RPL31;XPO1;TNPO1;RPLP0;TNRC6A;CIRBP;ZC3H14;APEX1;CPEB3;RPS12;CNOT6;RPL22;ETF1;CNOT1;FXR2;NT5C3B;RPL13A;RPL7A;PAN3;LARP1;RPL30;RPL26;EXOSC1;EXOSC10;RPL35A;SND1;RPL12;TTC37;RPL10A
0007018	microtubule-based movement	KIF1B;PRKCZ;CDC42;KIFAP3;MAP2;PCM1;RFX3;TNPO1;SUN2;IFT27;ARHGAP21;IFT43;IFT22;DYNC1LI2;MAPK8IP3;KIF21A;BICD1;WDR19;DYNC1I1;MAPT;IFT140;OPA1;DCTN1
0051656	establishment of organelle localization	TRAPPC6A;KIF1B;PRKCZ;CAMK2A;CDC42;ATP6AP1;CLASP1;DLG1;KIFAP3;MAP2;PCM1;SAR1A;RIMS1;XPO1;PIBF1;TMEM230;SUN2;SNPH;NAPA;ARHGAP21;PPP6R3;UNC13A;CHMP1A;STXBP1;BICD1;DYNC1I1;CLASP2;ADCY1;CTNNB1;RIMS2;PIP5K1C;MAPT;DNM3;OPA1;DCTN1;DOC2B
0006091	generation of precursor metabolites and energy	CS;PFKP;PKM;AACS;OXCT1;AKR1B1;NDUFB2;SORBS1;NDUFB7;IDH3B;GSR;NDUFS8;GAPDH;TPI1;ENO2;COX7C;POR;NDUFA10;MYBBP1A;SDHC;MDH2;ALDOA;DLAT;PFKM;AK9;PHKG2;FDXR;IDH3A;NDUFV1;STAT3;ZBTB20;IDH2;NDUFA4L2;PPP1R3E
0010975	regulation of neuron projection development	KDM1A;CAMK2B;PPP2R5B;FGFR1;MAP2;RIMS1;ARHGAP4;NDRG4;CRTC1;SCN1B;CPEB3;FKBP1B;PTK2B;RNF6;UNC13A;ACAP3;EPHA7;AVIL;SEMA6C;NTRK2;SPOCK1;NSMF;KNDC1;RIMS2;CAMK1D;CIB1;MAPT;SHTN1;PLXNB2;SYNGAP1;DNM3;PLXNB3;OPA1;L1CAM

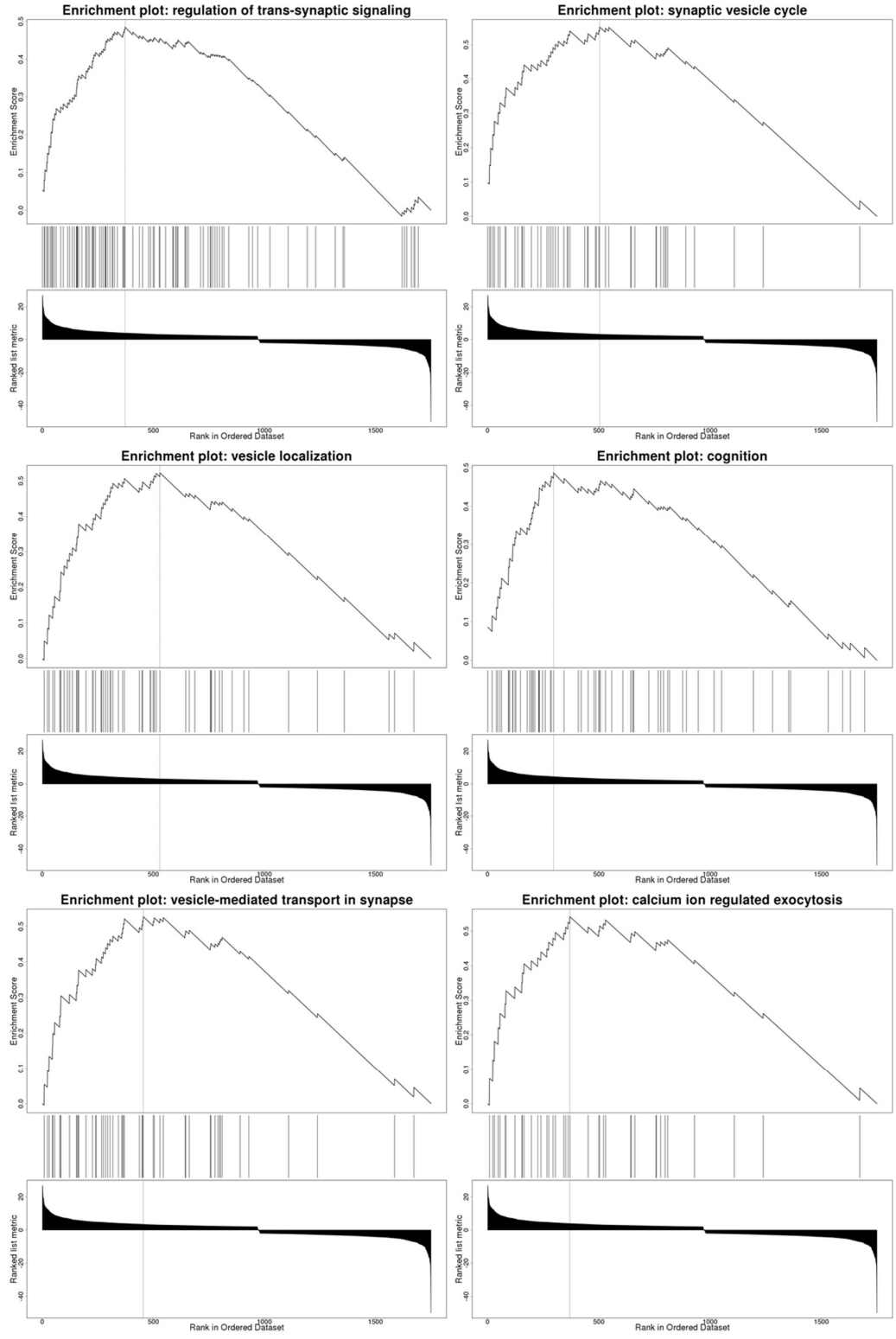
Table 7.3.8 List of genes from ORA analysis that show significant differential 5' splice site selection between cerebellum and the frontal cortex.

GO: gene set	GO: description	Overlap
0051656	establishment of organelle localization	GAB2;KIF1B;SYNE2;AP3D1;SYT1;PFN2;CAMK2A;DLG1;KIF22;RIMS1;CADPS2;GSK3B;NSFL1C;SNAP23; STX1A;WASL;DNM1;GBF1;ARHGAP21;GIT1;STK25;TRAK2;RIMS3;NAPB;MAP1S;SNAP25;MYH10;BLOC1S1; CDK5RAP2;ACTR2;RHOT2;SYT2;CENPC;SHROOM2;SYBU;ARFGAP2;KIF5A;DYNC1I1;SYNJ1;TRAPPC10; CLASP2;YWHAZ;CTNNB1;KIF5C;CEP120;RASGRP1;CNIH2;RIMS2;PPFIA3;PIP5K1C;BACE1;LYN;DOC2B
0051648	vesicle localization	KIF1B;AP3D1;SYT1;PFN2;CAMK2A;RIMS1;CADPS2;GSK3B;SNAP23;STX1A;WASL;DNM1;GBF1;GIT1;TRAK2; RIMS3;NAPB;SNAP25;BLOC1S1;SYT2;SHROOM2;SYBU;ARFGAP2;KIF5A;DYNC1I1;SYNJ1;TRAPPC10; CLASP2;CTNNB1;KIF5C;RASGRP1;CNIH2;RIMS2;PPFIA3;PIP5K1C;BACE1;DOC2B
0099003	vesicle-mediated transport in synapse	AP3D1;SYT1;PFN2;CAMK2A;RIMS1;CADPS2;GSK3B;SNAP23;SLC17A7;STX1A;DNM1;GIT1;RIMS3;NAPB; SNAP25;BLOC1S1;SYT2;KIF5A;SYNJ1;CTNNB1;KIF5C;CLSTN1;CNIH2;RIMS2;PPFIA3;GAK;PIP5K1C;BACE1; DOC2B
0099504	synaptic vesicle cycle	AP3D1;SYT1;PFN2;CAMK2A;RIMS1;CADPS2;GSK3B;RAPGEF4;SNAP23;SLC17A7;STX1A;DNM1;GIT1;RIMS3; NAPB;SNAP25;SYT2;SYNJ1;CTNNB1;RIMS2;PPFIA3;GAK;NRXN1;PIP5K1C;BACE1;DOC2B
1990778	protein localization to cell periphery	ITGA3;ARHGAP44;KIF1B;ATP1B3;DLG1;EPB41L3;GGA2;IKBKB;AKT2;C2CD5;OPTN;LRP1;GGA3;LAMA5; FLOT2;SNAP25;ROCK2;MAP7;TMBIM1;DENND4C;SYTL2;RAB15;AKT1;ANK3;ZFYVE27;LDLRAP1;EPB41; GRIN2C;CLASP2;RAB26;CLSTN1;DPP10;GAK;ZDHHC23
0060627	regulation of vesicle-mediated transport	ARHGAP44;GAB2;ZFYVE16;TNK2;SYT1;PFN2;CAMK2A;RIMS1;CADPS2;GSK3B;RAPGEF4;TF;PICK1;ARFGAP 1;NDRG4;TSC2;EEF2K;SLC17A7;AKT2;STX1A;WASL;DNM1;GIT1;C2CD5;RIMS3;LRP1;NAPB;RINT1;RAB15;LD LRAP1;SYNJ1;VPS28;CLASP2;PACSIN3;RAB26;RAB4A;CNIH2;MCTP1;RIMS2;ANKFY1;BACE1;BCR;SCAMP5; INPP5F;RUFY2;LYN;DOC2B
0017156	calcium ion regulated exocytosis	SYT1;PFN2;CAMK2A;SDF4;RIMS1;CADPS2;GSK3B;RAPGEF4;SNAP23;STX1A;GIT1;RIMS3;NAPB;SNAP25; SYT2;SYNJ1;RIMS2;PPFIA3;PIP5K1C;BACE1;SCAMP5;DOC2B
0099177	regulation of trans-synaptic signalling	NISCH;CAMK2B;SYT1;PFN2;CAMK2A;RIMS1;GSK3B;SSH1;JAK2;PICK1;STX1A;DNM1;GIT1;PPP1R9B;RIMS3; SLC8A2;PTK2B;PHF24;PLCG1;GRM4;NAPB;SNAP25;DGKB;CACNA1A;SYBU;NPTN;LRP8;GRIN2C;RAB26; CLSTN1;CNIH2;MCTP1;RIMS2;PPFIA3;NRXN1;BACE1;BCR;RELN;MTOR
0010975	regulation of neuron projection development	ITGA3;ARHGAP44;CAMK2B;SYT1;RIMS1;GSK3B;SSH1;NIN;PQBP1;NDRG4;EEF2K;MEGF8;MAG;COBL; CAPRIN2;FN1;STK25;TRAK2;PTK2B;LRP1;OBSL1;SNAP25;KIDINS220;ADGRB3;PLXNC1;ACTR2;ARHGDIA; AKT1;CARM1;SYT2;CPNE9;ZFYVE27;NPTN;LRP8;KNDC1;RIMS2;GAK;RELN;MTOR;INPP5F;L1CAM;LYN
0140029	exocytic process	SYT1;CAMK2A;CADPS2;SNAP23;STX1A;NAPB;SNAP25;VPS45;SYTL2;RAB15;DMTN;SYNJ1;PPFIA3;LYN

Table 7.3.9: List of genes from ORA analysis that show significant differential 3' splice site selection between cerebellum and the frontal cortex.

GO: gene set	GO: description	Leading Edge
0099177	**regulation of trans-synaptic signalling**	ABAT;APBA2;ARC;ATP2A2;CACNG3;CALB1;CALB2;CAMK2A;CLSTN1;CLSTN3;CPLX2;CPLX3;DNM1;EFNB3;EPHA4;GRIK5;GRIN1;JPH4;KCTD13;LGMN;LRFN2;MAPT;MEF2C;NAPA;NAPB;NCDN;NPTX2;NPTXR;NRGN;PFN2;PLK2;PRKAR1B;PRKCG;PRKCZ;PRNP;PRRT2;PTGS2;PTK2B;RAB3A;RGS4;SLC8A2;SNAP25;SNCA;STXBP1;SYN1;SYN3;SYP;SYT1;VAMP2
0099504	**synaptic vesicle cycle**	ADCY1;APBA2;ATP2A2;BRSK2;CADPS;CAMK2A;CHRNB2;CPLX2;CPLX3;DNM1;GRIK5;NAPA;NAPB;NLGN2;PACSIN1;PFN2;PRKAR1B;PRKCG;PRRT2;RAB27B;RAB3A;SLC32A1;SNAP25;SNCA;STXBP1;SYN1;SYN2;SYN3;SYP;SYT1;SYT5;TRIM9;UNC13A;VAMP2
0051648	**vesicle localization**	ADCY1;AP3S1;APBA2;ATP2A2;BRSK2;CADPS;CAMK2A;CHRNB2;CNR1;COL7A1;CPLX2;CPLX3;DCTN2;DNM1;GRIK5;HTT;MAP2;NAPA;NAPB;NLGN2;NSF;PAFAH1B1;PFN2;PRKCG;PRKCZ;PRRT2;RAB27B;RAB3A;SNAP25;SNCA;STXBP1;SYN1;SYN2;SYN3;SYP;SYT1;SYT5;TRIM9;UNC13A;VAMP2
0050890	**cognition**	ARC;CALB1;CAMK4;CHL1;CNTNAP2;GPI;GPR88;GRIN1;HTT;JPH4;LGMN;MAPT;MEF2C;NDRG4;NPTX2;NRGN;PAFAH1B1;PJA2;PLK2;PRKAR1B;PRKCG;PRKCZ;PRNP;PTGS2;SERPINF1;SLC8A2;SNAP25;TUSC3
0099003	**vesicle-mediated transport in synapse**	AP3S1;APBA2;ARC;ATP2A2;CADPS;CALY;CAMK2A;CHRNB2;CLSTN1;CPLX2;CPLX3;DNM1;GRIK5;HPCA;MAP2;NAPA;NAPB;NLGN2;PACSIN1;PFN2;PRKCG;PRRT2;RAB27B;RAB3A;SNAP25;SNCA;STXBP1;SYN1;SYP;SYT1;SYT5;TRIM9;VAMP2
0017156	**calcium ion regulated exocytosis**	APBA2;ATP2A2;CADPS;CAMK2A;CDK5R2;CPLX2;CPLX3;GRIK5;NAPA;NAPB;PFN2;PRKCG;PRRT2;RAB3A;SNAP25;STXBP1;SYN1;SYP;SYT1;SYT5;TRIM9;VAMP2
0140029	**exocytic process**	CAMK2A;CPLX2;CPLX3;GRIK5;NAPA;NAPB;PRRT2;RAB3A;SNAP25;STXBP1;SYT1;VAMP2
0051656	**establishment of organelle localization**	ADCY1;AP3S1;APBA2;ATP2A2;BICD2;CADPS;CAMK2A;CDCA5;CHGA;CHRNB2;COL7A1;CPLX2;CPLX3;DCTN2;DNM1;GRIK5;HTT;MAP2;MAPT;MYH10;NAPA;NAPB;NEFL;NSF;PAFAH1B1;PFN2;PRKCG;PRKCZ;PRRT2;PTK2;RAB27B;RAB3A;SNAP25;SNCA;STXBP1;SYN1;SYP;SYT1;SYT5;TRIM9;UCHL1;UNC13A;VAMP2;YWHAZ
0035249	**synaptic transmission, glutamatergic**	CACNG3;CDH8;CLSTN3;GRIA2;GRIK5;GRIN1;MEF2C;NAPA;NAPB;PTGS2;PTK2B;STXBP1;SYT1
0030534	**adult behaviour**	ABAT;CHL1;CNTNAP2;CXCL12;EFNB3;EPHA4;GABRG2;GRIN1;INPP5F;NRXN2;PAFAH1B1;SNCA;SPTBN2;UCHL1
0050886	endocrine process	APLN;FOXD1;HSD11B2;PCSK5
0061614	pri-miRNA transcription by RNA polymerase II	APLN;ATOH8;NFATC4;RELA
0043062	extracellular structure organization	ADAMTS2;ADAMTS9;AEBP1;BGN;BMP1;CCN2;COL16A1;COL1A2;COL27A1;COL5A3;COL6A2;COL8A1;COL9A2;COLGALT1;DNAJB6;ELN;FBLN1;FLOT1;FN1;FOXF1;GFAP;GSN;HPN;HPSE2;ICAM1;ITGA10;ITGA5;ITGA8;ITGAX;ITGB5;LAMB2;LCAT;MMP14;PECAM1;PLTP;RGCC;SERPINE1;SERPINH1;SH3PXD2B;SPP1;VCAN
0030856	regulation of epithelial cell differentiation	ASCL1;ATOH8;CLDN5;FOXJ1;MAFF;NOTCH4;PRKX;SERPINE1;SMO;VEZF1;WWTR1;ZFP36L1
0007162	negative regulation of cell adhesion	ANGPT2;APOD;ATP5F1B;DUSP1;FAM107A;FOXJ1;IRF1;LRRC32;MAP4K4;MBP;PLXNB1;PLXNB3;SERPINE1;SWAP70;VSIR

Table 7.3.10 List of genes from GSEA analysis that have significantly different transcriptional expression in control and clinical AD in the ROSMAP dataset (based on clinical diagnosis).


Enrichment plot: regulation of trans-synaptic signaling
Enrichment plot: synaptic vesicle cycle
Enrichment plot: vesicle localization
Enrichment plot: cognition
Enrichment plot: vesicle-mediated transport in synapse
Enrichment plot: calcium ion regulated exocytosis
Enrichment Score
Ranked list metric
Rank in Ordered Dataset

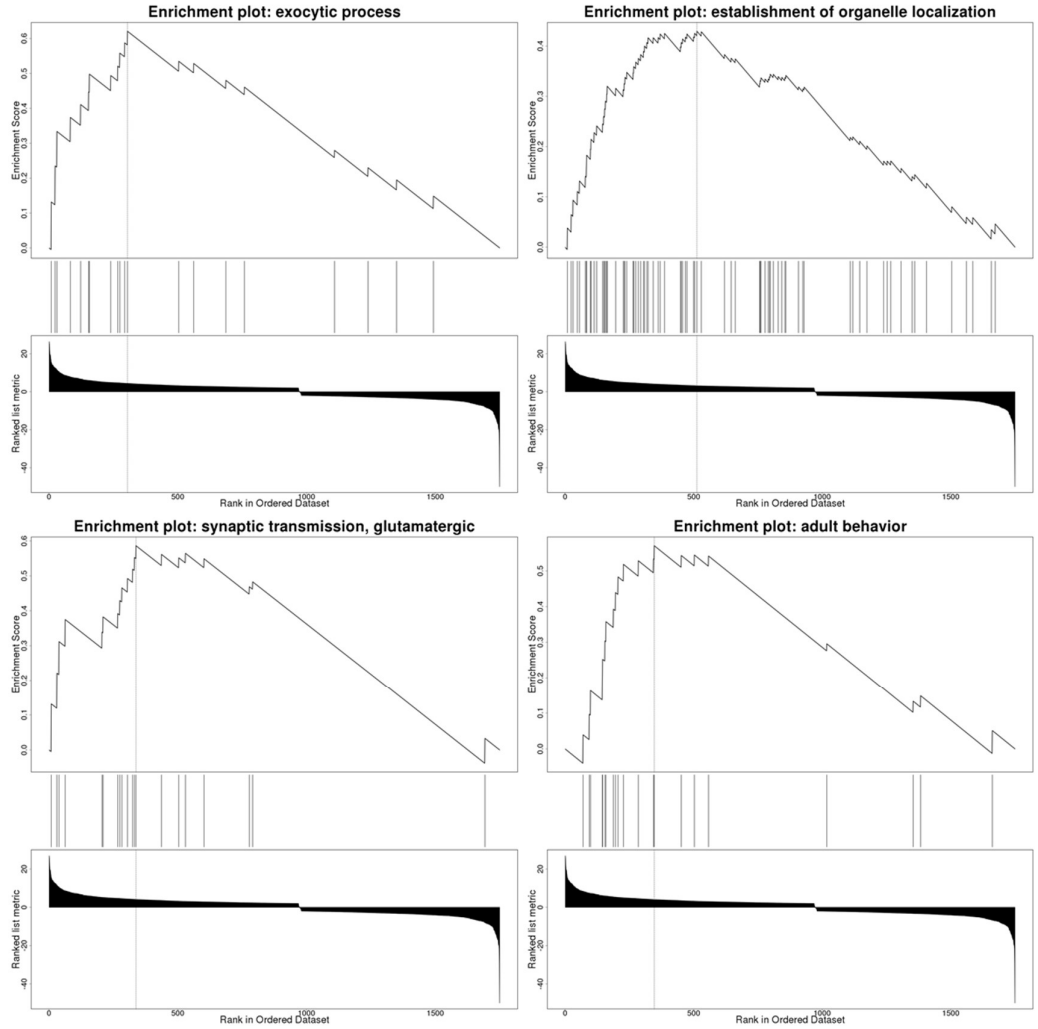
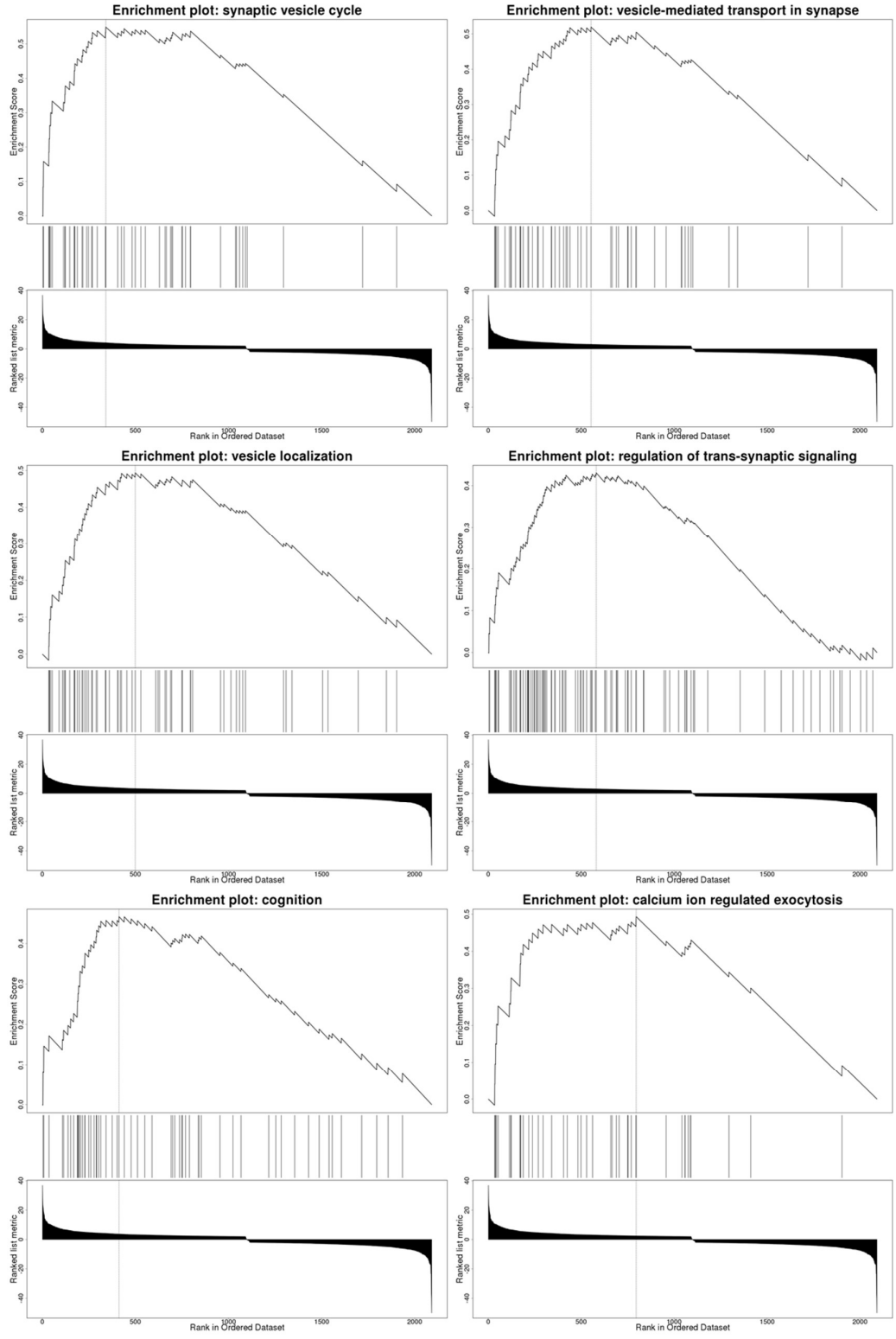


Figure 7.3.2 Enrichment plots for biological processes that are significantly enriched in gene list of differential expression between the control and clinical AD. Lines show 'hits' or genes at relevant rank in ordered dataset and resultant enrichment score. Produced by Webgestalt.

GO: gene set	GO: description	Leading Edge
0099177	**regulation of trans-synaptic signalling**	APBA2;ATP2A2;CADPS;CAMK2A;CPLX2;DNM1;GRIK5;NAPB;NLGN2;PFN2;PRKAR1B;PRKCG;PRRT2;RAB27B;RAB3A;SLC32A1;SNAP25;SNCA;STXBP1;SYN1;SYN3;SYP;SYT1;VAMP2
0099504	**synaptic vesicle cycle**	AP3S1;APBA2;ATP2A2;CADPS;CALY;CAMK2A;CLSTN1;CPLX1;CPLX2;DNM1;DVL1;GRIK5;GRIN3A;MAP2;NAPB;NLGN2;PACSIN1;PFN2;PRKCG;PRRT2;RAB27B;RAB3A;SNAP25;SNCA;SNCB;STXBP1;SYN1;SYP;SYT1;SYT5;TRIM9;VAMP2
0051648	**vesicle localization**	AP3S1;APBA2;ATP2A2;CADPS;CAMK2A;COL7A1;CPLX1;CPLX2;DCTN2;DNM1;DVL1;GRIK5;HTT;MAP2;NAPB;NLGN2;NSF;PAFAH1B1;PDCD6;PFN2;PRKCG;PRKCZ;PRRT2;RAB27B;RAB3A;SNAP25;SNCA;STXBP1;SYN1;SYN3;SYP;SYT1;SYT5;TRIM9;VAMP2
0050890	**cognition**	ABAT;APBA2;ATP2A2;CACNA1A;CALB1;CALB2;CAMK2A;CLSTN1;CLSTN3;CPLX1;CPLX2;DNM1;DRD5;DVL1;EFNB3;EPHA4;GRIK5;GRIN1;GRIN3A;JPH4;KCTD13;LGMN;LRFN2;MAPT;MEF2C;NAPB;NCDN;NETO1;NLGN2;NPTX2;NPTXR;NRGN;NSMF;NTNG1;PFN2;PLK2;PRKAR1B;PRKCG;PRKCZ;PRNP;PRRT2;PTK2B;RAB3A;SHANK1;SLC8A2;SNAP25;SNCA;SQSTM1;STAR;STXBP1;SYN1;SYN3;SYNGAP1;SYP;SYT1;TPRG1L;TUBB2B;VAMP2
0099003	**vesicle-mediated transport in synapse**	CALB1;CCK;CHL1;CNTNAP2;CRHBP;DRD5;GPI;GRIN1;HTT;JPH4;MAPT;MEF2C;NDRG4;NETO1;NPTX2;NRGN;NRXN2;PAFAH1B1;PJA2;PLK2;PRKAR1B;PRKCG;PRKCZ;PRNP;SERPINF1;SHANK1;SLC8A2;SNAP25
0017156	**calcium ion regulated exocytosis**	APBA2;ATP2A2;CADPS;CAMK2A;CDK5R2;CHRNB2;CNR1;CPLX1;CPLX2;DVL1;GRIK5;GRIN3A;NAPA;NAPB;PFN2;PPFIA3;PPP3CB;PRKCG;PRRT2;RAB3A;SDF4;SNAP25;STX1A;STX1B;STXBP1;SYN1;SYP;SYT1;SYT5;TRIM9;VAMP1;VAMP2
0140029	**exocytic process**	DVL1;GPR88;GRIN1;GRIN3A;JPH4;KCNAB2;MYH10;NEFL;NLGN2;PAFAH1B1;PRRT2;PSAP;SHANK1;UCHL1
0051656	**establishment of organelle localization**	CLSTN1;CLSTN3;GRASP;GRIN1;KLC1;LRRC7;MAPT;NLGN2;NRXN2;PRKCZ;RAB27B;SHANK1;SNAP25
0035249	**synaptic transmission, glutamatergic**	AP3S1;APBA2;ATP2A2;BICD2;CADPS;CAMK2A;CHGA;COL7A1;CPLX2;DCTN2;DNM1;GRIK5;HTT;MAP2;MAPT;MYH10;NAPB;NEFL;NSF;PAFAH1B1;PFN2;PRKCG;PRKCZ;PRRT2;RAB27B;RAB3A;SNAP25;SNCA;STXBP1;SYN1;SYP;SYT1;SYT5;TRIM9;UCHL1;VAMP2
0030534	**adult behaviour**	AGRN;C1QL3;CBLN2;CFL1;CHCHD10;CLSTN1;CLSTN3;DLGAP3;DVL1;EPHA4;FRMPD4;GRIN1;IL1RAP;LGMN;LRFN2;LZTS3;MAPT;MEF2C;MYH10;NEFL;NLGN2;NRXN2;NTNG1;PAFAH1B1;PCDH8;PCDHGC5;PFN2;PRNP;RAB3A;SHANK1;SNCA;SNCB;SPTBN2;SYN1;SYNGAP1;YWHAZ;ZNF365
0050886	endocrine process	ADAMTS2;ADAMTS9;AEBP1;ANTXR1;BMP1;CCN2;COL1A2;COL27A1;COL6A2;COL8A1;ECM2;ETS1;FLOT1;FN1;FOXC1;FOXF1;GFAP;GSN;HAPLN2;HPSE2;ITGA10;ITGA5;ITGAX;ITGB5;LCAT;PECAM1;PLTP;RGCC;SFRP2;SPARC;SPP1;VCAN
0061614	pri-miRNA transcription by RNA polymerase II	GPER1;MTRNR2L1;MTRNR2L8;RPS3
0043062	extracellular structure organization	C4A;CFH;CLU;FN1;HPR
0030856	regulation of epithelial cell differentiation	AZGP1;ERCC5;RPS27A
0007162	negative regulation of cell adhesion	PABPC1;PAIP2B;RPL10;RPL18;RPL21;RPL28;RPS2;RPS24;RPS27A;RPS3

Table 7.3.11 List of genes from GSEA analysis that have significantly different transcriptional expression in control and pathological AD in the ROSMAP dataset (based on CERAD score).


Enrichment plot: synaptic vesicle cycle
Enrichment plot: vesicle-mediated transport in synapse
Enrichment plot: vesicle localization
Enrichment plot: regulation of trans-synaptic signaling
Enrichment plot: cognition
Enrichment plot: calcium ion regulated exocytosis
Enrichment Score
Ranked list metric
Rank in Ordered Dataset

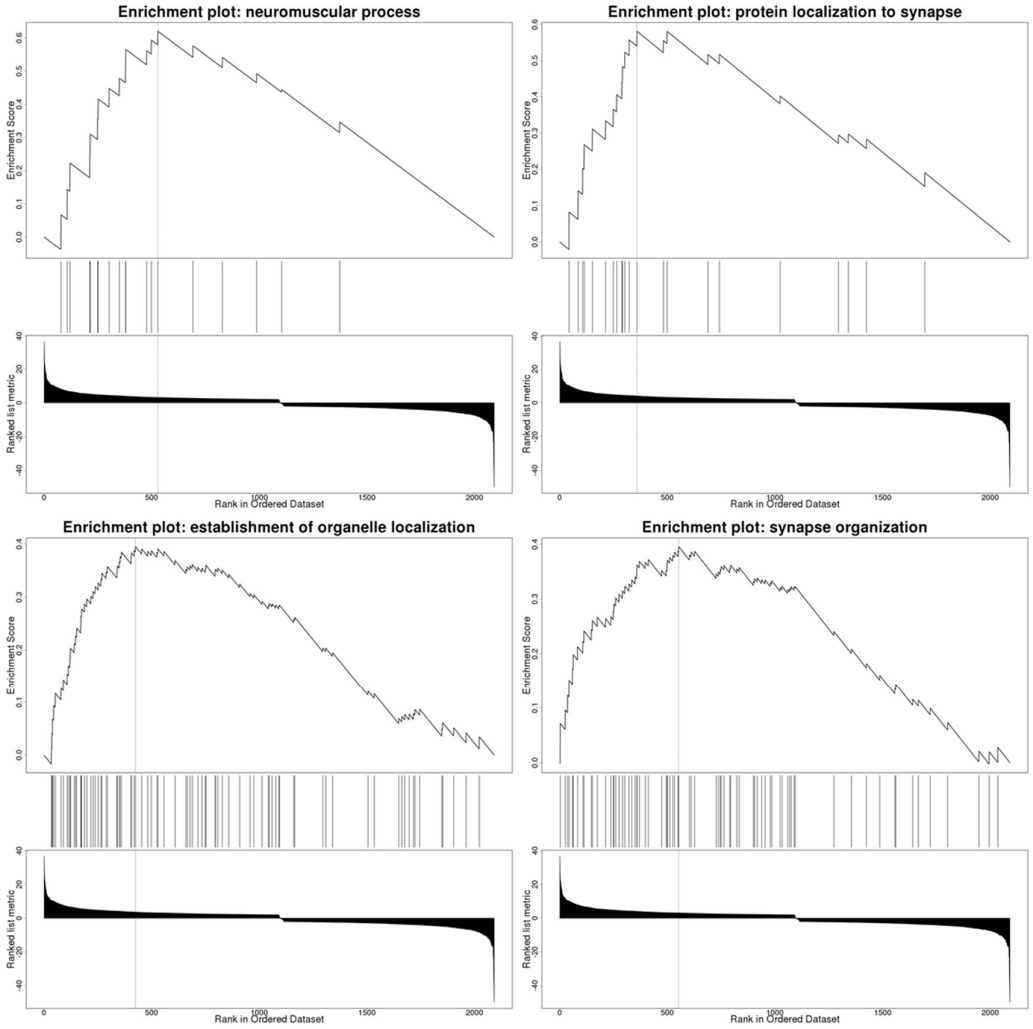
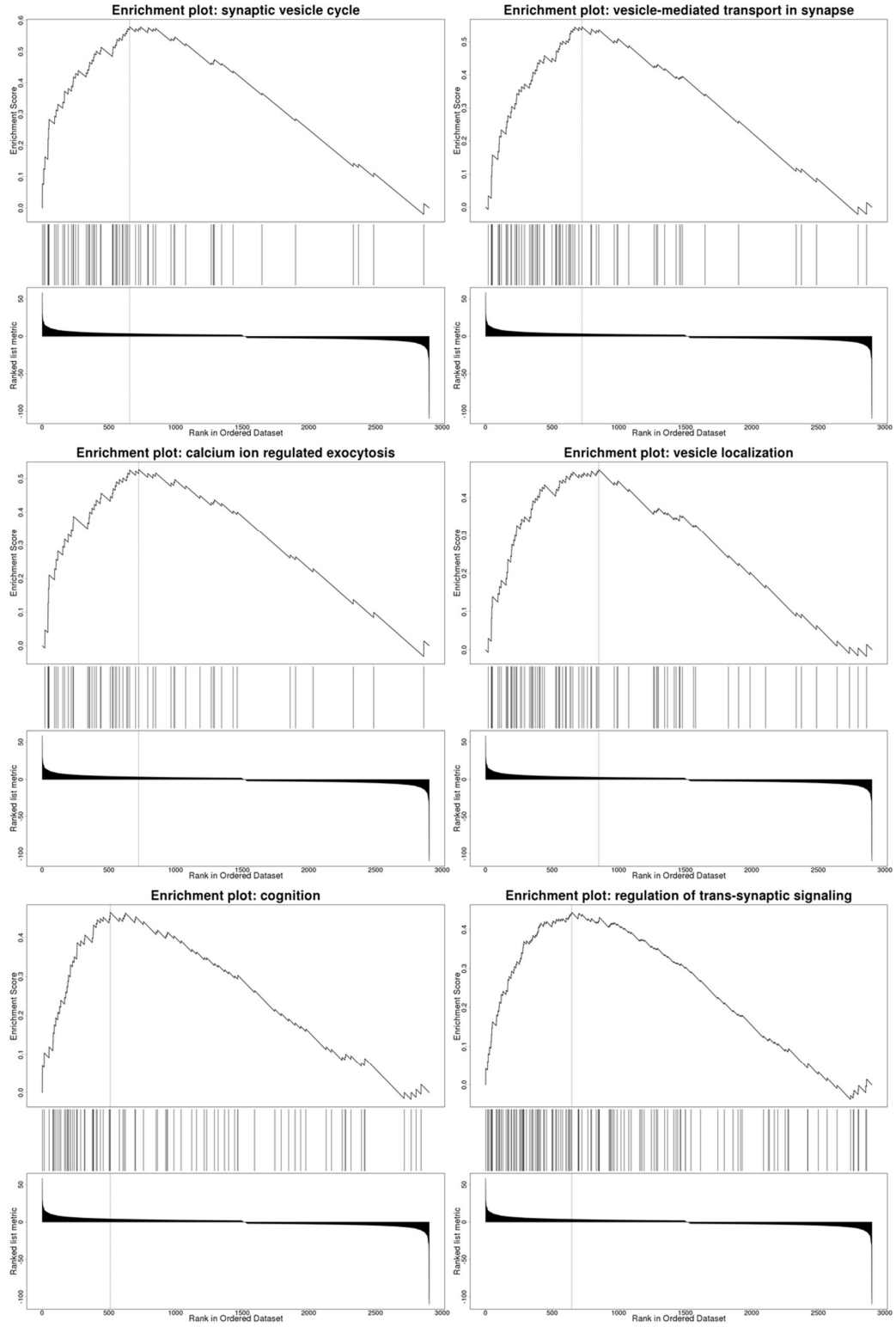


Figure 7.3.3 Enrichment plots for biological processes that are significantly enriched in gene list of differential expression between control and pathological AD (grouped by CERAD score). Lines show 'hits' or genes at relevant rank in ordered dataset and resultant enrichment score. Produced by Webgestalt.

GO: gene set	GO: description	Leading Edge
0099504	**synaptic vesicle cycle**	ACTG1;ADCY1;APBA2;ATP2A2;CADPS;CHRNB2;CPLX1;CPLX2;CPLX3;DNAJC5;DNM1;GRIK5;NAPA;NAPB;PACSIN1;PFN2;PPP3CB;PRKAR1B;PRKCG;PRRT2;RAB27B;RAB3A;SH3GL2;SLC17A7;SLC32A1;SNAP25;SNCA;SNCB;STX1B;STXBP1;SYN1;SYN2;SYN3;SYP;SYT1;SYT13;SYT4;SYT5;TRIM9;UNC13A;VAMP1;VAMP2
0099003	**vesicle-mediated transport in synapse**	ACTG1;ADCY1;AP3S1;APBA2;ARC;ATP2A2;CADPS;CALY;CHRNB2;CLSTN1;CNR1;CPLX1;CPLX2;CPLX3;DNAJC5;DNM1;DRD4;GRIK5;HPCA;MAP2;NAPA;NAPB;PACSIN1;PFN2;PPP3CB;PRKCG;PRRT2;RAB27B;RAB3A;SH3GL2;SLC17A7;SNAP25;SNCA;SNCB;STX1A;STX1B;STXBP1;SYN1;SYP;SYT1;SYT13;SYT4;SYT5;TRIM9;UNC13A;VAMP1;VAMP2
0017156	**calcium ion regulated exocytosis**	ADCY1;APBA2;ATP2A2;CADPS;CDK5R2;CHRNB2;CNR1;CPLX1;CPLX2;CPLX3;DNAJC5;GRIK5;NAPA;NAPB;PFN2;PPP3CB;PRKCG;PRRT2;RAB3A;SDF4;SNAP25;STX1A;STX1B;STXBP1;SYN1;SYP;SYT1;SYT13;SYT4;SYT5;TRIM9;UNC13A;VAMP1;VAMP2
0051648	**vesicle localization**	ADCY1;AP3S1;APBA2;ATP2A2;BRSK2;CADPS;CHRM2;CHRNB2;CNR1;COL7A1;CPLX1;CPLX2;CPLX3;DCTN2;DNAJC5;DNM1;GRIK5;HTT;MAP2;NAPA;NAPB;NDEL1;NLGN2;NSF;PAFAH1B1;PDCD6;PFN2;PRKCG;PRKCZ;PRRT2;RAB27B;RAB3A;RIMS3;SNAP25;SNCA;STX1A;STX1B;STXBP1;STXBP5L;SYN1;SYN2;SYN3;SYP;SYT1;SYT13;SYT4;SYT5;TRAPPC9;TRIM9;UNC13A;VAMP1;VAMP2;VPS33B
0050890	**cognition**	ARC;CALB1;CAMK4;CCK;CHL1;CHRM1;CHRNB2;CNTNAP2;GPI;GPR88;GRIN1;HTT;JPH4;LGMN;MAPT;MEF2C;NDRG4;NETO1;NPTX2;NRGN;NRXN2;NTRK2;PAFAH1B1;PJA2;PLCB1;PLK2;PPP3CB;PRKAR1B;PRKCG;PRKCZ;PRNP;PTGS2;SERPINF1;SLC8A2;SNAP25;TUSC3
0099177	**regulation of trans-synaptic signalling**	ABAT;ADCY1;APBA2;ARC;ATP2A2;CACNA1A;CACNG3;CALB1;CHRNB2;CLSTN1;CLSTN3;CPLX1;CPLX2;CPLX3;DBN1;DNM1;DRD4;EFNB3;EPHA4;FABP5;GRIK5;GRIN1;JPH4;LGMN;LRFN2;MAPT;MEF2C;NAPA;NAPB;NCDN;NETO1;NPTX2;NPTXR;NRGN;NTRK2;PFN2;PLCB1;PLK2;PNKD;PPP3CB;PRKAR1B;PRKCG;PRKCZ;PRNP;PRRT2;PTGS2;PTK2B;RAB3A;RGS4;SLC8A2;SNAP25;SNCA;STAR;STX1B;STXBP1;SYN1;SYN3;SYNGR1;SYP;SYT1;SYT4;TUBB2B;UNC13A;VAMP1;VAMP2
0015837	**amine transport**	ABAT;CCK;CHGA;CHRNB2;CNR1;CXCL12;DRD4;RGS4;SNCA;STX1A;STXBP1;SYT1;SYT13;SYT4;SYT5
0015844	**monoamine transport**	ABAT;ACTB;CHGA;CHRNB2;CNR1;CXCL12;DRD4;HTR1A;SNCA;STX1A;SYT1;SYT13;SYT4;SYT5
0140029	**exocytic process**	CPLX1;CPLX2;CPLX3;NAPA;NAPB;PRRT2;RAB3A;RAB3C;SNAP25;STX1B;STXBP1;SYT1;UNC13A;VAMP1;VAMP2;VPS33B
0051656	**establishment of organelle localization**	ADCY1;AP3S1;APBA2;ATP2A2;ATP6AP1;CADPS;CDC42;CDCA5;CENPF;CHGA;CHRNB2;COL7A1;CPLX1;CPLX2;CPLX3;DCTN2;DNAJC5;DNM1;GRIK5;HTT;MAP2;MAPT;MYH10;NAPA;NAPB;NEFL;NSF;PAFAH1B1;PDCD6;PFN2;PRKCG;PRKCZ;PRRT2;PTK2;RAB27B;RAB3A;SNAP25;SNCA;STX1B;STXBP1;SYN1;SYP;SYT1;SYT13;SYT4;SYT5;TRIM9;UBB;UCHL1;UNC13A;VAMP1;VAMP2;YWHAZ
0042063	gliogenesis	APP;ASCL1;BACE2;CDKN2C;CLU;CNTN2;CSF1;DAAM2;DLL1;EGFR;ERBB3;GFAP;GLI3;GSN;HDAC1;HDAC10;HES1;ID4;KCNJ10;KLF15;LAMB2;LPAR1;LRP2;MMP14;MT3;MYRF;NFIB;NKX22;NOTCH1;OLIG1;OLIG2;PAX6;PHGDH;PLP1;POU3F2;PPP1CC;RELA;RHOA;SLC45A3;SMO;SRSF1;SUN2;TAL1;TLR4
0007265	Ras protein signal transduction	ABCA1;APOE;ARHGAP29;ARHGAP42;ARHGAP5;ARHGEF37;ARHGEF40;COL1A2;CSF1;DNM2;DOK3;GNA12;GNA13;GPR4;GPSM2;GRAP;ITPKB;KANK2;LPAR1;MAP4K4;MAPKAP1;MCF2L2;MRAS;NOTCH2;PDGFRB;PECAM1;PREX1;PSD2;RAB13;RAB20;RAB29;RAB9A;RAPGEF3;RHOA;RHOC;RHOJ;RHOQ;RHOU;RREB1;RTKN;SOS2;TAX1BP3;VANGL2;VAV2;VAV3
0007389	pattern specification process	ASCL1;COBL;CRB2;DAAM2;DLL1;DLL4;EMX2;FOXC1;FOXD1;FOXF1;FOXJ1;GDF11;HES1;HIPK2;LRP2;LRP4;MSX1;RFX4;SEMA3F;SFRP2;SMAD6;SMARCD3;SMO;STC1;TBX18;TBX6
0045785	positive regulation of cell adhesion	ADA;CARD11;CD74;COL16A1;COL8A1;CSF1;DNM2;DOCK1;DOCK5;EBI3;ECM2;EMID1;EMP2;ETS1;FOXC2;FOXF1;GLI3;GPAM;HES1;HLADMB;HLADPA1;HLADPB1;ICAM1;IQGAP1;ITGA5;ITPKB;JUP;LGALS9;MAP4K4;MMRN2;PREX1;RELA;RHOA;RREB1;SASH3;SFRP2;TGM2;VAV3;VEGFA;VSIR;ZBTB1
0002064	epithelial cell development	ARHGEF26;ARID4A;BMP6;CLDN5;DLL1;EPHA2;EZR;FAT1;FOXJ1;GPR4;GSTM3;HAPLN2;ICAM1;IQGAP1;LAMB2;MYO1E;NKX22;NOTCH1;NOTCH4;PAX6;PECAM1;PGR;RAB13;RAPGEF3;SCRIB;SMO;SOX8;STC1;TJP1;VEZF1;WHRN

Table 7.3.12 List of genes from GSEA analysis that have significantly different transcriptional expression in control and SCI groups of the ROSMAP dataset (based on MMSE score).


Enrichment plot: synaptic vesicle cycle
Enrichment plot: vesicle-mediated transport in synapse
Enrichment plot: calcium ion regulated exocytosis
Enrichment plot: vesicle localization
Enrichment plot: cognition
Enrichment plot: regulation of trans-synaptic signaling
Enrichment Score
Ranked list metric
Rank in Ordered Dataset

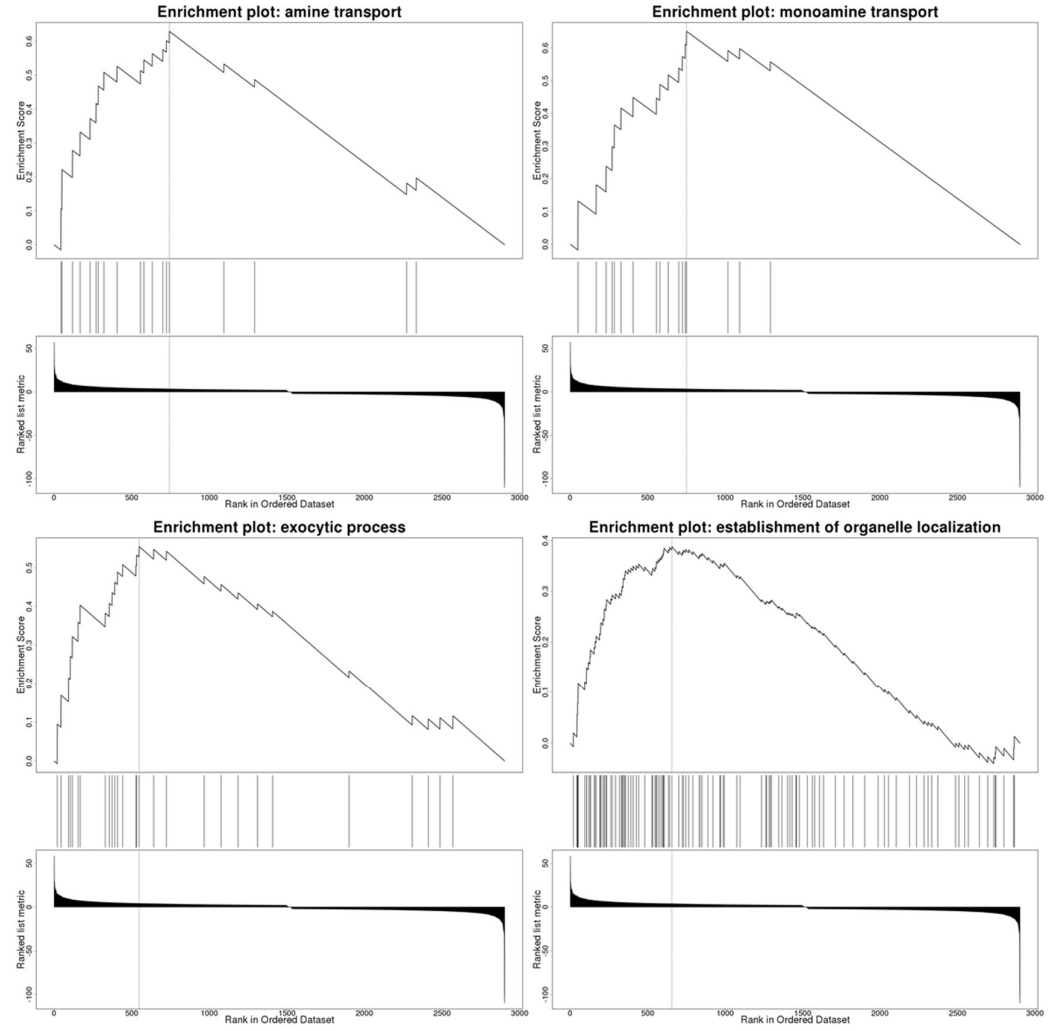


Figure 7.3.4 Enrichment plots for biological processes that are significantly enriched in gene list of differential expression between the NCI and SCI (grouped by MMSE score). Lines show 'hits' or genes at relevant rank in ordered dataset and resultant enrichment score. Produced by Webgestalt.

References

Abbassi R, Johns TG, Kassiou M & Munoz L. (2015). DYRK1A in neurodegeneration and cancer: Molecular basis and clinical implications. *Pharmacology & Therapeutics* **151,** 87-98.

Adusumalli S, Ngian ZK, Lin WQ, Benoukraf T & Ong CT. (2019). Increased intron retention is a post-transcriptional signature associated with progressive aging and Alzheimer's disease. *Aging Cell* **18,** e12928.

Al-Ali H, Ding Y, Slepak T, Wu W, Sun Y, Martinez Y, Xu XM, Lemmon VP & Bixby JL. (2017). The mTOR Substrate S6 Kinase 1 (S6K1) Is a Negative Regulator of Axon Regeneration and a Potential Drug Target for Central Nervous System Injury. *J Neurosci* **37,** 7079-7095.

Alkallas R, Fish L, Goodarzi H & Najafabadi HS. (2017). Inference of RNA decay rate from transcriptional profiling highlights the regulatory programs of Alzheimer's disease. *Nat Commun* **8,** 909.

Allen C, Horton K, Malhi N, Batson J & Bates D. (2017). The SRPK1 inhibitor SPHINX31 prevents increased retinal permeability in a rodent model of diabetes. *Acta Ophthalmologica* **95**.

Altafaj X, Dierssen M, Baamonde C, Martí E, Visa J, Guimerà J, Oset M, González JR, Flórez J, Fillat C & Estivill X. (2001). Neurodevelopmental delay, motor abnormalities and cognitive deficits in transgenic mice overexpressing Dyrk1A (minibrain), a murine model of Down's syndrome. *Hum Mol Genet* **10,** 1915-1923.

Alzheimer A, Stelzmann R, Schnitzlein H & Murtagh F. (1995). An English translation of Alzheimer's 1907 paper, "Uber eine eigenartige Erkankung der Hirnrinde", pp. 429-431. Clinical Anatomy.

Amador-Ortiz C, Lin WL, Ahmed Z, Personett D, Davies P, Duara R, Graff-Radford NR, Hutton ML & Dickson DW. (2007). TDP-43 immunoreactivity in hippocampal sclerosis and Alzheimer's disease. *Ann Neurol* **61,** 435-445.

Amin EM, Oltean S, Hua J, Gammons MVR, Hamdollah-Zadeh M, Welsh GI, Cheung MK, Ni L, Kase S, Renne ES, Symonds KE, Nowak DG, Royer-Pokora B, Saleem MA, Hagiwara M, Schumacher VA, Harper SJ, Hinton DR, Bates DO & Ladomery MR. (2011). WT1 Mutants Reveal SRPK1 to Be a Downstream Angiogenesis Target by Altering VEGF Splicing. *Cancer Cell* **20,** 768-780.

Anandatheerthavarada HK, Biswas G, Robin M-A & Avadhani NG. (2003). Mitochondrial targeting and a novel transmembrane arrest of Alzheimer's amyloid precursor protein impairs mitochondrial function in neuronal cells. *Journal of Cell Biology* **161,** 41-54.

Anderson RM, Hadjichrysanthou C, Evans S & Wong MM. (2017). Why do so many clinical trials of therapies for Alzheimer's disease fail? *Lancet* **390,** 2327-2329.

Andreadis A. (2005). Tau gene alternative splicing: expression patterns, regulation and modulation of function in normal brain and neurodegenerative diseases. *Biochim Biophys Acta* **1739,** 91-103.

Angarola BL & Anczuków O. (2021). Splicing alterations in healthy aging and disease. *Wiley Interdiscip Rev RNA***,** e1643.

Annese A, Manzari C, Lionetti C, Picardi E, Horner DS, Chiara M, Caratozzolo MF, Tullo A, Fosso B, Pesole G & D'Erchia AM. (2018). Whole transcriptome profiling of Late-Onset Alzheimer's Disease patients provides insights into the molecular changes involved in the disease. *Scientific Reports* **8,** 4282.

Araki S, Dairiki R, Nakayama Y, Murai A, Miyashita R, Iwatani M, Nomura T & Nakanishi O. (2015). Inhibitors of CLK protein kinases suppress cell growth and induce apoptosis by modulating pre-mRNA splicing. *PLoS One* **10,** e0116929.

Arber C, Lovejoy C & Wray S. (2017). Stem cell models of Alzheimer's disease: progress and challenges. *Alzheimers Res Ther* **9,** 42.

Arbones ML, Thomazeau A, Nakano-Kobayashi A, Hagiwara M & Delabar JM. (2019). DYRK1A and cognition: A lifelong relationship. *Pharmacol Ther* **194,** 199-221.

Armstrong RA, Lantos PL & Cairns NJ. (2005). Overlap between neurodegenerative disorders. *Neuropathology* **25,** 111-124.

Ashford JW. (2015). Treatment of Alzheimer's Disease: The Legacy of the Cholinergic Hypothesis, Neuroplasticity, and Future Directions. *J Alzheimers Dis* **47,** 149-156.

Aubol BE, Jamros MA, McGlone ML & Adams JA. (2013). Splicing Kinase SRPK1 Conforms to the Landscape of Its SR Protein Substrate. *Biochemistry* **52,** 7595-7605.

Aubol Brandon E, Plocinik Ryan M, Keshwani Malik M, McGlone Maria L, Hagopian Jonathan C, Ghosh G, Fu X-D & Adams Joseph A. (2014). N-terminus of the protein kinase CLK1 induces SR protein hyperphosphorylation. *Biochemical Journal* **462,** 143-152.

Aubol BE, Wu G, Keshwani MM, Movassat M, Fattet L, Hertel KJ, Fu XD & Adams JA. (2016). Release of SR Proteins from CLK1 by SRPK1: A Symbiotic Kinase System for Phosphorylation Control of Pre-mRNA Splicing. *Mol Cell* **63,** 218-228.

Avila J, Lucas JJ, Perez M & Hernandez F. (2004). Role of tau protein in both physiological and pathological conditions. *Physiol Rev* **84,** 361-384.

Bai B, Hales CM, Chen PC, Gozal Y, Dammer EB, Fritz JJ, Wang X, Xia Q, Duong DM, Street C, Cantero G, Cheng D, Jones DR, Wu Z, Li Y, Diner I, Heilman CJ, Rees HD, Wu H, Lin L, Szulwach KE, Gearing M, Mufson EJ, Bennett DA, Montine TJ, Seyfried NT, Wingo TS, Sun YE, Jin P, Hanfelt J, Willcock DM, Levey A, Lah JJ & Peng J. (2013). U1 small nuclear ribonucleoprotein complex and RNA splicing alterations in Alzheimer's disease. *Proc Natl Acad Sci U S A* **110,** 16562-16567.

Balliu B, Durrant M, de Goede O, Abell N, Li X, Liu B, Gloudemans M, Cook N, Smith K, Knowles D, Pala M, Cucca F, Schlessinger D, Jaiswal S, Sabatti C, Lind L, Ingelsson E & Montgomery S. (2019). Genetic regulation of gene expression and splicing during a 10-year period of human aging. *Genome Biology* **20**.

Ballmer-Hofer K, Andersson AE, Ratcliffe LE & Berger P. (2011). Neuropilin-1 promotes VEGFR-2 trafficking through Rab11 vesicles thereby specifying signal output. *Blood* **118,** 816-826.

Bancher C, Brunner C, Lassmann H, Budka H, Jellinger K, Wiche G, Seitelberger F, Grundke-Iqbal I, Iqbal K & Wisniewski HM. (1989). Accumulation of abnormally phosphorylated tau precedes the formation of neurofibrillary tangles in Alzheimer's disease. *Brain Res* **477,** 90-99.

Barnes DE & Yaffe K. (2011). The projected effect of risk factor reduction on Alzheimer's disease prevalence. *Lancet Neurol* **10,** 819-828.

Bates DO, Cui TG, Doughty JM, Winkler M, Sugiono M, Shields JD, Peat D, Gillatt D & Harper SJ. (2002). VEGF(165)b, an inhibitory splice variant of vascular endothelial growth factor, is down-regulated in renal cell carcinoma. *Cancer Research* **62,** 4123-4131.

Bates DO, Morris JC, Oltean S & Donaldson LF. (2017). Pharmacology of Modulators of Alternative Splicing. *Pharmacological reviews* **69,** 63-79.

Batson J, Toop HD, Redondo C, Babaei-Jadidi R, Chaikuad A, Wearmouth SF, Gibbons B, Allen C, Tallant C, Zhang J, Du C, Hancox JC, Hawtrey T, Da Rocha J, Griffith R, Knapp S, Bates DO & Morris JC. (2017). Development of Potent, Selective SRPK1 Inhibitors as Potential Topical Therapeutics for Neovascular Eye Disease. *ACS Chem Biol* **12,** 825-832.

Bayer AJ, Bullock R, Jones RW, Wilkinson D, Paterson KR, Jenkins L, Millais SB & Donoghue S. (2005). Evaluation of the safety and immunogenicity of synthetic Abeta42 (AN1792) in patients with AD. *Neurology* **64,** 94-101.

Beazley-Long N, Hua J, Jehle T, Hulse RP, Dersch R, Lehrling C, Bevan H, Qiu Y, Lagreze WA, Wynick D, Churchill AJ, Kehoe P, Harper SJ, Bates DO & Donaldson LF. (2013). VEGF-A(165)b Is an Endogenous Neuroprotective Splice Isoform of Vascular Endothelial Growth Factor A in Vivo and in Vitro. *American Journal of Pathology* **183,** 918-929.

Becker W, Weber Y, Wetzel K, Eirmbter K, Tejedor FJ & Joost HG. (1998). Sequence characteristics, subcellular localization, and substrate specificity of DYRK-related kinases, a novel family of dual specificity protein kinases. *J Biol Chem* **273,** 25893-25902.

Belin S, Nawabi H, Wang C, Tang S, Latremoliere A, Warren P, Schorle H, Uncu C, Woolf CJ, He Z & Steen JA. (2015). Injury-induced decline of intrinsic regenerative ability revealed by quantitative proteomics. *Neuron* **86,** 1000-1014.

Bennett DA, Buchman AS, Boyle PA, Barnes LL, Wilson RS & Schneider JA. (2018). Religious Orders Study and Rush Memory and Aging Project. *J Alzheimers Dis* **64,** S161-s189.

Bennett DA, Schneider JA, Arvanitakis Z & Wilson RS. (2012). Overview and findings from the religious orders study. *Curr Alzheimer Res* **9,** 628-645.

Berchtold NC, Sabbagh MN, Beach TG, Kim RC, Cribbs DH & Cotman CW. (2014). Brain gene expression patterns differentiate mild cognitive impairment from normal aged and Alzheimer's disease. *Neurobiology of aging* **35,** 1961-1972.

Bernabeu-Zornoza A & Zambrano A. (2019). Physiological and pathological effects of amyloid-β species in neural stem cell biology. *Neural Regeneration Research* **14**.

Berridge MJ. (2009). Inositol trisphosphate and calcium signalling mechanisms. *Biochimica et Biophysica Acta (BBA) - Molecular Cell Research* **1793,** 933-940.

Berson A, Barbash S, Shaltiel G, Goll Y, Hanin G, Greenberg DS, Ketzef M, Becker AJ, Friedman A & Soreq H. (2012). Cholinergic-associated loss of hnRNP-A/B in Alzheimer's disease impairs cortical splicing and cognitive function in mice. *EMBO Mol Med* **4,** 730-742.

Bhowmick S, D'Mello V & Abdul-Muneer PM. (2019). Synergistic Inhibition of ERK1/2 and JNK, Not p38, Phosphorylation Ameliorates Neuronal Damages After Traumatic Brain Injury. *Mol Neurobiol* **56,** 1124-1136.

Biamonti G, Amato A, Belloni E, Di Matteo A, Infantino L, Pradella D & Ghigna C. (2019). Alternative splicing in Alzheimer's disease. *Aging Clin Exp Res*.

Bidinosti M, Botta P, Krüttner S, Proenca CC, Stoehr N, Bernhard M, Fruh I, Mueller M, Bonenfant D, Voshol H, Carbone W, Neal SJ, McTighe SM, Roma G, Dolmetsch RE, Porter JA, Caroni P, Bouwmeester T, Lüthi A & Galimberti I. (2016). CLK2 inhibition ameliorates autistic features associated with SHANK3 deficiency. *Science* **351,** 1199-1203.

Biselli-Chicote PM, Biselli J, Cunha B, Castro R, Maniglia JV, Neto DdS, Tajara EH, Góis Filho JFd, Fukuyama EE, Pavarino ÉC & Goloni-Bertollo EM. (2017). Overexpression of Antiangiogenic Vascular Endothelial Growth Factor Isoform and Splicing Regulatory Factors in Oral, Laryngeal and Pharyngeal Squamous Cell Carcinomas. *Asian Pacific Journal of Cancer Prevention* **18,** 2171-2177.

Boban M, Babic Leko M, Miskic T, Hof PR & Simic G. (2019). Human neuroblastoma SH-SY5Y cells treated with okadaic acid express phosphorylated high molecular weight tau-immunoreactive protein species. *J Neurosci Methods* **319,** 60-68.

Bogetti ME, Pozo Devoto VM, Rapacioli M, Flores V & Fiszer de Plazas S. (2018). NGF, TrkA-P and neuroprotection after a hypoxic event in the developing central nervous system. *Int J Dev Neurosci* **71,** 111-121.

Bonello S, Zahringer C, BelAiba RS, Djordjevic T, Hess J, Michiels C, Kietzmann T & Gorlach A. (2007). Reactive oxygen species activate the HIF-1alpha promoter via a functional NFkappaB site. *Arterioscler Thromb Vasc Biol* **27,** 755-761.

Bossers K, Wirz KTS, Meerhoff GF, Essing AHW, van Dongen JW, Houba P, Kruse CG, Verhaagen J & Swaab DF. (2010). Concerted changes in transcripts in the prefrontal cortex precede neuropathology in Alzheimer's disease. *Brain* **133,** 3699-3723.

Bowler E & Oltean S. (2019). Alternative Splicing in Angiogenesis. *International journal of molecular sciences* **20,** 2067.

Boyce JJ & Shea TB. (1997). Phosphorylation events mediated by protein kinase C alpha and epsilon participate in regulation of tau steady-state levels and generation of certain "Alzheimer-like" phospho-epitopes. *Int J Dev Neurosci* **15,** 295-307.

Braak H & Braak E. (1991). Neuropathological stageing of Alzheimer-related changes. *Acta Neuropathol* **82,** 239-259.

Bruno V, Black R, Leon JT, Nick CF, Daniels M, McLennan G, Tompkins C, Leibman C & Grundman MPaM. (2009). Long-Term Follow-Up of Patients Immunized with AN1792: Reduced Functional Decline in Antibody Responders. *Current Alzheimer Research* **6,** 144-151.

Bruns AF, Herbert SP, Odell AF, Jopling HM, Hooper NM, Zachary IC, Walker JH & Ponnambalam S. (2010). Ligand-Stimulated VEGFR2 Signaling is Regulated by Co-Ordinated Trafficking and Proteolysis. *Traffic* **11,** 161-174.

Bryant AG, Hu M, Carlyle BC, Arnold SE, Frosch MP, Das S, Hyman BT & Bennett RE. (2020). Cerebrovascular Senescence Is Associated With Tau Pathology in Alzheimer's Disease. *Front Neurol* **11,** 575953.

Bullock N & Oltean S. (2017). The many faces of SRPK1. *The Journal of pathology* **241,** 437-440.

Carmeliet P & Storkebaum E. (2002). Vascular and neuronal effects of VEGF in the nervous system: implications for neurological disorders. *Seminars in Cell & Developmental Biology* **13,** 39-53.

Caughey B & Lansbury PT. (2003). Protofibrils, pores, fibrils, and neurodegeneration: separating the responsible protein aggregates from the innocent bystanders. *Annu Rev Neurosci* **26,** 267-298.

Chakraborty A, Chatterjee M, Twaalfhoven H, Del Campo Milan M, Teunissen CE, Scheltens P, Fontijn RD, van Der Flier WM & de Vries HE. (2018). Vascular Endothelial Growth Factor remains unchanged in cerebrospinal fluid of patients with Alzheimer's disease and vascular dementia. *Alzheimers Res Ther* **10,** 58.

Chan CB & Ye K. (2013). Serine-arginine protein kinases: New players in neurodegenerative diseases? *Reviews in the neurosciences* **24,** 1-13.

Chappell S, Patel T, Guetta-Baranes T, Sang F, Francis PT, Morgan K & Brookes KJ. (2018). Observations of extensive gene expression differences in the cerebellum and potential relevance to Alzheimer's disease. *BMC Res Notes* **11,** 646.

Cheignon C, Tomas M, Bonnefont-Rousselot D, Faller P, Hureau C & Collin F. (2018). Oxidative stress and the amyloid beta peptide in Alzheimer's disease. *Redox Biol* **14,** 450-464.

Chen C, Jin N, Qian W, Liu W, Tan X, Ding F, Gu X, Iqbal K, Gong CX, Zuo J & Liu F. (2014). Cyclic AMP-dependent protein kinase enhances SC35-promoted Tau exon 10 inclusion. *Mol Neurobiol* **49,** 615-624.

Chen H, Yang J, Low PS & Cheng J-X. (2008). Cholesterol Level Regulates Endosome Motility via Rab Proteins. *Biophysical Journal* **94,** 1508-1520.

Chen X-Q & Mobley WC. (2019). Alzheimer Disease Pathogenesis: Insights From Molecular and Cellular Biology Studies of Oligomeric Aβ and Tau Species. *Frontiers in Neuroscience* **13,** 659.

Chen Y, Fu AKY & Ip NY. (2019). Synaptic dysfunction in Alzheimer's disease: Mechanisms and therapeutic strategies. *Pharmacol Ther* **195,** 186-198.

Claesson-Welsh L & Welsh M. (2013). VEGFA and tumour angiogenesis. *J Intern Med* **273,** 114-127.

Clark LN, Poorkaj P, Wszolek Z, Geschwind DH, Nasreddine ZS, Miller B, Li D, Payami H, Awert F, Markopoulou K, Andreadis A, D'Souza I, Lee VM, Reed L, Trojanowski JQ, Zhukareva V, Bird T, Schellenberg G & Wilhelmsen KC. (1998). Pathogenic implications of mutations in the tau gene in pallido-ponto-nigral degeneration and related neurodegenerative disorders linked to chromosome 17. *Proc Natl Acad Sci U S A* **95,** 13103-13107.

Colasanti T, Barbati C, Rosano G, Malorni W & Ortona E. (2010). Autoantibodies in patients with Alzheimer's disease: pathogenetic role and potential use as biomarkers of disease progression. *Autoimmun Rev* **9,** 807-811.

Colwill K, Pawson T, Andrews B, Prasad J, Manley JL, Bell JC & Duncan PI. (1996). The Clk/Sty protein kinase phosphorylates SR splicing factors and regulates their intranuclear distribution. *The EMBO journal* **15,** 265-275.

Corder EH, Saunders AM, Strittmatter WJ, Schmechel DE, Gaskell PC, Small GW, Roses AD, Haines JL & Pericak-Vance MA. (1993). Gene dose of apolipoprotein E type 4 allele and the risk of Alzheimer's disease in late onset families. *Science* **261,** 921.

Czubaty A & Piekiełko-Witkowska A. (2017). Protein kinases that phosphorylate splicing factors: Roles in cancer development, progression and possible therapeutic options. *Int J Biochem Cell Biol* **91,** 102-115.

D'Souza GX, Rose SE, Knupp A, Nicholson DA, Keene CD & Young JE. (2021). The application of in vitro-derived human neurons in neurodegenerative disease modeling. *J Neurosci Res* **99,** 124-140.

Daniilidou M, Tsolaki M, Giannakouros T & Nikolakaki E. (2011). Detection of elevated antibodies against SR protein kinase 1 in the serum of Alzheimer's disease patients. *Journal of Neuroimmunology* **238,** 67-72.

De Jager PL, Ma Y, McCabe C, Xu J, Vardarajan BN, Felsky D, Klein H-U, White CC, Peters MA, Lodgson B, Nejad P, Tang A, Mangravite LM, Yu L, Gaiteri C, Mostafavi S, Schneider JA & Bennett DA. (2018). A multi-omic atlas of the human frontal cortex for aging and Alzheimer's disease research. *Scientific Data* **5,** 180142.

de Medeiros LM, De Bastiani MA, Rico EP, Schonhofen P, Pfaffenseller B, Wollenhaupt-Aguiar B, Grun L, Barbé-Tuana F, Zimmer ER, Castro MAA, Parsons RB & Klamt F. (2019). Cholinergic Differentiation of Human Neuroblastoma SH-SY5Y Cell Line and Its Potential Use as an In vitro Model for Alzheimer's Disease Studies. *Mol Neurobiol* **56,** 7355-7367.

De Strooper B. (2014). Lessons from a failed γ-secretase Alzheimer trial. *Cell* **159,** 721-726.

De Strooper B, Saftig P, Craessaerts K, Vanderstichele H, Guhde G, Annaert W, Von Figura K & Van Leuven F. (1998). Deficiency of presenilin-1 inhibits the normal cleavage of amyloid precursor protein. *Nature* **391,** 387-390.

Del Bo R, Ghezzi S, Scarpini E, Bresolin N & Comi GP. (2009). VEGF genetic variability is associated with increased risk of developing Alzheimer's disease. *Journal of the Neurological Sciences* **283,** 66-68.

Delabar JM, Ortner M, Simon S, Wijkhuisen A, Feraudet-Tarisse C, Pegon J, Vidal E, Hirschberg Y, Dubois B & Potier MC. (2020). Altered age-linked regulation of plasma DYRK1A in elderly cognitive complainers (INSIGHT-preAD study) with high brain amyloid load. *Alzheimers Dement (N Y)* **6,** e12046.

Delatorre JC & Mussivand T. (1993). CAN DISTURBED BRAIN MICROCIRCULATION CAUSE ALZHEIMERS-DISEASE. *Neurological Research* **15,** 146-153.

DeMattos RB, Bales KR, Cummins DJ, Dodart JC, Paul SM & Holtzman DM. (2001). Peripheral anti-A beta antibody alters CNS and plasma A beta clearance and decreases brain A beta burden in a mouse model of Alzheimer's disease. *Proc Natl Acad Sci U S A* **98,** 8850-8855.

Devi L, Prabhu BM, Galati DF, Avadhani NG & Anandatheerthavarada HK. (2006). Accumulation of amyloid precursor protein in the mitochondrial import channels of human Alzheimer's disease brain is associated with mitochondrial dysfunction. *J Neurosci* **26,** 9057-9068.

Di Santo SG, Prinelli F, Adorni F, Caltagirone C & Musicco M. (2013). A meta-analysis of the efficacy of donepezil, rivastigmine, galantamine, and memantine in relation to severity of Alzheimer's disease. *J Alzheimers Dis* **35,** 349-361.

Ding S, Shi J, Qian W, Iqbal K, Grundke-Iqbal I, Gong C-X & Liu F. (2012). Regulation of alternative splicing of tau exon 10 by 9G8 and Dyrk1A. *Neurobiology of aging* **33,** 1389-1399.

Dominguez D, Tsai Y-H, Weatheritt R, Wang Y, Blencowe BJ & Wang Z. (2016). An extensive program of periodic alternative splicing linked to cell cycle progression. *eLife* **5,** e10288.

Donahue CP, Muratore C, Wu JY, Kosik KS & Wolfe MS. (2006). Stabilization of the tau exon 10 stem loop alters pre-mRNA splicing. *The Journal of biological chemistry* **281,** 23302-23306.

Doody RS, Raman R, Farlow M, Iwatsubo T, Vellas B, Joffe S, Kieburtz K, He F, Sun X, Thomas RG, Aisen PS, Siemers E, Sethuraman G & Mohs R. (2013). A phase 3 trial of semagacestat for treatment of Alzheimer's disease. *N Engl J Med* **369,** 341-350.

Draberova E, Lukas Z, Ivanyi D, Viklicky V & Draber P. (1998). Expression of class III beta-tubulin in normal and neoplastic human tissues. *Histochem Cell Biol* **109,** 231-239.

Drewes G, Lichtenberg-Kraag B, Döring F, Mandelkow EM, Biernat J, Goris J, Dorée M & Mandelkow E. (1992). Mitogen activated protein (MAP) kinase transforms tau protein into an Alzheimer-like state. *The EMBO journal* **11,** 2131-2138.

Dubois B, Chupin M, Hampel H, Lista S, Cavedo E, Croisile B, Louis Tisserand G, Touchon J, Bonafe A, Ousset PJ, Ait Ameur A, Rouaud O, Ricolfi F, Vighetto A, Pasquier F, Delmaire C, Ceccaldi M, Girard N, Dufouil C, Lehericy S, Tonelli I, Duveau F, Colliot O, Garnero L, Sarazin M & Dormont D. (2015). Donepezil decreases annual rate of hippocampal atrophy in suspected prodromal Alzheimer's disease. *Alzheimers Dement* **11,** 1041-1049.

Duncan P, Howell B, Marius R, Drmanic S, Douville E & Bell J. (1995). Alternative Splicing of STY, a Nuclear Dual Specificity Kinase. *The Journal of biological chemistry* **270,** 21524-21531.

Duncan PI, Stojdl DF, Marius RM & Bell JC. (1997). In vivo regulation of alternative pre-mRNA splicing by the Clk1 protein kinase. *Molecular and cellular biology* **17,** 5996-6001.

Edelstein J, Hao T, Cao Q, Morales L & Rockwell P. (2011). Crosstalk between VEGFR2 and muscarinic receptors regulates the mTOR pathway in serum starved SK-N-SH human neuroblastoma cells. *Cell Signal* **23,** 239-248.

Effenberger KA, Urabe VK & Jurica MS. (2017). Modulating splicing with small molecular inhibitors of the spliceosome. *Wiley Interdiscip Rev RNA* **8**.

Eperon LP, Graham IR, Griffiths AD & Eperon IC. (1988). Effects of RNA secondary structure on alternative splicing of Pre-mRNA: Is folding limited to a region behind the transcribing RNA polymerase? *Cell* **54,** 393-401.

Ertekin-Taner N. (2007). Genetics of Alzheimer's disease: a centennial review. *Neurol Clin* **25,** 611-667, v.

Esparza TJ, Zhao H, Cirrito JR, Cairns NJ, Bateman RJ, Holtzman DM & Brody DL. (2013). Amyloid-β oligomerization in Alzheimer dementia versus high-pathology controls. *Annals of neurology* **73,** 104-119.

Espindola SL, Damianich A, Alvarez RJ, Sartor M, Belforte JE, Ferrario JE, Gallo JM & Avale ME. (2018). Modulation of Tau Isoforms Imbalance Precludes Tau Pathology and Cognitive Decline in a Mouse Model of Tauopathy. *Cell Rep* **23,** 709-715.

Evans TG. (2015). Considerations for the use of transcriptomics in identifying the 'genes that matter' for environmental adaptation. *J Exp Biol* **218,** 1925-1935.

Faller P & Hureau C. (2020). Reproducibility Problems of Amyloid-β Self-Assembly and How to Deal With Them. *Front Chem* **8,** 611227.

Fan C, Chen K, Zhou J, Wong P-p, He D, Huang Y, Wang X, Ling T, Yang Y & Zhao H. (2020). Systematic analysis to identify transcriptome-wide dysregulation of Alzheimer's disease in genes and isoforms. *Human Genetics*.

Farrer LA, Cupples LA, Haines JL, Hyman B, Kukull WA, Mayeux R, Myers RH, Pericak-Vance MA, Risch N & van Duijn CM. (1997). Effects of age, sex, and ethnicity on the

association between apolipoprotein E genotype and Alzheimer disease. A meta-analysis. APOE and Alzheimer Disease Meta Analysis Consortium. *Jama* **278,** 1349-1356.

Faul F, Erdfelder E, Lang AG & Buchner A. (2007). G*Power 3: a flexible statistical power analysis program for the social, behavioral, and biomedical sciences. *Behav Res Methods* **39,** 175-191.

Feki A & Hibaoui Y. (2018). DYRK1A Protein, A Promising Therapeutic Target to Improve Cognitive Deficits in Down Syndrome. *Brain Sci* **8**.

Fernandez MA, Klutkowski JA, Freret T & Wolfe MS. (2014). Alzheimer presenilin-1 mutations dramatically reduce trimming of long amyloid β-peptides (Aβ) by γ-secretase to increase 42-to-40-residue Aβ. *The Journal of biological chemistry* **289,** 31043-31052.

Ferrer I & Blanco R. (2000). N-myc and c-myc expression in Alzheimer disease, Huntington disease and Parkinson disease. *Brain Res Mol Brain Res* **77,** 270-276.

Folkman J. (1974). TUMOR ANGIOGENESIS FACTOR. *Cancer Research* **34,** 2109-2113.

Folkman J, Merler E, Abernathy C & Williams G. (1971). ISOLATION OF A TUMOR FACTOR RESPONSIBLE FOR ANGIOGENESIS. *Journal of Experimental Medicine* **133,** 275-+.

Forette F, Seux ML, Staessen JA, Thijs L, Birkenhager WH, Babarskiene MR, Babeanu S, Bossini A, Gil-Extremera B, Girerd X, Laks T, Lilov E, Moisseyev V, Tuomilehto J, Vanhanen H, Webster J, Yodfat Y, Fagard R & Syst-Eur I. (1998). Prevention of dementia in randomised double-blind placebo-controlled Systolic Hypertension in Europe (Syst-Eur) trial. *Lancet* **352,** 1347-1351.

Foster EM, Dangla-Valls A, Lovestone S, Ribe EM & Buckley NJ. (2019). Clusterin in Alzheimer's Disease: Mechanisms, Genetics, and Lessons From Other Pathologies. *Front Neurosci* **13,** 164.

Fukuhara T, Hosoya T, Shimizu S, Sumi K, Oshiro T, Yoshinaka Y, Suzuki M, Yamamoto N, Herzenberg LA, Herzenberg LA & Hagiwara M. (2006). Utilization of host SR protein kinases and RNA-splicing machinery during viral replication. *Proceedings of the National Academy of Sciences* **103,** 11329.

Gali CC, Fanaee-Danesh E, Zandl-Lang M, Albrecher NM, Tam-Amersdorfer C, Stracke A, Sachdev V, Reichmann F, Sun Y, Avdili A, Reiter M, Kratky D, Holzer P, Lass A, Kandimalla KK & Panzenboeck U. (2019). Amyloid-beta impairs insulin signaling by accelerating autophagy-lysosomal degradation of LRP-1 and IR-β in blood-brain barrier endothelial cells in vitro and in 3XTg-AD mice. *Mol Cell Neurosci* **99,** 103390.

Gammons MV, Fedorov O, Ivison D, Du C, Clark T, Hopkins C, Hagiwara M, Dick AD, Cox R, Harper SJ, Hancox JC, Knapp S & Bates DO. (2013). Topical antiangiogenic SRPK1 inhibitors reduce choroidal neovascularization in rodent models of exudative AMD. *Invest Ophthalmol Vis Sci* **54,** 6052-6062.

Gammons MV, Lucas R, Dean R, Coupland SE, Oltean S & Bates DO. (2014). Targeting SRPK1 to control VEGF-mediated tumour angiogenesis in metastatic melanoma. *Br J Cancer* **111,** 477-485.

Gao QS, Memmott J, Lafyatis R, Stamm S, Screaton G & Andreadis A. (2000). Complex regulation of tau exon 10, whose missplicing causes frontotemporal dementia. *J Neurochem* **74,** 490-500.

Gao Y, Tan L & Yu JT. (2018a). Tau in Alzheimer's Disease: Mechanisms and Therapeutic Strategies. *Curr Alzheimer Res* **15,** 283-300.

Gao Y-L, Wang N, Sun F-R, Cao X-P, Zhang W & Yu J-T. (2018b). Tau in neurodegenerative disease. *Annals of Translational Medicine; Vol 6, No 10 (May 2018): Annals of Translational Medicine (Focus on "Translational Neurodegeneration")*.

Garcimartin A, Lopez-Oliva ME, Gonzalez MP, Sanchez-Muniz FJ & Benedi J. (2017). Hydrogen peroxide modifies both activity and isoforms of acetylcholinesterase in human neuroblastoma SH-SY5Y cells. *Redox Biol* **12,** 719-726.

Gatz M, Reynolds CA, Fratiglioni L, Johansson B, Mortimer JA, Berg S, Fiske A & Pedersen NL. (2006). Role of genes and environments for explaining Alzheimer disease. *Arch Gen Psychiatry* **63,** 168-174.

Geldmacher DS. (2004). Differential diagnosis of dementia syndromes. *Clin Geriatr Med* **20,** 27-43.

George A, Aubol BE, Fattet L & Adams JA. (2019). Disordered protein interactions for an ordered cellular transition: Cdc2-like kinase 1 is transported to the nucleus via its Ser-Arg protein substrate. *J Biol Chem* **294,** 9631-9641.

Ghosh G & Adams JA. (2011). Phosphorylation mechanism and structure of serine-arginine protein kinases. *The FEBS journal* **278,** 587-597.

Giannakopoulos P, Herrmann F, Bussière T, Bouras C, Kovari E, Perl D, Morrison J, Gold G & Hof PR. (2003). Tangle and neuron numbers, but not amyloid load, predict cognitive status in Alzheimer's disease. *Neurology* **60,** 1495-1500.

Giannakouros T, Nikolakaki E, Mylonis I & Georgatsou E. (2011). Serine-arginine protein kinases: a small protein kinase family with a large cellular presence. *Febs j* **278,** 570-586.

Glatz DC, Rujescu D, Tang Y, Berendt FJ, Hartmann AM, Faltraco F, Rosenberg C, Hulette C, Jellinger K, Hampel H, Riederer P, Möller HJ, Andreadis A, Henkel K & Stamm S. (2006). The alternative splicing of tau exon 10 and its regulatory proteins CLK2 and TRA2-BETA1 changes in sporadic Alzheimer's disease. *J Neurochem* **96,** 635-644.

Glenner GG & Wong CW. (1984). ALZHEIMERS-DISEASE - INITIAL REPORT OF THE PURIFICATION AND CHARACTERIZATION OF A NOVEL CEREBROVASCULAR AMYLOID PROTEIN. *Biochemical and Biophysical Research Communications* **120,** 885-890.

Goedert M & Jakes R. (1990). Expression of separate isoforms of human tau protein: correlation with the tau pattern in brain and effects on tubulin polymerization. *Embo j* **9,** 4225-4230.

Goedert M, Spillantini MG, Cairns NJ & Crowther RA. (1992). Tau proteins of alzheimer paired helical filaments: Abnormal phosphorylation of all six brain isoforms. *Neuron* **8,** 159-168.

Goedert M, Spillantini MG, Jakes R, Rutherford D & Crowther RA. (1989). Multiple isoforms of human microtubule-associated protein tau: sequences and localization in neurofibrillary tangles of Alzheimer's disease. *Neuron* **3,** 519-526.

Gong CX & Iqbal K. (2008). Hyperphosphorylation of microtubule-associated protein tau: a promising therapeutic target for Alzheimer disease. *Curr Med Chem* **15,** 2321-2328.

Gong CX, Shaikh S, Wang JZ, Zaidi T, Grundke-Iqbal I & Iqbal K. (1995). Phosphatase activity toward abnormally phosphorylated tau: decrease in Alzheimer disease brain. *J Neurochem* **65,** 732-738.

Gonçalves V & Jordan P. (2015). Posttranscriptional Regulation of Splicing Factor SRSF1 and Its Role in Cancer Cell Biology. *BioMed Research International* **2015,** 287048.

Gorelick PB, Counts SE & Nyenhuis D. (2016). Vascular cognitive impairment and dementia. *Biochimica Et Biophysica Acta-Molecular Basis of Disease* **1862,** 860-868.

Gorelick PB, Scuteri A, Black SE, Decarli C, Greenberg SM, Iadecola C, Launer LJ, Laurent S, Lopez OL, Nyenhuis D, Petersen RC, Schneider JA, Tzourio C, Arnett DK, Bennett DA, Chui HC, Higashida RT, Lindquist R, Nilsson PM, Roman GC, Sellke FW & Seshadri S. (2011). Vascular contributions to cognitive impairment and dementia: a statement for healthcare professionals from the american heart association/american stroke association. *Stroke* **42,** 2672-2713.

Grammas P. (2011). Neurovascular dysfunction, inflammation and endothelial activation: Implications for the pathogenesis of Alzheimer's disease. *Journal of Neuroinflammation* **8**.

Grand JH, Caspar S & Macdonald SW. (2011). Clinical features and multidisciplinary approaches to dementia care. *Journal of multidisciplinary healthcare* **4,** 125-147.

Gratuze M & Holtzman DM. (2021). Targeting pre-synaptic tau accumulation: a new strategy to counteract tau-mediated synaptic loss and memory deficits. *Neuron* **109,** 741-743.

Greenberg DA & Jin KL. (2005). From angiogenesis to neuropathology. *Nature* **438,** 954-959.

Grover A, Houlden H, Baker M, Adamson J, Lewis J, Prihar G, Pickering-Brown S, Duff K & Hutton M. (1999). 5' splice site mutations in tau associated with the inherited dementia FTDP-17 affect a stem-loop structure that regulates alternative splicing of exon 10. *J Biol Chem* **274,** 15134-15143.

Gu J, Shi J, Wu S, Jin N, Qian W, Zhou J, Iqbal IG, Iqbal K, Gong CX & Liu F. (2012). Cyclic AMP-dependent protein kinase regulates 9G8-mediated alternative splicing of tau exon 10. *FEBS Lett* **586,** 2239-2244.

Guimera J, Casas C, Estivill X & Pritchard M. (1999). Human minibrain homologue (MNBH/DYRK1): characterization, alternative splicing, differential tissue expression, and overexpression in Down syndrome. *Genomics* **57,** 407-418.

Guo Y, Wang Q, Chen S & Xu C. (2021). Functions of amyloid precursor protein in metabolic diseases. *Metabolism* **115,** 154454.

Gómez-Isla T, Price JL, McKeel DW, Jr., Morris JC, Growdon JH & Hyman BT. (1996). Profound loss of layer II entorhinal cortex neurons occurs in very mild Alzheimer's disease. *J Neurosci* **16,** 4491-4500.

Haass C & Selkoe DJ. (2007). Soluble protein oligomers in neurodegeneration: lessons from the Alzheimer's amyloid β-peptide. *Nature Reviews Molecular Cell Biology* **8,** 101-112.

Habekost M, Qvist P, Denham M, Holm IE & Jørgensen AL. (2021). Directly Reprogrammed Neurons Express MAPT and APP Splice Variants Pertinent to Ageing and Neurodegeneration. *Molecular Neurobiology*.

Hales CM, Dammer EB, Deng Q, Duong DM, Gearing M, Troncoso JC, Thambisetty M, Lah JJ, Shulman JM, Levey AI & Seyfried NT. (2016). Changes in the detergent-insoluble brain proteome linked to amyloid and tau in Alzheimer's Disease progression. *Proteomics* **16,** 3042-3053.

Hampel H, Mesulam MM, Cuello AC, Farlow MR, Giacobini E, Grossberg GT, Khachaturian AS, Vergallo A, Cavedo E, Snyder PJ & Khachaturian ZS. (2018). The cholinergic system in the pathophysiology and treatment of Alzheimer's disease. *Brain* **141,** 1917-1933.

Han S, Miller JE, Byun S, Kim D, Risacher SL, Saykin AJ, Lee Y & Nho K. (2019). Identification of exon skipping events associated with Alzheimer's disease in the human hippocampus. *BMC Med Genomics* **12,** 13.

Hannon E, Shireby GL, Brookes K, Attems J, Sims R, Cairns NJ, Love S, Thomas AJ, Morgan K, Francis PT & Mill J. (2020). Genetic risk for Alzheimer's disease influences neuropathology via multiple biological pathways. *Brain Commun* **2,** fcaa167.

Harada H, Andersen JS, Mann M, Terada N & Korsmeyer SJ. (2001). p70S6 kinase signals cell survival as well as growth, inactivating the pro-apoptotic molecule BAD. *Proc Natl Acad Sci U S A* **98,** 9666-9670.

Harari O, Cruchaga C, Kauwe JS, Ainscough BJ, Bales K, Pickering EH, Bertelsen S, Fagan AM, Holtzman DM, Morris JC & Goate AM. (2014). Phosphorylated tau-Abeta42 ratio as a continuous trait for biomarker discovery for early-stage Alzheimer's disease in multiplex immunoassay panels of cerebrospinal fluid. *Biol Psychiatry* **75,** 723-731.

Hardie DG. (1990). Roles of protein kinases and phosphatases in signal transduction. *Symp Soc Exp Biol* **44,** 241-255.

Hardy J. (2017). The discovery of Alzheimer-causing mutations in the APP gene and the formulation of the "amyloid cascade hypothesis". *Febs Journal* **284,** 1040-1044.

Hardy JA & Higgins GA. (1992). ALZHEIMERS-DISEASE - THE AMYLOID CASCADE HYPOTHESIS. *Science* **256,** 184-185.

Harold D, Abraham R, Hollingworth P, Sims R, Gerrish A, Hamshere ML, Pahwa JS, Moskvina V, Dowzell K, Williams A, Jones N, Thomas C, Stretton A, Morgan AR, Lovestone S, Powell J, Proitsi P, Lupton MK, Brayne C, Rubinsztein DC, Gill M, Lawlor B, Lynch A, Morgan K, Brown KS, Passmore PA, Craig D, McGuinness B, Todd S, Holmes C, Mann D, Smith AD, Love S, Kehoe PG, Hardy J, Mead S, Fox N, Rossor M, Collinge J, Maier W, Jessen F, Schürmann B, Heun R, van den Bussche H, Heuser I, Kornhuber J, Wiltfang J, Dichgans M, Frölich L, Hampel H, Hüll M, Rujescu D, Goate AM, Kauwe JS, Cruchaga C, Nowotny P, Morris JC, Mayo K, Sleegers K, Bettens K, Engelborghs S, De Deyn PP, Van Broeckhoven C, Livingston G, Bass NJ, Gurling H, McQuillin A, Gwilliam R, Deloukas P, Al-Chalabi A, Shaw CE, Tsolaki M, Singleton AB, Guerreiro R, Mühleisen TW, Nöthen MM, Moebus S, Jöckel KH, Klopp N, Wichmann HE, Carrasquillo MM, Pankratz VS, Younkin SG, Holmans PA, O'Donovan M, Owen MJ & Williams J. (2009). Genome-wide association study identifies variants at CLU and PICALM associated with Alzheimer's disease. *Nat Genet* **41,** 1088-1093.

Harper SJ & Bates DO. (2008). VEGF-A splicing: the key to anti-angiogenic therapeutics? *Nature Reviews Cancer* **8,** 880-887.

Harris R, Miners JS, Allen S & Love S. (2018). VEGFR1 and VEGFR2 in Alzheimer's Disease. *J Alzheimers Dis* **61,** 741-752.

Hartmann AM, Rujescu D, Giannakouros T, Nikolakaki E, Goedert M, Mandelkow EM, Gao QS, Andreadis A & Stamm S. (2001). Regulation of alternative splicing of human tau exon 10 by phosphorylation of splicing factors. *Mol Cell Neurosci* **18,** 80-90.

Haug LS, Østvold AC, Cowburn RF, Garlind A, Winblad B, Bogdanovich N & Walaas SI. (1996). Decreased Inositol (1,4,5)-Trisphosphate Receptor Levels in Alzheimer's Disease Cerebral Cortex: Selectivity of Changes and Possible Correlation to Pathological Severity. *Neurodegeneration* **5,** 169-176.

Hayashi T, Abe K & Itoyama Y. (1998). Reduction of ischemic damage by application of vascular endothelial growth factor in rat brain after transient ischemia. *J Cereb Blood Flow Metab* **18,** 887-895.

Henley DB, Sundell KL, Sethuraman G, Dowsett SA & May PC. (2014). Safety profile of semagacestat, a gamma-secretase inhibitor: IDENTITY trial findings. *Curr Med Res Opin* **30,** 2021-2032.

Hermida MA, Dinesh Kumar J & Leslie NR. (2017). GSK3 and its interactions with the PI3K/AKT/mTOR signalling network. *Adv Biol Regul* **65,** 5-15.

Hernández F, Pérez M, Lucas JJ, Mata AM, Bhat R & Avila J. (2004). Glycogen synthase kinase-3 plays a crucial role in tau exon 10 splicing and intranuclear distribution of SC35. Implications for Alzheimer's disease. *J Biol Chem* **279,** 3801-3806.

Hettiarachchi NT, Dallas ML, Al-Owais MM, Griffiths HH, Hooper NM, Scragg JL, Boyle JP & Peers C. (2014). Heme oxygenase-1 protects against Alzheimer's amyloid-beta(1-42)-induced toxicity via carbon monoxide production. *Cell Death & Disease* **5**.

Hirsch-Reinshagen V, Zhou S, Burgess BL, Bernier L, McIsaac SA, Chan JY, Tansley GH, Cohn JS, Hayden MR & Wellington CL. (2004). Deficiency of ABCA1 impairs apolipoprotein E metabolism in brain. *J Biol Chem* **279,** 41197-41207.

Hishimoto A, Pletnikova O, Lang D, Troncoso J, Egan J & Liu Q-R. (2019). Neurexin 3 transmembrane and soluble isoform expression and splicing haplotype are associated with neuron inflammasome and Alzheimer's disease. *Alzheimer's Research & Therapy* **11**.

Hobson MI, Green CJ & Terenghi G. (2000). VEGF enhances intraneural angiogenesis and improves nerve regeneration after axotomy. *Journal of Anatomy* **197,** 591-605.

Hoeben A, Landuyt B, Highley MS, Wildiers H, Van Oosterom AT & De Bruijn EA. (2004). Vascular endothelial growth factor and angiogenesis. *Pharmacol Rev* **56,** 549-580.

Hollingworth P, Harold D, Sims R, Gerrish A, Lambert JC, Carrasquillo MM, Abraham R, Hamshere ML, Pahwa JS, Moskvina V, Dowzell K, Jones N, Stretton A, Thomas C, Richards A, Ivanov D, Widdowson C, Chapman J, Lovestone S, Powell J, Proitsi P, Lupton MK, Brayne C, Rubinsztein DC, Gill M, Lawlor B, Lynch A, Brown KS, Passmore PA, Craig D, McGuinness B, Todd S, Holmes C, Mann D, Smith AD, Beaumont H, Warden D, Wilcock G, Love S, Kehoe PG, Hooper NM, Vardy ER, Hardy J, Mead S, Fox NC, Rossor M, Collinge J, Maier W, Jessen F, Rüther E, Schürmann B, Heun R, Kölsch H, van den Bussche H, Heuser I, Kornhuber J, Wiltfang J, Dichgans M, Frölich L, Hampel H, Gallacher J, Hüll M, Rujescu D, Giegling I, Goate AM, Kauwe JS, Cruchaga C, Nowotny P, Morris JC, Mayo K, Sleegers K, Bettens K, Engelborghs S, De Deyn PP, Van Broeckhoven C, Livingston G, Bass NJ, Gurling H, McQuillin A, Gwilliam R, Deloukas P, Al-Chalabi A, Shaw CE, Tsolaki M, Singleton AB, Guerreiro R, Mühleisen TW, Nöthen MM, Moebus S, Jöckel KH, Klopp N, Wichmann HE, Pankratz VS, Sando SB, Aasly JO, Barcikowska M, Wszolek ZK, Dickson DW, Graff-Radford NR, Petersen RC, van Duijn CM, Breteler MM, Ikram MA, DeStefano AL, Fitzpatrick AL, Lopez O, Launer LJ, Seshadri S, Berr C, Campion D, Epelbaum J, Dartigues JF, Tzourio C, Alpérovitch A, Lathrop M, Feulner TM, Friedrich P, Riehle C, Krawczak M, Schreiber S, Mayhaus M, Nicolhaus S, Wagenpfeil S, Steinberg S, Stefansson H, Stefansson K, Snaedal J, Björnsson S, Jonsson PV, Chouraki V, Genier-Boley B, Hiltunen M, Soininen H, Combarros O, Zelenika D, Delepine M, Bullido MJ, Pasquier F, Mateo I, Frank-Garcia A, Porcellini E, Hanon O, Coto E, Alvarez V, Bosco P, Siciliano G, Mancuso M, Panza F, Solfrizzi V, Nacmias B, Sorbi S, Bossù P, Piccardi P, Arosio B, Annoni G, Seripa D, Pilotto A, Scarpini E, Galimberti D, Brice A, Hannequin D, Licastro F, Jones L, Holmans PA, Jonsson T, Riemenschneider M, Morgan K, Younkin SG, Owen MJ, O'Donovan M, Amouyel P & Williams J. (2011). Common variants at ABCA7, MS4A6A/MS4A4E, EPHA1, CD33 and CD2AP are associated with Alzheimer's disease. *Nat Genet* **43,** 429-435.

Holmes C, Boche D, Wilkinson D, Yadegarfar G, Hopkins V, Bayer A, Jones RW, Bullock R, Love S, Neal JW, Zotova E & Nicoll JA. (2008). Long-term effects of Abeta42 immunisation in Alzheimer's disease: follow-up of a randomised, placebo-controlled phase I trial. *Lancet* **372,** 216-223.

Hong M, Zhukareva V, Vogelsberg-Ragaglia V, Wszolek Z, Reed L, Miller BI, Geschwind DH, Bird TD, McKeel D, Goate A, Morris JC, Wilhelmsen KC, Schellenberg GD, Trojanowski JQ & Lee VM. (1998). Mutation-specific functional impairments in distinct tau isoforms of hereditary FTDP-17. *Science* **282,** 1914-1917.

Hong Y, Chan CB, Kwon IS, Li X, Song M, Lee HP, Liu X, Sompol P, Jin P, Lee HG, Yu SP & Ye K. (2012). SRPK2 phosphorylates tau and mediates the cognitive defects in Alzheimer's disease. *J Neurosci* **32,** 17262-17272.

Honig LS, Vellas B, Woodward M, Boada M, Bullock R, Borrie M, Hager K, Andreasen N, Scarpini E, Liu-Seifert H, Case M, Dean RA, Hake A, Sundell K, Poole Hoffmann V, Carlson C, Khanna R, Mintun M, DeMattos R, Selzler KJ & Siemers E. (2018). Trial of Solanezumab for Mild Dementia Due to Alzheimer's Disease. *N Engl J Med* **378,** 321-330.

Howard JM & Sanford JR. (2015). The RNAissance family: SR proteins as multifaceted regulators of gene expression. *Wiley Interdiscip Rev RNA* **6,** 93-110.

Hua J, Spee C, Kase S, Rennel ES, Magnussen AL, Qiu Y, Varey A, Dhayade S, Churchill AJ, Harper SJ, Bates DO & Hinton DR. (2010). Recombinant human VEGF165b inhibits experimental choroidal neovascularization. *Invest Ophthalmol Vis Sci* **51,** 4282-4288.

Huang L, Jia J & Liu R. (2013). Decreased serum levels of the angiogenic factors VEGF and TGF-β1 in Alzheimer's disease and amnestic mild cognitive impairment. *Neurosci Lett* **550,** 60-63.

Hulse RP, Beazley-Long N, Hua J, Kennedy H, Prager J, Bevan H, Qiu Y, Fernandes ES, Gammons MV, Ballmer-Hofer K, Gittenberger de Groot AC, Churchill AJ, Harper SJ, Brain SD, Bates DO & Donaldson LF. (2014). Regulation of alternative VEGF-A mRNA splicing is a therapeutic target for analgesia. *Neurobiol Dis* **71,** 245-259.

Hulse RP, Beazley-Long N, Ved N, Bestall SM, Riaz H, Singhal P, Ballmer Hofer K, Harper SJ, Bates DO & Donaldson LF. (2015). Vascular endothelial growth factor-A165b prevents diabetic neuropathic pain and sensory neuronal degeneration. *Clin Sci (Lond)* **129,** 741-756.

Hutton M, Lendon CL, Rizzu P, Baker M, Froelich S, Houlden H, Pickering-Brown S, Chakraverty S, Isaacs A, Grover A, Hackett J, Adamson J, Lincoln S, Dickson D, Davies P, Petersen RC, Stevens M, de Graaff E, Wauters E, van Baren J, Hillebrand M, Joosse M, Kwon JM, Nowotny P, Che LK, Norton J, Morris JC, Reed LA, Trojanowski J, Basun H, Lannfelt L, Neystat M, Fahn S, Dark F, Tannenberg T, Dodd PR, Hayward N, Kwok JB, Schofield PR, Andreadis A, Snowden J, Craufurd D, Neary D, Owen F, Oostra BA, Hardy J, Goate A, van Swieten J, Mann D, Lynch T & Heutink P. (1998). Association of missense and 5'-splice-site mutations in tau with the inherited dementia FTDP-17. *Nature* **393,** 702-705.

Idda ML, Munk R, Abdelmohsen K & Gorospe M. (2018). Noncoding RNAs in Alzheimer's disease. *Wiley Interdiscip Rev RNA* **9**.

Iqbal K, Liu F, Gong CX & Grundke-Iqbal I. (2010). Tau in Alzheimer disease and related tauopathies. *Curr Alzheimer Res* **7,** 656-664.

Ishiguro K, Omori A, Takamatsu M, Sato K, Arioka M, Uchida T & Imahori K. (1992). Phosphorylation sites on tau by tau protein kinase I, a bovine derived kinase generating an epitope of paired helical filaments. *Neurosci Lett* **148,** 202-206.

Ishiguro K, Shiratsuchi A, Sato S, Omori A, Arioka M, Kobayashi S, Uchida T & Imahori K. (1993). Glycogen synthase kinase 3β is identical to tau protein kinase I generating several epitopes of paired helical filaments. *FEBS Letters* **325,** 167-172.

Ito K, Tatebe T, Suzuki K, Hirayama T, Hayakawa M, Kubo H, Tomita T & Makino M. (2017). Memantine reduces the production of amyloid-β peptides through modulation of amyloid precursor protein trafficking. *Eur J Pharmacol* **798,** 16-25.

Jack CR, Jr., Knopman DS, Jagust WJ, Shaw LM, Aisen PS, Weiner MW, Petersen RC & Trojanowski JQ. (2010). Hypothetical model of dynamic biomarkers of the Alzheimer's pathological cascade. *Lancet Neurol* **9,** 119-128.

Jacobs HIL, Hopkins DA, Mayrhofer HC, Bruner E, van Leeuwen FW, Raaijmakers W & Schmahmann JD. (2018). The cerebellum in Alzheimer's disease: evaluating its role in cognitive decline. *Brain* **141,** 37-47.

Jain P, Karthikeyan C, Moorthy NS, Waiker DK, Jain AK & Trivedi P. (2014). Human CDC2-like kinase 1 (CLK1): a novel target for Alzheimer's disease. *Curr Drug Targets* **15,** 539-550.

Jakubauskienė E, Vilys L, Pečiulienė I & Kanopka A. (2021). The role of hypoxia on Alzheimer's disease-related APP and Tau mRNA formation. *Gene* **766,** 145146.

James BD, Bennett DA, Boyle PA, Leurgans S & Schneider JA. (2012). Dementia from Alzheimer disease and mixed pathologies in the oldest old. *JAMA* **307,** 1798-1800.

Jiang Q, Lee CYD, Mandrekar S, Wilkinson B, Cramer P, Zelcer N, Mann K, Lamb B, Willson TM, Collins JL, Richardson JC, Smith JD, Comery TA, Riddell D, Holtzman DM, Tontonoz P & Landreth GE. (2008). ApoE promotes the proteolytic degradation of Abeta. *Neuron* **58,** 681-693.

Jiang T, Yu JT, Hu N, Tan MS, Zhu XC & Tan L. (2014). CD33 in Alzheimer's disease. *Mol Neurobiol* **49,** 529-535.

Jiang Z, Tang H, Havlioglu N, Zhang X, Stamm S, Yan R & Wu JY. (2003). Mutations in tau gene exon 10 associated with FTDP-17 alter the activity of an exonic splicing enhancer to interact with Tra2 beta. *The Journal of biological chemistry* **278,** 18997-19007.

Jin N, Yin X, Gu J, Zhang X, Shi J, Qian W, Ji Y, Cao M, Gu X, Ding F, Iqbal K, Gong CX & Liu F. (2015a). Truncation and Activation of Dual Specificity Tyrosine Phosphorylation-regulated Kinase 1A by Calpain I: A MOLECULAR MECHANISM LINKED TO TAU PATHOLOGY IN ALZHEIMER DISEASE. *J Biol Chem* **290,** 15219-15237.

Jin N, Yin X, Yu D, Cao M, Gong CX, Iqbal K, Ding F, Gu X & Liu F. (2015b). Truncation and activation of GSK-3β by calpain I: a molecular mechanism links to tau hyperphosphorylation in Alzheimer's disease. *Sci Rep* **5,** 8187.

Johnson DK, Storandt M, Morris JC & Galvin JE. (2009). Longitudinal study of the transition from healthy aging to Alzheimer disease. *Arch Neurol* **66,** 1254-1259.

Johnson ECB, Dammer EB, Duong DM, Yin L, Thambisetty M, Troncoso JC, Lah JJ, Levey AI & Seyfried NT. (2018). Deep proteomic network analysis of Alzheimer's disease brain reveals alterations in RNA binding proteins and RNA splicing associated with disease. *Mol Neurodegener* **13,** 52.

Johnson KW & Smith KA. (1991). Molecular cloning of a novel human cdc2/CDC28-like protein kinase. *J Biol Chem* **266,** 3402-3407.

Jonsson T, Stefansson H, Steinberg S, Jonsdottir I, Jonsson PV, Snaedal J, Bjornsson S, Huttenlocher J, Levey AI, Lah JJ, Rujescu D, Hampel H, Giegling I, Andreassen OA,

Engedal K, Ulstein I, Djurovic S, Ibrahim-Verbaas C, Hofman A, Ikram MA, van Duijn CM, Thorsteinsdottir U, Kong A & Stefansson K. (2013). Variant of TREM2 associated with the risk of Alzheimer's disease. *N Engl J Med* **368,** 107-116.

Jurica MS & Moore MJ. (2003). Pre-mRNA splicing: awash in a sea of proteins. *Mol Cell* **12,** 5-14.

Kalaria RN, Cohen DL, Premkumar DRD, Nag S, LaManna JC & Lust WD. (1998). Vascular endothelial growth factor in Alzheimer's disease and experimental cerebral ischemia. *Molecular Brain Research* **62,** 101-105.

Kawamura H, Li X, Harper SJ, Bates DO & Claesson-Welsh L. (2008). Vascular endothelial growth factor (VEGF)-A165b is a weak in vitro agonist for VEGF receptor-2 due to lack of coreceptor binding and deficient regulation of kinase activity. *Cancer Res* **68,** 4683-4692.

Keck PJ, Hauser SD, Krivi G, Sanzo K, Warren T, Feder J & Connolly DT. (1989). Vascular permeability factor, an endothelial cell mitogen related to PDGF. *Science* **246,** 1309-1312.

Kendall RL & Thomas KA. (1993). Inhibition of vascular endothelial cell growth factor activity by an endogenously encoded soluble receptor. *Proceedings of the National Academy of Sciences of the United States of America* **90,** 10705-10709.

Kentrup H, Becker W, Heukelbach J, Wilmes A, Schürmann A, Huppertz C, Kainulainen H & Joost H-G. (1996). Dyrk, a Dual Specificity Protein Kinase with Unique Structural Features Whose Activity Is Dependent on Tyrosine Residues between Subdomains VII and VIII. *The Journal of biological chemistry* **271,** 3488-3495.

Keshwani MM, Aubol BE, Fattet L, Ma CT, Qiu J, Jennings PA, Fu XD & Adams JA. (2015). Conserved proline-directed phosphorylation regulates SR protein conformation and splicing function. *Biochem J* **466,** 311-322.

Kester MI & Scheltens P. (2009). Dementia: the bare essentials. *Pract Neurol* **9,** 241-251.

Kilic U, Kilic E, Jarve A, Guo ZY, Spudich A, Bieber K, Barzena U, Bassetti CL, Marti HH & Hermann DM. (2006). Human vascular endothelial growth factor protects axotomized retinal ganglion cells in vivo by activating ERK-1/2 and Akt pathways. *Journal of Neuroscience* **26,** 12439-12446.

Killick R, Ribe EM, Al-Shawi R, Malik B, Hooper C, Fernandes C, Dobson R, Nolan PM, Lourdusamy A, Furney S, Lin K, Breen G, Wroe R, To AWM, Leroy K, Causevic M, Usardi A, Robinson M, Noble W, Williamson R, Lunnon K, Kellie S, Reynolds CH, Bazenet C, Hodges A, Brion JP, Stephenson J, Paul Simons J & Lovestone S. (2014). Clusterin regulates β-amyloid toxicity via Dickkopf-1-driven induction of the wnt–PCP–JNK pathway. *Molecular Psychiatry* **19,** 88-98.

Kim E, Magen A & Ast G. (2007a). Different levels of alternative splicing among eukaryotes. *Nucleic Acids Res* **35,** 125-131.

Kim J, Onstead L, Randle S, Price R, Smithson L, Zwizinski C, Dickson DW, Golde T & McGowan E. (2007b). Abeta40 inhibits amyloid deposition in vivo. *J Neurosci* **27,** 627-633.

Kim YS, Ahn KH, Kim SY & Jeong JW. (2009). Okadaic acid promotes angiogenesis via activation of hypoxia-inducible factor-1. *Cancer Lett* **276,** 102-108.

Kisko K, Brozzo MS, Missimer J, Schleier T, Menzel A, Leppanen VM, Alitalo K, Walzthoeni T, Aebersold R & Ballmer-Hofer K. (2011). Structural analysis of vascular endothelial growth factor receptor-2/ligand complexes by small-angle X-ray solution scattering. *Faseb j* **25,** 2980-2986.

Koizumi J, Okamoto Y, Onogi H, Mayeda A, Krainer A & Hagiwara M. (1999). The subcellular localization of SF2/ASF is regulated by direct interaction with SR protein kinases (SRPKs). *The Journal of biological chemistry* **274,** 11125-11131.

Kolisnyk B, Al-Onaizi M, Soreq L, Barbash S, Bekenstein U, Haberman N, Hanin G, Kish MT, Souza da Silva J, Fahnestock M, Ule J, Soreq H, Prado VF & Prado MAM. (2017). Cholinergic Surveillance over Hippocampal RNA Metabolism and Alzheimer's-Like Pathology. *Cereb Cortex* **27,** 3553-3567.

Kondo S, Yamamoto N, Murakami T, Okumura M, Mayeda A & Imaizumi K. (2004). Tra2 beta, SF2/ASF and SRp30c modulate the function of an exonic splicing enhancer in exon 10 of tau pre-mRNA. *Genes Cells* **9,** 121-130.

Kong W, Li S & Mou X. (2012). *ICA-based Gene Expression Modules Exploring for Alzheimer's Disease*.

Kopeikina KJ, Hyman BT & Spires-Jones TL. (2012). Soluble forms of tau are toxic in Alzheimer's disease. *Transl Neurosci* **3,** 223-233.

Kosel F, Pelley JMS & Franklin TB. (2020). Behavioural and psychological symptoms of dementia in mouse models of Alzheimer's disease-related pathology. *Neurosci Biobehav Rev* **112,** 634-647.

Kosik KS, Orecchio LD, Bakalis S & Neve RL. (1989). Developmentally regulated expression of specific tau sequences. *Neuron* **2,** 1389-1397.

Kovacic JC, Castellano JM & Fuster V. (2012). The links between complex coronary disease, cerebrovascular disease, and degenerative brain disease. *Ann N Y Acad Sci* **1254,** 99-105.

Kuroyanagi N, Onogi H, Wakabayashi T & Hagiwara M. (1998). Novel SR-Protein-Specific Kinase, SRPK2, Disassembles Nuclear Speckles. *Biochemical and Biophysical Research Communications* **242,** 357-364.

Kurumatani T, Fastbom J, Bonkale WL, Bogdanovic N, Winblad B, Ohm TG & Cowburn RF. (1998). Loss of inositol 1,4,5-trisphosphate receptor sites and decreased PKC levels correlate with staging of Alzheimer's disease neurofibrillary pathology. *Brain Res* **796,** 209-221.

LaDu M, Falduto M, Manelli A, Reardon C, Getz G & Frail D. (1994). Isoform-specific binding of apolipoprotein E to beta-amyloid. *The Journal of biological chemistry* **269,** 23403-23406.

LaFerla FM. (2002). Calcium dyshomeostasis and intracellular signalling in Alzheimer's disease. *Nat Rev Neurosci* **3,** 862-872.

Lahoz C, Schaefer EJ, Cupples LA, Wilson PWF, Levy D, Osgood D, Parpos S, Pedro-Botet J, Daly JA & Ordovas JM. (2001). Apolipoprotein E genotype and cardiovascular disease in the Framingham Heart Study. *Atherosclerosis* **154,** 529-537.

Lai MC, Lin RI & Tarn WY. (2001). Transportin-SR2 mediates nuclear import of phosphorylated SR proteins. *Proceedings of the National Academy of Sciences of the United States of America* **98,** 10154-10159.

Lambert JC, Heath S, Even G, Campion D, Sleegers K, Hiltunen M, Combarros O, Zelenika D, Bullido MJ, Tavernier B, Letenneur L, Bettens K, Berr C, Pasquier F, Fiévet N, Barberger-Gateau P, Engelborghs S, De Deyn P, Mateo I, Franck A, Helisalmi S, Porcellini E, Hanon O, de Pancorbo MM, Lendon C, Dufouil C, Jaillard C, Leveillard T, Alvarez V, Bosco P, Mancuso M, Panza F, Nacmias B, Bossù P, Piccardi P, Annoni G, Seripa D, Galimberti D, Hannequin D, Licastro F, Soininen H, Ritchie K, Blanché H, Dartigues JF, Tzourio C, Gut I, Van Broeckhoven C, Alpérovitch A, Lathrop M & Amouyel P. (2009). Genome-wide association study identifies variants at CLU and CR1 associated with Alzheimer's disease. *Nat Genet* **41,** 1094-1099.

Lambrechts D, Storkebaum E, Morimoto M, Del-Favero J, Desmet F, Marklund SL, Wyns S, Thijs V, Andersson J, van Marion I, Al-Chalabi A, Bornes S, Musson R, Hansen V, Beckman L, Adolfsson R, Pall HS, Prats H, Vermeire S, Rutgeerts P, Katayama S, Awata T, Leigh N, Lang-Lazdunski L, Dewerchin M, Shaw C, Moons L, Vlietinck R, Morrison KE, Robberecht W, Van Broeckhoven C, Collen D, Andersen PM & Carmeliet P. (2003). VEGF is a modifier of amyotrophic lateral sclerosis in mice and humans and protects motoneurons against ischemic death. *Nature Genetics* **34,** 383-394.

Lane CA, Hardy J & Schott JM. (2018). Alzheimer's disease. *Eur J Neurol* **25,** 59-70.

Lanz T, Karmilowicz M, Wood K, Pozdnyakov N, Du P, Piotrowski M, Brown T, Nolan C, Richter K, Finley J, Fei Q, Ebbinghaus C, Chen Y, Spracklin D, Tate B, Geoghegan K, Lau L-F, Auperin D & Schachter J. (2006). Concentration-Dependent Modulation of Amyloid-β in Vivo and in Vitro Using the γ-Secretase Inhibitor, LY-450139. *The Journal of pharmacology and experimental therapeutics* **319,** 924-933.

Lareau LF, Inada M, Green RE, Wengrod JC & Brenner SE. (2007). Unproductive splicing of SR genes associated with highly conserved and ultraconserved DNA elements. *Nature* **446,** 926-929.

Ledesma MD, Correas I, Avila J & Diaz-Nido J. (1992). Implication of brain cdc2 and MAP2 kinases in the phosphorylation of tau protein in Alzheimer's disease. *FEBS Letters* **308,** 218-224.

Lee CYD, Tse W, Smith JD & Landreth GE. (2012). Apolipoprotein E promotes β-amyloid trafficking and degradation by modulating microglial cholesterol levels. *The Journal of biological chemistry* **287,** 2032-2044.

Lee HJ, Woo H, Lee HE, Jeon H, Ryu KY, Nam JH, Jeon SG, Park H, Lee JS, Han KM, Lee SM, Kim J, Kang RJ, Lee YH, Kim JI & Hoe HS. (2020). The novel DYRK1A inhibitor KVN93 regulates cognitive function, amyloid-beta pathology, and neuroinflammation. *Free Radic Biol Med* **160,** 575-595.

Lee KY, Clark AW, Rosales JL, Chapman K, Fung T & Johnston RN. (1999). Elevated neuronal Cdc2-like kinase activity in the Alzheimer disease brain. *Neurosci Res* **34,** 21-29.

Lee SJ, Nam E, Lee HJ, Savelieff MG & Lim MH. (2017). Towards an understanding of amyloid-β oligomers: characterization, toxicity mechanisms, and inhibitors. *Chem Soc Rev* **46,** 310-323.

Lee Y, Ha J, Kim HJ, Kim YS, Chang EJ, Song WJ & Kim HH. (2009). Negative feedback Inhibition of NFATc1 by DYRK1A regulates bone homeostasis. *J Biol Chem* **284,** 33343-33351.

Lemmon MA & Schlessinger J. (2010). Cell signaling by receptor tyrosine kinases. *Cell* **141,** 1117-1134.

Leung DW, Cachianes G, Kuang WJ, Goeddel DV & Ferrara N. (1989). Vascular endothelial growth factor is a secreted angiogenic mitogen. *Science* **246,** 1306-1309.

Levin JZ, Yassour M, Adiconis X, Nusbaum C, Thompson DA, Friedman N, Gnirke A & Regev A. (2010). Comprehensive comparative analysis of strand-specific RNA sequencing methods. *Nature Methods* **7,** 709-715.

Li HD, Funk CC, McFarland K, Dammer EB, Allen M, Carrasquillo MM, Levites Y, Chakrabarty P, Burgess JD, Wang X, Dickson D, Seyfried NT, Duong DM, Lah JJ, Younkin SG, Levey AI, Omenn GS, Ertekin-Taner N, Golde TE & Price ND. (2021). Integrative functional genomic analysis of intron retention in human and mouse brain with Alzheimer's disease. *Alzheimers Dement*.

Li K, Wei Q, Liu FF, Hu F, Xie AJ, Zhu LQ & Liu D. (2018). Synaptic Dysfunction in Alzheimer's Disease: Aβ, Tau, and Epigenetic Alterations. *Mol Neurobiol* **55,** 3021-3032.

Liang N, Zeng C, Tao KP, Sou WH, Hsia HP, Qu D, Lau SN & Ngo JC. (2014). Primary structural features of SR-like protein acinusS govern the phosphorylation mechanism by SRPK2. *Biochem J* **459,** 181-191.

Liao F, Jiang H, Srivatsan S, Xiao Q, Lefton KB, Yamada K, Mahan TE, Lee JM, Shaw AS & Holtzman DM. (2015). Effects of CD2-associated protein deficiency on amyloid-β in neuroblastoma cells and in an APP transgenic mouse model. *Mol Neurodegener* **10,** 12.

Lindwall G & Cole RD. (1984). Phosphorylation affects the ability of tau protein to promote microtubule assembly. *J Biol Chem* **259,** 5301-5305.

Liu F, Liang Z, Shi J, Yin D, El-Akkad E, Grundke-Iqbal I, Iqbal K & Gong CX. (2006). PKA modulates GSK-3beta- and cdk5-catalyzed phosphorylation of tau in site- and kinase-specific manners. *FEBS Lett* **580,** 6269-6274.

Liu F, Liang Z, Wegiel J, Hwang YW, Iqbal K, Grundke-Iqbal I, Ramakrishna N & Gong CX. (2008). Overexpression of Dyrk1A contributes to neurofibrillary degeneration in Down syndrome. *Faseb j* **22,** 3224-3233.

Love JE, Hayden EJ & Rohn TT. (2015). Alternative Splicing in Alzheimer's Disease. *J Parkinsons Dis Alzheimers Dis* **2**.

Lovestone S, Reynolds CH, Latimer D, Davis DR, Anderton BH, Gallo JM, Hanger D, Mulot S, Marquardt B, Stabel S & et al. (1994). Alzheimer's disease-like phosphorylation of the microtubule-associated protein tau by glycogen synthase kinase-3 in transfected mammalian cells. *Curr Biol* **4,** 1077-1086.

Lu M & Kosik KS. (2001). Competition for microtubule-binding with dual expression of tau missense and splice isoforms. *Molecular biology of the cell* **12,** 171-184.

Luengo-Fernandez R, Leal J & Gray A. (2015). UK research spend in 2008 and 2012: comparing stroke, cancer, coronary heart disease and dementia. *BMJ Open* **5,** e006648.

Ma C-T, Velazquez-Dones A, Hagopian JC, Ghosh G, Fu X-D & Adams JA. (2008). Ordered Multi-site Phosphorylation of the Splicing Factor ASF/SF2 By SRPK1. *Journal of Molecular Biology* **376,** 55-68.

Maenz B, Hekerman P, Vela EM, Galceran J & Becker W. (2008). Characterization of the human DYRK1A promoter and its regulation by the transcription factor E2F1. *BMC Mol Biol* **9,** 30.

Magistri M, Velmeshev D, Makhmutova M & Faghihi MA. (2015). Transcriptomics Profiling of Alzheimer's Disease Reveal Neurovascular Defects, Altered Amyloid-β Homeostasis, and Deregulated Expression of Long Noncoding RNAs. *J Alzheimers Dis* **48,** 647-665.

Magnussen AL, Rennel ES, Hua J, Bevan HS, Beazley Long N, Lehrling C, Gammons M, Floege J, Harper SJ, Agostini HT, Bates DO & Churchill AJ. (2010). VEGF-A165b is cytoprotective and antiangiogenic in the retina. *Invest Ophthalmol Vis Sci* **51,** 4273-4281.

Mahley RW & Rall SC. (2000). Apolipoprotein E: Far More Than a Lipid Transport Protein. *Annual Review of Genomics and Human Genetics* **1,** 507-537.

Malkani R, D'Souza I, Gwinn-Hardy K, Schellenberg GD, Hardy J & Momeni P. (2006). A MAPT mutation in a regulatory element upstream of exon 10 causes frontotemporal dementia. *Neurobiol Dis* **22,** 401-403.

Manning C. (2004). Beyond memory: neuropsychologic features in differential diagnosis of dementia. *Clin Geriatr Med* **20,** 45-58.

Manolio TA, Collins FS, Cox NJ, Goldstein DB, Hindorff LA, Hunter DJ, McCarthy MI, Ramos EM, Cardon LR, Chakravarti A, Cho JH, Guttmacher AE, Kong A, Kruglyak L, Mardis E, Rotimi CN, Slatkin M, Valle D, Whittemore AS, Boehnke M, Clark AG, Eichler EE, Gibson G, Haines JL, Mackay TFC, McCarroll SA & Visscher PM. (2009). Finding the missing heritability of complex diseases. *Nature* **461,** 747-753.

Mantile F & Prisco A. (2020). Vaccination against β-Amyloid as a Strategy for the Prevention of Alzheimer's Disease. *Biology (Basel)* **9**.

Martin L, Page G & Terro F. (2011). Tau phosphorylation and neuronal apoptosis induced by the blockade of PP2A preferentially involve GSK3beta. *Neurochem Int* **59,** 235-250.

Martinez A, González-Pérez A, Gayán J, Antúnez C, Marín J, Boada M, López-Arrieta J, Fernández E, Ramírez-Lorca R, Saez M, Ruiz A, Scholl F & Real L. (2013). Genetic Study of Neurexin and Neuroligin Genes in Alzheimer's Disease. *Journal of Alzheimer's disease : JAD* **35**.

Martín Moyano P, Němec V & Paruch K. (2020). Cdc-Like Kinases (CLKs): Biology, Chemical Probes, and Therapeutic Potential. *Int J Mol Sci* **21**.

Mastroeni D, Nolz J, Sekar S, Delvaux E, Serrano G, Cuyugan L, Liang WS, Beach TG, Rogers J & Coleman PD. (2018). Laser-captured microglia in the Alzheimer's and Parkinson's brain reveal unique regional expression profiles and suggest a potential role for hepatitis B in the Alzheimer's brain. *Neurobiology of aging* **63,** 12-21.

Matsunaga S, Kishi T, Nomura I, Sakuma K, Okuya M, Ikuta T & Iwata N. (2018). The efficacy and safety of memantine for the treatment of Alzheimer's disease. *Expert Opin Drug Saf* **17,** 1053-1061.

Matsuzaki H, Tamatani M, Yamaguchi A, Namikawa K, Kiyama H, Vitek MP, Mitsuda N & Tohyama M. (2001). Vascular endothelial growth factor rescues hippocampal neurons from glutamate-induced toxicity: signal transduction cascades. *Faseb j* **15,** 1218-1220.

Mavrou A, Brakspear K, Hamdollah-Zadeh M, Damodaran G, Babaei-Jadidi R, Oxley J, Gillatt DA, Ladomery MR, Harper SJ, Bates DO & Oltean S. (2015). Serine-arginine protein kinase 1 (SRPK1) inhibition as a potential novel targeted therapeutic strategy in prostate cancer. *Oncogene* **34,** 4311-4319.

Mavrou A & Oltean S. (2016). SRPK1 inhibition in prostate cancer: A novel anti-angiogenic treatment through modulation of VEGF alternative splicing. *Pharmacological Research* **107,** 276-281.

Mazin P, Xiong J, Liu X, Yan Z, Zhang X, Li M, He L, Somel M, Yuan Y, Phoebe Chen Y-P, Li N, Hu Y, Fu N, Ning Z, Zeng R, Yang H, Chen W, Gelfand M & Khaitovich P. (2013). Widespread splicing changes in human brain development and aging. *Molecular Systems Biology* **9,** 633.

McCarthy A, Lonergan R, Olszewska DA, O'Dowd S, Cummins G, Magennis B, Fallon EM, Pender N, Huey ED, Cosentino S, O'Rourke K, Kelly BD, O'Connell M, Delon I, Farrell M, Spillantini MG, Rowland LP, Fahn S, Craig P, Hutton M & Lynch T. (2015). Closing the tau loop: the missing tau mutation. *Brain : a journal of neurology* **138,** 3100-3109.

McKhann GM, Knopman DS, Chertkow H, Hyman BT, Jack CR, Jr., Kawas CH, Klunk WE, Koroshetz WJ, Manly JJ, Mayeux R, Mohs RC, Morris JC, Rossor MN, Scheltens P, Carrillo MC, Thies B, Weintraub S & Phelps CH. (2011). The diagnosis of dementia due to Alzheimer's disease: recommendations from the National Institute on Aging-Alzheimer's Association workgroups on diagnostic guidelines for Alzheimer's disease. *Alzheimer's & dementia : the journal of the Alzheimer's Association* **7,** 263-269.

McShane R, Westby MJ, Roberts E, Minakaran N, Schneider L, Farrimond LE, Maayan N, Ware J & Debarros J. (2019). Memantine for dementia. *Cochrane Database Syst Rev* **3,** Cd003154.

Melchior B, Mittapalli GK, Lai C, Duong-Polk K, Stewart J, Güner B, Hofilena B, Tjitro A, Anderson SD, Herman DS, Dellamary L, Swearingen CJ, Sunil KC & Yazici Y. (2019). Tau pathology reduction with SM07883, a novel, potent, and selective oral DYRK1A inhibitor: A potential therapeutic for Alzheimer's disease. *Aging Cell* **18,** e13000.

Melincovici CS, Boşca AB, Şuşman S, Mărginean M, Mihu C, Istrate M, Moldovan IM, Roman AL & Mihu CM. (2018). Vascular endothelial growth factor (VEGF) - key factor in normal and pathological angiogenesis. *Rom J Morphol Embryol* **59,** 455-467.

Mendez MF. (2019). Early-onset Alzheimer Disease and Its Variants. *Continuum (Minneapolis, Minn)* **25,** 34-51.

Menegay HJ, Myers MP, Moeslein FM & Landreth GE. (2000). Biochemical characterization and localization of the dual specificity kinase CLK1. *J Cell Sci* **113 (Pt 18),** 3241-3253.

Metin-Armagan D, Gezen-Ak D, Dursun E, Atasoy IL, Karabay A, Yilmazer S & Ozturk M. (2018). Okadaic acid-induced tau hyperphosphorylation and the downregulation of Pin1 expression in primary cortical neurons. *J Chem Neuroanat* **92,** 41-47.

Michikawa M, Fan QW, Isobe I & Yanagisawa K. (2000). Apolipoprotein E exhibits isoform-specific promotion of lipid efflux from astrocytes and neurons in culture. *J Neurochem* **74,** 1008-1016.

Mielke MM, Vemuri P & Rocca WA. (2014). Clinical epidemiology of Alzheimer's disease: assessing sex and gender differences. *Clin Epidemiol* **6,** 37-48.

Mikoshiba K, Furuichi T & Miyawaki A. (1994). Structure and function of IP3 receptors. *Semin Cell Biol* **5,** 273-281.

Milind N, Preuss C, Haber A, Ananda G, Mukherjee S, John C, Shapley S, Logsdon BA, Crane PK & Carter GW. (2020). Transcriptomic stratification of late-onset Alzheimer's cases reveals novel genetic modifiers of disease pathology. *PLoS Genet* **16,** e1008775.

Mirakhur A, Craig D, Hart DJ, McLlroy SP & Passmore AP. (2004). Behavioural and psychological syndromes in Alzheimer's disease. *Int J Geriatr Psychiatry* **19,** 1035-1039.

Mirra SS, Heyman A, McKeel D, Sumi SM, Crain BJ, Brownlee LM, Vogel FS, Hughes JP, van Belle G & Berg L. (1991). The Consortium to Establish a Registry for Alzheimer's Disease (CERAD). Part II. Standardization of the neuropathologic assessment of Alzheimer's disease. *Neurology* **41,** 479-486.

Mitchelmore C, Büchmann-Møller S, Rask L, West MJ, Troncoso JC & Jensen NA. (2004). NDRG2: a novel Alzheimer's disease associated protein. *Neurobiol Dis* **16,** 48-58.

Miyawaki A, Furuichi T, Ryou Y, Yoshikawa S, Nakagawa T, Saitoh T & Mikoshiba K. (1991). Structure-function relationships of the mouse inositol 1,4,5-trisphosphate receptor. *Proc Natl Acad Sci U S A* **88,** 4911-4915.

Morgan D, Diamond DM, Gottschall PE, Ugen KE, Dickey C, Hardy J, Duff K, Jantzen P, DiCarlo G, Wilcock D, Connor K, Hatcher J, Hope C, Gordon M & Arendash GW. (2000). A

beta peptide vaccination prevents memory loss in an animal model of Alzheimer's disease. *Nature* **408,** 982-985.

Mukaetova-Ladinska EB, Garcia-Siera F, Hurt J, Gertz HJ, Xuereb JH, Hills R, Brayne C, Huppert FA, Paykel ES, McGee M, Jakes R, Honer WG, Harrington CR & Wischik CM. (2000). Staging of cytoskeletal and beta-amyloid changes in human isocortex reveals biphasic synaptic protein response during progression of Alzheimer's disease. *Am J Pathol* **157,** 623-636.

Murakami M & Simons M. (2009). Regulation of vascular integrity. *Journal of Molecular Medicine-Jmm* **87,** 571-582.

Muraki M, Ohkawara B, Hosoya T, Onogi H, Koizumi J, Koizumi T, Sumi K, Yomoda J, Murray MV, Kimura H, Furuichi K, Shibuya H, Krainer AR, Suzuki M & Hagiwara M. (2004). Manipulation of alternative splicing by a newly developed inhibitor of Clks. *J Biol Chem* **279,** 24246-24254.

Myers MP, Murphy MB & Landreth G. (1994). The dual-specificity CLK kinase induces neuronal differentiation of PC12 cells. *Mol Cell Biol* **14,** 6954-6961.

Müller S, Chaikuad A, Gray NS & Knapp S. (2015). The ins and outs of selective kinase inhibitor development. *Nature Chemical Biology* **11,** 818-821.

Nakagawa O, Arnold M, Nakagawa M, Hamada H, Shelton JM, Kusano H, Harris TM, Childs G, Campbell KP, Richardson JA, Nishino I & Olson EN. (2005). Centronuclear myopathy in mice lacking a novel muscle-specific protein kinase transcriptionally regulated by MEF2. *Genes & development* **19,** 2066-2077.

Nakagawa T, Okano H, Furuichi T, Aruga J & Mikoshiba K. (1991). The subtypes of the mouse inositol 1,4,5-trisphosphate receptor are expressed in a tissue-specific and developmentally specific manner. *Proceedings of the National Academy of Sciences of the United States of America* **88,** 6244-6248.

Namba Y, Tomonaga M, Kawasaki H, Otomo E & Ikeda K. (1991). Apolipoprotein E immunoreactivity in cerebral amyloid deposits and neurofibrillary tangles in Alzheimer's disease and kuru plaque amyloid in Creutzfeldt-Jakob disease. *Brain Research* **541,** 163-166.

Naro C & Sette C. (2013). Phosphorylation-Mediated Regulation of Alternative Splicing in Cancer. *International Journal of Cell Biology* **2013,** 151839.

Nasu R, Furukawa A, Suzuki K, Takeuchi M & Koriyama Y. (2020). The Effect of Glyceraldehyde-Derived Advanced Glycation End Products on β-Tubulin-Inhibited Neurite Outgrowth in SH-SY5Y Human Neuroblastoma Cells. *Nutrients* **12**.

National Institute for Health and Care E. (2018). National Institute for Health and Care Excellence: Clinical Guidelines. In *Dementia: Assessment, management and support for people living with dementia and their carers*. National Institute for Health and Care Excellence (UK)

Copyright © NICE 2018., London.

Nayler O, Stamm S & Ullrich A. (1997). Characterization and comparison of four serine- and arginine-rich (SR) protein kinases. *The Biochemical journal* **326 (Pt 3),** 693-700.

Ngo J, Chakrabarti S, Ding J-H, Velazquez-Dones A, Nolen B, Aubol B, Adams J, Fu X-D & Ghosh G. (2005). Interplay between SRPK and Clk/Sty kinases in phosphorylation of the splicing factor ASF/SF2 is regulated by a docking motif in ASF/SF2. *Molecular cell* **20,** 77-89.

Ngo JCK, Gullingsrud J, Giang K, Yeh MJ, Fu X-D, Adams JA, McCammon JA & Ghosh G. (2007). SR Protein Kinase 1 Is Resilient to Inactivation. *Structure* **15,** 123-133.

Niblock M & Gallo J-M. (2012). Tau alternative splicing in familial and sporadic tauopathies. *Biochemical Society Transactions* **40,** 677-680.

Nicoll JAR, Buckland GR, Harrison CH, Page A, Harris S, Love S, Neal JW, Holmes C & Boche D. (2019). Persistent neuropathological effects 14 years following amyloid-β immunization in Alzheimer's disease. *Brain* **142,** 2113-2126.

Nikolakaki E, Kohen R, Hartmann AM, Stamm S, Georgatsou E & Giannakouros T. (2001). Cloning and characterization of an alternatively spliced form of SR protein kinase 1 that interacts specifically with scaffold attachment factor-B. *J Biol Chem* **276,** 40175-40182.

Nikolic M, Chou MM, Lu W, Mayer BJ & Tsai L-H. (1998). The p35/Cdk5 kinase is a neuron-specific Rac effector that inhibits Pak1 activity. *Nature* **395,** 194-198.

Nilsen TW & Graveley BR. (2010). Expansion of the eukaryotic proteome by alternative splicing. *Nature* **463,** 457-463.

Nowak DG, Amin EM, Rennel ES, Hoareau-Aveilla C, Gammons M, Damodoran G, Hagiwara M, Harper SJ, Woolard J, Ladomery MR & Bates DO. (2010). Regulation of Vascular Endothelial Growth Factor (VEGF) Splicing from Pro-angiogenic to Anti-angiogenic Isoforms A NOVEL THERAPEUTIC STRATEGY FOR ANGIOGENESIS. *Journal of Biological Chemistry* **285,** 5532-5540.

Nowak DG, Woolard J, Amin EM, Konopatskaya O, Saleem MA, Churchill AJ, Ladomery MR, Harper SJ & Bates DO. (2008). Expression of pro- and anti-angiogenic isoforms of VEGF is differentially regulated by splicing and growth factors. *Journal of Cell Science* **121,** 3487-3495.

Oh J, Lee HJ, Song JH, Park SI & Kim H. (2014). Plasminogen activator inhibitor-1 as an early potential diagnostic marker for Alzheimer's disease. *Exp Gerontol* **60,** 87-91.

Olivares D, Deshpande VK, Shi Y, Lahiri DK, Greig NH, Rogers JT & Huang X. (2012). N-methyl D-aspartate (NMDA) receptor antagonists and memantine treatment for Alzheimer's disease, vascular dementia and Parkinson's disease. *Curr Alzheimer Res* **9,** 746-758.

Oltean S, Neal CR, Mavrou A, Patel P, Ahad T, Alsop C, Lee T, Sison K, Qiu Y, Harper SJ, Bates DO & Salmon AH. (2012). VEGF165b overexpression restores normal glomerular water permeability in VEGF164-overexpressing adult mice. *Am J Physiol Renal Physiol* **303,** F1026-1036.

Oosthuyse B, Moons L, Storkebaum E, Beck H, Nuyens D, Brusselmans K, Van Dorpe J, Hellings P, Gorselink M, Heymans S, Theilmeier G, Dewerchin M, Laudenbach V, Vermylen P, Raat H, Acker T, Vleminckx V, Van Den Bosch L, Cashman N, Fujisawa H, Drost MR, Sciot R, Bruyninckx F, Hicklin DJ, Ince C, Gressens P, Lupu F, Plate KH, Robberecht W, Herbert JM, Collen D & Carmeliet P. (2001). Deletion of the hypoxia-response element in the vascular endothelial growth factor promoter causes motor neuron degeneration. *Nat Genet* **28,** 131-138.

Ossola B, Lantto TA, Puttonen KA, Tuominen RK, Raasmaja A & Mannisto PT. (2012). Minocycline protects SH-SY5Y cells from 6-hydroxydopamine by inhibiting both caspase-dependent and -independent programmed cell death. *J Neurosci Res* **90,** 682-690.

Pan Q, Shai O, Lee LJ, Frey BJ & Blencowe BJ. (2008). Deep surveying of alternative splicing complexity in the human transcriptome by high-throughput sequencing. *Nat Genet* **40,** 1413-1415.

Paquet D, Kwart D, Chen A, Sproul A, Jacob S, Teo S, Olsen KM, Gregg A, Noggle S & Tessier-Lavigne M. (2016). Efficient introduction of specific homozygous and heterozygous mutations using CRISPR/Cas9. *Nature* **533,** 125-129.

Paris D, Townsend K, Quadros A, Humphrey J, Sun J, Brem S, Wotoczek-Obadia M, DelleDonne A, Patel N, Obregon DF, Crescentini R, Abdullah L, Coppola D, Rojiani AM, Crawford F, Sebti SM & Mullan M. (2004). Inhibition of angiogenesis by Abeta peptides. *Angiogenesis* **7,** 75-85.

Park SA, Ahn SI & Gallo J-M. (2016). Tau mis-splicing in the pathogenesis of neurodegenerative disorders. *BMB reports* **49,** 405-413.

Park SJ, Jeong J, Park Y-U, Park K-S, Lee H, Lee N, Kim S-M, Kuroda K, Nguyen MD, Kaibuchi K & Park SK. (2015). Disrupted-in-schizophrenia-1 (DISC1) Regulates Endoplasmic Reticulum Calcium Dynamics. *Scientific reports* **5,** 8694-8694.

Patel NS, Mathura VS, Bachmeier C, Beaulieu-Abdelahad D, Laporte V, Weeks O, Mullan M & Paris D. (2010). Alzheimer's beta-amyloid peptide blocks vascular endothelial growth factor mediated signaling via direct interaction with VEGFR-2. *J Neurochem* **112,** 66-76.

Paudel HK, Lew J, Ali Z & Wang JH. (1993). Brain proline-directed protein kinase phosphorylates tau on sites that are abnormally phosphorylated in tau associated with Alzheimer's paired helical filaments. *J Biol Chem* **268,** 23512-23518.

Pei JJ, Braak H, An WL, Winblad B, Cowburn RF, Iqbal K & Grundke-Iqbal I. (2002). Up-regulation of mitogen-activated protein kinases ERK1/2 and MEK1/2 is associated with the progression of neurofibrillary degeneration in Alzheimer's disease. *Brain Res Mol Brain Res* **109,** 45-55.

Peretti D, Bastide A, Radford H, Verity N, Molloy C, Martin MG, Moreno JA, Steinert JR, Smith T, Dinsdale D, Willis AE & Mallucci GR. (2015). RBM3 mediates structural plasticity and protective effects of cooling in neurodegeneration. *Nature* **518,** 236-239.

Perrin RM, Konopatskaya O, Qiu Y, Harper S, Bates DO & Churchill AJ. (2005). Diabetic retinopathy is associated with a switch in splicing from anti- to pro-angiogenic isoforms of vascular endothelial growth factor. *Diabetologia* **48,** 2422-2427.

Persson T, Popescu BO & Cedazo-Minguez A. (2014). Oxidative Stress in Alzheimer's Disease: Why Did Antioxidant Therapy Fail? *Oxidative Medicine and Cellular Longevity* **2014,** 427318.

Pink J, O'Brien J, Robinson L & Longson D. (2018). Dementia: assessment, management and support: summary of updated NICE guidance. *bmj* **361**.

Poduslo JF, Curran GL & Berg CT. (1994). Macromolecular permeability across the blood-nerve and blood-brain barriers. *Proc Natl Acad Sci U S A* **91,** 5705-5709.

Prince M, Knapp M, Guerchet M, McCrone P, Prina M, Comas-Herrera A, Wittenberg R, Adelaja B, Hu B & King D. (2014). Dementia UK: -overview.

Provias J & Jeynes B. (2008). Neurofibrillary tangles and senile plaques in Alzheimer's brains are associated with reduced capillary expression of vascular endothelial growth factor and endothelial nitric oxide synthase. *Curr Neurovasc Res* **5,** 199-205.

Qian W, Iqbal K, Grundke-Iqbal I, Gong CX & Liu F. (2011a). Splicing factor SC35 promotes tau expression through stabilization of its mRNA. *FEBS Lett* **585,** 875-880.

Qian W, Liang H, Shi J, Jin N, Grundke-Iqbal I, Iqbal K, Gong C-X & Liu F. (2011b). Regulation of the alternative splicing of tau exon 10 by SC35 and Dyrk1A. *Nucleic acids research* **39,** 6161-6171.

Qiu Y, Hoareau-Aveilla C, Oltean S, Harper SJ & Bates DO. (2009). The anti-angiogenic isoforms of VEGF in health and disease. *Biochem Soc Trans* **37,** 1207-1213.

Rabin JS, Schultz AP, Hedden T, Viswanathan A, Marshall GA, Kilpatrick E, Klein H, Buckley RF, Yang H-S, Properzi M, Rao V, Kirn DR, Papp KV, Rentz DM, Johnson KA, Sperling RA & Chhatwal JP. (2018). Interactive Associations of Vascular Risk and β-Amyloid Burden With Cognitive Decline in Clinically Normal Elderly Individuals: Findings From the Harvard Aging Brain Study. *JAMA neurology* **75,** 1124-1131.

Rabin JS, Yang H-S, Schultz AP, Hanseeuw BJ, Hedden T, Viswanathan A, Gatchel JR, Marshall GA, Kilpatrick E, Klein H, Rao V, Buckley RF, Yau W-YW, Kirn DR, Rentz DM, Johnson KA, Sperling RA & Chhatwal JP. (2019). Vascular Risk and β-Amyloid Are Synergistically Associated with Cortical Tau. *Annals of neurology* **85,** 272-279.

Raj T, Li YI, Wong G, Humphrey J, Wang M, Ramdhani S, Wang YC, Ng B, Gupta I, Haroutunian V, Schadt EE, Young-Pearse T, Mostafavi S, Zhang B, Sklar P, Bennett DA & De Jager PL. (2018). Integrative transcriptome analyses of the aging brain implicate altered splicing in Alzheimer's disease susceptibility. *Nat Genet* **50,** 1584-1592.

Rapp A, Gmeiner B & Hüttinger M. (2006). Implication of apoE isoforms in cholesterol metabolism by primary rat hippocampal neurons and astrocytes. *Biochimie* **88,** 473-483.

Rebeck GW, Reiter JS, Strickland DK & Hyman BT. (1993). Apolipoprotein E in sporadic Alzheimer's disease: allelic variation and receptor interactions. *Neuron* **11,** 575-580.

Reiman EM, Chen K, Liu X, Bandy D, Yu M, Lee W, Ayutyanont N, Keppler J, Reeder SA, Langbaum JBS, Alexander GE, Klunk WE, Mathis CA, Price JC, Aizenstein HJ, DeKosky ST & Caselli RJ. (2009). Fibrillar amyloid-beta burden in cognitively normal people at 3 levels of genetic risk for Alzheimer's disease. *Proceedings of the National Academy of Sciences of the United States of America* **106,** 6820-6825.

Robbins JP, Perfect L, Ribe EM, Maresca M, Dangla-Valls A, Foster EM, Killick R, Nowosiad P, Reid MJ, Polit LD, Nevado AJ, Ebner D, Bohlooly YM, Buckley N, Pangalos MN, Price J & Lovestone S. (2018). Clusterin Is Required for β-Amyloid Toxicity in Human iPSC-Derived Neurons. *Front Neurosci* **12,** 504.

Rodgers JT, Vogel RO & Puigserver P. (2011). Clk2 and B56β Mediate Insulin-Regulated Assembly of the PP2A Phosphatase Holoenzyme Complex on Akt. *Molecular Cell* **41,** 471-479.

Rodrigue KM, Rieck JR, Kennedy KM, Devous MD, Diaz-Arrastia R & Park DC. (2013). Risk Factors for beta-Amyloid Deposition in Healthy Aging. *Jama Neurology* **70,** 600-606.

Rogawski MA & Wenk GL. (2003). The neuropharmacological basis for the use of memantine in the treatment of Alzheimer's disease. *CNS Drug Rev* **9,** 275-308.

Rowen L, Young J, Birditt B, Kaur A, Madan A, Philipps DL, Qin S, Minx P, Wilson RK, Hood L & Graveley BR. (2002). Analysis of the human neurexin genes: alternative splicing and the generation of protein diversity. *Genomics* **79,** 587-597.

Ruggiu M, Herbst R, Kim N, Jevsek M, Fak JJ, Mann MA, Fischbach G, Burden SJ & Darnell RB. (2009). Rescuing Z+ agrin splicing in Nova null mice restores synapse formation and unmasks a physiologic defect in motor neuron firing. *Proc Natl Acad Sci U S A* **106,** 3513-3518.

Ryoo S-R, Jeong H-K, Radnaabazar C, Yoo J-J, Cho H-J, Lee H-W, Kim I-S, Cheon Y-H, Ahn Y, Chung S-H & Song W-J. (2007). DYRK1A-mediated hyperphosphorylation of Tau - A functional link between Down syndrome and Alzheimer disease. *The Journal of biological chemistry* **282,** 34850-34857.

Sakono M & Zako T. (2010). Amyloid oligomers: formation and toxicity of A beta oligomers. *Febs Journal* **277,** 1348-1358.

Salomon-Zimri S, Glat MJ, Barhum Y, Luz I, Boehm-Cagan A, Liraz O, Ben-Zur T, Offen D & Michaelson DM. (2016). Reversal of ApoE4-Driven Brain Pathology by Vascular Endothelial Growth Factor Treatment. *J Alzheimers Dis* **53,** 1443-1458.

Santacruz K, Lewis J, Spires T, Paulson J, Kotilinek L, Ingelsson M, Guimaraes A, DeTure M, Ramsden M, McGowan E, Forster C, Yue M, Orne J, Janus C, Mariash A, Kuskowski M, Hyman B, Hutton M & Ashe KH. (2005). Tau suppression in a neurodegenerative mouse model improves memory function. *Science* **309,** 476-481.

Saraswat D, Nehra S, Chaudhary K & Cvs SP. (2015). Novel vascular endothelial growth factor blocker improves cellular viability and reduces hypobaric hypoxia-induced vascular leakage and oedema in rat brain. *Clin Exp Pharmacol Physiol* **42,** 475-484.

Saura CA, Servián-Morilla E & Scholl FG. (2011). Presenilin/γ-secretase regulates neurexin processing at synapses. *PLoS One* **6,** e19430.

Scheiffele P, Fan J, Choih J, Fetter R & Serafini T. (2000). Neuroligin Expressed in Nonneuronal Cells Triggers Presynaptic Development in Contacting Axons. *Cell* **101,** 657-669.

Schenk D. (2002). Amyloid-beta immunotherapy for Alzheimer's disease: the end of the beginning. *Nat Rev Neurosci* **3,** 824-828.

Schenk D, Barbour R, Dunn W, Gordon G, Grajeda H, Guido T, Hu K, Huang J, Johnson-Wood K, Khan K, Kholodenko D, Lee M, Liao Z, Lieberburg I, Motter R, Mutter L, Soriano F, Shopp G, Vasquez N, Vandevert C, Walker S, Wogulis M, Yednock T, Games D & Seubert P. (1999). Immunization with amyloid-beta attenuates Alzheimer-disease-like pathology in the PDAPP mouse. *Nature* **400,** 173-177.

Scheuner D, Eckman C, Jensen M, Song X, Citron M, Suzuki N, Bird TD, Hardy J, Hutton M, Kukull W, Larson E, Levy-Lahad L, Viitanen M, Peskind E, Poorkaj P, Schellenberg G, Tanzi R, Wasco W, Lannfelt L, Selkoe D & Younkin S. (1996). Secreted amyloid β–protein similar to that in the senile plaques of Alzheimer's disease is increased in vivo by the presenilin 1 and 2 and APP mutations linked to familial Alzheimer's disease. *Nature Medicine* **2,** 864-870.

Schlessinger J & Ullrich A. (1992). Growth factor signaling by receptor tyrosine kinases. *Neuron* **9,** 383-391.

Schmechel DE, Saunders AM, Strittmatter WJ, Crain BJ, Hulette CM, Joo SH, Pericak-Vance MA, Goldgaber D & Roses AD. (1993). Increased amyloid beta-peptide deposition in cerebral cortex as a consequence of apolipoprotein E genotype in late-onset Alzheimer disease. *Proceedings of the National Academy of Sciences of the United States of America* **90,** 9649-9653.

Schneider JA, Arvanitakis Z, Bang W & Bennett DA. (2007). Mixed brain pathologies account for most dementia cases in community-dwelling older persons. *Neurology* **69,** 2197.

Schneider JA, Wilson RS, Bienias JL, Evans DA & Bennett DA. (2004). Cerebral infarctions and the likelihood of dementia from Alzheimer disease pathology. *Neurology* **62,** 1148-1155.

Schoch Kathleen M, DeVos Sarah L, Miller Rebecca L, Chun Seung J, Norrbom M, Wozniak David F, Dawson Hana N, Bennett CF, Rigo F & Miller Timothy M. (2016). Increased 4R-Tau Induces Pathological Changes in a Human-Tau Mouse Model. *Neuron* **90,** 941-947.

Schonberger SJ, Edgar PF, Kydd R, Faull RLM & Cooper GJS. (2001). Proteomic analysis of the brain in Alzheimer's disease: Molecular phenotype of a complex disease process. *PROTEOMICS* **1,** 1519-1528.

Schumacher VA, Jeruschke S, Eitner F, Becker JU, Pitschke G, Ince Y, Miner JH, Leuschner I, Engers R, Everding AS, Bulla M & Royer-Pokora B. (2007). Impaired glomerular maturation and lack of VEGF165b in Denys-Drash syndrome. *J Am Soc Nephrol* **18,** 719-729.

Selkoe DJ. (2001). Alzheimer's disease: Genes, proteins, and therapy. *Physiological Reviews* **81,** 741-766.

Selkoe DJ. (2004). Cell biology of protein misfolding: the examples of Alzheimer's and Parkinson's diseases. *Nat Cell Biol* **6,** 1054-1061.

Selkoe DJ & Hardy J. (2016). The amyloid hypothesis of Alzheimer's disease at 25 years. *EMBO Mol Med* **8,** 595-608.

Senger DR, Connolly DT, Van de Water L, Feder J & Dvorak HF. (1990). Purification and NH2-terminal amino acid sequence of guinea pig tumor-secreted vascular permeability factor. *Cancer Res* **50,** 1774-1778.

Senger DR, Perruzzi CA, Feder J & Dvorak HF. (1986). A highly conserved vascular permeability factor secreted by a variety of human and rodent tumor cell lines. *Cancer Res* **46,** 5629-5632.

Sengupta A, Novak M, Grundke-Iqbal I & Iqbal K. (2006). Regulation of phosphorylation of tau by cyclin-dependent kinase 5 and glycogen synthase kinase-3 at substrate level. *FEBS Lett* **580,** 5925-5933.

Seo J, Byun MS, Yi D, Lee JH, Jeon SY, Shin SA, Kim YK, Kang KM, Sohn CH, Jung G, Park JC, Han SH, Byun J, Mook-Jung I, Lee DY & Choi M. (2020). Genetic associations of in vivo pathology influence Alzheimer's disease susceptibility. *Alzheimers Res Ther* **12,** 156.

Seshadri S, Fitzpatrick AL, Ikram MA, DeStefano AL, Gudnason V, Boada M, Bis JC, Smith AV, Carassquillo MM, Lambert JC, Harold D, Schrijvers EM, Ramirez-Lorca R, Debette S, Longstreth WT, Jr., Janssens AC, Pankratz VS, Dartigues JF, Hollingworth P, Aspelund T, Hernandez I, Beiser A, Kuller LH, Koudstaal PJ, Dickson DW, Tzourio C, Abraham R, Antunez C, Du Y, Rotter JI, Aulchenko YS, Harris TB, Petersen RC, Berr C, Owen MJ, Lopez-Arrieta J, Varadarajan BN, Becker JT, Rivadeneira F, Nalls MA, Graff-Radford NR, Campion D, Auerbach S, Rice K, Hofman A, Jonsson PV, Schmidt H, Lathrop M, Mosley TH, Au R, Psaty BM, Uitterlinden AG, Farrer LA, Lumley T, Ruiz A, Williams J, Amouyel P, Younkin SG, Wolf PA, Launer LJ, Lopez OL, van Duijn CM & Breteler MM. (2010). Genome-wide analysis of genetic loci associated with Alzheimer disease. *Jama* **303,** 1832-1840.

Shahnur A, Nakano M, Ishihara S, Kakuda N, Miyasaka T, Uchiyama H, Shirai Y, Moniruzzaman M, Saito T, Saido TC, Nishimura M & Funamoto S. (2021). A potential defense mechanism against amyloid deposition in cerebellum. *Biochem Biophys Res Commun* **535,** 25-32.

Shankar GM, Bloodgood BL, Townsend M, Walsh DM, Selkoe DJ & Sabatini BL. (2007). Natural oligomers of the Alzheimer amyloid-beta protein induce reversible synapse loss by modulating an NMDA-type glutamate receptor-dependent signaling pathway. *J Neurosci* **27,** 2866-2875.

Shen J & Kelleher RJ, 3rd. (2007). The presenilin hypothesis of Alzheimer's disease: evidence for a loss-of-function pathogenic mechanism. *Proceedings of the National Academy of Sciences of the United States of America* **104,** 403-409.

Shen K, Hines AC, Schwarzer D, Pickin KA & Cole PA. (2005). Protein kinase structure and function analysis with chemical tools. *Biochim Biophys Acta* **1754,** 65-78.

Shi J, Qian W, Yin X, Iqbal K, Grundke-Iqbal I, Gu X, Ding F, Gong CX & Liu F. (2011). Cyclic AMP-dependent protein kinase regulates the alternative splicing of tau exon 10: a mechanism involved in tau pathology of Alzheimer disease. *J Biol Chem* **286,** 14639-14648.

Shi J, Zhang T, Zhou C, Chohan MO, Gu X, Wegiel J, Zhou J, Hwang YW, Iqbal K, Grundke-Iqbal I, Gong CX & Liu F. (2008). Increased dosage of Dyrk1A alters alternative splicing factor (ASF)-regulated alternative splicing of tau in Down syndrome. *J Biol Chem* **283,** 28660-28669.

Shi XL, Yan N, Cui YJ & Liu ZP. (2020). A Unique GSK-3β inhibitor B10 Has a Direct Effect on Aβ, Targets Tau and Metal Dyshomeostasis, and Promotes Neuronal Neurite Outgrowth. *Cells* **9**.

Shibuya M. (2001). Structure and dual function of vascular endothelial growth factor receptor-1 (Flt-1). *The International Journal of Biochemistry & Cell Biology* **33,** 409-420.

Shilling D, Muller M, Takano H, Mak D-O, Abel T, Coulter D & Foskett J. (2014). Suppression of InsP(3) Receptor-Mediated Ca2+ Signaling Alleviates Mutant Presenilin-Linked Familial Alzheimer's Disease Pathogenesis. *The Journal of neuroscience : the official journal of the Society for Neuroscience* **34,** 6910-6923.

Shorbagi S & Brown IR. (2016). Dynamics of the association of heat shock protein HSPA6 (Hsp70B') and HSPA1A (Hsp70–1) with stress-sensitive cytoplasmic and nuclear structures in differentiated human neuronal cells. *Cell Stress and Chaperones* **21,** 993-1003.

Silverman WF, Krum JM, Mani N & Rosenstein JM. (1999). Vascular, glial and neuronal effects of vascular endothelial growth factor in mesencephalic explant cultures. *Neuroscience* **90,** 1529-1541.

Simons M, Gordon E & Claesson-Welsh L. (2016). Mechanisms and regulation of endothelial VEGF receptor signalling. *Nat Rev Mol Cell Biol* **17,** 611-625.

Siqueira RP, Barbosa Éde A, Polêto MD, Righetto GL, Seraphim TV, Salgado RL, Ferreira JG, Barros MV, de Oliveira LL, Laranjeira AB, Almeida MR, Júnior AS, Fietto JL, Kobarg J, de Oliveira EB, Teixeira RR, Borges JC, Yunes JA & Bressan GC. (2015). Potential Antileukemia Effect and Structural Analyses of SRPK Inhibition by N-(2-(Piperidin-1-yl)-5-(Trifluoromethyl)Phenyl)Isonicotinamide (SRPIN340). *PLoS One* **10,** e0134882.

Sondell M, Lundborg G & Kanje M. (1999). Vascular endothelial growth factor has neurotrophic activity and stimulates axonal outgrowth, enhancing cell survival and Schwann cell proliferation in the peripheral nervous system. *J Neurosci* **19,** 5731-5740.

Sondell M, Sundler F & Kanje M. (2000). Vascular endothelial growth factor is a neurotrophic factor which stimulates axonal outgrowth through the flk-1 receptor. *Eur J Neurosci* **12,** 4243-4254.

Song JS & Yang SD. (1995). Tau protein kinase I/GSK-3 beta/kinase FA in heparin phosphorylates tau on Ser199, Thr231, Ser235, Ser262, Ser369, and Ser400 sites phosphorylated in Alzheimer disease brain. *J Protein Chem* **14,** 95-105.

Song W-J, Sternberg LR, Kasten-Sportès C, Keuren MLV, Chung S-H, Slack AC, Miller DE, Glover TW, Chiang P-W, Lou L & Kurnit DM. (1996). Isolation of Human and Murine

Homologues of theDrosophilaMinibrain Gene: Human Homologue Maps to 21q22.2 in the Down Syndrome “Critical Region”. *Genomics* **38,** 331-339.

Sonoda Y, Tooyama I, Mukai H, Maeda K, Akiyama H & Kawamata T. (2016). S6 kinase phosphorylated at T229 is involved in tau and actin pathologies in Alzheimer's disease. *Neuropathology* **36,** 325-332.

Sperling RA, Aisen PS, Beckett LA, Bennett DA, Craft S, Fagan AM, Iwatsubo T, Jack CR, Jr., Kaye J, Montine TJ, Park DC, Reiman EM, Rowe CC, Siemers E, Stern Y, Yaffe K, Carrillo MC, Thies B, Morrison-Bogorad M, Wagster MV & Phelps CH. (2011). Toward defining the preclinical stages of Alzheimer's disease: recommendations from the National Institute on Aging-Alzheimer's Association workgroups on diagnostic guidelines for Alzheimer's disease. *Alzheimer's & dementia : the journal of the Alzheimer's Association* **7,** 280-292.

Spillantini MG & Goedert M. (2013). Tau pathology and neurodegeneration. *Lancet Neurol* **12,** 609-622.

Spires-Jones TL, Kopeikina KJ, Koffie RM, de Calignon A & Hyman BT. (2011). Are tangles as toxic as they look? *Journal of molecular neuroscience : MN* **45,** 438-444.

Spires-Jones TL, Stoothoff WH, de Calignon A, Jones PB & Hyman BT. (2009). Tau pathophysiology in neurodegeneration: a tangled issue. *Trends Neurosci* **32,** 150-159.

Stanford PM, Shepherd CE, Halliday GM, Brooks WS, Schofield PW, Brodaty H, Martins RN, Kwok JB & Schofield PR. (2003). Mutations in the tau gene that cause an increase in three repeat tau and frontotemporal dementia. *Brain* **126,** 814-826.

Stevens M & Oltean S. (2018). Modulation of VEGF-A Alternative Splicing as a Novel Treatment in Chronic Kidney Disease. *Genes (Basel)* **9**.

Stine WB, Jungbauer L, Yu CJ & Ladu MJ. (2011). Preparing Synthetic A beta in Different Aggregation States. *Alzheimer's Disease and Frontotemporal Dementia: Methods and Protocols* **670,** 13-32.

Storkebaum E, Lambrechts D & Carmeliet P. (2004). VEGF: once regarded as a specific angiogenic factor, now implicated in neuroprotection. *Bioessays* **26,** 943-954.

Stroo E, Janssen L, Sin O, Hogewerf W, Koster M, Harkema L, Youssef S, beschorner N, Wolters A, Bakker B, Thathiah A, Foijer F, Sluis B, Deursen J, Jucker M, Bruin A & Nollen E. (2021). *Deletion of Serf2 shifts amyloid conformation in an Aβ amyloid mouse model*.

Tamagnini F, Scullion S, Brown JT & Randall AD. (2015). Intrinsic excitability changes induced by acute treatment of hippocampal CA1 pyramidal neurons with exogenous amyloid β peptide. *Hippocampus* **25,** 786-797.

Tan CC, Yu JT, Wang HF, Tan MS, Meng XF, Wang C, Jiang T, Zhu XC & Tan L. (2014). Efficacy and safety of donepezil, galantamine, rivastigmine, and memantine for the treatment of Alzheimer's disease: a systematic review and meta-analysis. *J Alzheimers Dis* **41,** 615-631.

Tariot PN, Farlow MR, Grossberg GT, Graham SM, McDonald S & Gergel I. (2004). Memantine treatment in patients with moderate to severe Alzheimer disease already receiving donepezil: a randomized controlled trial. *Jama* **291,** 317-324.

Tarkowski E, Issa R, Sjogren M, Wallin A, Blennow K, Tarkowski A & Kumar P. (2002). Increased intrathecal levels of the angiogenic factors VEGF and TGF-beta in Alzheimer's disease and vascular dementia. *Neurobiology of Aging* **23,** 237-243.

Thal DR, Rüb U, Orantes M & Braak H. (2002). Phases of A beta-deposition in the human brain and its relevance for the development of AD. *Neurology* **58,** 1791-1800.

Theofilas P, Ehrenberg AJ, Nguy A, Thackrey JM, Dunlop S, Mejia MB, Alho AT, Paraizo Leite RE, Rodriguez RD, Suemoto CK, Nascimento CF, Chin M, Medina-Cleghorn D, Cuervo AM, Arkin M, Seeley WW, Miller BL, Nitrini R, Pasqualucci CA, Filho WJ, Rueb U, Neuhaus J, Heinsen H & Grinberg LT. (2018). Probing the correlation of neuronal loss, neurofibrillary tangles, and cell death markers across the Alzheimer's disease Braak stages: a quantitative study in humans. *Neurobiol Aging* **61,** 1-12.

Thomas T, Miners S & Love S. (2015). Post-mortem assessment of hypoperfusion of cerebral cortex in Alzheimer's disease and vascular dementia. *Brain* **138,** 1059-1069.

Tokar T, Pastrello C & Jurisica I. (2020). GSOAP: a tool for visualization of gene set over-representation analysis. *Bioinformatics* **36,** 2923-2925.

Tollervey JR, Wang Z, Hortobágyi T, Witten JT, Zarnack K, Kayikci M, Clark TA, Schweitzer AC, Rot G, Curk T, Zupan B, Rogelj B, Shaw CE & Ule J. (2011). Analysis of alternative splicing associated with aging and neurodegeneration in the human brain. *Genome Res* **21,** 1572-1582.

Trabzuni D, Wray S, Vandrovcova J, Ramasamy A, Walker R, Smith C, Luk C, Gibbs JR, Dillman A, Hernandez DG, Arepalli S, Singleton AB, Cookson MR, Pittman AM, de Silva R, Weale ME, Hardy J & Ryten M. (2012). MAPT expression and splicing is differentially regulated by brain region: relation to genotype and implication for tauopathies. *Human Molecular Genetics* **21,** 4094-4103.

Tzelepis K, De Braekeleer E, Aspris D, Barbieri I, Vijayabaskar MS, Liu WH, Gozdecka M, Metzakopian E, Toop HD, Dudek M, Robson SC, Hermida-Prado F, Yang YH, Babaei-Jadidi R, Garyfallos DA, Ponstingl H, Dias JML, Gallipoli P, Seiler M, Buonamici S, Vick B, Bannister AJ, Rad R, Prinjha RK, Marioni JC, Huntly B, Batson J, Morris JC, Pina C, Bradley A, Jeremias I, Bates DO, Yusa K, Kouzarides T & Vassiliou GS. (2018). SRPK1 maintains acute myeloid leukemia through effects on isoform usage of epigenetic regulators including BRD4. *Nat Commun* **9,** 5378.

Ved N, Hulse RP, Bestall SM, Donaldson LF, Bainbridge JW & Bates DO. (2017). Vascular endothelial growth factor-A(165)b ameliorates outer-retinal barrier and vascular dysfunction in the diabetic retina. *Clin Sci (Lond)* **131,** 1225-1243.

Veeranna, Kaji T, Boland B, Odrljin T, Mohan P, Basavarajappa BS, Peterhoff C, Cataldo A, Rudnicki A, Amin N, Li BS, Pant HC, Hungund BL, Arancio O & Nixon RA. (2004). Calpain mediates calcium-induced activation of the erk1,2 MAPK pathway and cytoskeletal phosphorylation in neurons: relevance to Alzheimer's disease. *Am J Pathol* **165,** 795-805.

Wakiya K & Shibuya M. (1999). Okadaic acid stimulates the expression of vascular endothelial growth factor gene. *Biochem Biophys Res Commun* **265,** 584-588.

Walsh DM, Klyubin I, Fadeeva JV, Cullen WK, Anwyl R, Wolfe MS, Rowan MJ & Selkoe DJ. (2002). Naturally secreted oligomers of amyloid β protein potently inhibit hippocampal long-term potentiation in vivo. *Nature* **416,** 535-539.

Wang G, Yang H, Yan S, Wang CE, Liu X, Zhao B, Ouyang Z, Yin P, Liu Z, Zhao Y, Liu T, Fan N, Guo L, Li S, Li XJ & Lai L. (2015a). Cytoplasmic mislocalization of RNA splicing factors and aberrant neuronal gene splicing in TDP-43 transgenic pig brain. *Mol Neurodegener* **10,** 42.

Wang HY, Lin W, Dyck JA, Yeakley JM, Songyang Z, Cantley LC & Fu XD. (1998). SRPK2: a differentially expressed SR protein-specific kinase involved in mediating the interaction and localization of pre-mRNA splicing factors in mammalian cells. *J Cell Biol* **140,** 737-750.

Wang J, Gao QS, Wang Y, Lafyatis R, Stamm S & Andreadis A. (2004). Tau exon 10, whose missplicing causes frontotemporal dementia, is regulated by an intricate interplay of cis elements and trans factors. *J Neurochem* **88,** 1078-1090.

Wang JZ, Xia YY, Grundke-Iqbal I & Iqbal K. (2013). Abnormal hyperphosphorylation of tau: sites, regulation, and molecular mechanism of neurofibrillary degeneration. *J Alzheimers Dis* **33 Suppl 1,** S123-139.

Wang Y, Liu J, Huang BO, Xu YM, Li J, Huang LF, Lin J, Zhang J, Min QH, Yang WM & Wang XZ. (2015b). Mechanism of alternative splicing and its regulation. *Biomed Rep* **3,** 152-158.

Wang Z & Burge C. (2008). Splicing regulation: From a parts list of regulatory elements to an integrated splicing code. *RNA (New York, NY)* **14,** 802-813.

Wang Z, Gerstein M & Snyder M. (2009). RNA-Seq: a revolutionary tool for transcriptomics. *Nat Rev Genet* **10,** 57-63.

Wang Z-H, Liu P, Liu X, Yu SP, Wang J-Z & Ye K. (2018). Delta-secretase (AEP) mediates tau-splicing imbalance and accelerates cognitive decline in tauopathies. *The Journal of experimental medicine* **215,** 3038-3056.

Weingarten MD, Lockwood AH, Hwo SY & Kirschner MW. (1975). A protein factor essential for microtubule assembly. *Proceedings of the National Academy of Sciences of the United States of America* **72,** 1858-1862.

Weinreb O, Amit T, Bar-Am O & Youdim MB. (2012). Ladostigil: a novel multimodal neuroprotective drug with cholinesterase and brain-selective monoamine oxidase inhibitory activities for Alzheimer's disease treatment. *Curr Drug Targets* **13,** 483-494.

Wilkinson ME, Charenton C & Nagai K. (2020). RNA Splicing by the Spliceosome. *Annu Rev Biochem* **89,** 359-388.

Will CL & Lührmann R. (2011). Spliceosome structure and function. *Cold Spring Harbor perspectives in biology* **3,** a003707.

Wilson RS, Leurgans SE, Boyle PA & Bennett DA. (2011). Cognitive decline in prodromal Alzheimer disease and mild cognitive impairment. *Arch Neurol* **68,** 351-356.

Wilson RS, Segawa E, Boyle PA, Anagnos SE, Hizel LP & Bennett DA. (2012). The natural history of cognitive decline in Alzheimer's disease. *Psychol Aging* **27,** 1008-1017.

Wisniewski KE, Wisniewski HM & Wen GY. (1985). Occurrence of neuropathological changes and dementia of Alzheimer's disease in Down's syndrome. *Ann Neurol* **17,** 278-282.

Wittmann CW, Wszolek MF, Shulman JM, Salvaterra PM, Lewis J, Hutton M & Feany MB. (2001). Tauopathy in Drosophila: Neurodegeneration Without Neurofibrillary Tangles. *Science* **293,** 711.

World Health O. (2017). Global action plan on the public health response to dementia 2017–2025.

Xiao S, Song LL, Li JT, Wang H, Yu N, Wang ZQ, Zhang Y, He JS & Hung T. (2020). Intraperitoneal Administration of Monoclonal Antibody Against Pathologic Aβ42 Aggregates Alleviated Cognitive Deficits and Synaptic Lesions in APP/PS1 Mice. *J Alzheimers Dis* **73,** 657-670.

Xu J, Patassini S, Rustogi N, Riba-Garcia I, Hale BD, Phillips AM, Waldvogel H, Haines R, Bradbury P, Stevens A, Faull RLM, Dowsey AW, Cooper GJS & Unwin RD. (2019). Regional protein expression in human Alzheimer's brain correlates with disease severity. *Commun Biol* **2,** 43.

Yang J, Välineva T, Hong J, Bu T, Yao Z, Jensen ON, Frilander MJ & Silvennoinen O. (2007). Transcriptional co-activator protein p100 interacts with snRNP proteins and facilitates the assembly of the spliceosome. *Nucleic Acids Res* **35,** 4485-4494.

Yang M, Ke Y, Kim P & Zhou X. (2021). ExonSkipAD provides the functional genomic landscape of exon skipping events in Alzheimer's disease. *Brief Bioinform*.

Yang SP, Bae DG, Kang HJ, Gwag BJ, Gho YS & Chae CB. (2004). Co-accumulation of vascular endothelial growth factor with beta-amyloid in the brain of patients with Alzheimer's disease. *Neurobiology of Aging* **25,** 283-290.

Yap K & Makeyev EV. (2016). Functional impact of splice isoform diversity in individual cells. *Biochem Soc Trans* **44,** 1079-1085.

Yin X, Jin N, Gu J, Shi J, Zhou J, Gong CX, Iqbal K, Grundke-Iqbal I & Liu F. (2012). Dual-specificity tyrosine phosphorylation-regulated kinase 1A (Dyrk1A) modulates serine/arginine-rich protein 55 (SRp55)-promoted Tau exon 10 inclusion. *J Biol Chem* **287,** 30497-30506.

Yon Rhee S, Wood V, Dolinski K & Draghici S. (2008). Use and misuse of the gene ontology annotations. *Nature Reviews Genetics* **9,** 509-515.

Zhang L, Yue Y, Ouyang M, Liu H & Li Z. (2017). The Effects of IGF-1 on TNF-α-Treated DRG Neurons by Modulating ATF3 and GAP-43 Expression via PI3K/Akt/S6K Signaling Pathway. *Neurochem Res* **42,** 1403-1421.

Zhang YW, Thompson R, Zhang H & Xu HX. (2011). APP processing in Alzheimer's disease. *Molecular Brain* **4**.

Zhao J & Pei G. (2008). Evoking plasmin for beta-amyloid clearance. *Cell Res* **18,** 803-804.

Zhao QF, Yu JT, Tan MS & Tan L. (2015). ABCA7 in Alzheimer's Disease. *Mol Neurobiol* **51,** 1008-1016.

Zhao WQ, De Felice FG, Fernandez S, Chen H, Lambert MP, Quon MJ, Krafft GA & Klein WL. (2008). Amyloid beta oligomers induce impairment of neuronal insulin receptors. *Faseb j* **22,** 246-260.

Zheng CL, Fu XD & Gribskov M. (2005). Characteristics and regulatory elements defining constitutive splicing and different modes of alternative splicing in human and mouse. *Rna* **11,** 1777-1787.

Zheng XL, Xie ZH, Zhu ZY, Liu Z, Wang Y, Wei LF, Yang H, Yang HN, Liu YQ & Bi JZ. (2014). Methyllycaconitine Alleviates Amyloid-beta Peptides-Induced Cytotoxicity in SH-SY5Y Cells. *Plos One* **9**.

Zhong XY, Ding JH, Adams JA, Ghosh G & Fu XD. (2009). Regulation of SR protein phosphorylation and alternative splicing by modulating kinetic interactions of SRPK1 with molecular chaperones. *Genes Dev* **23,** 482-495.

Zlokovic BV. (2011). Neurovascular pathways to neurodegeneration in Alzheimer's disease and other disorders. *Nat Rev Neurosci* **12,** 723-738.

Šimić G, Babić Leko M, Wray S, Harrington CR, Delalle I, Jovanov-Milošević N, Bažadona D, Buée L, de Silva R, Di Giovanni G, Wischik CM & Hof PR. (2017). Monoaminergic neuropathology in Alzheimer's disease. *Progress in neurobiology* **151,** 101-138.